NASA Contractor Report 3322

Satellite Power Systems (SPS) Concept Definition Study

Volume V - Special Emphasis Studies

G. M. Hanley

CONTRACT NAS8-32475
SEPTEMBER 1980

NASA

NASA Contractor Report 3322

Satellite Power Systems (SPS) Concept Definition Study

Volume V - Special Emphasis Studies

G. M. Hanley
Rockwell International
Downey, California

Prepared for
Marshall Space Flight Center
under Contract NAS8-32475

National Aeronautics
and Space Administration

**Scientific and Technical
Information Branch**

1980

FOREWORD

This is Volume V - *Special Emphasis Studies*, of the SPS Concept Definition Study final report as submitted by Rockwell International through the Satellite Systems Division. All work was completed in response to the NASA/MSFC Contract NAS8-32475, Exhibit C, dated March 28, 1978.

The SPS final report will provide the NASA with additional information on the selection of a viable SPS concept and will furnish a basis for subsequent technology advancement and verification activities. Other volumes of the final report are listed as follows:

Volume	Title
I	Executive Summary
II	Systems Engineering
III	Experimentation/Verification Element Definition
IV	Transportation Analyses
VI	In-Depth Element Investigations
VII	Systems/Subsystems Requirements Data Book

The SPS Program Manager, G. M. Hanley, may be contacted on any of the technical or management aspects of this report. He may be reached at 213/594-3911, Seal Beach, California.

CONTENTS

Section Page

ILLUSTRATIONS

TABLES

1.0 INTRODUCTION

1.0 INTRODUCTION

At the beginning of the current study, five specific areas which previously had been analyzed to varying depths of detail were identified as high priority for more in-depth analysis. These areas were:

- Rectenna Constructability
- Satellite Constructability
- Support Systems Constructability
- Space Environmental Analysis
- Special End-to-End Analyses

Subsequent to submission of the First Quarterly Review, new program baseline requirements were issued by NASA. These requirements specified coplanar solar blankets and an end mounted antenna, utilizing either GaAlAs solar cells and employing a CR of 2, or Si cells. Several configurations were analyzed and are reported herein. One configuration, selected as the preferred concept, is shown in Figure 1.0-1. Utilizing the preferred configuration as a baseline, a satellite construction base was defined, precursor operations incident to establishment of orbital support facilities identified, and the satellite construction sequence and procedures developed. Since the new baseline specifies sixty instead of one hundred and twenty satellites to be constructed in a thirty year period, mass flow to orbit requirements were revised and new traffic models established. Launch site requirements (exclusive of actual launch operations) in terms of manpower and building space were defined.

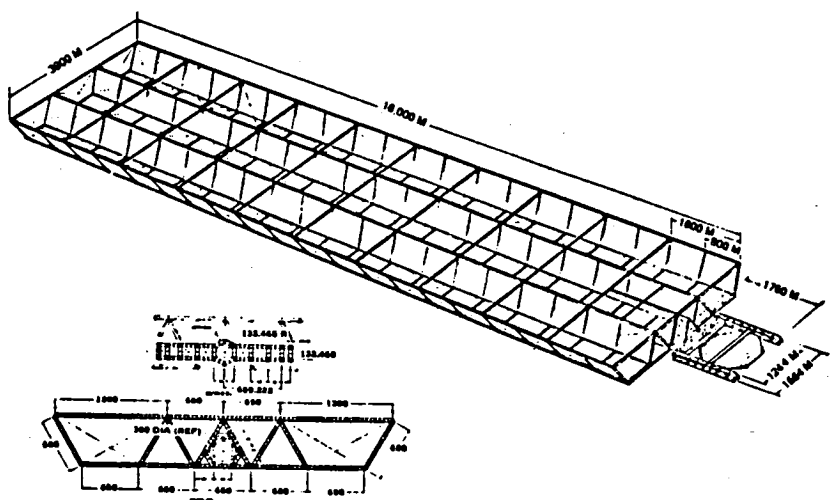

Figure 1.0-1. Reference Configuration SPS

Although considerable rectenna design effort has been done, very little analysis of the implications of actually constructing a rectenna site had been accomplished. Therefore, the sequence of operations incident to the construction was developed, procedures established, and manpower and equipment requirements defined.

In the special end-to-end area, analyses were initially conducted to determine satellite control, resources, manufacturing, propellant requirements, and space environmental effects. An additional subtask, Laser Environmental Impact Study, was added in November 1978.

The satellite control analysis evaluated the satellite and ground receiver operations to determine probable operating sequences and interfaces. Since most of the subsystems detailed operating procedures and timeline data was yet to be determined the study was limited to the identification of major operating sequences and the definition of major operating functions. A major goal of the study was to identify and define any major issues that were, or could become, 'showstoppers'.

A resource analysis, which was conducted utilizing the Rockwell Point Design as a basis, is considered generally applicable to the Reference Concept, except for composites, which have been added to the analysis. Manufacturing implications relating to high usage items also have been identified.

The fleet of transportation vehicles which will support the satellite construction program includes growth shuttles, electric orbital transfer vehicles (EOTV), personnel orbital transfer vehicles (POTV), intra-orbit transfer vehicles (IOTV), and heavy lift launch vehicle (HLLV). Propellant requirements reflecting annual anticipated usage of these vehicles were determined and production implications identified.

The laser study was established to, primarily, determine the impact of the laser beam upon the intervening atmosphere, as well as the inverse effects. To accomplish this objective within the available funds it was specified that the selected laser system would be limited to existing gas laser devices. Included in the study was a requirement to prepare a preliminary definition/description of the ground receptor and sufficient data to permit a first order comparison between the laser transitter and its microwave equivalent as described for the Rockwell reference concept.

The significant space environments (nuclear radiation, micrometeoroids, hot and cold plasma, etc.) and their effects on spacecraft components (materials, electronics, men) are summarized. While the size of an OTV reduces plasma effects (as compared to those for a smaller spacecraft) the opposite is true for micrometeoroids. Solar cell degradation (sensitive to the duration of the transfer orbit) and human EVA duration (sensitive to the altitude at LEO) were also considered. The purpose of these investigations was to more accurately define the design and operational limits imposed by the environments on an OTV. The results show that LEO altitudes $\lesssim$300 nmi and transfer orbit durations $\lesssim$6 months are preferrable.

2.0 RECTENNA CONSTRUCTABILITY

2.0 RECTENNA CONSTRUCTABILITY

2.1 RECTENNA SITE CHARACTERISTICS

2.1.1 SITE REQUIREMENTS

A rectenna site requires approximately 35,000 acres. Figure 2.1-1 shows a layout of a typical site. The inner ellipse containing the rectenna panels, 10×13 km, is about 25,200 acres or 72% of the total acreage. The area surrounding the inner ellipse is utilized for maintenance facilities, access roads, converter stations and the two peripheral rows of towers which support the 40 kV dc and 500 kV ac cables. The outer perimeter of the area is fenced for security reasons. The towers which support the 500 kV ac cables are constructed of steel girders footed in concrete and are approximately 230 ft (70 meters) high. The inner towers are each comprised of four tapered steel columns 60 feet (18.3 meters) tall. Fifty-four of the larger towers and 401 of the smaller towers are required, the latter figure translating into 1604 tubular members because of the configuration.

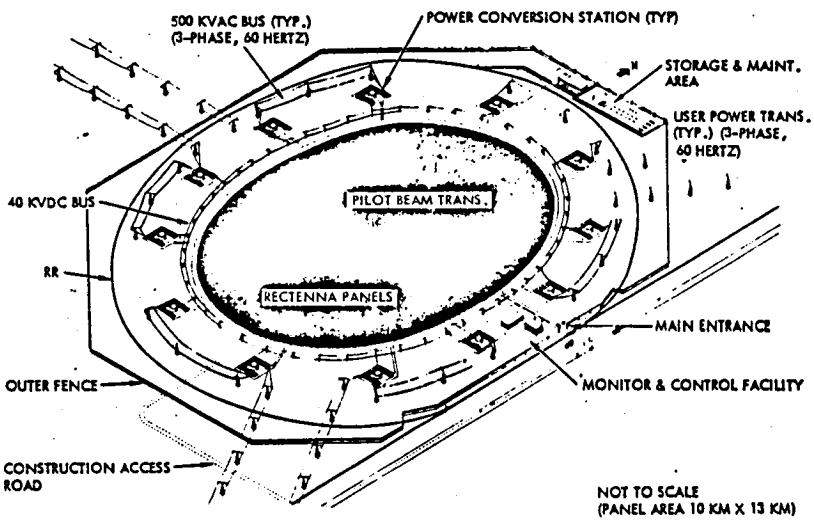

Figure 2.1-1. Operational Ground Receiving Facility (Rectenna) - Typical

2.1.2 PANEL INSTALLATION

Figure 2.1-2 shows a panel in the installed position. The panels are 9.33×14.69 meters and are attached to continuous concrete footings at eight points as shown. A trade-off which considered eight individual footings versus continuous footings was made. A maximum wind force of 90 mph was

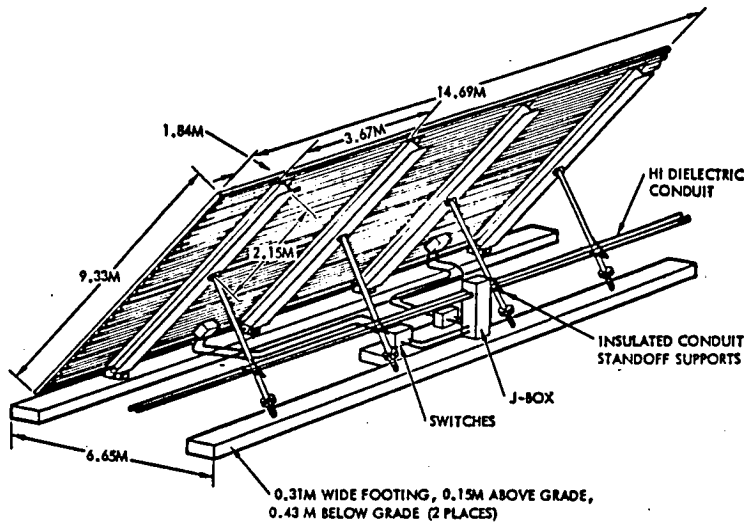

Figure 2.1-2. Panel Installation

assumed. It was determined that the amount of concrete required for either approach was essentially the same but that the continuous footing concept was easier to install.

Threaded inserts are placed in the concrete during the pouring process and provide the means for mounting the panel attach fittings which are capable of longitudinaland laternal adjustment. Screw jacks are installed at each of the four rear attach points to allow for panel adjustment and alignment.

Details of panel construction are shown in Figure 2.1-3. Four standard size eight inch I beams, to which the attach fittings are secured, are spaced in the lateral (14.69 meters) direction. Galvanized steel hat sections (thin sheet, 0.020 inches thickness) of the dimensions as shown are mounted in the longitudinal direction (14.69 meters) and provide the mounting for the substrate containing the electronic components. The substrate (with components) is delivered to the on-site assembly plant, in strips of 9.33×0.74 meters. The panels are supported in the inclined position by tubular steel members which provide an angle from the horizontal of 40° for this example, (latitude = 34°N). Each panel weighs 2080 kg, of which approximately 85% is steel.

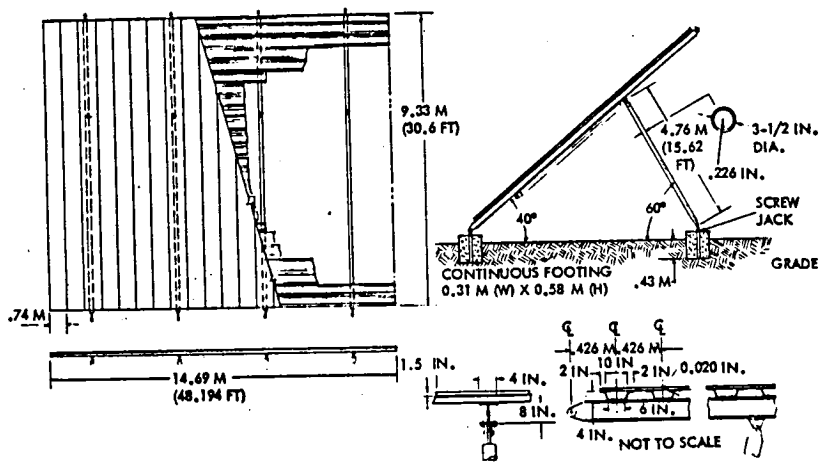

Figure 2.1-3. Rectenna Array Support Structure

2.2 RECTENNA CONSTRUCTION SEQUENCE

2.2.1 SEQUENCE OF OPERATIONS

The sequence of the nine primary operations attendant to construction of a rectenna site are shown in Figure 2.2-1. It is assumed that land acquisition has been completed and that the environmental impact report and other necessary permits have been approved.

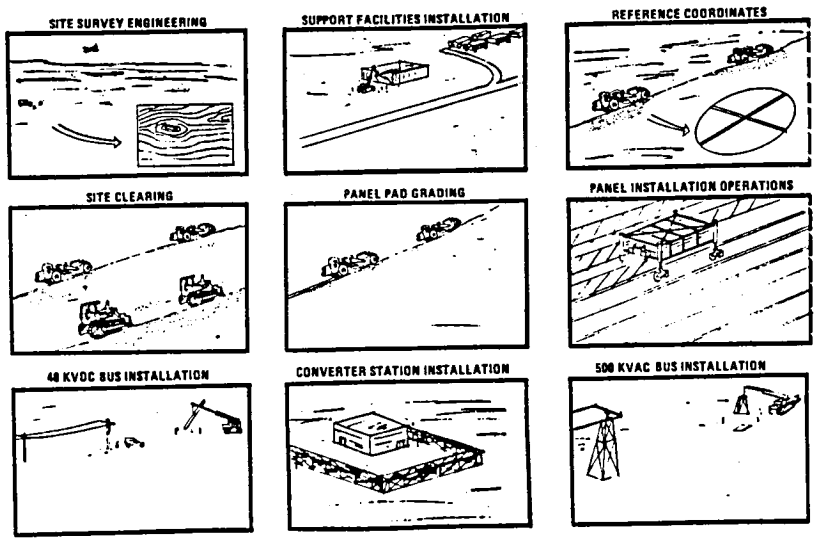

Figure 2.2-1. Rectenna Construction Sequence

Initially, site survey and engineering activities must take place. When these are completed, the first step is to install utilities (water, power, etc.), access roads and railroad spurs. Facilities must then be provided for equipment maintenance and servicing, logistics (material receiving and distribution), concrete production, panel assembly, crew support, and an operations center which coordinates all site construction activity.

Upon completion of support facilities installation, reference coordinates for the clearing and grading of the 10×13 km ellipse must be established. This operation is followed by site clearing and panel pad grading.

The panel installation operations, the next series of events in the overall sequence, entail establishment of string lines (although use of lasers with multiple reflectors is a viable alternative), footing excavation, concrete pouring, panel fabrication and installation, and electrical hookup of the panels.

Two periphery cable runs around the perimeter of the panel ellipse must be installed. The 40 kV dc row will be located approximately 50 meters outside the ellipse; the 500 kV ac lines about 500 meters outside. These two rows of cabling will be separated by converter stations. Although installation of this equipment is shown as the last steps in the complete operation, installation of the towers and stations could be started earlier on a noninterference basis with panel installation. Table 2.2-1 summarizes the operational activities required for construction of the rectenna.

Table 2.2-1. Rectenna Construction Sequence

SITE SURVEY & ENGINEERING
SUPPORT FACILITIES INSTALLATION
UTILITIES, ROAD & RAIL SPUR
EQUIPMENT MAINTENANCE & SERVICING
MATERIALS DISTRIBUTION CENTER
CONCRETE PLANT
PANEL ASSY FACTORY
CONSTRUCTION CONTROL CENTER
CREW SUPPORT
REFERENCE COORDINATES CLEARING & GRADING
SITE CLEARING
PANEL PAD GRADING
PANEL INSTALLATION OPERATIONS
SET STRING LINES
EXCAVATE FOR FOOTINGS
POUR FOOTINGS & SET & ALIGN ATTACH FITTINGS
FABRICATE & TRANSPORT PANELS
INSTALL & ALIGN PANELS
DISTRIBUTE & INSTALL SWITCHES & FEEDERS
ELECTRICAL CONNECT & C/O PANELS, SWITCHES & FEEDERS
40 KVDC BUS INSTALLATION
DISTRIBUTE AND INSTALL POLES, SWITCHES & BUSES
ELECTRICAL CONNECT & C/O POLES, SWITCHES & BUSES
CONVERTER STATION INSTALLATION
500 KVAC BUS INSTALLATION

2.2.2 CONSTRUCTION SCHEDULE

The time allocated for construction of a rectenna site, exclusive of land acquisition and permits, is between 14 and 15 months. Figure 2.2-2 shows a schedule for the major activities which have been discussed in the preceding section. The equipment and crew requirements for each task which are developed in subsequent sections are predicated in this schedule. It is noted that approximately 270 days each are allocated for the major activities. The schedule is based on a site location featuring relatively benign characteristics relative to timber and slope. Selection of a site featuring more extreme slopes or extensive timber would affect either the timeline or the manpower and equipment requirements.

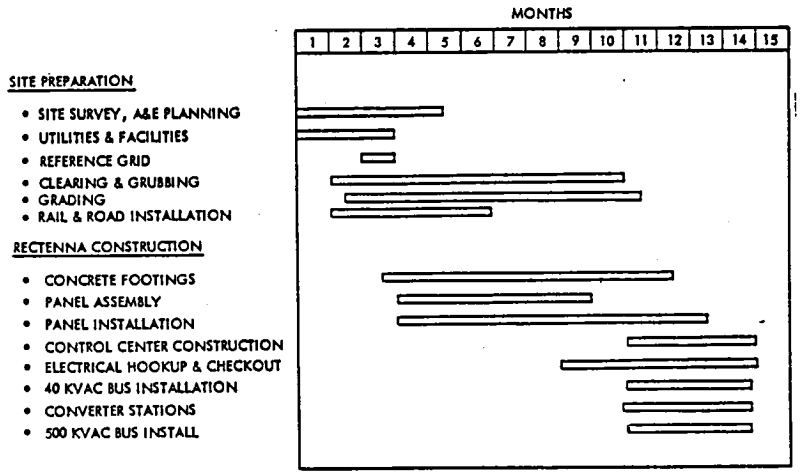

Figure 2.2-2. Rectenna Site Construction Schedule

2.3 CONSTRUCTION OPERATIONS

2.3.1 INDUSTRY CONTACTS

A number of industry contacts were made to acquire more insight into procedures involved in clearing large land areas and in large scale equipment installation. These contacts, summarized in Table 2.3-1, included organizations which produce heavy, earth moving equipment, pour concrete for freeways, supervise construction of installations such as the Sandia Thermal Test Facility, or which are involved in other activities having a bearing on the SPS program. The data derived from these contacts are reflected in the types of equipment, equipment capabilities, and supporting manpower described in subsequent sections.

2.3.2 SUPPORT FACILITIES

Approximately three months have been allocated for installation of the facilities required to support construction of the rectenna panel farm.

Table 2.3-1. Industry Contacts

ORGANIZATION	PURPOSE
• SME (SOCIETY OF MANUFACTURING) ENGINEERS)	OBTAIN TECHNICAL DATA ON ROBOTICALS AND TECHNOLOGY STATUS
• RIVERSIDE CEMENT CO.	RECTENNA CEMENT/CONCRETE REQUIREMENTS AND PROCESSES
• MODERN ALLOYS, INC.	METHODS & EQUIPMENT FOR CONTINUOUS PLACEMENT OF RECTENNA PANEL CONCRETE FOOTINGS
• SANDIA-SOLAR THERMAL	COMPARISON OF STTF CONSTRUCTION/HANDLING APPROACH WITH SPS RECTENNA REQ'TS
• TOWNSEND & BOTTUM, CONST. MGRS, 10 MW SOLAR PLANT IN BARSTOW, CA	SITE PREPARATION AND CONSTRUCTION OPERATIONS
• AMERICAN BRIDGE - A DIVISION OF UNITED STATES STEEL	STEEL REQ'TS & CONSTRUCTION APPROACH FOR INSTALLATION OF RECTENNA PANELS
• ALPHA-BETA DISTRIBUTION CENTER	ANALYSIS OF MATERIALS HANDLING SYSTEMS
• CATAPILLAR	EARTH MOVING & GRADING EQUIPMENT
• INTERNATIONAL HARVESTER	EARTH MOVING & GRADING EQUIPMENT
• SOUTHERN CALIFORNIA EDISON	DC/AC POWER DISTRIBUTION LINES/TOWERS

Initially provisions must be made for availability of utilities, primarily water and electrical power. Existing roads and railroads must be supplemented by access roads and railroad spurs to provide immediate access to selected portions of the overall site.

Because of the large concrete requirements, it has been determined that the most practical method for satisfying these requirements is to establish a concrete mixing facility on the site. This facility would require some 25 acres which would provide space for the concrete factory, a concrete truck loading area with multiple loading hoppers, and a storage area for the concrete ingredients. This latter area would be equipped with largely automated conveyor systems which would transport the material to the mixing facility. This procedure and supporting equipment is inherent in modern large concrete producing facilities.

Since the rectenna panels are too large for delivery in the assembled configuration, a panel assembly facility also must be provided. Details of a facility concept are contained in a subsequent section.

In addition to these specific facilities, provisions must be made for maintaining the extensive rolling stock inventory and for receiving and storing the large amounts of material which will be required. Figure 2.3-1 shows a typical site layout with those facilities which must be installed to support the construction of the rectenna panel farm and peripheral electrical feeder installation.

2.3.3 CLEARING AND LEVELING OPERATIONS

Figure 2.3-2 is a representation of activities incident to site preparation, and include bulldozing, grading, and dirt removal. The equipment

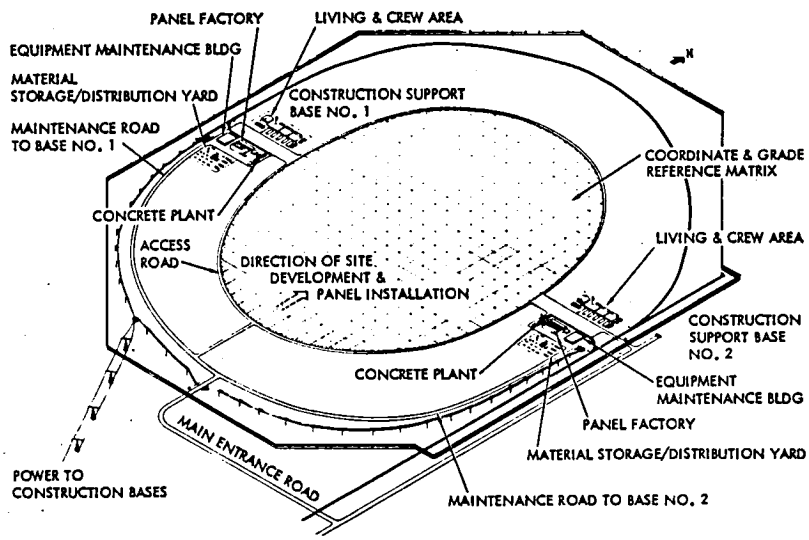

Figure 2.3-1. Support Facilities

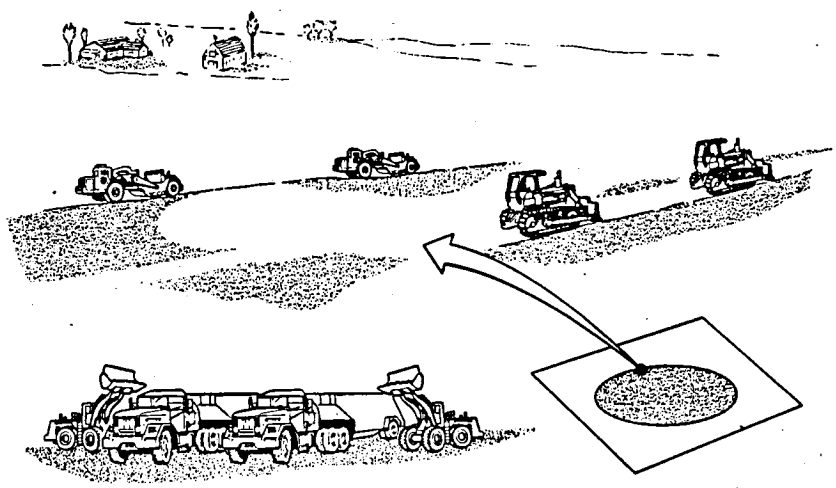

Figure 2.3-2. Clearing and Leveling Operations

pictured is based on current inventories of large, earth moving equipment available on today's market.

The clearing and leveling operations will occur at a number of locations within the panel farm perimeter. These operations consist of tree removal (if required), grading and leveling the terrain to acceptable slope angles, and removing excess dirt. Sixteen areas of the ellipse would be cleared and leveled simultaneously.

Table 2.3-2 summarizes the equipment and crew size required to complete the clearing and leveling operations in 9 months. Based on information obtained from industry sources, a 13 man crew equipped as indicated in the table can clear 8 acres per day. This factor was used to project the total requirements. It is noted that this operation has been restricted to one daily shift, or essentially daylight hours.

Table 2.3-2. Clearing and Leveling

1 SHIFT OPERATION		
1:30 MAX AVG. GRADE		
NON-FORRESTED LAND		
9-MONTH SCHEDULE		
35000 ACRES/SITE		
130 ACRES/DAY		
CREW REQUIREMENTS 8 ACRES/DAY/13 MAN CREW		
CREW COMPOSITION:	4	ROAD GRADERS
	3	BULL DOZERS
	3	DUMP TRUCKS
	2	CRANES
	1	BACK HOE
	13	OPERATORS
16 CREWS REQ'D	208	OPERATORS
SUPPORT PERSONNEL	72	15% MAINT., 10% SERVICING, 10% SUPR.
TOTAL ON SITE CREW	280	
3 CREWS/ROW, 5 + ROWS/DAY		
MAJ. EQUIP'T REQUIREMENTS (FOR 16 CREWS + 5% STANDBY)		
	67	ROAD GRADERS
	50	BULL DOZERS
	50	DUMP TRUCKS
	34	CRANES
	17	BACK HOES

2.3.4 FOOTING EXCAVATIONS

Conventional trenchers are utilized to excavate the 0.31×0.43 meter trenches which will be filled with concrete to form the panel footings. Figure 2.3-3 shows a typical operation with two sets of trenchers in operation. Each set of trenchers excavates the front and rear trench simultaneously and feeds the removed dirt into trucks which are stationed between the trenchers and which move at the same pace. When the truck is filled, it proceeds to the dumping area and another truck moves into position.

Approximately 17×10^6 meters of trench must be excavated in 278 days. An excavation rate of 90 meters per hour per trencher has been established as a figure representative of the capabilities of current equipment. At this excavation rate, 38 trenchers and the dump trucks will be required. A round trip time of 1 hour was assumed for the dump trucks. These requirements are predicted on a 20 hour day, 7 days a week.

Personnel requirements for this operation include trencher and truck operations, maintenance crews, and supervision, totaling 324 men for 4 shifts (3 shifts per day, 7 days per week, 2 days off per shift week). Table 2.3-3 summarizes both equipment and crew requirements.

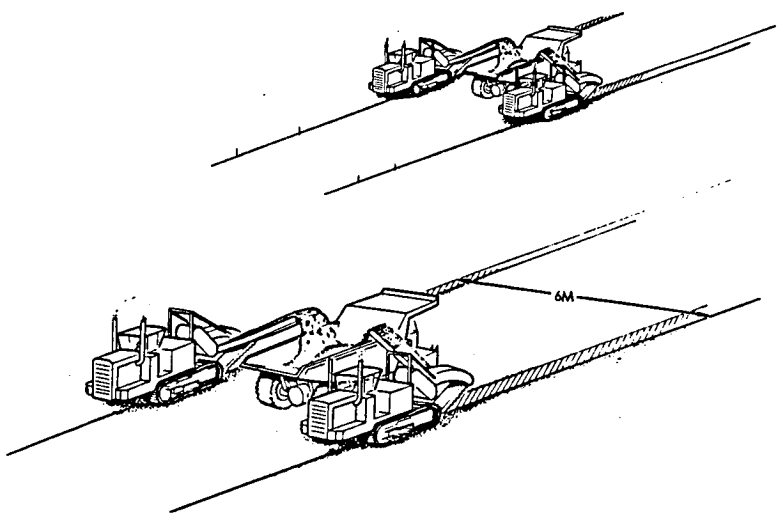

Figure 2.3-3. Footing Excavation

Table 2.3-3. Footing Installation (Trenching)

3-SHIFT OPERATION, 20 HRS/DAY
ROWS LEVEL AND GUIDELINES ESTABLISHED
9 MONTH SCHEDULE
17 x 10^6 M OF TRENCHES (8.5 x 10 M OF DOUBLE FOOTINGS)
3140 M/HR OF TRENCH
.31 M x .31 M TRENCH SECTION (≈0.1 M^3 /M LENGTH
302 M^3/DAY EXCAVATION
18 EQUIPMENT UNITS OF 2 TRENCHERS (1 FRONT FOOTING, 1 REAR FOOTING) + 1 DUMP TRUCK
EQUIPMENT REQUIREMENTS INCL. 5% STANDBY
38 TRENCHERS (≈ 90 LIN. M/HR/8.5 M^3/HR EA. MACHINE)
26 DUMP TRUCKS (52 M^3 CAPACITY, 1 HR R.T. DUMP TIME)
CREW REQUIREMENTS
38 TRENCHER OPERATORS
26 TRUCK OPERATORS
64 OPERATORS
7 SUPERVISION 10%
10 SERVICING/MAINTENANCE 15%
81 TOTAL/SHIFT
324 TOTAL/4 SHIFTS

2.3.5 CONCRETE INSTALLATION

Concrete formers such as are used in freeway or road curb installation are utilized to pour the concrete in the trenches. Figure 2.3-4 shows a former in operation. The formers, fed by concrete trucks, extrude a shaped ribbon at rates of up to 6 meters per minute, including the 0.15 meter extension above ground level. No forms are required. The concrete is poured into a hopper as shown, where it is transported upward by an auger to a second hopper which feeds the mules. Within the mules the concrete is hydraulically vibrated to remove air pockets and consolidate the concrete into a homogeneous

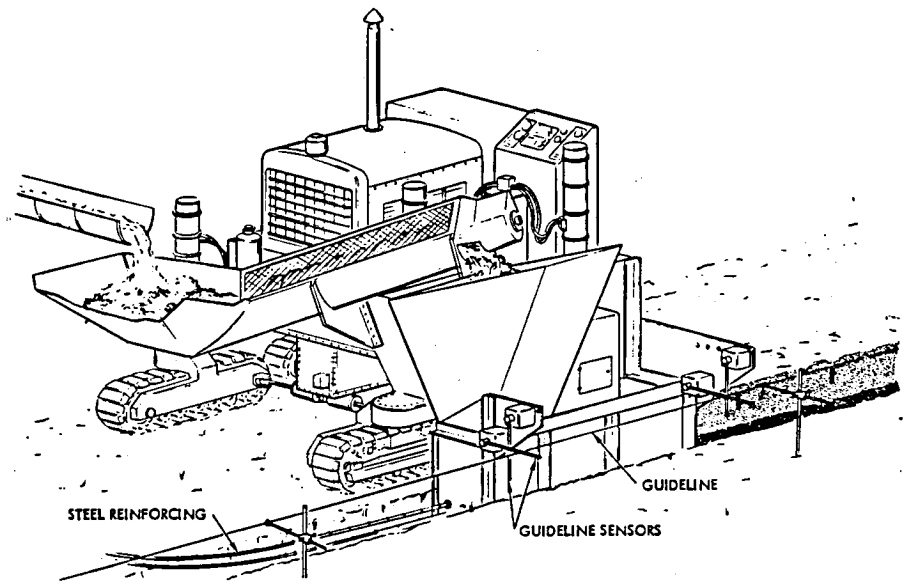

Figure 2.3-4. Concrete Installation

solid mass before extrusion. Reinforcing steel bars are fed into the mule and inserted into the concrete during the extrusion process. Additionally, the attach points (e.g., threaded inserts) for the panel attach fittings are inserted into the concrete prior to extrusion. Guideline sensors are provided as shown so that the rig can accurately follow a line or wire, although laser control is a viable alternative.

Ten of these machines, including one spare, are required to install concrete in the 17×10^6 meters of trenches. Two days have been allocated for concrete curing after installation. Table 2.3-4 summarizes equipment and manpower requirements for completing the concrete installation in 270 days on a 3 shift 20 hour a day, 7 days a week basis.

After the concrete has cured, 8 attach fittings per panel, or a total of 4.6×10^6 fittings must be secured to the attach inserts imbeded in the concrete. The equipment and crew required to deliver and install these attach fittings are shown in the lower portion of Table 2.3-4.

2.3.6 PANEL FABRICATION AND INSTALLATION

Because of the panel dimensions, shipping completed panels from an off-site manufacturing facility to the rectenna site is not practical. The alternatives are to ship the prefabricated materials to the rectenna site and assemble the panels at either a centralized factory or on a mobile fabricator. The former concept has the advantages of centralized material receiving and a protected environment, but requires delivery of completed panels to the point of installation. The mobile concept requires delivery of materials to many locations, which complicates logistics, and provides no environmental protection during the assembly process. However, double handling of the finished panels is not required. The centralized facility was selected for this study. A concept for

Table 2.3-4. Footing Installation (Concrete & Attach Fittings)

CONCRETE POURING

- REQUIREMENT
  - 17×10^6 M OF FOOTING
  - 4×10^6 CU. YDS TOTAL
  - 6.8 CU. YDS/PANEL, 14,620 CU. YDS/DAY
  - 139×10^6 KG REINFORCING STEEL, 0.5×10^6 KG/DAY
- EQUIPMENT
  - 190 CONCRETE DELIVERY TRUCKS @ 10 CU. YDS/TRUCK
  - 10 CONCRETE FORMING MACHINES, 6 M/MIN
- CREW SIZE
  - 289 PER SHIFT x 4 SHIFTS + SUPPORT = 1,156 TOTAL

PANEL ATTACH FITTING INSTALLATION AND ALIGNMENT

- REQUIREMENT
  - 4.6×10^6 ATTACH FITTINGS, 17,200 PER DAY
- EQUIPMENT
  - 40 TRACTOR-TRAILERS
- CREW REQUIREMENT
  - 80 PER SHIFT INCL. SUPPORT x 4 SHIFTS = 320 TOTAL

such a facility is shown in Figure 2.3-5. The factory has multiple assembly lines, each line consisting of a materials feed station, panel assembly, electrical hookup of the 14.69×0.74 meter substrates containing the electronics and finally, checkout. It was assumed that one line using automated procedures could assemble and checkout a panel in 40 minutes. On this basis, seventy-two assembly lines operating 20 hours per day, seven days a week are required to produce 580,500 panels in the allocated 270 days. Eight additional assembly lines have been specified as spares.

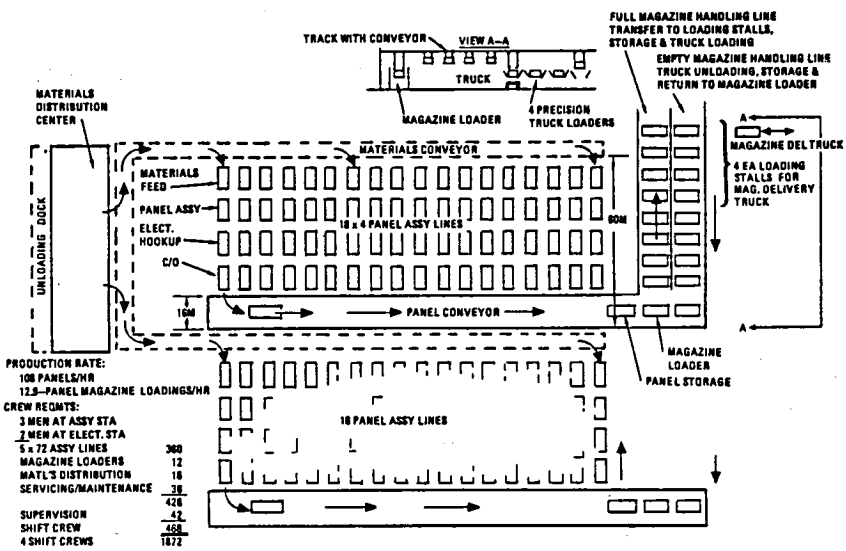

Figure 2.3-5. Central Panel Factory

After the panels have been checked, they are placed on an overhead conveying system and transported to loading stalls, where they are assembled into 9-panel magazines and loaded on specially designed trucks for delivery to the point of installation. Production rates and crew requirements are summarized in the lower left of the figure.

Specialized equipment is required to deliver the panels from the factory to the installation point and to install them because of their large dimensions. Use of cranes for lifting the panels from a delivery vehicle and lowering them to the attach position was considered but discarded because of potential difficulties involving wind loads on a suspended object with a large surface area. After consultation with industry sources (see Section 2.3.1), a concept for a specialized machine was developed (Figure 2.3-6). The machine can carry up to nine panels. The front and rear wheel pairs are each steerable as a unit and have provisions for height adjustment. Although dual wheels are shown at each corner, the bearing load could result in substitution of caterpillar track units. Power packages for vehicle movement and hydraulic power are located on either side of the central stations located at both ends of the vehicle. The panels (not shown) can be translated laterally and longitudinally for final positioning before attachment to the footings.

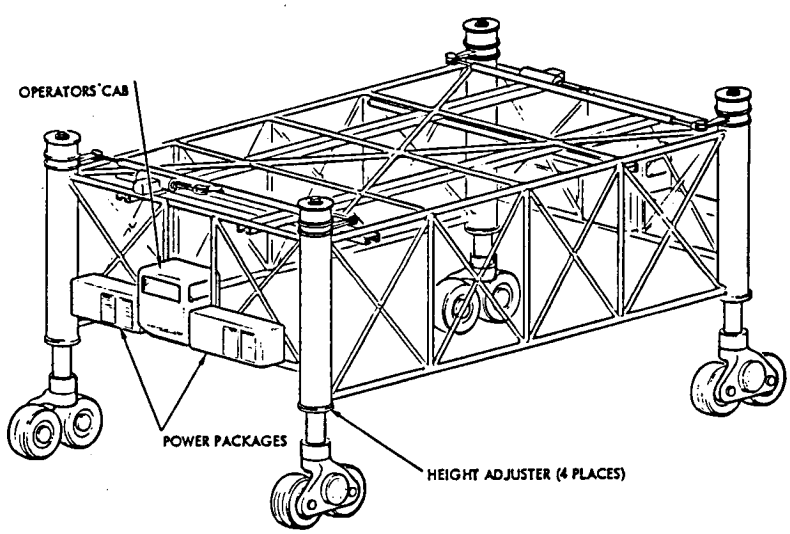

Figure 2.3-6. Panel Installation Machine

Figure 2.3-7 shows a concept for a panel magazine delivery truck which loads magazines of up to 9 panels each at the panel factory (Figure 2.3-5) and transports them to the panel installation site. There they are transferred to the panel installation machine. The delivery truck can be driven directly beneath the installation machine in order to transfer the panels. The panels are secured in the magazines by means of fixtures mounted in a vertical assembly which attach to the panel I beams as shown in Figure 2.3-8. When the truck is positioned beneath the installer machine, the vertical fixture assembly holding the panels is secured to the hoist as shown in the middle illustration of the figure and elevated sufficiently to permit departure by the truck. At the

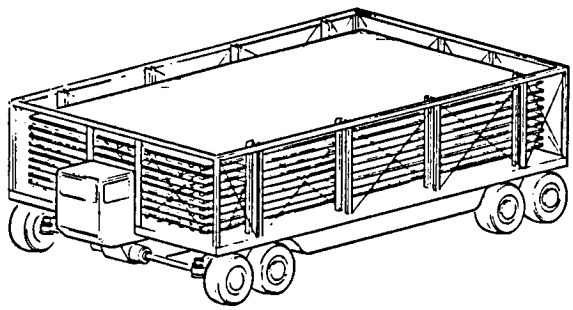

Figure 2.3-7. Magazine Delivery Truck

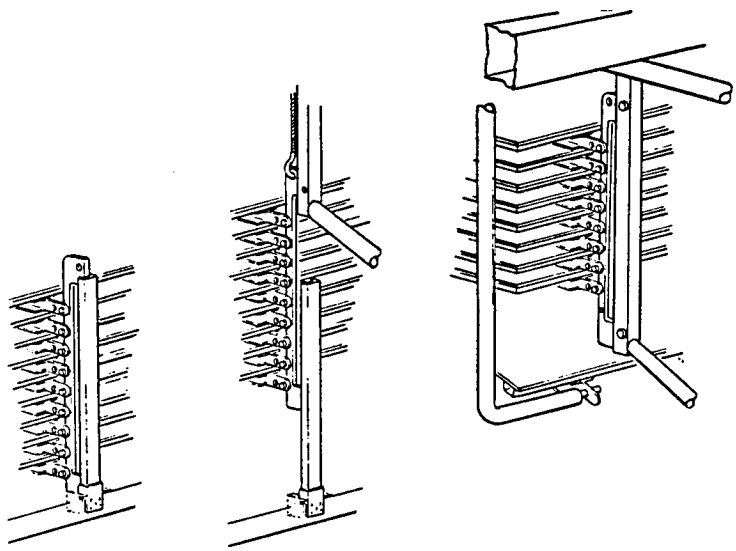

Figure 2.3-8. Panel Magazine Transfer

right of the figure are shown movable L-shaped arms which attach to the bottom panel retention fixture and lower it to the proper position and angle for attachment to the footings. The retention fixtures of the vertical fixture assembly are uncoupled when the panel has been secured to the movable L-shaped arms.

Figure 2.3-9 shows the sequence of events described above. Commencing at the upper left, the delivery truck approaches the installer machine and then is positioned for magazine transfer. The installer machine is then elevated (lower left), the magazine transferred and hoisted clear, and the truck departs. In the lower right of the figure, the bottom panel has been lowered into position for attachment. Figure 2.3-10 shows panel installation operations. The installer machine is straddling the two rows of footings. A panel has just been installed and the machine advanced into position for installing the next panel.

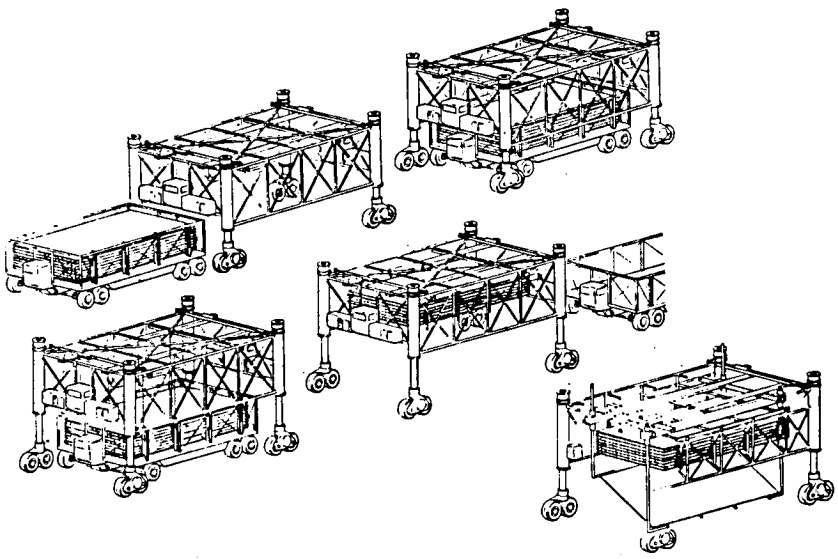

Figure 2.3-9. Panel Loading Sequence

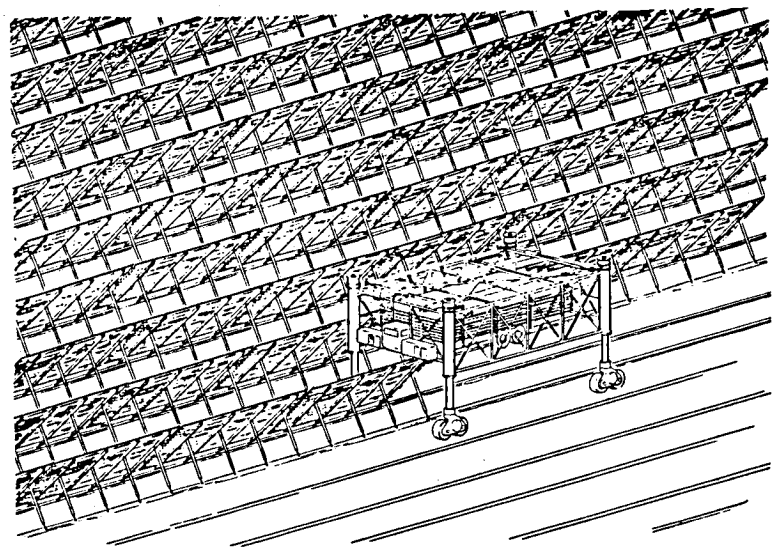

Figure 2.3-10. Panel Installation Operations

The equipment and personnel requirements to assemble and install the panels in a 9 month period are summarized in Table 2.3-5. The panel assembly requirements were discussed previously. An installation rate of 20 minutes per panel has been established. On this basis, 36 panel installation machines with 4 spares are required. Twelve panel delivery trucks (plus 2 spares) with a a round trip time of one hour maintain the panel flow to the installers, utilizing a total of 66 magazines. Approximately 900 men (4 shifts) are required to operate the vehicles, attach the panels, and conduct checkout operations. This,

Table 2.3-5. Panel Assembly and Installation

EQUIPMENT

ONE PANEL ASSY, FACTORY
72 ASSY LINES, 40 MIN/PANEL ASSY TIME, 108 PANELS/HR
8 ASSY LINES FOR SERVICING/MAINTENANCE DOWNTIME

36 PANEL INSTALLATION MACHINES, ON LINE (20 MIN/PANEL, 60 PANELS/20-HR DAY EA.)
4 PANEL INSTALLATION MACHINES FOR SERVICING/MAINTENANCE DOWNTIME
40 PANEL INSTALLATION MACHINES, TOTAL

12 MAGAZINE DELIVERY TRUCKS ON LINE (9 PANELS/DELIVERY, 108 PANELS/HR, 1-HR R.T. DELIVERY TIME)

2 MAGAZINE DELIVERY TRUCKS FOR SERVICING/MAINTENANCE DOWNTIME

14 MAGAZINE DELIVERY TRUCKS, TOTAL

66 9-PANEL MAGAZINES (36 ON INSTALLERS, 12 ON TRUCKS, 12 ON LOADING DOCK @ FACTORY, 6 SPARES)

CREW SIZE

(1872) PANEL ASSY FACTORY CREW

216	ASSY
144	ELECT. & C/O
12	LOAD
372	PANEL ASSY & C/O
18	MATERIALS DISTRIB.
36	SERV./MAINT.
426	
42	SUPERVISION
468	EA. SHIFT
1872	FOUR SHIFTS

(60) MAGAZINE DELIVERY TRUCK CREW

12	DRIVERS
2	SERV./MAINT.
1	SUPERVISION
15	EA. SHIFT
60	FOUR SHIFTS

(840) PANEL INSTALLATION CREW

720 · RIGGERS & MACHINE OPERATORS (4 RIGGERS, 1 MACHINE OPERATOR EA. CREW, 36 CREWS, 180 CREW MEMBERS/SHIFT · 4-SHIFT CREWS)

20 SERVICING/MAINTENANCE OF MACHINES

100 SUPERVISION

when added to the assembly factory crew of 1872, results in a total of 2772 men required to assemble, install and check the panels.

2.3.7 ELECTRICAL HOOKUP

A typical power transmission schematic for a portion of the panel farm is shown in Figure 2.3-11. Each row of panels is connected through switchgears to the inner periphery 40 kV dc buses. These buses, in turn, are connected to the outer periphery 500 kV ac buses through a series of twelve converter stations. There are 580,500 individual panels arranged in 1088 rows.

A total of 329,000 switchgears, 10×10^6 meters of feeder cables, plus conduit, miscellaneous junction boxes and other electrical components must be installed in the panel farm following completion of panel installation. As shown in Figure 2.3-12, the electrical components and conduits are off-loaded at the rear of each panel by flatbed trucks equipped with hoists. The feeder cable is reeled out by other, specially equipped trucks. The delivery operation is followed by electrical installation crews in conventional electrical installation trucks (not shown) who secure the switchgears, junction boxes and conduits, and complete the electrical hookup. As summarized in Table 2.3-6, 229 vehicles, including spares, are required.

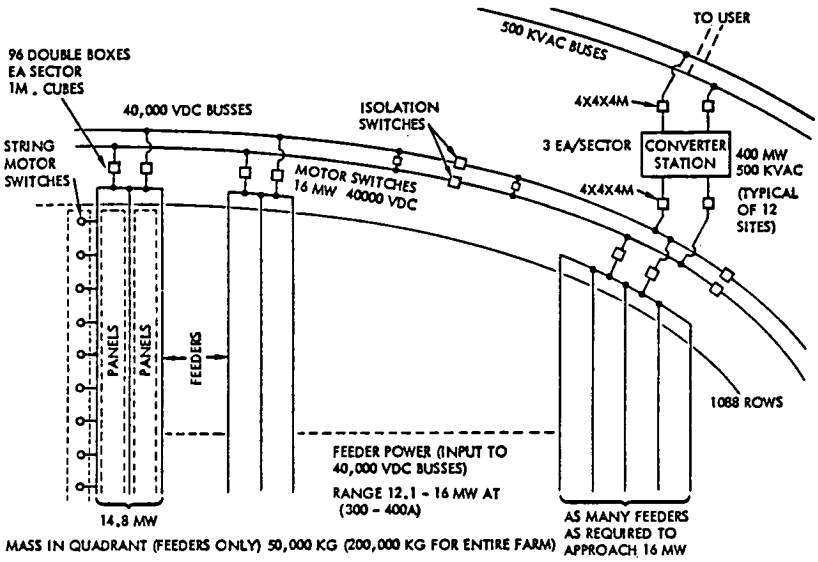

Figure 2.3-11. Rectenna Schematic Block Diagram - Preliminary

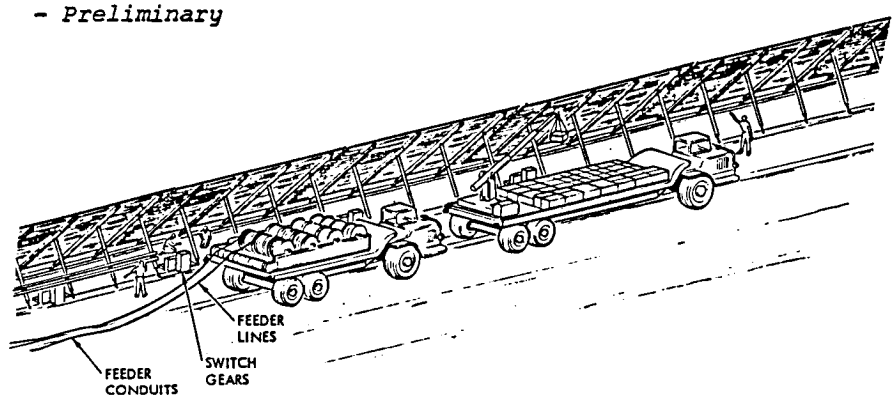

Figure 2.3-12. Electrical Installation and Hookup

Table 2.3-6. Electrical Hookup

REQUIREMENT - 329,000 SWITCH GEARS, 10^7 M FEEDER CABLES, MISC. JUNCTION BOXES, ETC.	
EQUIPMENT	
4	SWITCH & WIRE DELIVERY TRACTOR-TRAILERS W/CRANES
215	ELECTRICAL INSTALLATION CREW TRUCKS
10	FOR SERV./MAINT. DOWNTIME
229	TOTAL
CREW REQUIREMENTS	
(76)	SWITCH TRUCKS (1 DRIVER, 2 SW. UNLOADERS, 1 CABLE DISPENSER MONITOR 16 EA SHIFT)
64	4 SHIFTS
6	SUPERVISION
6	LOGISTICS SUPPORT
(4120)	PANEL ELECT. INSTALLATION
3440	ELECT. INSTALLERS (4 MEN/CREW, 2 HR CREWTIME/PANEL • 860 EA SHIFT, 4 SHIFTS
340	SUPERVISION
120	TRUCK & EQUIPMENT SERVICING/MAINT
120	LOGISTICS SUPPORT
SHIFT SIZE: EQUIP. 16	TOTAL • 76
INST. 860	4120
876	4196

The crew requirements (4 shifts) are the highest of any individual rectenna construction operation. Utility companies have estimated that approximately 8 manhours will be required to complete the electrical installation on one panel. An individual crew size of 4 men requiring 2 hours per panel has been established and 215 crews per shift will be required to complete the operation on schedule. This, when combined with drivers, logistics support, maintenance crews, and supervision, results in a four shift total of 4,196 men.

This is the last operation required for completion of the panel farm.

2.3.8 HIGH TENSION CABLE SUPPORTS

The periphery of the panel farm is ringed by 40 kV dc and 500 kV ac buses mounted on towers. The 40 kV dc bus is located approximately 50 meters outside the ellipse containing the panels; the 500 kV ac bus about 450 meters further out.

Based on Southern California Edison data, the 40 kV dc buses would be suspended on a series of hollow tapered steel poles. Four poles, connected by a crossbeam upon which the insulators are mounted, constitute one suspension unit. Each pole measures 0.46 meters diameter at the tip, 1.1 meters diameter at the base, and has a wall thickness of 0.013 meters. The poles are inserted into a 1.22 meter circular hole to a depth of 3 meters and surrounded by concrete. The spacing between pole units is about 91 meters; this requires 401 installations or a total of 1604 poles.

The 500 kV ac towers are similar to existing high tension towers, measuring 12.9 meters at the base with a height of about 70 meters above ground. The towers are spaced every 457 meters; since they do not completely rim the perimeter, only 54 towers are required, including 18 "deadend" towers.

The deadend towers are mounted on four concrete pilings 1.83 meters in diameter and extending 10.7 meters into the ground. The remainder of the towers require less footing and are secured to four concrete pilings measuring 1.1 meters in diameter and 6.1 meters deep.

Both the 40 kV dc and the 500 kV ac towers will be fabricated off-site, the latter in sections. Installation of the towers can commence as soon as the land is sufficiently cleared but on a noninterference basis with panel installation. Several 5-6 man crews can complete the installation within the overall schedule, working daylight hours only, seven days a week.

Table 2.3-7 summarizes the steel and concrete required for the towers.

Table 2.3-7. Tower Material Requirements

STEEL	MASS (kg)
40 kV dc TOWERS	8.2×10^6
500 kV ac TOWERS	3.68×10^6
	11.88×10^6
CONCRETE	
40 kV dc TOWERS	4.59×10^6
500 kV ac TOWERS	6.66×10^6
	11.25×10^6

2.4 SUMMARY

Total manpower requirement estimates for constructing a rectenna site are tabulated in Table 2.4-1. As indicated, except for the site preparation, the totals reflect 4 shifts. The single largest crew size is for electrical installation and hookup, followed by panel assembly and concrete pouring. Manpower for installation of the perimeter high-tension poles, estimated at twenty or less, is not included in the table.

Table 2.4-1. Construction Crew Requirements (4 Shifts)

	SHIFT SIZE	TOTAL	
SITE PREPARATION (SINGLE SHIFT)	280	280	
PANEL ASSEMBLY FACILITY	468	1872	
CONCRETE PRODUCTION	55	220	
FOOTING EXCAVATION	81	324	
CONCRETE POURING	289	1156	4 SHIFT TOTAL
PANEL ATTACH FITTINGS	80	320	
PANEL INSTALLATION	225	900	
ELEC. INS. & HOOKUP	1050	4200	
TOTAL	2528	9272	

NOTE: 3 8-HR SHIFTS/DAY, 7 DAYS PER WEEK, 2 DAYS OFF PER SHIFT/WEEK, 4 SHIFTS TOTAL

A summary of material and equipment is shown in Table 2.4-2. The steel and concrete for high tension towers, not included, is contained in Table 2.3-7. It is noted that the panel mass is composed of approximately 85% steel, the remainder being substrate and electronics. The manpower and equipment estimates reflect a relatively level site with a minimum of timber removal.

Table 2.4-2. Construction Summary

● SCHEDULE: 15 MONTHS		
RECTENNA MASS -	PANELS	1207×10^6 kg
	CONCRETE	7176
	FEEDERS	1
	REINFORCE STEEL	51
		8435×10^6 kg
● CREW		
	SHIFT SIZE	2474
	TOTAL CREW FOR 24 HR/7DAY OPERATION	9272
● EQUIPMENT		
	SCRAPERS/GRADERS	67
	DUMP TRUCKS	50
	BULLDOZERS	50
	CRANES	34
	BACK HOES	17
	TRACTOR/TRAILER TRUCKS	48
	CONCRETE TRUCKS	190
	CONCRETE POURING RIGS	10
	PANEL INSTALLERS	40
	PANEL MAGAZINE TRUCKS	14
	ELECTRICAL INSTALLATION TRUCKS	229
	MISC. JEEPS, PICKUPS, ETC.	

2.4.1 KEY ISSUES

Five key issues which can affect rectenna constructabability have been identified.

- Site Selection - The characteristics of a proposed rectenna site can have significant impact on schedule, manpower and equipment requirements. Important factors in site selection include overall topography, drainage, type of soil, prevailing weather, and location relative to industry and transportation.

- Environmental Impact - Considerable advance planning will be required to assure that the environmental impact report and other necessary permits are prepared and submitted well ahead of planned construction go-ahead. In some instances, up to five years have been required for approval of these documents.

- Site Operational Control - A site operational control plan is vital to effective construction operations of this magnitude. The plan must provide for communications, disposition of incoming material, traffic control of the many vehicles involved, and a detailed operational sequence of events.

- Lightning Protection - Studies conducted at Rice University under contract to the George C. Marshall Space Flight Center indicate a high probability of multiple lightning strikes in an area the size of the panel farm. Lightning could result in both localized physical damage to panels and propagating damage to circuitry. The effects on rectenna reception of erecting a protecting rod on each panel have not been determined. The amount of copper required for grounding would be

significant for this type of approach. This overall area requires additional study relevant to effects and feasible preventive measures.

- Resource Availability - As indicated in Table 2.4-2, material, manpower and equipment requirements for construction of one rectenna site are considerable. Additional facilities, particularly for steel, may be required. The equipment requirements reflect, for the most part, vehicles which are produced currently; however, ample lead time for acquiring them in these numbers would be necessary. Sixty sites would be constructed in a 30 year period. While the equipment could be transferred to the next site and reused, the current postulated schedule would require that several sites be under construction at any one time.

Availability of manpower reflecting the required skills and in the required quantity constitutes a potential problem area, particularly in some areas, where the local labor market is inadequate.

2.4.2 SUMMARY AND CONCLUSIONS

- Existing construction equipment designs adequate for site construction excepting panel installation.
- Extensive manpower and equipment required to complete site in 15 months schedule.
- Variability in site characteristics can impact both schedule and crew/equipment requirements.
- Better definition of potential rectenna sites required.
- Considerable lead time necessary for environmental impact report and permit approvals.
- Availability of required materials is potential problem area.
- No major technology drivers for rectenna site construction.

2.4.3 RECOMMENDATIONS FOR FURTHER STUDY

- Determine rectenna resource requirements
- Update rectenna construction approach and panel fabrication.
- Implementation of lightning protection requirements.
- Define detailed construction sequences and operation routines.
- Integrate multi-rectenna site construction requirements.
- Iterate installed panel loads and footing concepts for potential reduction in concrete requirements.

3.0 PRECURSOR OPERATIONS

3.0 PRECURSOR OPERATIONS

3.1 OVERALL SCENARIO

The overall scenario leading to establishment of satellite construction support facilities and to satellite construction is shown in Figure 3.1-1. Initial operations entail use of the growth shuttle and the shuttle derived HLLV for transporting men and material to LEO for the precursor phase of the program. Subsequently, during the 30 year satellite construction phase, the HLLV will become the primary transportation element for delivering construction mass to LEO.

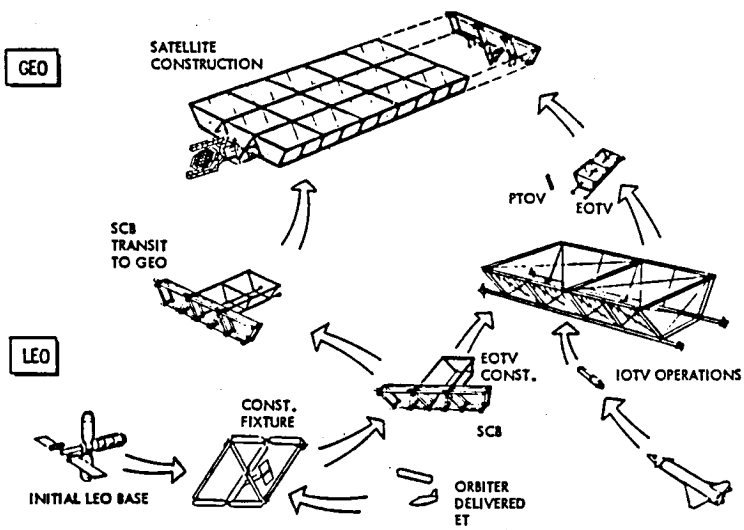

Figure 3.1-1. Overall Satellite Construction Scenario

The initial step in satellite precursor operations is establishment of a LEO base as shown in the lower left of the figure. Crew and power modules are transported to LEO by shuttle derivatives and assembled. When the base is fully operational, shuttle external tanks are delivered and mated to form construction fixtures for SCB construction. The figure shows a completed SCB. Since the more economical HLLV will not be available during this phase of the program and since overall plans specify an EOTV test vehicle, it os probable that only the center section of the SCB would be constructed initially. This trough would be used to fabricate the pilot plant EOTV with an end-mounted antenna. After proof of concept and SPS go-ahead, the remainder of the SCB would be completed, sufficient EOTV's constructed to support initial satellite construction operations, and the SCB then transferred to GEO, using one or more EOTV's for propulsion and attitude control. Upon reaching GEO, satellite construction would commence, with the logistics support as shown at the right of the figure. These operations are discussed in more detail in the following section.

3.2 SCB CONSTRUCTION OPERATIONS

3.2.1 SCB DESCRIPTION (REFERENCE SATELLITE CONFIGURATION)

The satellites are constructed in GEO, each satellite being constructed at its designated longitudinal location. All construction activities are supported by a single integrated construction base (SCB). The SCB supports construction of 2 satellites per year during the mature portion of the program. Upon completion of a satellite, the SCB is moved to the operational location of the next satellite for construction of that satellite.

The SCB (Figure 3.2-1), constructed of composites, consists of the construction fixture, construction equipment, and base support facilities. The construction fixture is in the form of three troughs, corresponding to the satellite configuration, which permits simultaneous construction of the three satellite troughs. Additional structural members are located in the middle trough and are used as fixtures for constructing the rotary joint, and supporting structure.

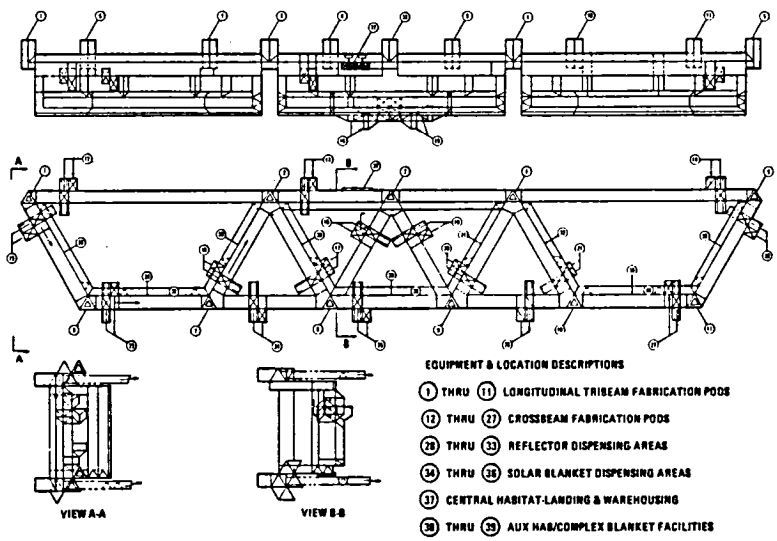

Figure 3.2-1. Satellite Construction Base (SCB)

The location of the major construction equipment item is identified in the figure. A total of twenty-seven 50-meter tribeam fabricators for both longerons and crossbeams are required. The solar blanket dispensers, (34), (35), and (36), are installed at the bottom of each trough, while the reflector dispensing areas, (28) through (33), are located on the inner side of each trough diagonal.

The central habitat, including docking and warehouse facilities, (37), are located on the top deck girder of the middle trough. Auxiliary habitats and facilities, (38) and (39), are installed at the bottom of each trough to reduce the time required for crew rotation at the end of each shift.

Figure 3.2-2 illustrates the SCB in perspective. Details of the installation equipment are contained in Section 4.0. Table 3.2-1 contains the SCB mass statement.

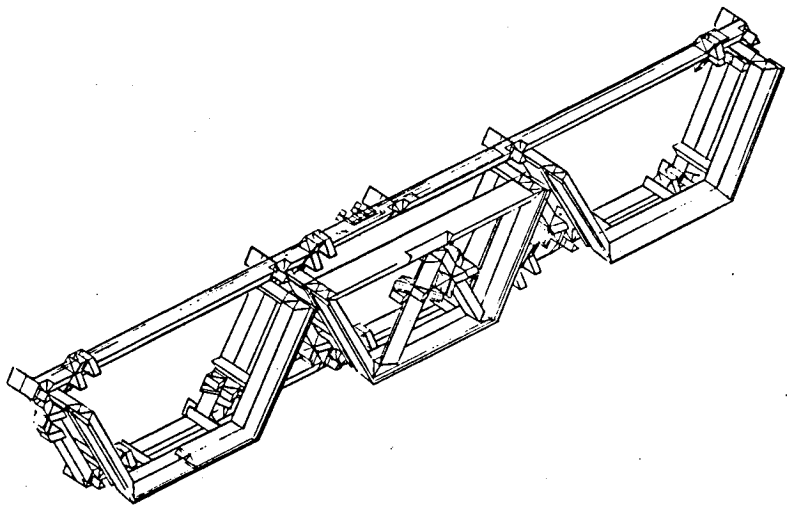

Figure 3.2-2. Integrated Satellite Construction Base

Table 3.2-1. SCB Mass Summary
(3 Trough - Single Pass)

TRIBEAM FABRICATORS	166000 KG
REFLECTOR INST. EQUIPMENT	120000
SOLAR BLANKET DISPENSORS (INC. CABLES & CATENARIES)	187000
	473000
MICROWAVE ANTENNA	409000 KG
FABRICATION FIXTURE	1499000
LOGISTICS VEHICLES & MANNED MANIPULATORS	252000
	2160000
HABITAT AND POWER SUPPLY	1617000
TOTAL	4250000 KG
TOTAL (INC. 25% GROWTH)	5312000 KG

3.2.2 SHUTTLE EXTERNAL TANK ASSEMBLY

The initial stages of the SPS program will be supported by STS derivatives, since the HLLV will not be operational. The growth shuttle on the left of Figure 3.2-3 has an option of two liquid propellant boosters which replace the solid propellants and permit larger payloads. In the shuttle-derived HLLV, the orbiter has been replaced by a larger payload module also equipped with liquid propellant engines, resulting in considerably larger payload capacity than the growth shuttle.

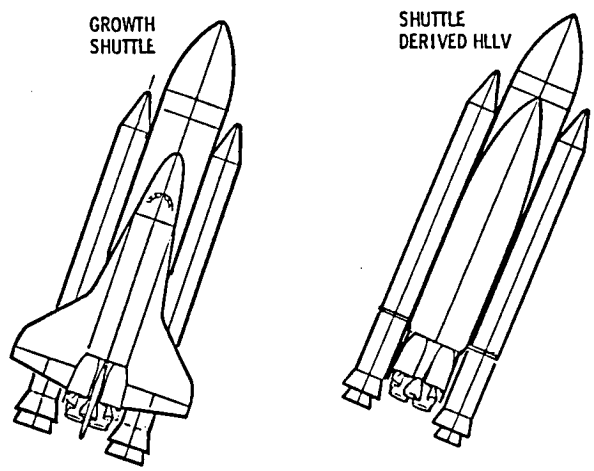

Figure 3.2-3. STS Derivatives

Figure 3.2-4 shows the docking and attaching of two external tanks, one attached to a growth shuttle and the other attached to a shuttle derived HLLV. The ET's have structural modifications incorporated prior to launch to accommodate the docking modules.

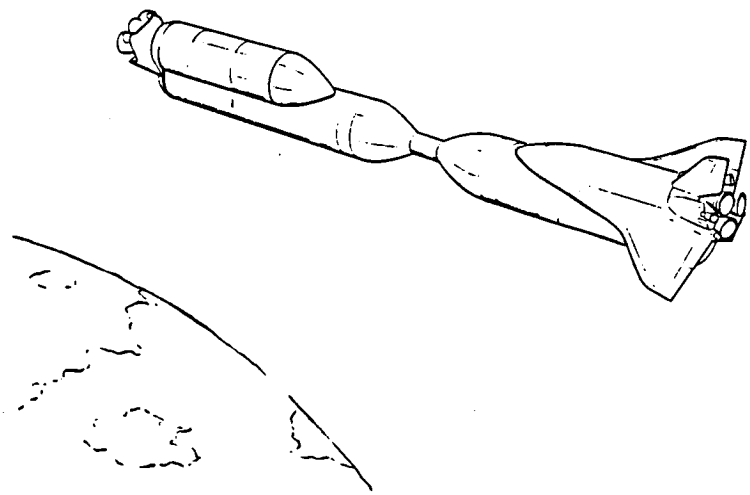

Figure 3.2-4. External Tank Docking

The module to which the two ET's are connected is carried to LEO via a shuttle flight and installed by free-flying manned manipulator modules.

The next step in the sequence is shown in Figure 3.2-5 where two ET's have been secured together by a module to which is docked a combination crew habitat and power module. A 2 meter beam machine has been installed by manned manipulator modules and has fabricated the beam shown at the bottom of the two ET's. This beam forms a part of the inner triangular structure which provides mounting for beam machines.

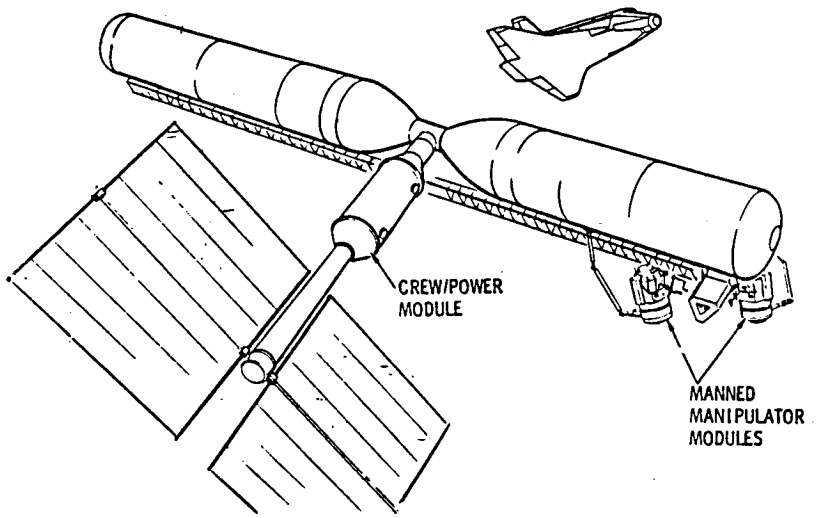

Figure 3.2-5. Rendezvous and Docking External Tanks

Details of a 60° intersection of two ET's is shown in Figure 3.2-6. The basic structure which secures the orbiter to the aft section of the ET is used for this purpose; any additional structural members required for added stiffness are prefabricated and transported as part of the Shuttle payload. Two manned manipulator modules are shown installing a 2 meter beam machine.

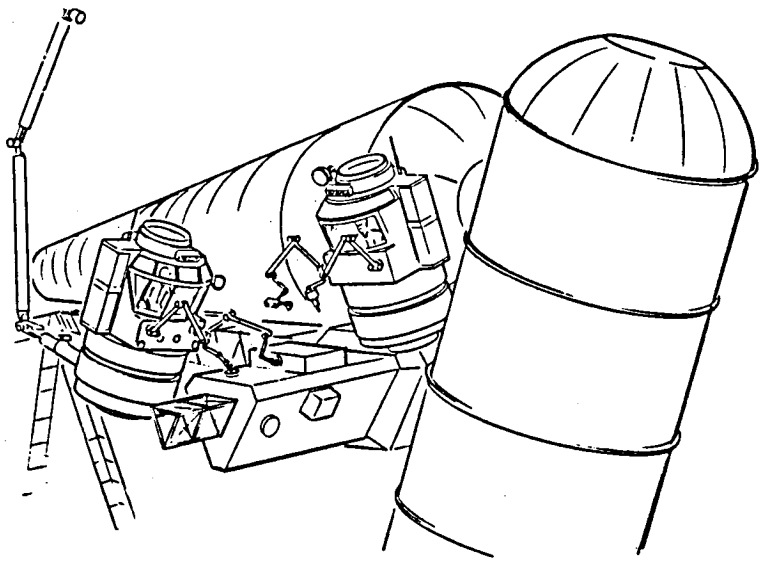

Figure 3.2-6. ET Facility Buildup

The facility (Figure 3.2-7) is for the purpose of producing the longitudinal and crossbeam pods which will be installed in the SCB for subsequent construction of EOTV and satellite tribeams. It is comprised of six shuttle ET's joined together as shown. The structure which attaches the orbiter to the aft section of the ET is utilized for joining the ET's and is augmented

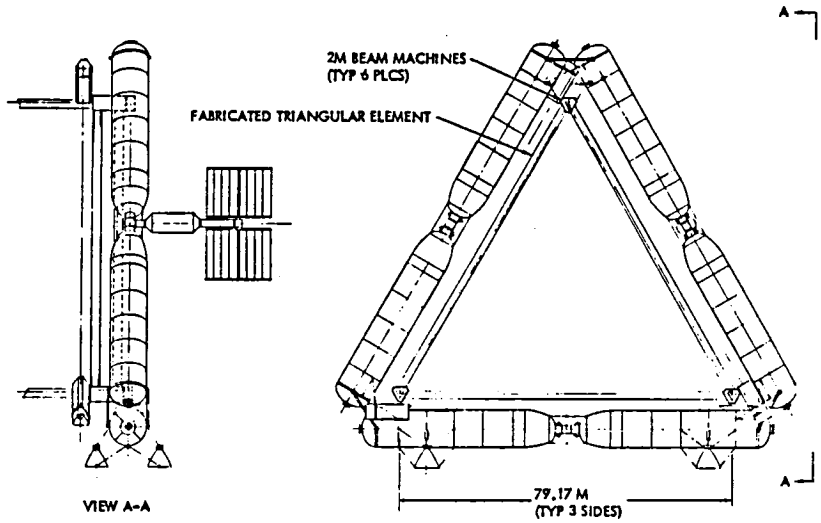

Figure 3.2-7. Triangular Element Fabrication Facility

by prefabricated bracing delivered by the orbiter. A triangular element comprised of 2 meter tribeams is mounted within the triangle formed by the ET's and provides the structure required for mounting the 2 meter beam machines which are used for constructing the outer triangle of the tribeam pod, or fabricator. A total of six beam machines are required; three for longitudinal beams and three for crossbeams. A crew facilities and power module, shown at the left of the figure, provides crew habitat and the electrical power required to operate life support and the beam machines. Reaction control pods attached to the ET's provide the required altitude control.

The primary structure of the SCB consists of a diamond cross section formed by two triangles. A mobile diamond-shaped fixture formed by joining 8 orbiter external tanks, depicted in Figure 3.2-8, is utilized for SCB primary structure fabrication. The beam machines are located at the tips of the structure enclosed by the external tanks. Nine machines are required to construct the four longerons, the four crossbeams and the diagonal beam. A combination crew and power module provides crew facilities and electrical power.

Figure 3.2-9 illustrates a mobile tribeam fabricator which subsequently will be utilized for construction of the antenna support structure, including slip rings, yoke, and antenna frame. The fabricator contains six beam machines; three to construct longerons and three for crossbeams. The machines used for the crossbeams are installed on track-mounted rotatable platforms. This permits rotation and translation of the machines to the rear section of the fabricator for servicing and reloading.

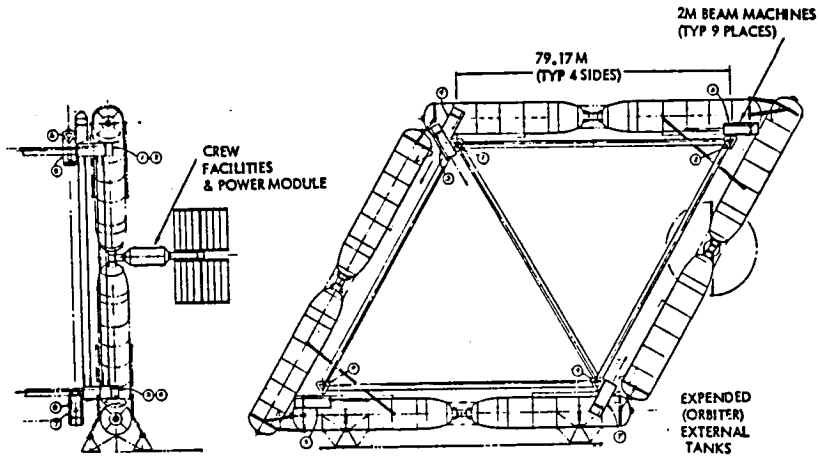

Figure 3.2-8. Mobile 79m Girder Fabrication Facility (Right-Hand Shown)

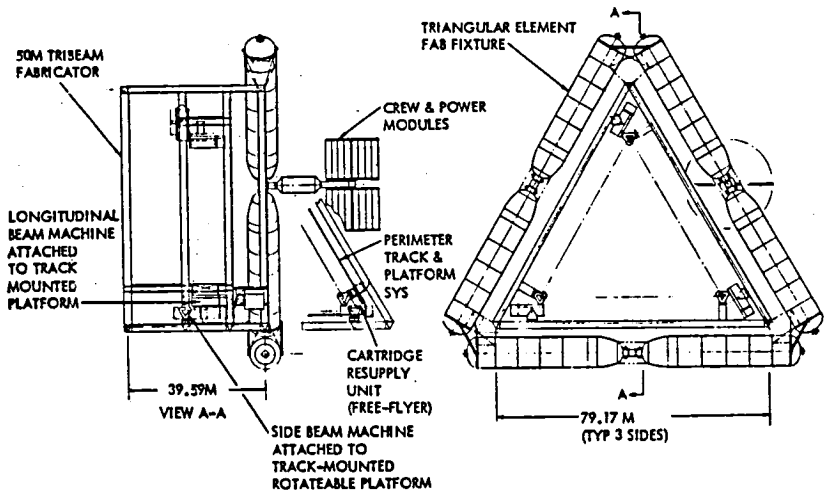

Figure 3.2-9. 50m Tribeam Fabricator Construction

3.2.3 SCB CONSTRUCTION

Total Integrated SCB

The SCB main structure consists of top and bottom transverse structural members connected by six diagonal members which match the three-trough reference satellite configuration. All members are constructed with a 80 meter diamond shaped cross section as shown in the explored view of the SCB main structure (Figure 3.2-10). The eleven 50 meter tribeam fabricators used for constructing the satellite longerons are shown in their ultimate positions at the intersection of the diagonals with the top and bottom members.

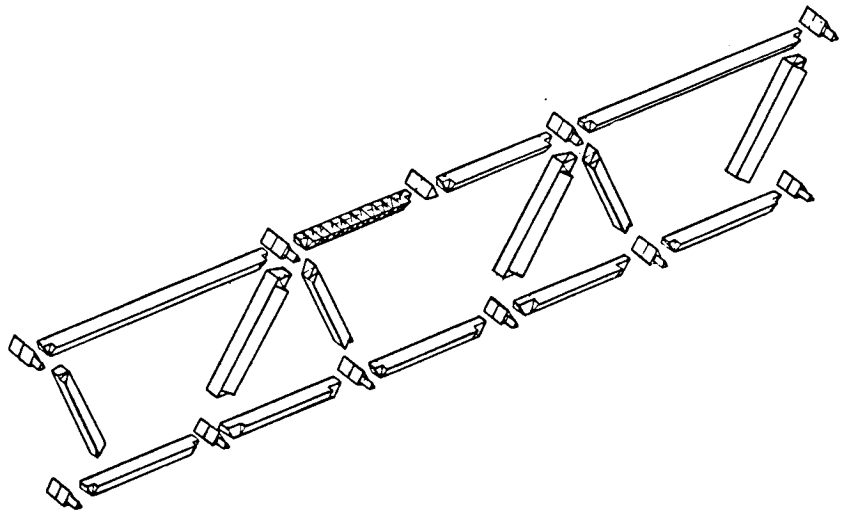

Figure 3.2-10. Components - SCB Main Structure

The initial step in the SCB construction is to fabricate a tribeam longeron pod, or fabricator, (upper right of Figure 3.2-11), described later. Two mobile 79 meter girder fabrication facilities (Figure 3.2-8) are then positioned on either side of the longeron pod and are used to fabricate sufficient lengths of the diamond-shaped girder to allow for attachment to the pod. When the attachment is complete, the girder fabricators resume fabrication, moving away in opposite directions from the pod as indicated in the upper left of the figure. At the proper spacing intervals additional pods are inserted until the entire upper deck of the SCB has been completed.

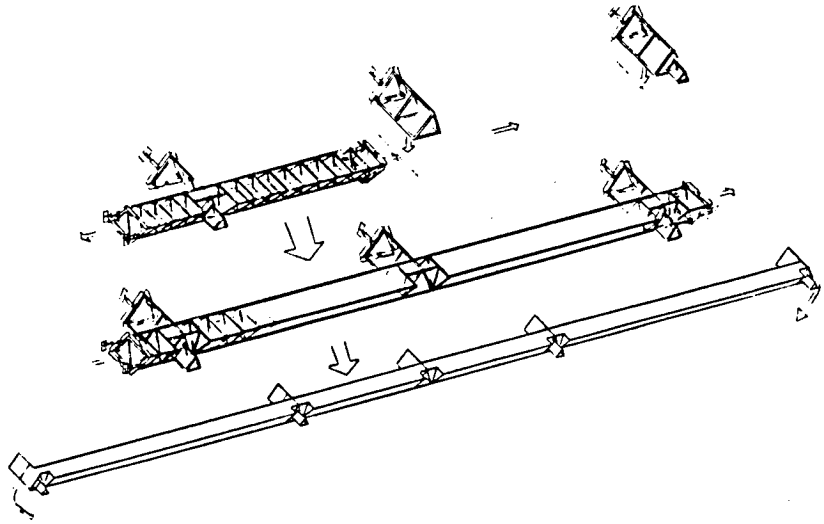

Figure 3.2-11. Construction of SCB Top Deck Girder

When the portion of the upper deck which ultimately will provide space for crew habitat and warehousing has been finished, facilities are installed and the logistics flow of materials commences.

The completed structural framework of the longeron fabricators which are installed in the SCB structure is depicted in Figure 3.2-12. A mobile 79 meter tribeam fabricator, including crew facilities and a power module (Reference Figure 3.2-7) is shown attached to the pod. The 50 meter tribeam longeron will be fabricated between the inner and outer triangular structures. Rigging and attach stations (not shown) will be located within the inner triangular structure. Section 4.4 contains additional details of fabricator operation. The structural interface details of the longitudinal pod intersection with the SCB diamond girder are contained in Figure 3.2-13. Two mobile girder fabrication facilities have made attachment to the pod and are progressing outward in opposite directions, fabricating the diamond girder as they advance.

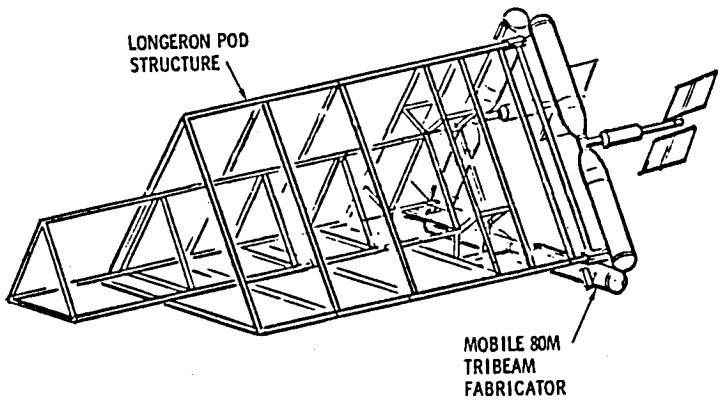

Figure 3.2-12. Longeron Pod Fabrication

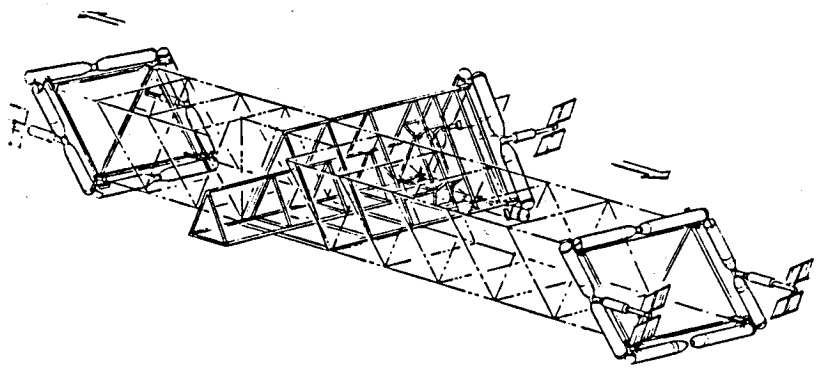

Figure 3.2-13. Intersection/Interface - Longitudinal Pod with Diamond Girder

As previously described, the initial step in the SCB construction is completion of the upper deck, with longeron pods installed as indicated in Figure 3.2-14. Upon completion of this deck, the two side diagonals are constructed at the proper angles, followed by completion of the Lower deck. The inner diagonals are then fabricated and attached in the sequence indicated in the figure by the circled numbers. This completes the SCB main structure.

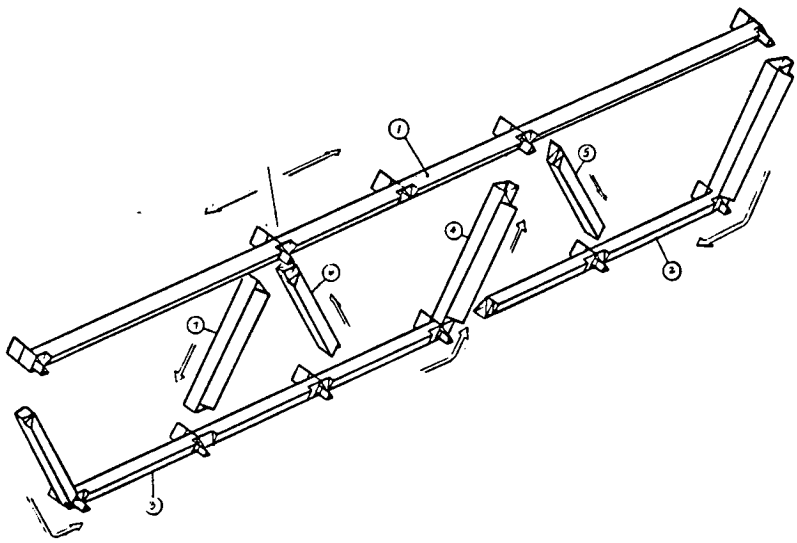

Figure 3.2-14. Assembly Sequence - SCB Main Structural Elements

The control complex, comprising crew facilities, power modules, and warehousing, is located on the central portion of the upper deck and is installed after this portion of the deck has been completed.

Figure 3.2-15 contains a representation of a typical 3-way intersection of the SCB structure. The longeron fabrication facility is shown installed in the SCB bottom girder, adjacent to a diagonal structural member. The moveable tribeam pod in the right center of the figure is used to construct a crossbeam and is then translated to the parking position, leaving a gap between the completed beam and the beam attach point. The closeout segment which is used to fill this gap is constructed by the fixed tribeam pod and is then translated into position for final attachment. An alternate approach understudy would be to translate the pod and build closeout segments using two beam machines external to the pod.

The secondary structure (Figure 3.2-16) is cantilevered to the main structure. The solar converter installation facilities and the auxiliary bases are installed on the secondary structure. The center section of the structure has additional structural elements as shown in the figure. These elements and the attached tribeam fabricators are used to construct the slip ring support interface structure. The slip rings, antenna yoke, and antennas are constructed using combinations of free-flying facilities, (see Section 4.4 and Figure 4.4-7).

Figure 3.2-17 shows the partially completed secondary structure. The center and left portions are almost complete. The beams comprising the right portion are in a partially completed state. When the secondary structure has been completed, auxiliary bases are established at the bottom of each trough and the solar converter installation equipment installed.

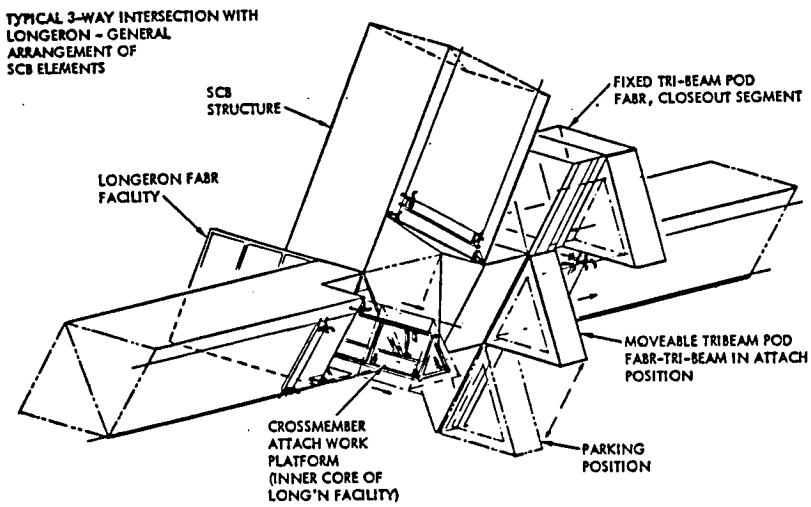

Figure 3.2-15. Typical 3-Way Intersection with Longeron

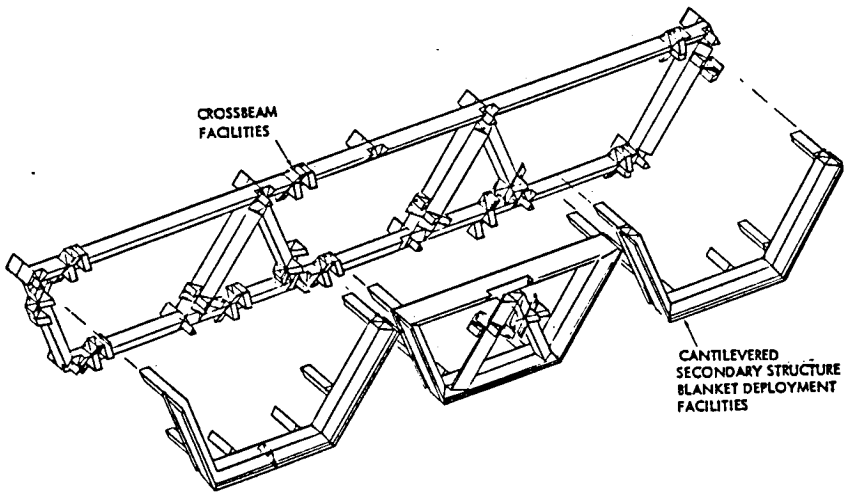

Figure 3.2-16. Secondary Structure

Upon completion of the SCB in LEO, construction of the EOTV fleet can commence. Since the EOTV cross section is the same as one trough of the satellite, the SCB is utilized for the EOTV construction. Two EOTV's can be constructed simultaneously, (Figure 3.2-18. However, it is probable that initial orbital operations would consist of constructing an EOTV with end-mounted antenna as a test article for proof of concept.

The basic EOTV configuration features extension beams at each of the four lower corners upon which the propulsion units are mounted. The overall scenario entails movement of the SCB from LEO to GEO by means of an EOTV constructed and still attached to the SCB center trough. In the event that dynamics studies indicate a requirement for an EOTV to be mounted on each

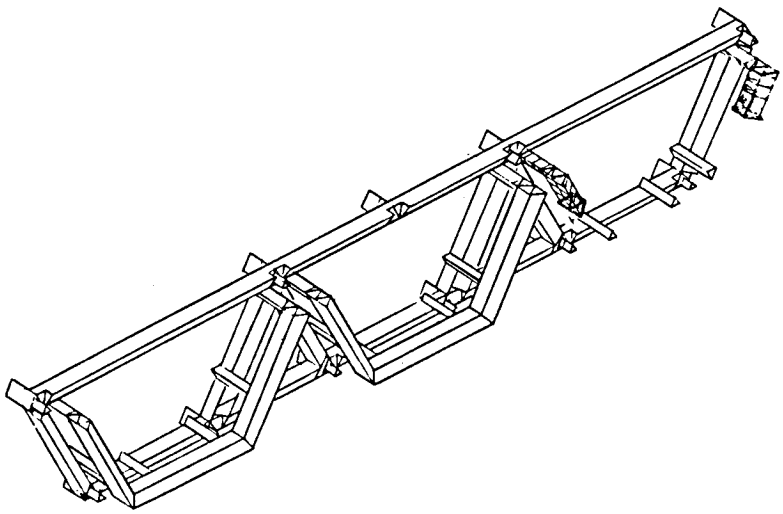

Figure 3.2-17. Construct Secondary Structure

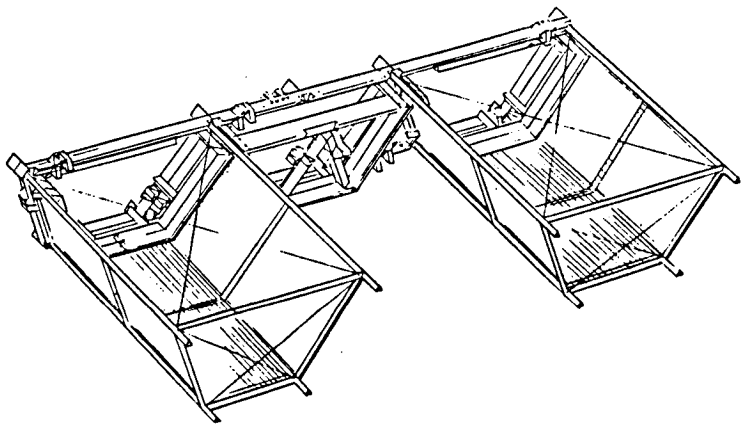

Figure 3.2-18. Parallel Fabrication of EOTV's

side of the SCB for this transit, the propulsion unit arms on one end of the EOTV would be modified (Figure 3.2-19) for docking on the face of the SCB opposite that which supports construction operations.

If it is desired to utilize an EOTV during the initial phases of a satellite construction to provide additional attitude control capability, the EOTV which transports the SCB to GEO could be docked in an inverted position (Figure 3.2-20). The satellite solar blankets should not be deployed in direct sunlight. By docking the EOTV in an inverted position, augmenting electrical power becomes available, while the satellite blankets may now be deployed outside of direct sunlight.

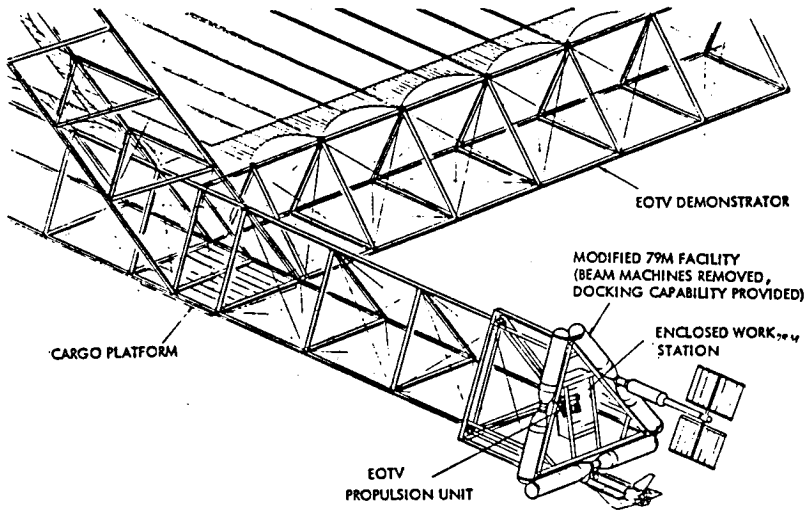

Figure 3.2-19. EOTV Propulsion Unit Installation

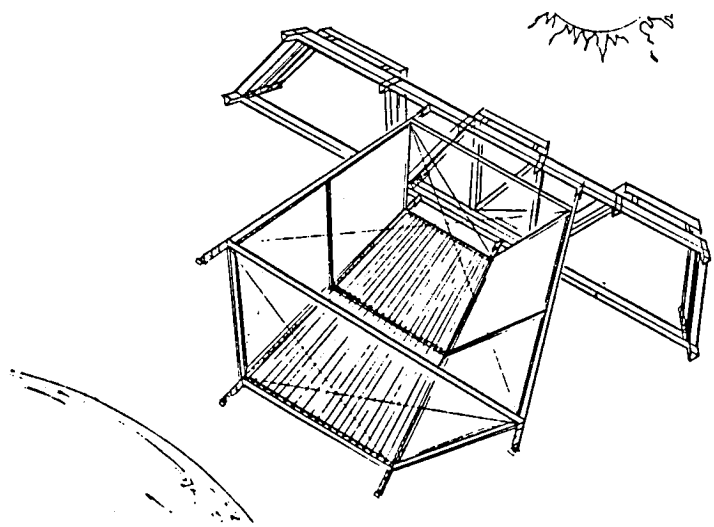

Figure 3.2-20. EOTV/SCB Orbit Transfer Configuration

Demonstration Program Configuration

Since at least initial precursor operations will be supported by shuttle derivatives, it is possible that the SCB will be constructed in increments, the first increment consisting of the center trough fixture. This fixture would support construction of the first EOTV (with end-mounted antenna) which would be used to establish proof of concept. Figure 3.2-21 contains three views of this configuration; a perspective is shown in Figure 3.2-22. The locations of the tribeam fabricators, solar converter dispensing area, and the habitat/warehouse facilities are as denoted by the legend in the upper left portion of the figure. The construction sequence for this configuration would be similar to that described for the integrated SCB in the preceding section, excluding the two side troughs.

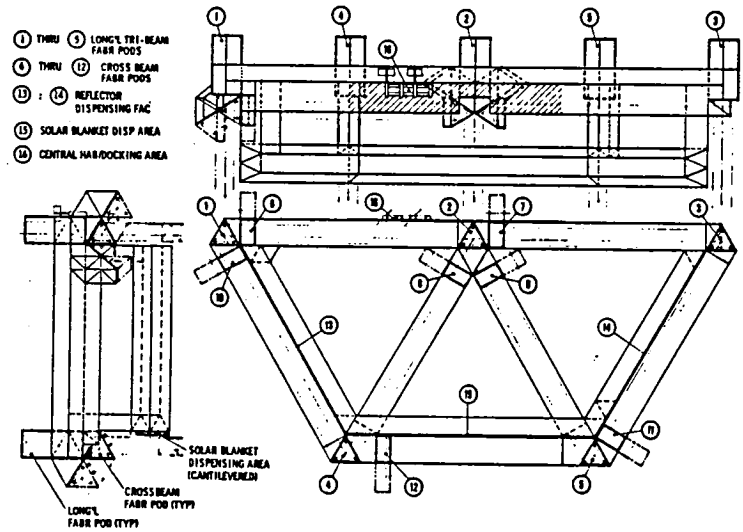

Figure 3.2-21. EOTV/DEMO SPS Satellite Construction Base

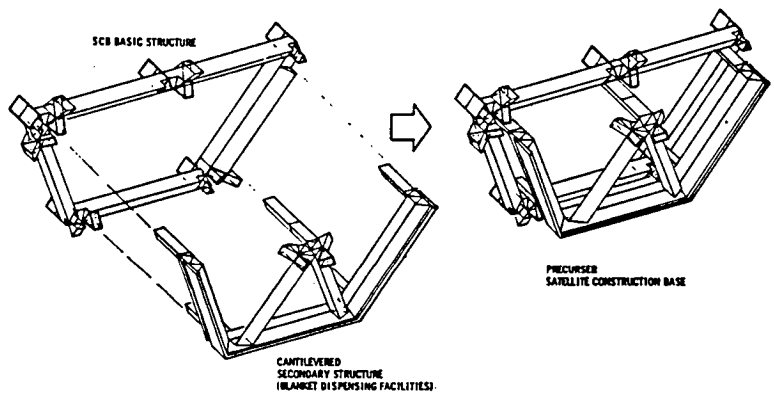

Figure 3.2-22. EOTV/DEMO SPS Satellite Construction Base (Perspective)

The space frame antenna which will be mounted on one end of the EOTV test article is identical to those which will be mounted on the satellites except that only sufficient structure to mount the reduced number of mechanical modules will be completed. Figure 3.2-23 contains three views of the basic antenna, which is composed of a primary structure 60 meters in depth upon which is mounted an 8 meter (depth) secondary structure. The RF elements are secured to the secondary structure. For the test article only sufficient (TBD) mechanical modules to provide the required test data will be installed.

An end view of the slip rings and antenna supporting structure is shown in Figure 3.2-24. The bottom view shows the location of the slip rings or rotary joint relative to the EOTV structure. This configuration is identical to the installation in the center trough of the satellite.

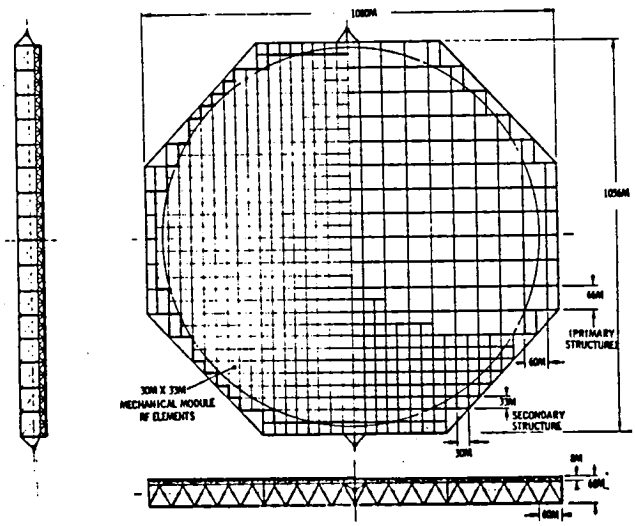

Figure 3.2-23. Space Frame Antenna Configuration

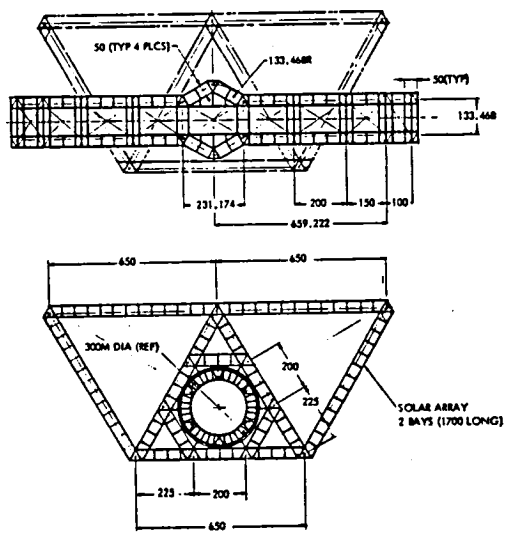

Figure 3.2-24. EOTV/DEMO SPS Reference Configuration

The upper portion of the figure shows the location of the structure which forms the rotating portion of the joint. The transverse element is the base of the U shaped structure which contains the trunnion joints and the antenna.

The construction of the EOTV test article, including the rotary joint housing, slip rings, antenna support, and antenna is shown in the sequence contained in Figure 3.2-25 through 3.2-29. Additional details of antenna fabrication procedures are contained in Section 4.4.3.

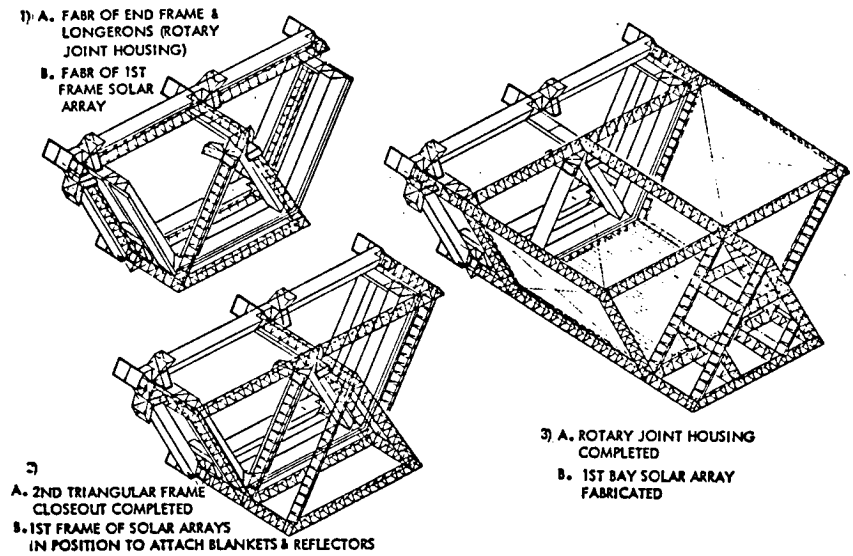

Figure 3.2-25. EOTV/DEMO SPS Construction Sequence Slip Ring/Rotary Joint Housing Structure

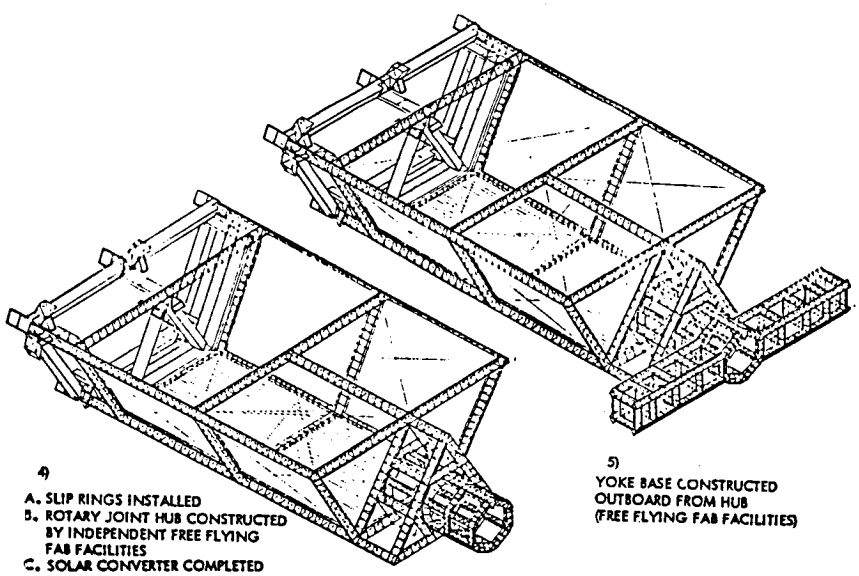

Figure 3.2-26. EOTV/DEMO SPS Construction Sequence Slip Ring, Rotary Hub and Yoke Base

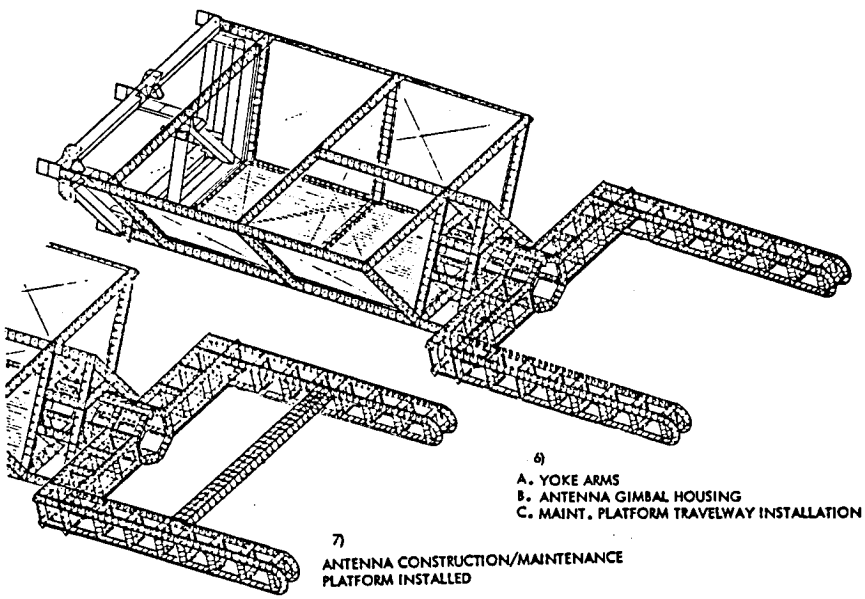

Figure 3.2-27. EOTV/DEMO SPS Construction Sequence Yoke Arms and Antenna Fab/Maintenance Platform

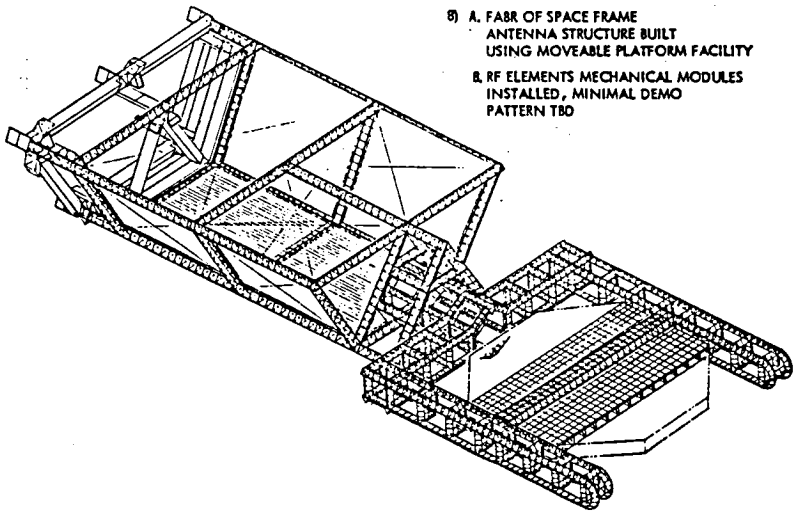

Figure 3.2-28. EOTV/DEMO SPS Construction Sequence Space Frame Antenna

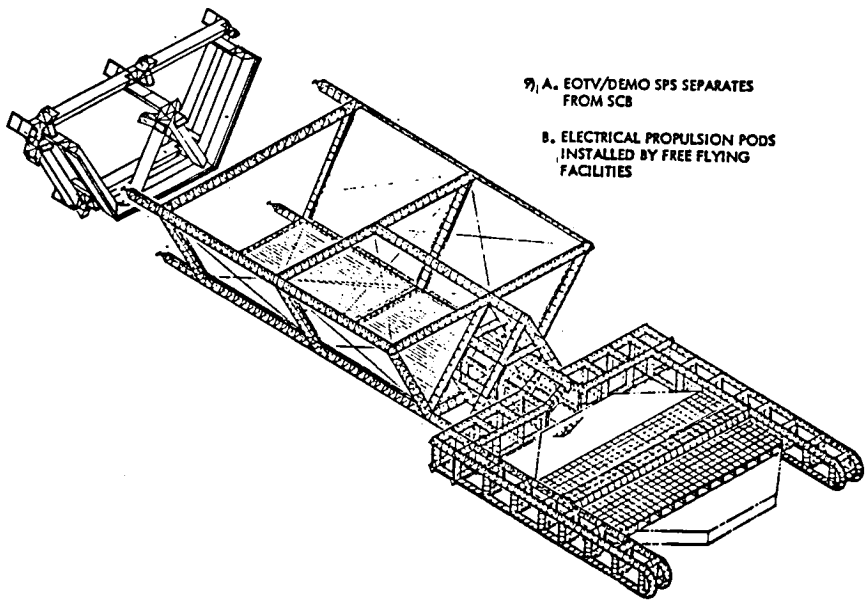

Figure 3.2-29. EOTV/DEMO SPS Construction Sequence Electrical Propulsion System Installation

3.2.4 SCB CONSTRUCTION SCHEDULE

Construction of the SCB has been programmed over a three year period. This includes a time allocation for construction of the EOTV test article (precursor satellite) following completion of the SCB center trough. Two months have been allocated for establishment of the LEO base, including crew habitat, support modules and a power module. The timeline is depicted in Figure 3.2-30. Initially the center trough of the SCB is completed, including the equipment and facilities required for installation of the solar converter and antenna fabrication. This activity is completed by the ninth month of the second year at which time the EOTV test article is constructed, utilizing the center trough of the SCB. Following this operation, the remainder of the SCB is constructed and the integrated facility is then checked out.

Estimated crew requirements are summarized at the bottom of the figure.

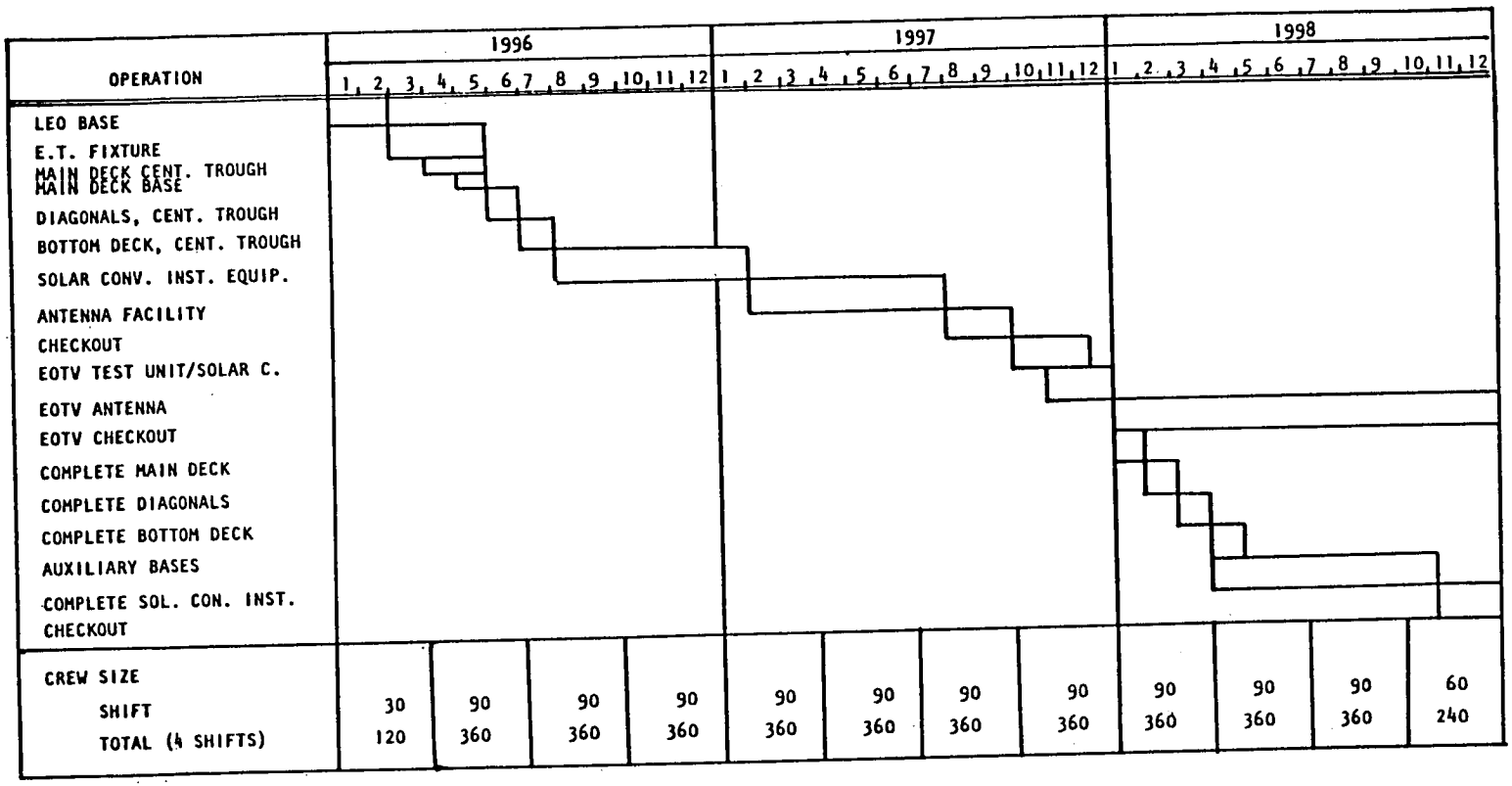

Figure 3.2-30. SCB Construction Schedule and Crew Size

4.0 SATELLITE CONSTRUCTION

4.0 SATELLITE CONSTRUCTION

Subsequent to the First Quarterly Review, redirection from NASA resulted in no additional effort being expended on the Rockwell Point Design. The current NASA ground rules applicable to satellite construction consist of:

- Coplanar configuration
- 5 Gigawatt system
- End-mounted antenna
- Composite structure
- GEO construction, two satellites per year
- Electric OTV
- GaAlAs solar cells, CR=2

In applying these ground rules to new configurations, a guideline of retaining desirable features of the Rockwell June 78 design relative to geometry and construction concept was utilized.

In addition, certain construction guidelines, developed for the previous design and modified by the above ground rules were followed. These are:

- Single integrated SCB
- Continuous structure fabrication
- Solar converter installation simultaneous with structural fabrication
- Antenna assembled in place concurrent with satellite structural fabrication
- No scheduled EVA
- 180 day construction schedule

4.1 CONFIGURATION AND CONSTRUCTION OPTIONS

A number of options reflecting both center and end mounted antennas, and varying numbers of troughs were examined. Figure 4.1-1 shows the 3-trough coplanar satellite with center mounted antenna and with an end mounted antenna together with their applicable optional construction techniques. (The effect of increasing the satellite width to four troughs, with attendant reduction in lengths, is shown in subsequent figures.) The serpentine construction technique offers the potential of a small SCB and smaller crew size but offers little flexibility for reducing construction time since each trough is constructed serially; also it is less appropriate for the center mounted antenna

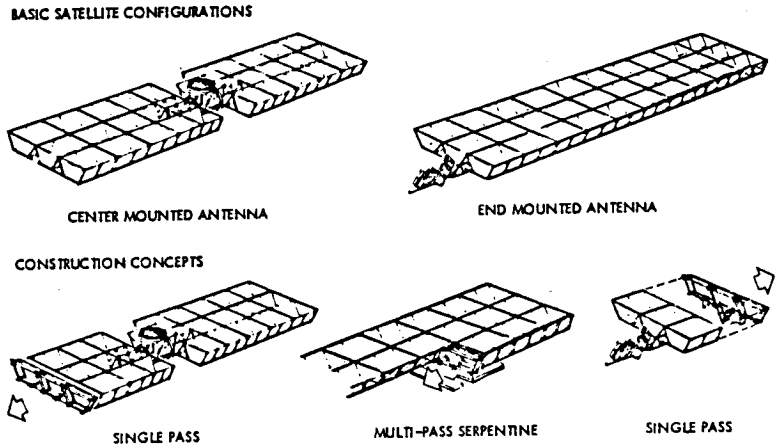

Figure 4.1-1. Satellite and Construction Options

configuration. The single pass construction technique has somewhat the opposite characteristics.

Three and four trough versions of the satellite end-mounted antenna configurations are shown in Figure 4.1-2. The solar blanket area is the same for each version. Two different construction concepts have been identified; parallel build single pass for the three troughs and serpentine for the four troughs. The single pass concept possess potential for shortening the nominal 180 day construction schedule; the serpentine concept, because of sequential trough construction, requires the entire 180 days. While the mass of the SCB used for serpentine construction is slightly less than for the single pass SCB, the serpentine SCB, featuring a large platform with sliding sections, is more complex.

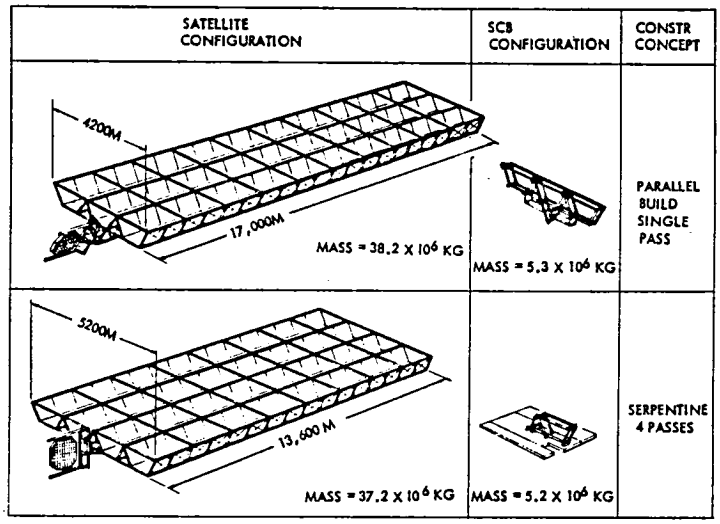

Figure 4.1-2. 3- and 4-Trough Satellites with End Mounted Antenna

The center mounted antenna is depicted in Figure 4.1-3 for the same trough configurations shown above. The difference in satellite mass for these configurations as compared to the end-mounted versions is largely attributable to power distribution. (Parallel build, single pass construction was selected for these configurations since the complexity associated with serpentine build of a center-mounted antenna configuration appeared to be excessive.)

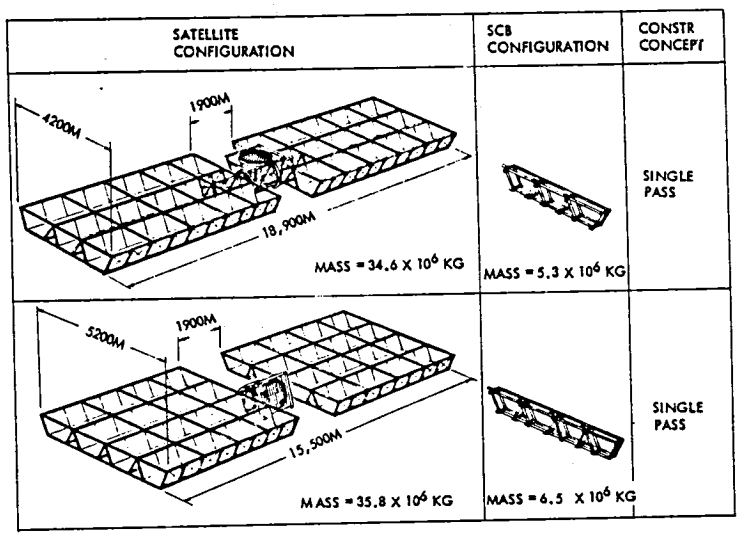

Figure 4.1-3. 3- and 4-Trough Satellites with Center Mounted Antenna

From a constructability standpoint the 3-trough satellite is more desirable than the 4-trough configuration because the SCB is narrower, of lower mass, and requires a smaller crew size.

4.2 ROCKWELL POINT DESIGN (JUNE 1978)

4.2.1 SATELLITE DESCRIPTION

The satellite is comprised of two wings and a center section upon which the slip ring and antenna is mounted. Each wing consists of 12 bays 800-m long, numbered as shown on the isometric representation of the satellite, Figure 4.2-1. Referring to the cross section view, solar blanket strips 750-m long and 25-m wide are installed along the bottom of the three troughs as indicated, while the reflector panels are installed in the trough sides.

The satellite structure is constructed from 50-m tribeams which are fabricated from the basic building block of 2-m tribeams as shown in the tribeam cross section. The overall construction concept entails use of a satellite construction base, to construct one wing, commencing with bay 1, complete the center section, and then fabricate the second wing, commencing with Bay 24. Installation of the power generating equipment is accomplished concurrently with fabrication of each bay.

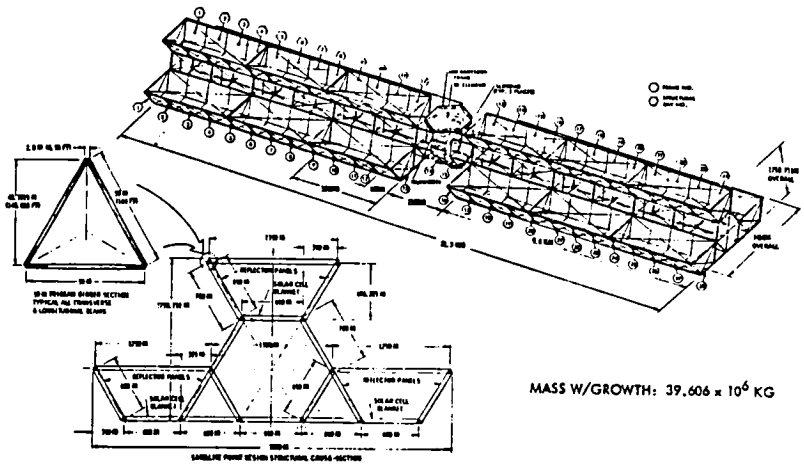

Figure 4.2-1. Rockwell Baseline Satellite Description, June 1978

4.2.2 SATELLITE CONSTRUCTION BASE (SCB)

Construction of the satellites takes place in GEO, each satellite being constructed at its designated longitudinal location. All construction activities are supported by a single integrated construction base which produces satellites at the rate of 4 per year (and later 5 per year) during the mature portion of the program. Upon completion of one satellite the base is moved to the operational location of the next satellite for construction of that satellite.

The construction base, Figure 4.2-2, consists of the satellite construction fixture, the construction equipment, and the base support facilities and equipment. The construction fixture is a rugged heavy gage metal structure on which all elements of the construction base are mounted. The fixture constitutes the reference surfaces for the construction operations and the locating jig for the equipment which constructs/installs various elements of the satellite in situ.

The major construction equipment includes the 50 m tribeam fabricators; the deployment equipment for the solar cell blankets, the solar reflector panels, the power distribution conductors, the cables for retention of the solar blankets, and the structure tensioning cables; the assembly facility for the MW antenna mechanical modules; and the equipment for installation of the MW antenna elements into the antenna frame. The location of most of these elements is identified on Figure 4.2-2.

4.2.3 SATELLITE CONSTRUCTION SCHEDULE

A single integrated construction facility builds the structure, installs the solar blankets, the reflectors, the power distribution system and other subsystem elements located in the wings. Construction starts with one wing tip and progresses toward the center section where the rotating joint for the MW antenna

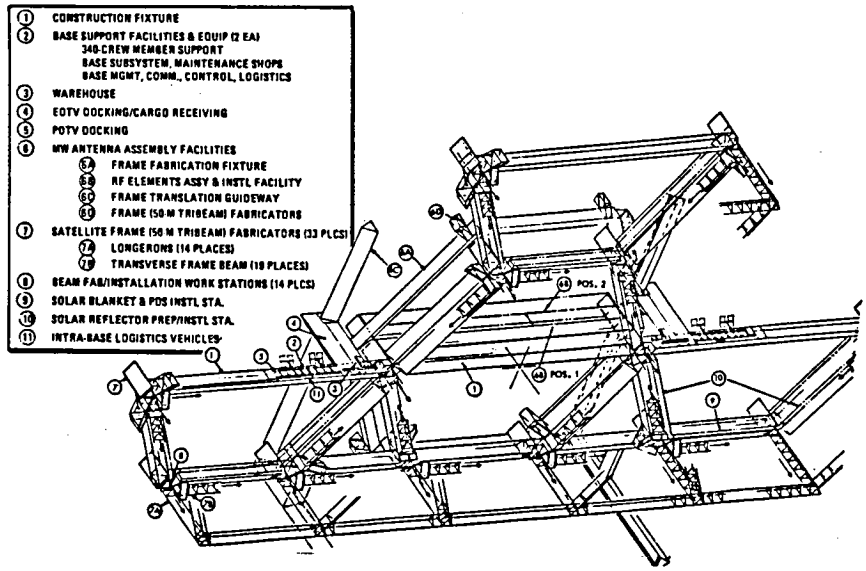

Figure 4.2-2. Rockwell Baseline Satellite Construction Base (SCB), June 1978

is to be located, and hence continues outboard building wing No. 2 and terminating at the wing tip. The sequence is shown in Figure 4.2-3.

The first eight days are designated for preparation of the construction facility, including distribution and installation into dispensers of material (e.g., structure cassettes, solar blankets, etc.) required to commence construction. During this time satellite materials are arriving from LEO daily with delivery scheduled for completion by the 60th day.

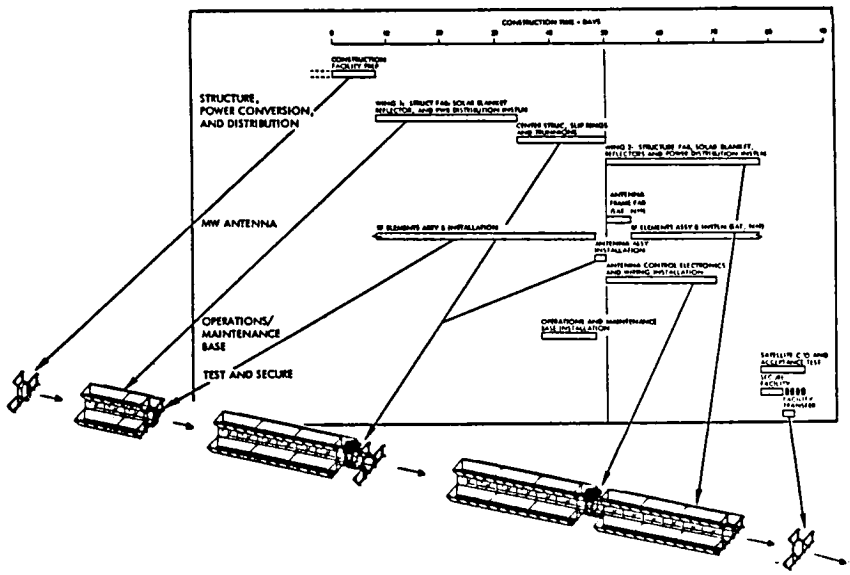

Figure 4.2-3. Construction Schedule for Rockwell Baseline Satellite, June 1978

Each satellite wing consists of 12 bays 800-m long. These are constructed at the rate of one every two days using three 8-hour shifts per day. The structure and installation of the power conversion system of wing No. 1 is completed on the 34th day. While the wing No. 1 construction is taking place the MW antenna crews are proceeding with the assembly, test, and installation of the antenna elements into the antenna frame. The antenna assembly continues during the construction of the center section.

Subsequent to completion of wing No. 1 the construction facility constructs the longerons and frames in the center section, installs the slip rings, constructs the tension supports, installs the trunions, and installs power wiring in the center. Although 16 days are scheduled for this activity, the timeline requires only 12 days with two additional days scheduled for transfer of the antenna to the trunion mounts. Two days are allowed for contingencies.

Immediately upon completion of the center section primary structure the facilities for the operation and maintenance are installed and the first operational maintenance crew arrives to support installation of the antenna control electronics and satellite checkout, which takes place from day 50 through day 69.

Final satellite checkout and acceptance testing is completed on day 86. Use of the construction facility is completed on day 78 and flyaway transfer to the construction site of the next satellite occurs on day 84.

4.3 SERPENTINE CONSTRUCTION SCENARIO

4.3.1 SCB DESCRIPTION

The fixture shown in Figure 4.3-1 is for the serpentine construction concept. This entails beam fabrication from each side of the fixture as shown, for example by the duplicate sets of longeron beam fabricators, denoted by (8A) and (8B). In addition to fabricators for the basic satellite structure, fabricators for the antenna frame are shown (8E). The concept for building the antenna frame a half at a time will be subsequently covered. Antenna RF elements are installed from the two assembly and installation stations, (15). Crew, power, warehousing and receiving facilities are grouped on the central portion of the fixture, indicated by (2) through (5). The rotating joint assembly fixture, (10), is located in the triangle formed by the two left diagonals.

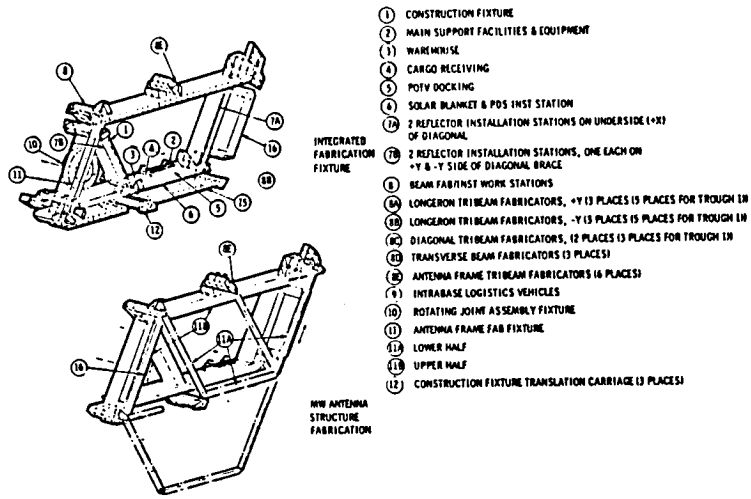

Figure 4.3-1. Integrated Fabrication Facility

Solar converter installation equipment (for solar blankets, reflectors, power distribution system elements, information management and control system, ACS) is located along the trough bottom and sides of the fixture. The construction fixture assembly constitutes the tooling jig for these major elements: solar converter primary structure, MW antenna structure, slip ring assembly, and antenna yoke. The fixture assembly is designed to allow construction of troughs 1 and 3 from the -Y face, and troughs 2 and 4 from the +Y face. This permits achievement of the serpentine construction pattern by translation of the SCB to the position for construction of the next trough, thus precluding a possibly untenable requirement to rotate the SCB. It is also designed so that the rotary joint can be fabricated anytime during construction of troughs 1 and 2, and the MW antenna is assembled (on the -Y face of the fixture), simultaneously with the construction of trough 2 (which is accomplished from the +Y face).

The fixture is mounted on a platform in tracks which provide for transverse and longitudinal movement. The movement is effected by means of 3 translation carriages, (12), which are attached to tracks in the platform.

Figure 4.3-2 shows the translation platform with the construction facility attached to the tracks, (18) by the three translating carriages. The platform consists of three sections attached to one another by means of sliding guideways, (17) which permit lateral relative movement during the repositioning operations as shown onthe bottom figure and as described later. The elevating frame attach fittings, (14), are used to secure the platform to the partially completed satellite and to thus permit movement of the construction facility relative to the satellite.

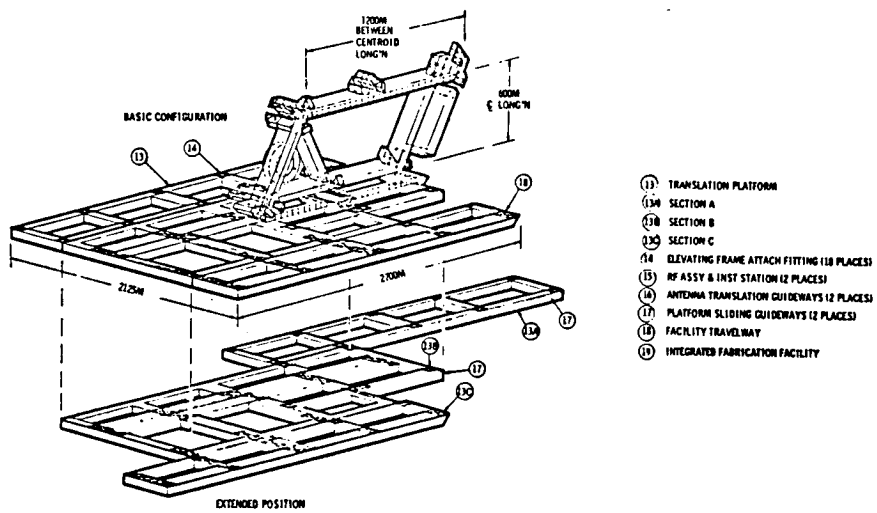

Figure 4.3-2. Satellite Construction Base (SCB) (Serpentine Construction)

The timeline for construction of a satellite is given in Figure 4.3-3 and the utilization of the SCB in constructing a satellite is illustrated in the sequence of Figures 4.3-4 through 4.3-8 which are discussed in the following subsections.

The serpentine construction concept requires that the troughs be constructed in sequence as shown in the timeline. This essentially becomes the pacing activity. The antenna frame is fabricated on the fixture during the second pass followed by installation of the antenna RF elements. Assembly of RF mechanical modules occurs during most of the 180 days except when RF elements are being installed, since these two operations are conducted by the same crew. Upon completion of the antenna, the assembly of mechanical modules for the next satellite commences, as shown by the second bar in Figure 4.3-3. This provides a greater time span for this task with a resultant reduction in crew and equipment.

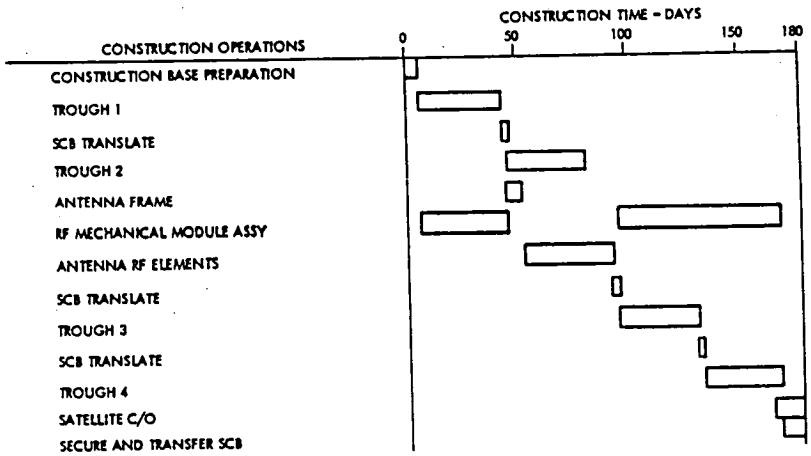

Figure 4.3-3. Satellite Construction Timeline

The time-phased crew size for the serpentine construction concept and the 180 day construction schedule previously described is contained in Table 4.3-1. The crew size remains constant during the first 164 days of the construction period at which time the operational maintenance crew (30 members total) arrives on board for their first 90 day tour of duty; during the last 15 days of the construction period they support test and checkout of satellite. Note that the size of the crew is not affected by the number of troughs in the satellite; i.e., a 3-trough satellite would also require a crew size of 264; the required construction time would remain (essentially) the same (180 days) providing the total solar converter area is constant.

Table 4.3-1. Crew Size
Serpentine Construction

OPERATIONS	NO. OF CREW MEMBERS SHIFT SIZE	
	DAY 1-165	DAY 166-180
CONSTRUCTION CREW		
SOLAR CONVERTER CONSTR.	20	20
ANTENNA RF ASSY/INSTLN.	24	24
CONSTRUCTION SUPPORT	6	6
MAINTENANCE	6	6
BASE MGMT	4	4
CREW SUPPORT	6	6
TOTAL SHIFT SIZE	66	66
TOTAL CREW - 4 SHIFTS	264	264
OPERATIONAL MAINTENANCE CREW		24
TOTAL CREW ON-BOARD	264	258

4.3.2 SOLAR CONVERTER CONSTRUCTION AND INSTALLATION

Five tribeam fabricators for making longerons are indicated in the upper right-hand view on Figure 4.3-4. All five are used in the first pass as trough 1 is built. In constructing the remaining troughs only three fabricators (1, 2, 3) are required. The longerons are continuous members for the entire 15,300 m length of the satellite. Only four tribeam fabricators are required for making the crossbeams except for the first pass which requires six. The crossbeams are continuous for their respective lengths. In making the solar converter troughs the initial frame is constructed using the fixture as the tooling jig. The longerons are then fabricated away from the face of the SCB moving the frame with them. As they move out, the solar blankets, reflectors, power feeders and other elements of the solar converter are dispensed. At the completion of the length of each bay, fabrication in the longitudinal direction is stopped, the beams for the next frame (which have been fabricated during construction of the longerons) are connected in place to the longerons and the solar blankets and reflectors are tensioned between the frames to complete the bay.

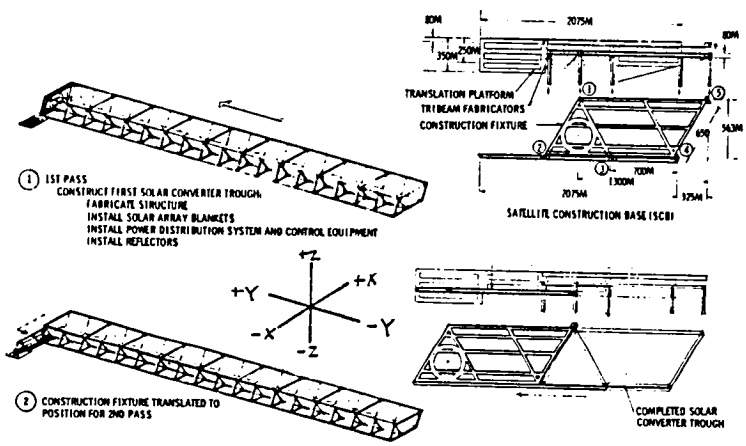

Figure 4.3-4. Trough 1 Construction

The translating platform supports the fixture assembly and all SCB facilities. It is designed to move with the rest of the SCB in the longitudinal direction but can also be locked to the completed structure to perform its functions at the end of each trough. The fixture assembly is mounted in tracks on the platform which permit movement of the fixture both laterally and longitudinally. The platform extends 775 m wider than the structure of the trough being constructed. After the last frame of trough 1 is completed the translation platform is clamped to the longerons of trough 1. The fixture assembly is first translated in the longitudinal direction to clear the last frame, then translated laterally to be in line for construction of trough 2. It is then translated longitudinally back along the side of trough 1 to be in position for fabrication of the first frame of trough 2. After the first frame of trough 2 is completed and tied into the last frame of trough 1, the translation platform is released from the trough 1 longerons and translated to the left to again be in the position with respect to the fixture assembly shown on the right-hand side of Figure 4.3-4.

4.3.3 MW ANTENNA ASSEMBLY AND INSTALLATION

The construction fixture is designed for simultaneous fabrication of the antenna on the -Y face while the second trough is being fabricated from the +Y face. The SCB geometry and the sequence of construction of the solar converter portion of the satellite make it necessary that the antenna and rotary joint installations be completed prior to starting construction of the third trough. The rotary joint can be assembled and checked out independently on the special circular jig any time during construction of the first two troughs. Antenna frame fabrication is initiated simultaneously with start of construction of trough No. 2. Installation of the RF elements is started as soon as the tension web installation is completed. Fabrication of the antenna yoke and rotary joint standoff support structure occurs after completion of trough No. 2 since those operations take place on the +Y side of the construction fixture.

The 50-m tribeam fabricators produce the structure for the antenna frame. Referring to the middle view on the right-hand side of Figure 4.3-5, the lower one-half portion of the frame is fabricated first using the part of the fixture indicated by the heavy dashed lines. This half-frame is closed out across the top with the temporary 50-m tribeam tie bar indicated for stabilization during the remainder of the assembly operations. This frame half is then translated to a position below the translation platform (arrows and phantom outline in the middle view) and the upper half is fabricated using the heavy solid line part of the fixture, and the two halfs are joined to form the hex-shaped frame.

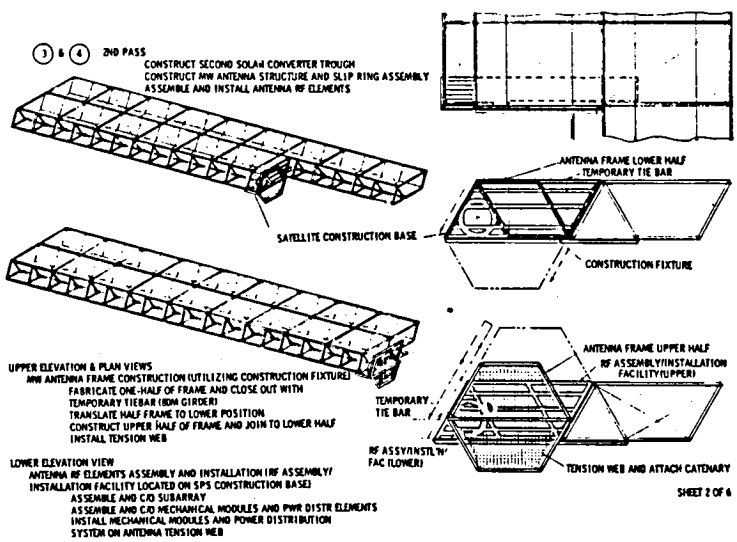

Figure 4.3-5. Trough 2 and MW Antenna Construction and RF Installation

The lower right-hand view on Figure 4.3-5 shows that the SCB provides for up-down translation of the antenna in the X-Z plane. The position of the tie bar is variable from the X-Y plane of the base of the translating platform to the X-Y plane of the upper cross frame of the construction fixture. This

permits installation of the tension web, installation of the RF mechanical modules (antenna upper-half installed from the upper RF assembly and installation facility, antenna bottom half installed from the lower RF facility), and alignment of the completed antenna with the rotary joint. Assembly and checkout of the subarrays and mechanical modules is also accomplished at the RF facilities.

Upon completion of trough No. 2 the slip ring supports and antenna yoke shown on Figure 4.3-6 are fabricated using one of the available 50-m tribeam fabricators. The slip ring supports are joined to the solar converter structure and the slip ring is removed from its jig and installed on the supports. The base of the antenna yoke is fabricated parallel to the translating base, the antenna is translated to be centered in the projection of the base, and the trunion support arms are built out in the -Y direction to pass through extensions of the antenna center line on which the trunions are located. Guideways are provided along the trunion support arms which engage the trunions as the support arms are fabricated outward. The translation platform is used to move the center line of the antenna/yoke coincident with the center line of the rotary joint and the yoke is attached to the rotary joint.

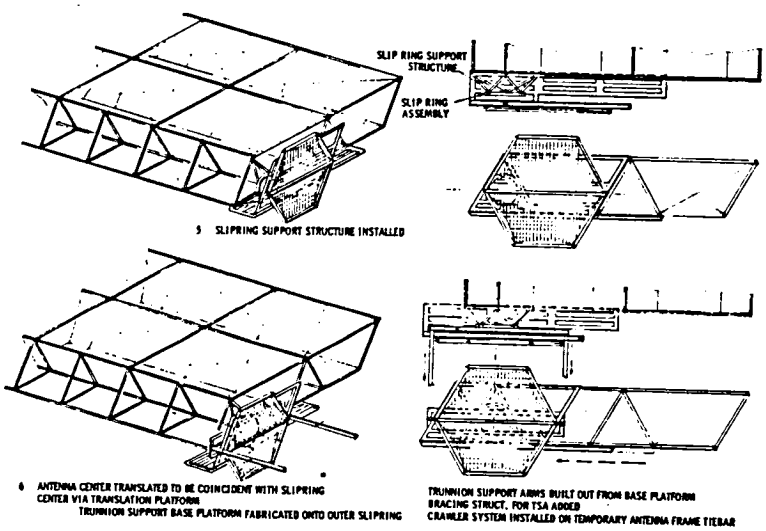

Figure 4.3-6. Antenna Rotary Joint and Yoke Construction

Referring to Figure 4.3-7 a crawler system installed on the temporary tie bar is used to translate the antenna along the trunion guideways to its gimble plane. The gimbles are secured, azimuth control elements are installed, and electrical power, information management and control system connections are made utilizing the crawler system. Since the slip ring and yoke base are necessarily constructed on opposite sides of the construction fixture it is necessary to rotate the slip ring and antenna assembly 120° as shown in Figure 4.3-7 to release the construction base. The construction base is then translated into position to start construction of trough No. 3 (see Figure 4.3-8) through a series of operations similar to those described for moving from trough No. 1.

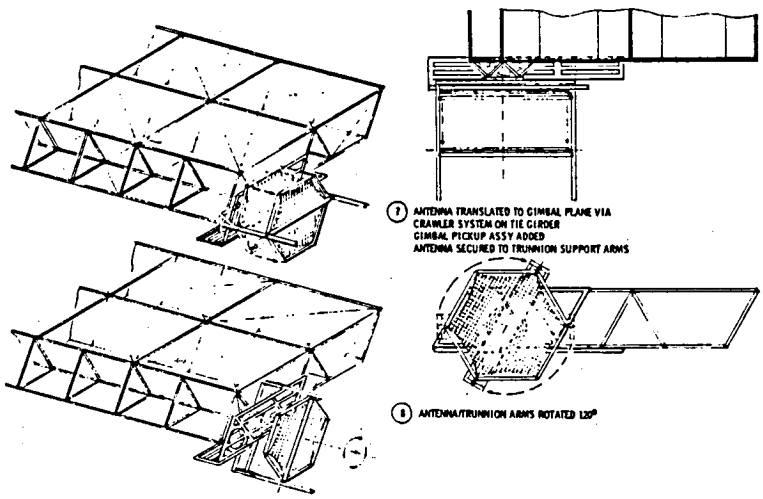

Figure 4.3-7. Antenna Mounting and Rotation

The completed antenna installation is shown in Figure 4.3-8. At this time the temporary tie bar is removed from the antenna frame and installed in the guideways of the trunion support arms to become the permanent antenna maintenance platform. Translation of the platform along the guideways, together with the crawler system which transverses its length, provides access to the entire antenna surface. The platform is stored at the base of the yoke during normal satellite operation.

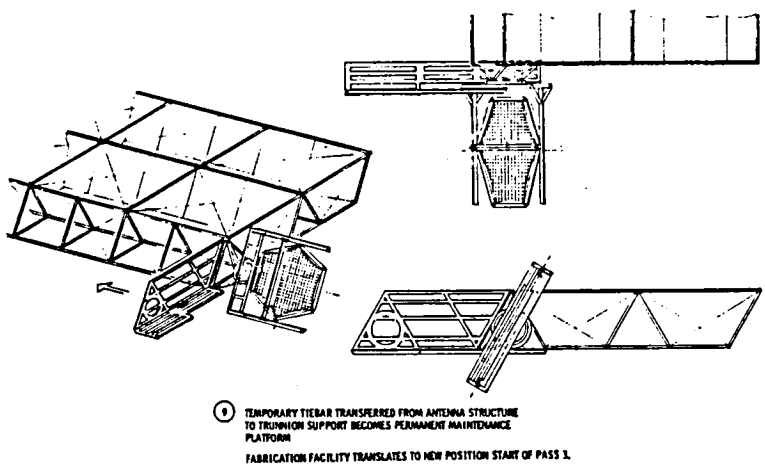

Figure 4.3-8. SCB Translation for Trough 3 Construction

Construction of troughs No. 3 and No. 4 is identical to construction of No's 1 and 2. The completed satellite has been shown in Figure 4.3-9. After checking out the satellite the SCB is secured and flown away to the site for construction of the next satellite.

The completed satellite is shown in Figure 4.3-9. The SCB, which has just finished the fourth pass, will now be detached from the satellite and moved to the next operational satellite location for construction of the satellite.

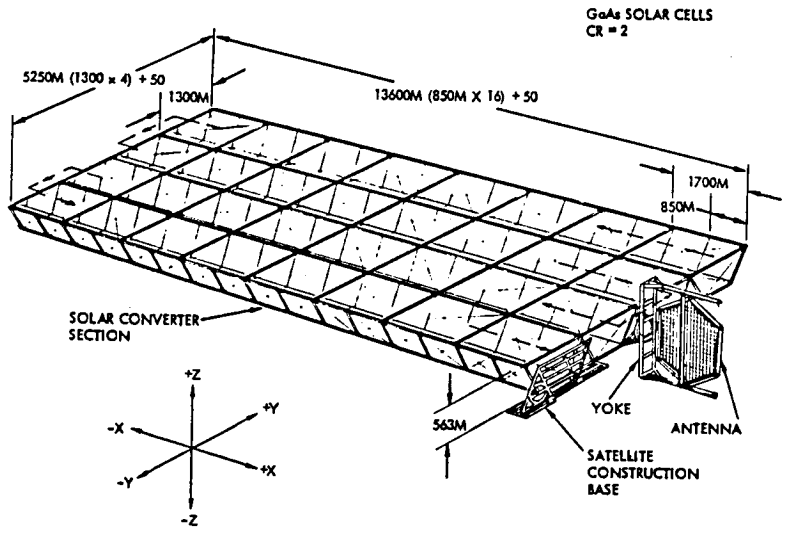

Figure 4.3-9. Completed Satellite

4.4 REFERENCE CONCEPT

4.4.1 SATELLITE DESCRIPTION

The Rockwell configuration (Reference concept) for a coplanar satellite with an end-mounted antenna is shown in Figure 4.4-1. The satellite has three troughs, each with ten bays, and is 3900 meters wide at the longeron points and 16,000 meters long (less antenna). Twenty-four solar blanket strips, measuring 25 meters by 750 meters, are installed in each bay along the bottom of the trough. The reflectors are attached to the inner diagonal sides of the troughs as indicated. The space frame end-mounted antenna with slip rings, support structure, and trunnion arms extends 1750 meters from the basic satellite. The general arrangement of the antenna is contained in Figure 4.4-2. The lower portion of the figure shows the location of the slip rings, or rotary joint with relationship to the cross section of the satellite structure. The support for the trunnion structure is attached to the rotary joint (middle illustration). The trunnion structure (upper view) extends about 625 meters either side of the centerline and provides support for the two longitudinal arms upon which the antenna is mounted. Additional details are contained in Section 2.0.

The satellite mass statement is contained in Table 4.4-1.

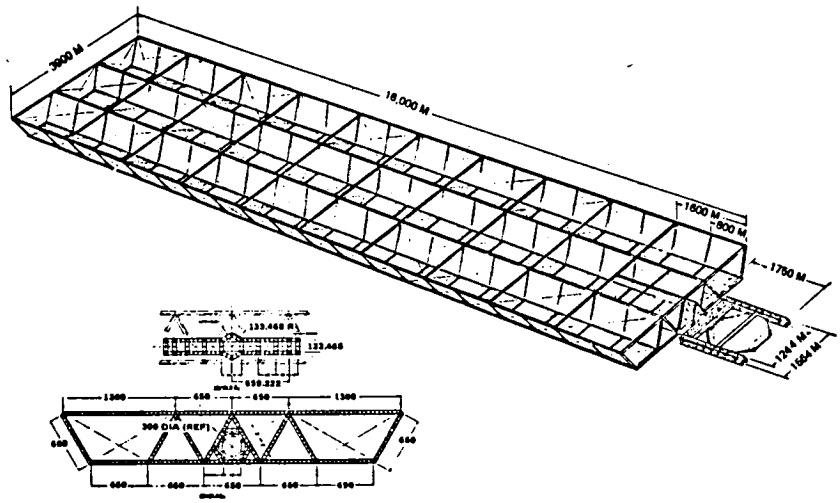

Figure 4.4-1. Reference Configuration SPS

Construction Schedule and Crew Size

Current program ground rules specify a satellite construction rate of two per year over a 30 year period, or 180 days per satellite. The timeline in Figure 4.4-3 conforms to that schedule.

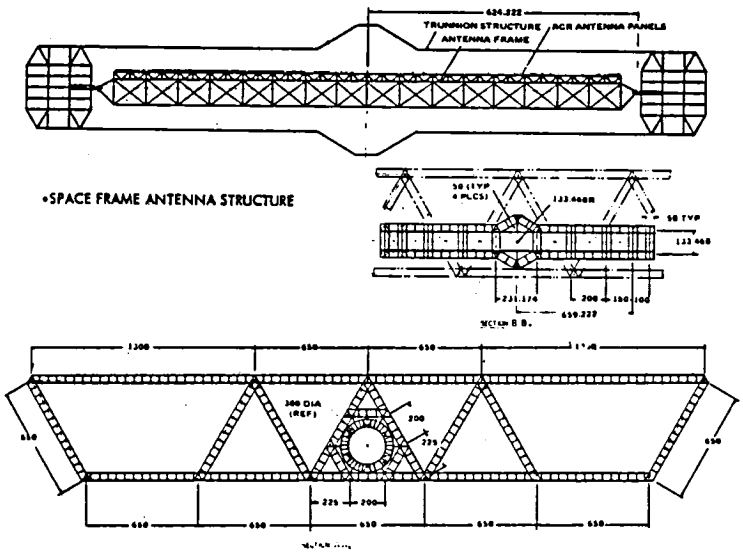

Figure 4.4-2. End Mounted Antenna/Yoke - Cross Section 3-Trough Configuration

Table 4.4-1. Mass Summary (Reference Concept) (10^6 kg)

ITEM	MASS
COLLECTOR ARRAY	
STRUCTURE AND MECHANISMS	1.260
ATTITUDE CONTROL	0.116
SOLAR CONVERTER	7.855
POWER DISTRIBUTION AND CONTROL	2.603
INFORMATION MANAGEMENT AND CONTROL	0.050
	11.884
ANTENNA SECTION	
STRUCTURE AND MECHANISMS	0.977
THERMAL CONTROL	1.408
MICROWAVE POWER	7.012
POWER DISTRIBUTION AND CONTROL	4.505
INFORMATION MANAGEMENT AND CONTROL	0.630
	14.532
TOTAL SATELLITE DRY	26.416
GROWTH 25%	6.604
TOTAL SHUTTLE DRY WITH GROWTH	33.02

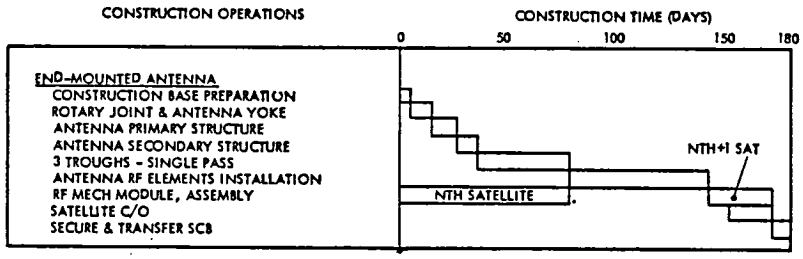

Figure 4.4-3. Satellite Construction Timeline

Table 4.4-2 contains the crew size required to support the construction schedule. The time phasing of the crew size reflects the major events on the timeline (Figure 4.4-3). The operation is based on four shifts; three shifts per day with two days off per week. While construction of the troughs could be started as soon as the slip ring structure is complete, it is not a pacing item and its deferral results in minor crew size reduction.

Table 4.4-2. Crew Size (Reference Concept)

	DAY 1 - 80	DAY 81 - 140	DAY 141 - 180
CONSTRUCTION CREW			
SOLAR CONVERTER CONSTRUCTION	60	-	-
ANTENNA RF ASSY/INSTALLATION	24	24	24
CONSTRUCTION SUPPORT	12	5	5
MAINTENANCE	10	5	5
BASE MANAGEMENT	8	4	4
CREW SUPPORT	12	4	4
TOTAL SHIFT CREW	126	42	42
TOTAL CONST. CREW - 4 SHIFTS	504	168	168
OPERATIONAL MAINTENANCE CREW	-	-	30
TOTAL CREW ON-BOARD	504	168	198

4.4.2 CONSTRUCTION OPERATIONS

Overview

The satellite structure and solar converter is constructed in a single pass, utilizing the integrated SCB described in Section 3.2.1. Initially construction of longitudinal members of the slip ring interface structure is initiated, the members fabricated to a length permitting attachment to the triangular frame (Figure 4.4-4). The first satellite frame is then constructed as shown in Figure 4.4-5, followed by additional fabrication of slip ring longitudinal members until the first triangular frame is positioned properly away from the SCB so that the second triangle can be completed. The SCB then proceeds to fabricate/install the remainder of the satellite structure and solar converter. Concurrently, construction of the slip rings (rotary joint) takes place, utilizing free flying fabrication facilities, (Figure 4.4-6). In the figure, the second satellite frame has been constructed and the slip ring structure has been completed.

Mobile free flying tribeam fabricators as described in Section 3.0 are utilized to construct the slip ring structure, the antenna yoke base, and the arms. The configuration of the fabricator and the structural elements to be fabricated are displayed in Figure 4.4-7.

A layout of the slip rings, yoke, and antenna structure is contained in Figure 4.4-8. The right of the upper illustration shows one 800 meter bay of the satellite, which contains the supporting structure for the slip rings and the slip rings themselves. The yoke is attached to the left-hand portion of the slip ring assembly. The antenna trunnion mountings are contained in the yoke arms as shown. Side elevations of the antenna, the antenna yoke, and the slip ring are in the lower part of the figure.

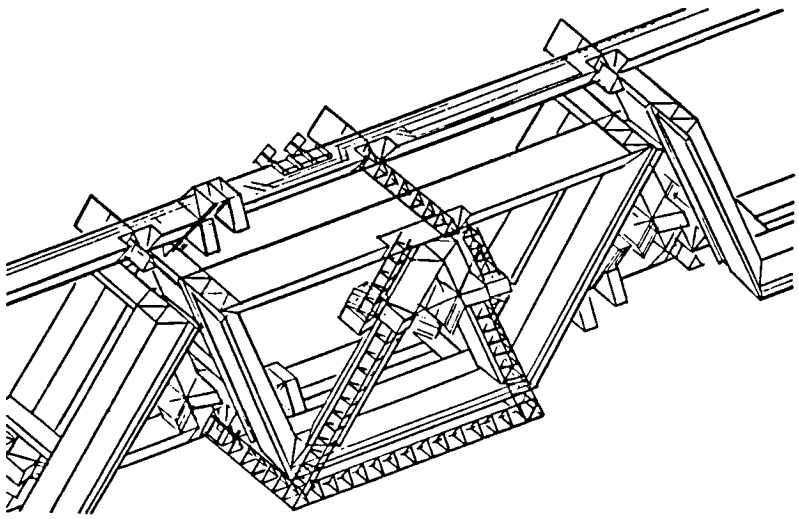

Figure 4.4-4. Slip Ring Interface Structure

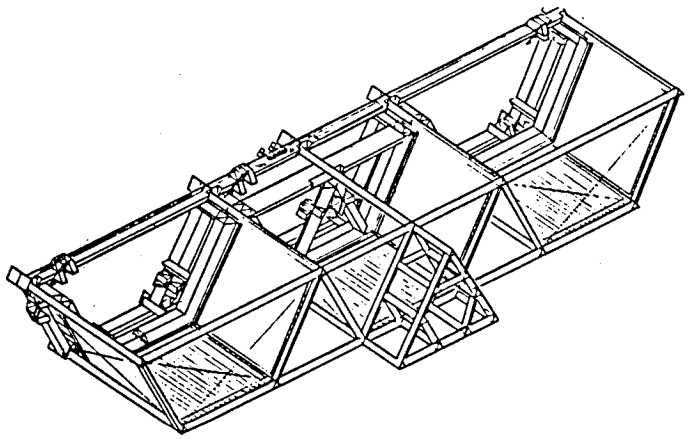

Figure 4.4-5. Solar Array First Frame and Slip Ring Interface Structure

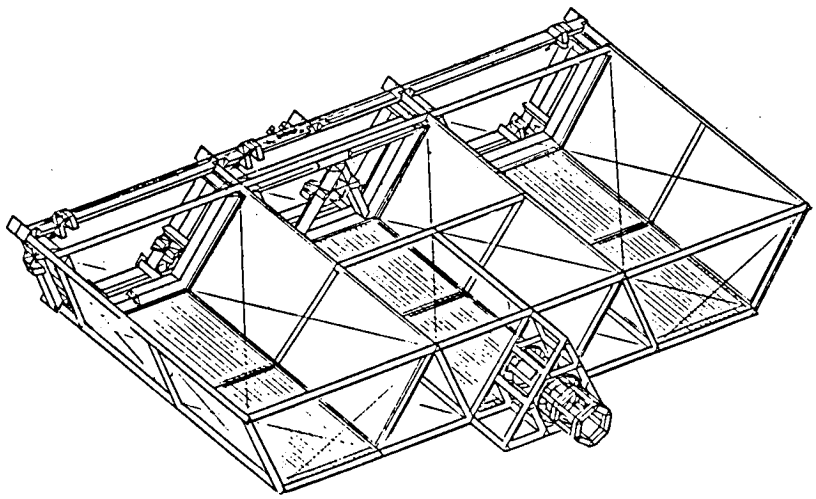

Figure 4.4-6. Slip Ring Structure Independent Fabrication

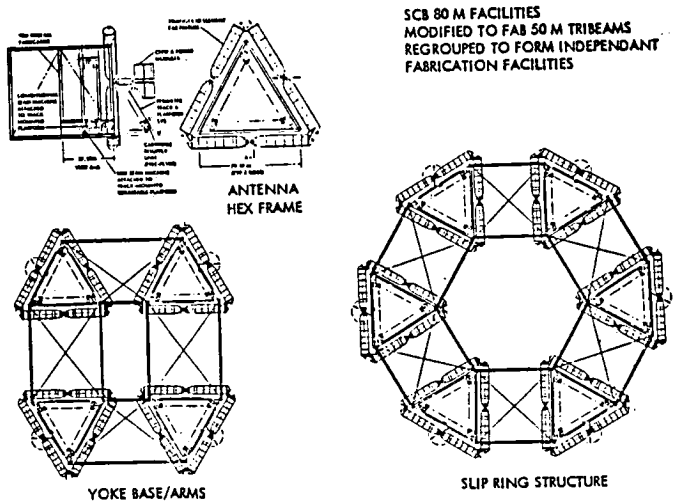

Figure 4.4-7. 50m Tribeam Facility Constellations Fabricates Antenna and Supporting Structure

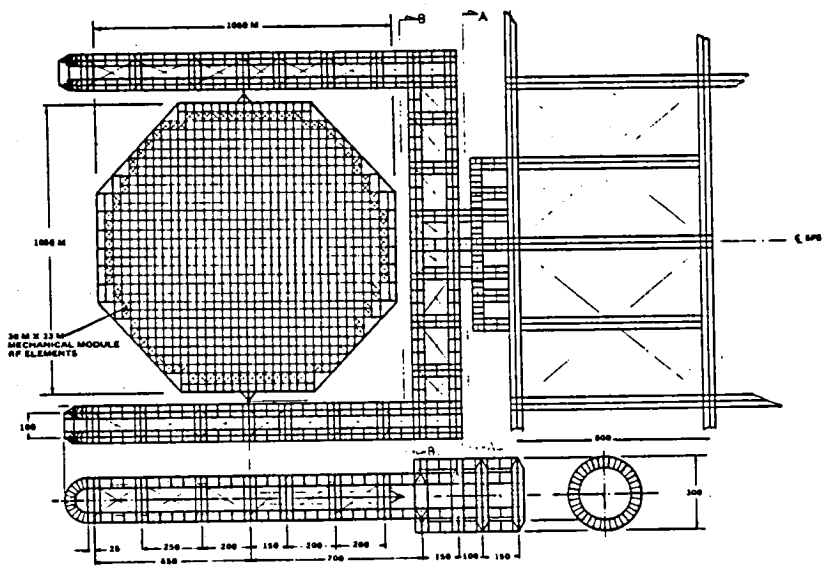

Figure 4.4-8. Slip Ring/Yoke/Antenna Structural Layout Spaceframe Antenna

The assembly operation described above is shown in sequence in Figure 4.4-9, starting with the configuration in the upper left, where the slip ring supporting structure has been completed. In the next view, the slip ring has been fabricated in its position and the yoke interface has been constructed. The last two views show the partially and fully completed yoke structure. The next step in the process consists of fabricating a movable beam which traverses both sides of the yoke arms in tracks and provides a platform for the equipment needed to construct the antenna and install the RF elements. Figures 2.2-26 and 2.2-27 in Section 2.2.3 illustrate the sequence of operations.

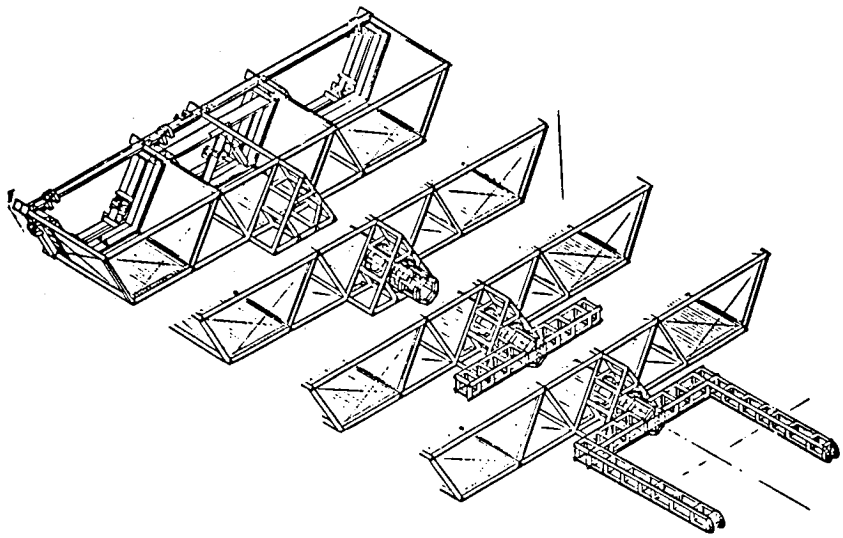

Figure 4.4-9. Antenna Supporting Structure Assembly Sequence

4.4.3 ASSEMBLY EQUIPMENT AND OPERATIONS

Primary Structure Fabrication

The overall satellite structural configuration (Figure 4.4-1) is 16,000 meters in length, divided into twenty 800 meter bays separated by 21 transverse frames.

The satellite primary structure is constructed of 50 meter tribeam girders which utilize the basic 2 meter triangular beam elements for the longitudinal elements at the three corners and for the transverse ties which occur at 50 meter intervals, (Figure 4.4-10). The basic structural 2 meter triangular beam is constructed as a continuous element by a single beam machine which is fed by three cassettes containing prepunched composite ribbons. (Shear stabilization of both the tribeams and the satellite structure is achieved by use of the X-tension cables.)

Tribeam Fabrication. The 50 meter tribeams are also fabricated as coninuous elements. The tribeam fabricator (Figure 4.4-11) is one concept for a unitized 50 meter tribeam builder. The concept utilizes six beam machines to construct each girder; one for each of the three longitudinal members and one for each of the three sides to fabricate the transverse ties.

A side and end elevation of the facility is shown in Figure 4.4-12. Referring to this figure, facilities are provided at the right of the structure for transferring and attaching the 2 meter crossbeams without shutting down the 2 meter longeron beam machines. Other necessary attach fittings also are installed at this station. After beam attachment, the 50 meter beam advances to the next two stations, where tensioning cables are installed and beam alignment completed. The 50 meter longeron is attached to the 50 meter crossbeam at the final station, utilizing manned manipulator modules with a 50-65 meter reach.

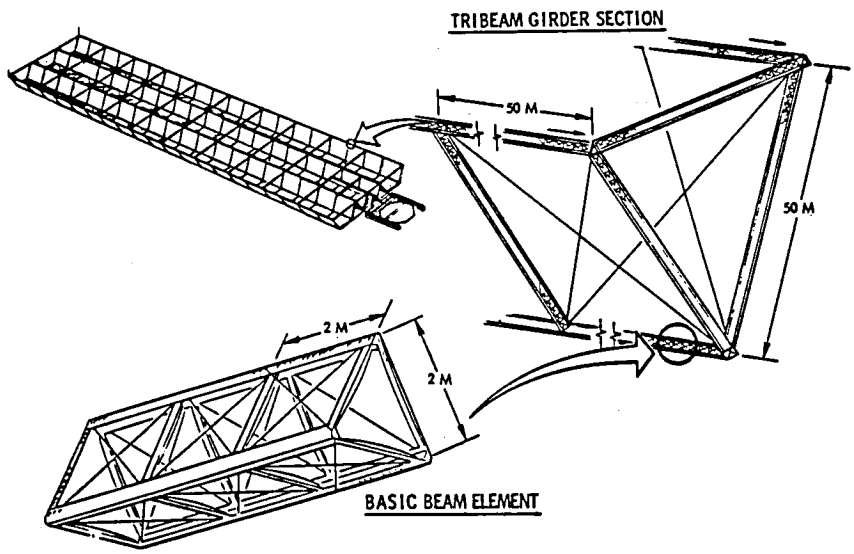

Figure 4.4-10. Primary Structure Evolution

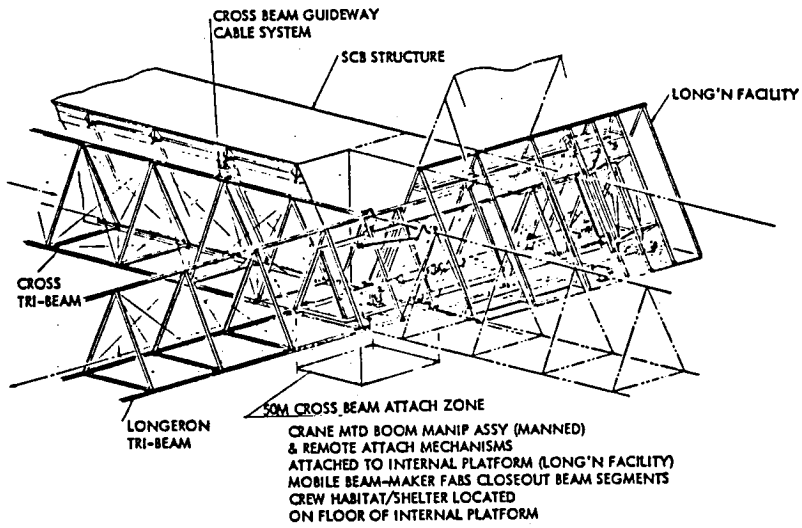

Figure 4.4-11. Longeron Facility (Typical)

Additional detail of this process is illustrated in Figure 4.4-13, which shows installation of a 50 meter crossbeam at the bottom of a trough section. Movable tribeam facilities (A) construct the 50 meter crossbeams, the completed beam advancing to the right in each case. When the beam has advanced to the longeron to which it will be attached, the movable facilities are translated downward to make room for installation of the beam closeout section. Fixed facilities, (B), then fabricate the closeout section, which is translated downward into the proper position for attachment. Figure 4.4-14 shows the cross tribeam and longeron in the process of construction; in Figure 4.4-15 the crossbeam has been completed and the closeout section installed.

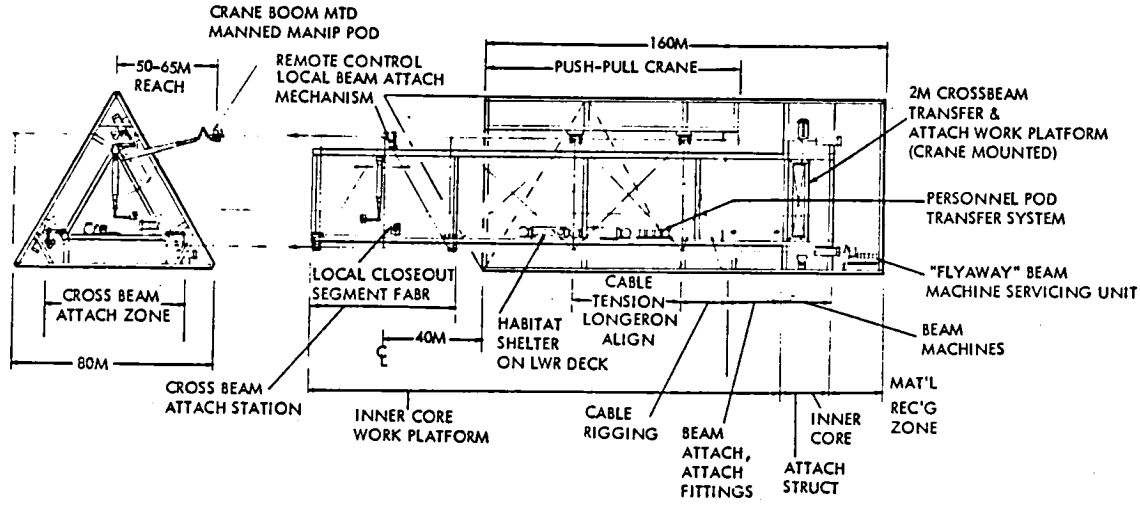

Figure 4.4-12. Longeron Fabrication Facility

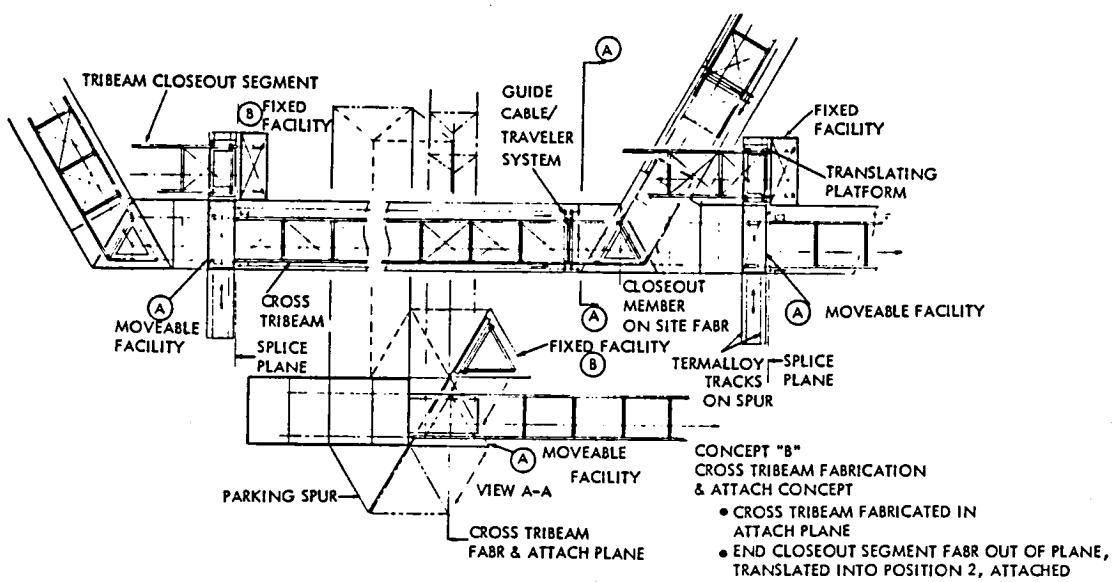

Figure 4.4-13. 50 Meter Crossbeam Installation

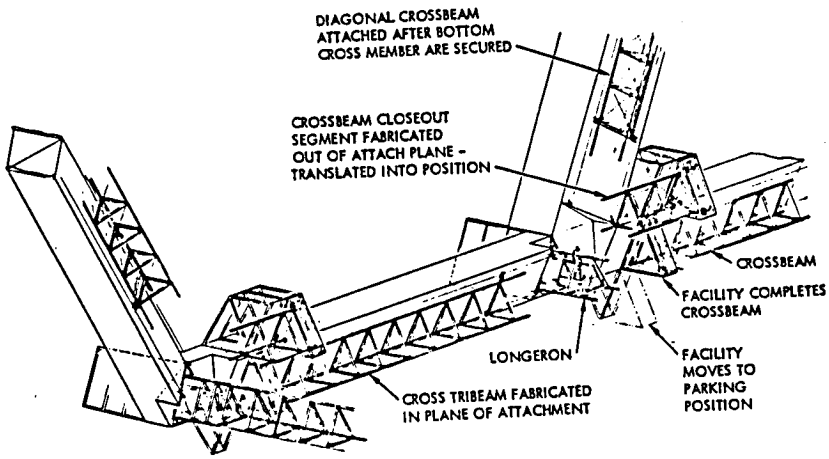

Figure 4.4-14. Typical 3-Way Intersection with Longeron

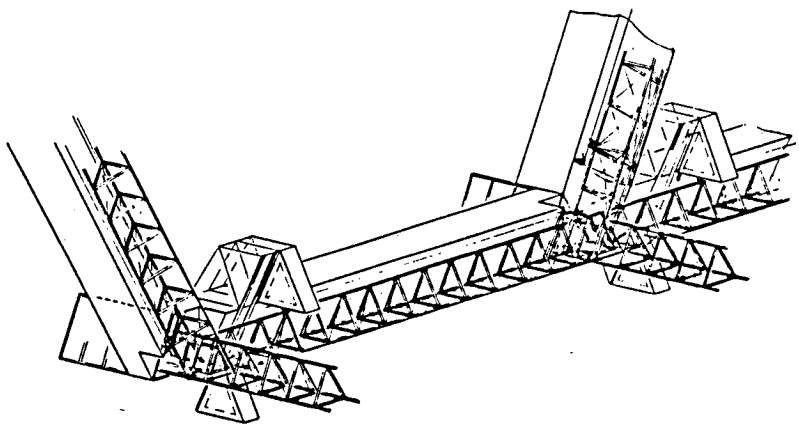

Figure 4.4-15. Crossbeam Attach Configuration

An alternative concept eliminates the need for the extra movable facility shown in Figure 4.4-13. In this concept (Figure 4.4-16), the movable facility has been replaced by relocating the crossbeam fabricator from inside the longitudinal tribeam pod to an adjacent site as shown at the left of the figure. A parking spur for the crossbeam fabricator is provided to permit translation of the fabricator in a downward direction as indicated in view A-A at the bottom of the figure. In addition to the beam machines which construct the basic 50 m crossbeam, additional beam machines are mounted external to the fabricator as shown.

Initially, the crossbeam is fabricated, progressing across the bottom element of the SCB as it advances. When the beam reaches the longitudinal tribeam fabricator, or pod, at the right of the trough bottom (Figure 4.4-17), the crossbeam fabricator is translated downward (view A-A) to position the external beam machines. The closeout elements which consist of 2 m beam sections are then fabricated by the external beam machines and translated into position by manned manipulator modules for attachment utilizing the attach concept described in the next section.

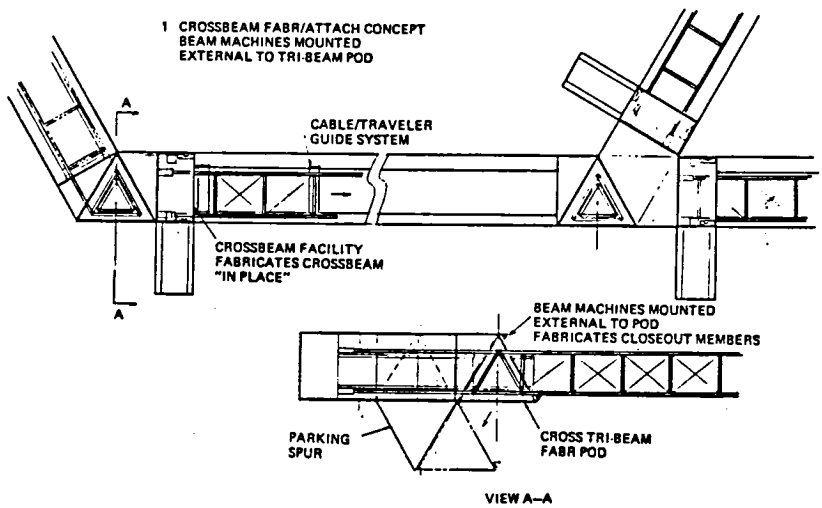

Figure 4.4-16. Construction Concept Crossbeam Fabr/Attach Seq. 1

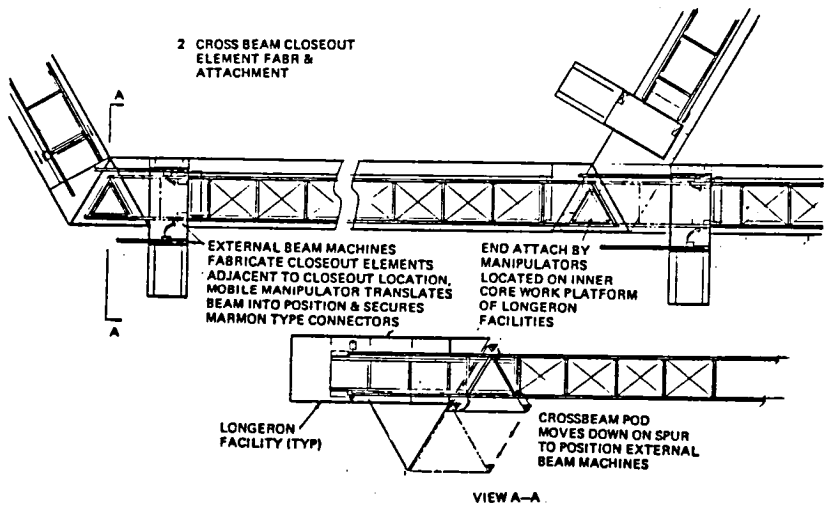

Figure 4.4-17. Construction Concept Crossbeam Fabr/Attach Seq. 2

A perspective of the arrangement contained in Figure 4.4-18 shows additional detail of the parking spur and the external machines locations relative to the longitudinal fabrication facility.

Beam Attach Concept

Various techniques for beam to beam attachment have been proposed. Generally, the large beams which comprise the main elements of a space structure consist of combinations of smaller beams of similar cross section. The Rockwell structural concept (Figure 4.4-10) consists of a basic building block of a

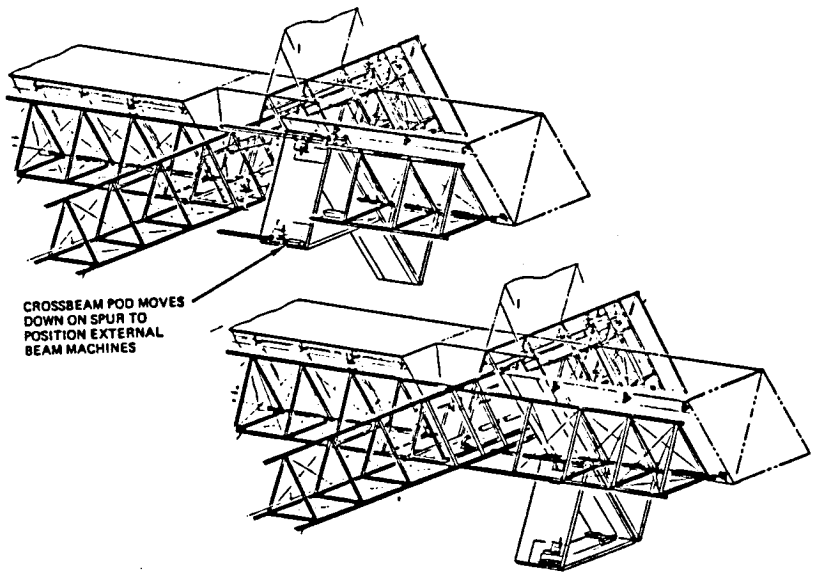

Figure 4.4-18. Construction Concept (Perspective) End Element Fabr. & Attachment

2.083 meter beam from which the 50 meter tribeams are formed. Beam joining, then, devolves into techniques for securing 2 meter beams to each other, since this is the essential element required for the intersection and attachment of the 50 meter tribeam. The operations entailed in the joining process must be adaptable to accomplishment by automatic or semi-automatic (man assist) equipment which does not require EVA.

Several concepts for attaching 2-meter beams have been defined. All of these concepts require further study to identify the specific operations and equipment involved. One such concept is described herein.

Figure 4.4-19 shows two views of the intersection of three 2-meter tribeams. The concept entails use of special fittings which are inserted into the cap section of the beam, either at the end or at locations along the beam length, as required by the geometry of the intersection. The sections marked A and A^1 on the figure are detailed in Figure 4.4-20. In detail A, two end fittings have been inserted into the cap section of the two bottom beams and spot welded in place. An insert fitting, capable of being inserted through lightening holes (Detail A^1) by a special tool has been welded into the proper position on the third beam and two fittings inserted and secured as shown in the upper section of Detail A. These fittings are then mated to the two end fittings and secured by clamps.

Figure 4.4-21 contains the details of B, B^1, C and C^1 of Figure 4.4-19. A tubular section formed in the shape of an angle is utilized to provide a connection between the outer caps of the intersecting beams, reaching from C to B in the left of Figure 4.4-19 and from B^1 to C^1 and then upwards to the cap in the right elevation of the same figure. The configuration of the tube is shown in Figure 4.4-21. Details B and B^1 show the attachment of one end of

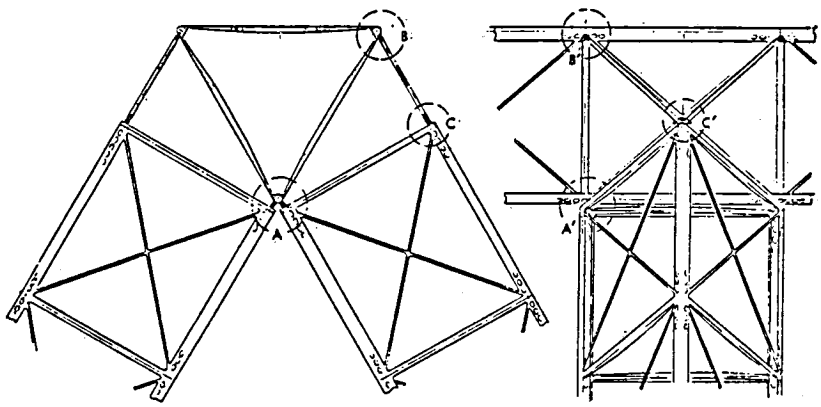

Figure 4.4-19. Reference Configuration Attach Fittings

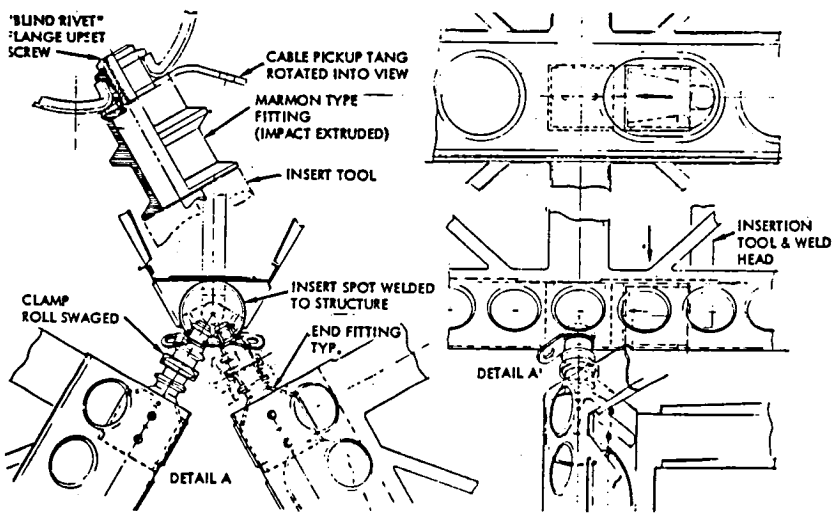

Figure 4.4-20. Reference Configuration Detail A & A[1]

the tube to the cap insert; Detail C and C[1] depict the attachment of the bent and elongated section to the beam end mount insert fitting. Tangs are provided as indicated for cable attach.

Tribeam Fabricator Servicing

There are 27 permanently installed tribeam fabricators utilized for satellite construction. These fabricators are installed in 12 general locations. Each fabricator must be loaded approximately 4 times with 18 cassettes (3 per each of 6 beam machines) to support construction of one satellite. The cassettes are transported from the warehouse area of the SCB to the various locations. This can be done either by a vehicle traveling on tracks or cables, or by a free flyer. The network of tracks (or cables) which would be required for servicing the various locations from the warehouse area is complex and involves

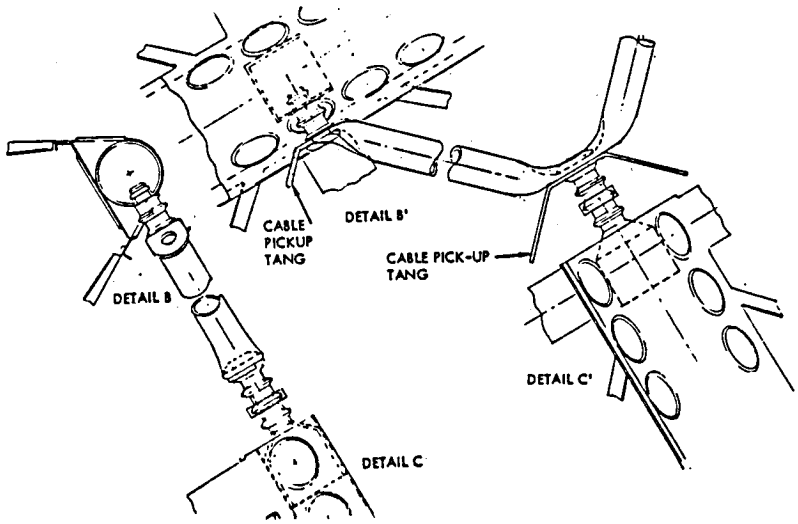

Figure 4.4-21. Reference Configuration

numerous changes of direction, some of which would be difficult to traverse. For these reasons, the free flying mode was selected. The concept (Figure 4.4-22) consists of a chemically propelled and stabilized manned logistics vehicle (LV) capable of transporting 18 cassettes. The cassettes are attached to a conveyor on a detachable flatbed, which permits preparation of one load while the other is being delivered. The loaded LV docks on a track-mounted magnetic docking pad located at the rear of the fabricator. The tracks traverse the three sides of the fabricator, thus providing access by the LV to the six beam machines. Each empty cassette, mounted in a swivel hub and secured at the other end by a yoke arrangement, is removed and replaced by a full cassette. It is noted that the beam machines which construct the cross-beams rotate and translate into position parallel to the longitudinal machines to facilitate unloading and loading.

The initial loading operation is conducted during preparation of the SCB for the next satellite construction. The second operation is conducted following completion of 5 800-m bays. Sufficient LV's are available to permit accomplishment of the estimated 8 hour operation at the various stations within the overall construction timeline. LV propellant requirements are minimal, amounting to approximately 850 kg per sortie.

Figure 4.4-23, a perspective of the previous figure, shows the LV in both the undocked and docked position. In the docked view, the manned module is in the process of removing an empty cassette for stowage on the platform prior to replacing it with a full cassette. The cassette is being removed from a transverse beam machine which has been rotated and translated into servicing position. The tracks to which the docking platform is attached are designed to permit travel to all three corners of the tribeam fabricator.

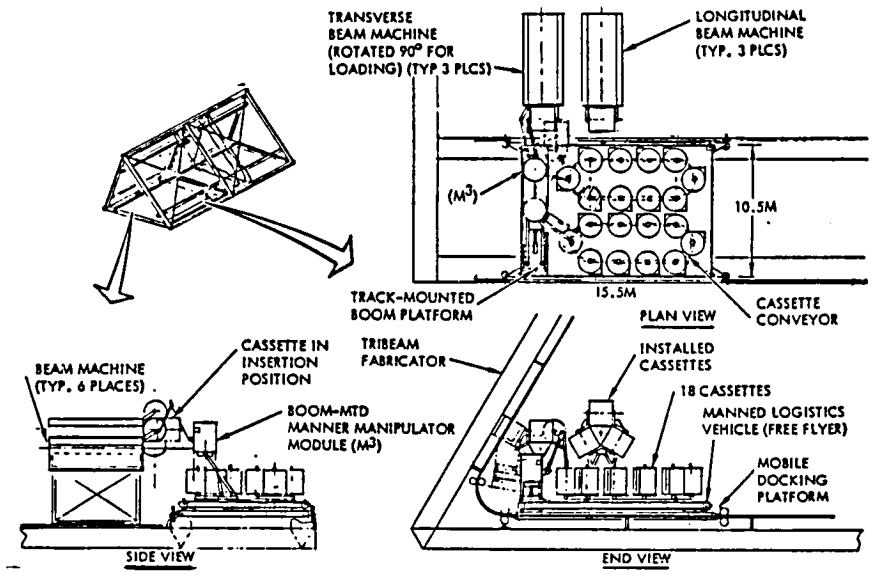

Figure 4.4-22. Tribeam Fabricator Servicing Concept

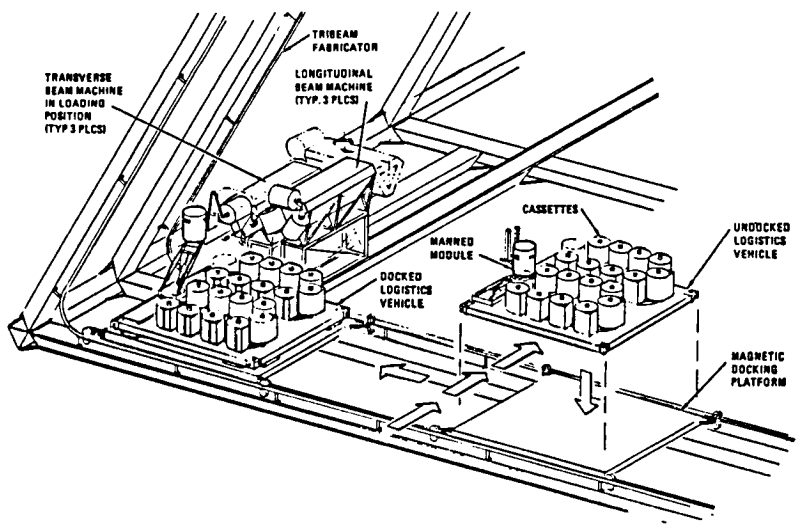

Figure 4.4-23. Free Flying Logistics Vehicle (LV)

Solar Blankets

Solar blankets are deployed along the bottom of each of the three troughs. The general arrangement of the deployment facilities is shown in Figure 4.4-24 for one trough, and is described in more detail later. The blanket dispensers are located on the lower deck (side elevation), and to the left of the blanket attach plane.

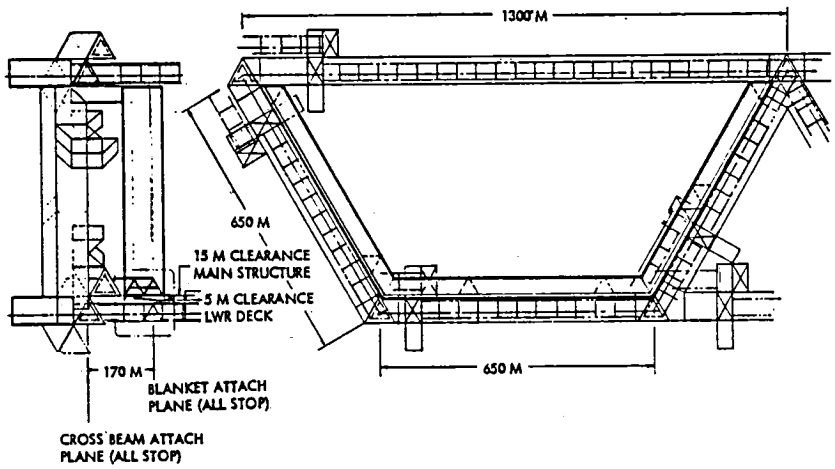

Figure 4.4-24. General Arrangement - Solar Blanket Deployment Facilities

An elevation of the solar blanket deployment facility is contained in Figure 4.4-25. This facility provides for the installation of tension cables, switchgears, distribution feeders, and other equipment associated with the solar blankets. An auxiliary base (15), including crew habitat (17), a docking and service module (16), and a power module (shown to the left of the crew habitat) has been established at each of the three deployment facilities. Previously, all such modules were located at the central habitat/warehousing area on the top of the SCB main deck girder. An evaluation of timelines and the estimated rate of travel of personnel vehicles traversing tracks from the central base to the various deployment areas indicated that considerable time over the nominal eight hour shift would be required for crew rotation. Therefore, the central base size was reduced and the three auxiliary bases added to the concept. Capability has been retained, however, for movement of logistics and personnel to and from the central base to the auxiliary bases, since more extensive warehousing and servicing facilities exist at the central location, and arriving payloads will be a mix.

The top deck of the facility contains a cargo loading deck which can receive cargo from either the central base or from an EOTV via transfer tugs (IOTV's). A warehousing area is provided on the next lower deck (23). Means of transferring material from this area to the main deck are provided by the inter-deck elevator (24), and the material transit system (22). Supply elevators (3) and (9) are utilized for deliveries of material or manned manipulator modules to the lower deck. POTV's arriving from LEO can dock as indicated at the right of the figure (20,21).

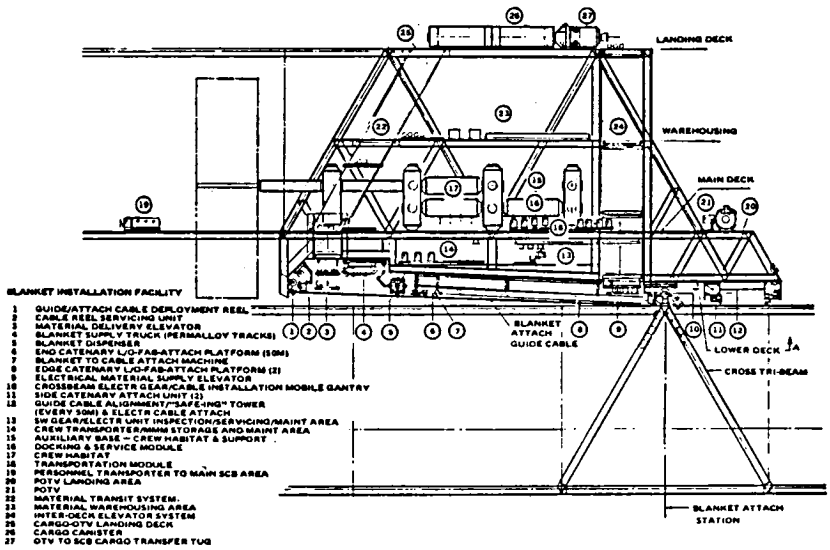

Figure 4.4-25. Solar Blanket Development Facility (Elevation)

The overall installation concept is similar to that described in the Satellite Power Systems Concept Definition Study, Final Report, Volume V, dated April 1978, in that cables and blankets are deployed as the crossbeams to which they are attached advance in the course of main structure fabrication. The satellite (and SCB) configuration has changed since submission of the final report; that factor plus concept update has resulted in the current facility.

The first step in solar blanket deployment is to load the blanket rolls in the twenty-four dispensers (5) installed in each of the three facilities. This is accomplished by a logistics vehicle (4) which traverses the entire trough width, loading each dispenser as it progresses. It is estimated that the vehicle can load the 24 dispensers in 6 hours (15 minutes per dispenser). The dispensers must be loaded prior to the fabrication of each bay, a six shift operation, so additional time is available if required by contingencies.

The blankets are attached to the tension cables which are strung at either side of the blanket strip by an attach machine (7). Other stations for attaching side and end catenaries and electrical components are also shown as indicated in the number index at the left.

The triangular section at the bottom right of Figure 4.4-25 represents the 50 meter crossbeam in the position for attachment of solar blankets, cables, etc., and installation of switchgears and other electrical components.

A perspective of the solar blanket deployment facility (Figure 4.4-26) shows the location of certain stations relative to the bottom of the SCB trough. The numbers are keyed to the numbering index in the preceding figure 4.4-25.

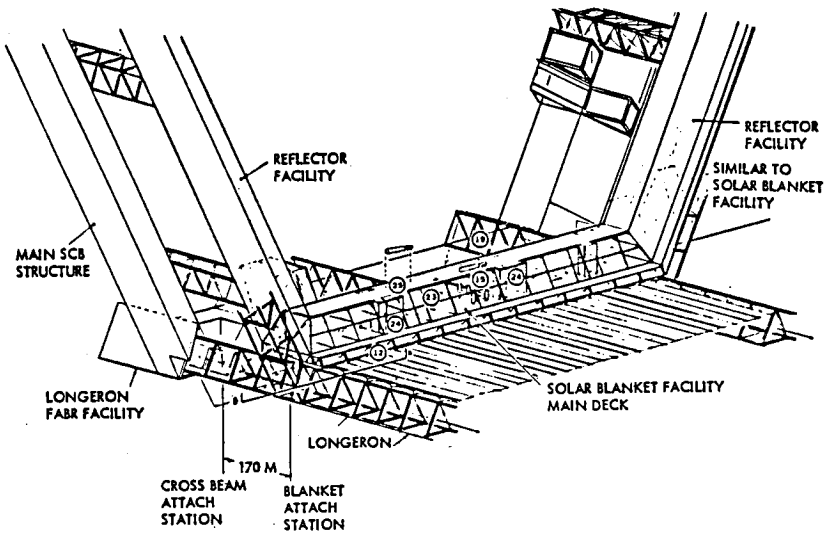

Figure 4.4-26. Solar Blanket Deployment Facilities

Figure 4.4-27 contains a plan view of the facility, looking upward at the lower deck. The apex of the 50 meter crossbeam (Figure 4.4-25) is indicated as the blanket attach station. The guide/attach cable deployment reels (1), are located at the left of the figure. The track-mounted cable reel servicing unit (2), can traverse the entire width of the SCB trough bottom to load the reels and perform any required maintenance. The blanket supply truck (4) is shown adjacent to the blanket dispensers (5). A solar blanket roll (25 m wide) to the left of the truck is being delivered by the elevator.

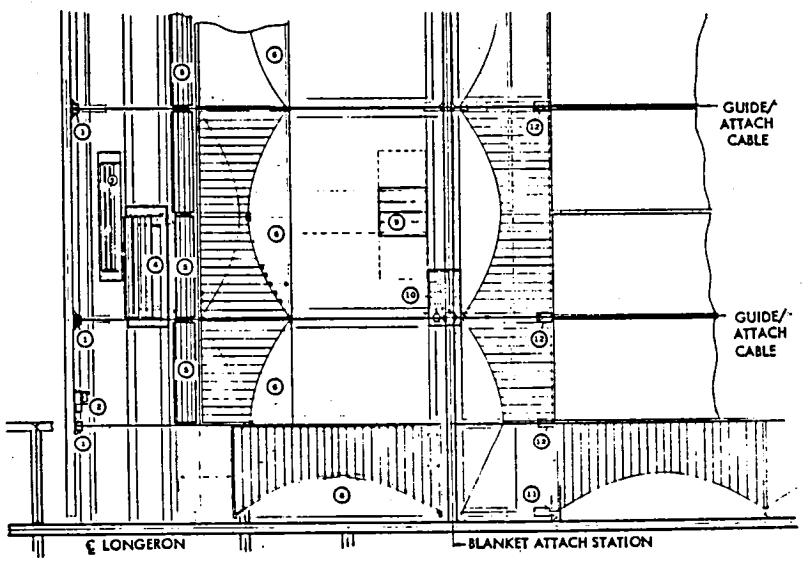

Figure 4.4-27. Solar Blanket Deployment Facilities (Plan View Looking up at Lower Deck)

The end catenaries are 50 m wide, each catenary being attached to two blanket strips. Each blanket roll has half of the catenary attached. These catenaries are attached to form a 50 m wide assembly on the platform (6) which extends across the trough. The side catenaries are assembled on platform (8) and attached to the two outboard solar blanket strips as they deploy.

The guide cable alignment tower (12) has the capability of moving on tracks on the longitudinal direction (see Figure 4.4-25). The tower is utilized to fasten the leading and trailing edge catenary cables to the crossbeam. Additionally, as the cables deploy with the advancing crossbeam, the towers restrain the cables from a direct line to the crossbeam by depressing them so that they are deployed in the proper plane.

A mobile gantry (10) traverses laterally and is used to install the switchgears, sending feeders and other ancillary electrical equipment on the crossbeams at the bottom of the trough. Additional details of this operation are described later.

Figure 4.4-28, a perspective of the preceding figure, shows the location of the numbered items relative to the overall facility structure. The crossbeam upon which the installations are being made is shaded and is to the right center of the figure.

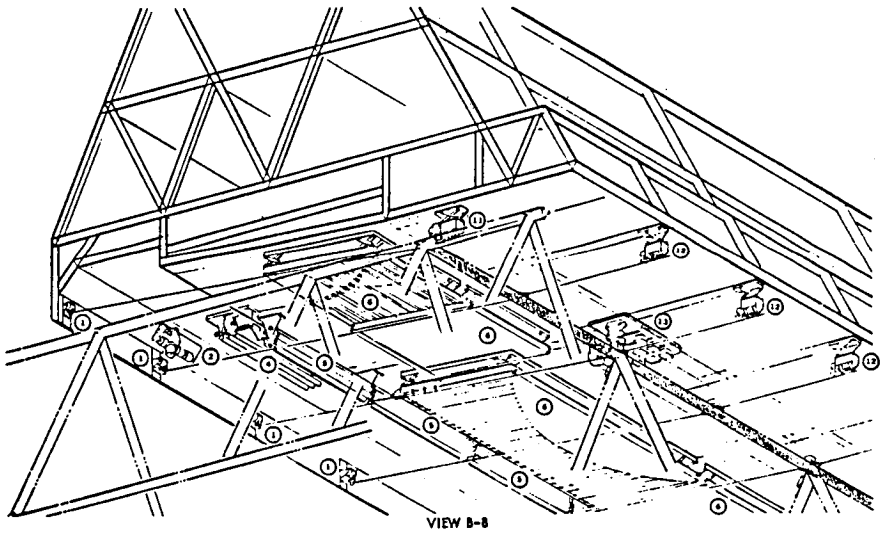

Figure 4.4-28. Solar Blanket Deployment Facility (View Looking Up)

Installation Operations at Crossbeams

Upon completion of crossbeam structure fabrication, the saddle clamps, switch assemblies, and DM&C equipment are installed. Figure 4.4-29 represents the general arrangement of the installation. Secondary feeders and their insulation mounts are included in this installation for alternate crossbeams. The solar blanket trailing edge catenaries and longitudinal cable tensioning

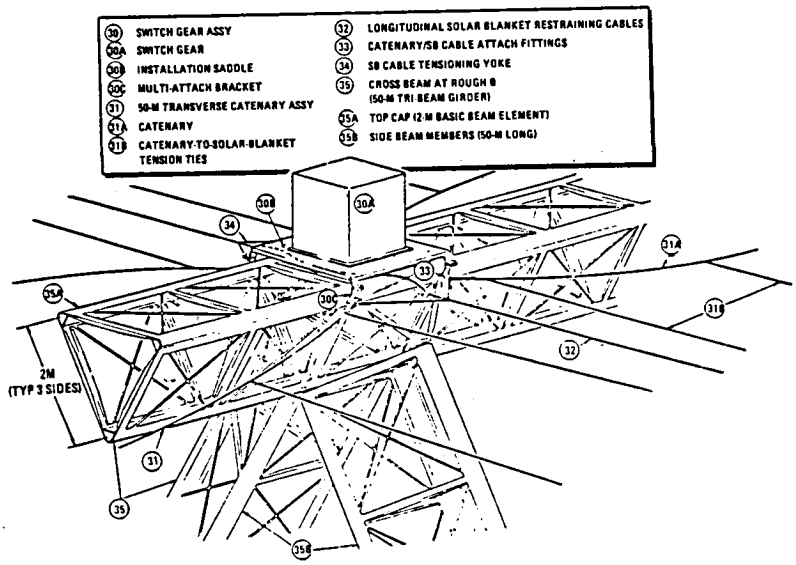

Figure 4.4-29. Installation Operations at Crossbeams

ties are then attached, followed by tensioning and clamping of the transverse catenaries and longitudinal cables. Following this operation, the leading edge of the solar blanket transverse catenaries are attached to the trailing edge of the crossbeam by means of brackets installed on the saddle. The operation at each station is completed by attaching the blanket connectors to the switch assemblies, connecting the DM&C bus, and connecting the switchgears to secondary feeders (alternate crossbeams). Construction of the longerons and crossbeams for the next bay is then initiated.

A timeline encompassing the operations incident to construction of 1 bay is contained in Figure 4.4-30. Two days or six shifts have been allocated for the operation.

OPERATION	DAY	1			2		
	SHIFT	1	2	3	1	2	3
CONSTRUCT & INSTALL BAY N							
FAB LONGERONS & DISPENSE SB'S & REFL'S BAY N							
FAB CB N+1							
BEAM							
END FITTINGS							
ATTACH CB N+1 TO LONGERONS							
ALIGN STRUCTURE							
RELOAD SOLAR BLNKT & REFL. DISPENSERS							
INSTALL EQUIPMENT, MAKE ATTACHMENTS & TENSION AT CBN+1							
INSTALL HARDWARE							
ATTACH & TENSION BLANKETS							
INSTALL/CONNECT ELECT., PWR/DM&C BUSES							
CHECKOUT							

Figure 4.4-30. Solar Converter Construction Sequence Typical Bay

One of the satellite construction guidelines entailed no planned EVA. Accordingly, construction and installation operations concepts have leaned heavily on automated activities, assisted by manned manipulator modules. A typical manipulator module is shown in Figure 4.4-31. It's primary elements

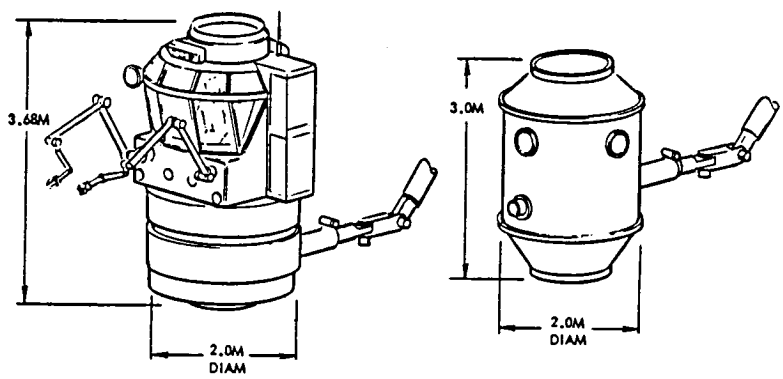

Figure 4.4-31. Manned Manipulator Module and Crew Transport Module

are the control cab, the support base, and the bilateral manipulator. The base rotates around the center line of the boom attach wrist and the control cab rotates 360° around the vertical axis of its base. The cab provides a shirt-sleeve environment, and can be operated by one man, but has sufficient space to accommodate two suited astronauts. The life support system is sized to support three persons for short periods of time (e.g., a rescue operation). One docking port is located at the top of the cab and one at the bottom of the base, providing dual exits. Facility power is provided through the boom. The boom operation is controlled from the cab with secondary control capability at the platform. The MMM contains provisions for lights and TV cameras.

A crew transport module is depicted to the right of the MMM. It's life support capabilities are less than the MMM. It's primary purpose is to rotate MMM crews for operations requiring more than one shift (e.g., solar blanket electrical installation) without having to remove the MMM and replace it with a similar unit.

A traveling gantry, or platform [Item (10) on Figure 4.4-27) installs and connects the electrical components, and attaches and tensions the various cables. The gantry (Figure 4.4-32) is equipped with two MMMs and a switchgear assembly dispenser. The saddle clamp already has been installed on the crossbeam, (this operation taking place in the tribeam fabrication facility) and the cables attached. The MMM to the right has a tensioning tool used to apply the correct tension to the cables and then clamp them. Another view of the tensioning tool is shown in Figure 4.4-33. The tensioning yokes are attached to the brackets (Figure 4.4-32) with the clamp already attached. MMM's apply the tensioning screw jack at the left of the figure until the longitudinal cable is tensioned to the proper value. The end of the tool pushes against the clamp mounted on the yoke to maintain tautness. The cable clamp is then secured to the longitudinal cable.

In Figure 4.4-34, which shows additional detail, the magazine has been indexed to the proper position for installing the switchgear assembly, which is automatically inserted into the keyway on the saddle clamp and locked into position. An electrical connector attached to wiring from the solar array is automatically inserted into its mating receptacle as the assembly advances into position.

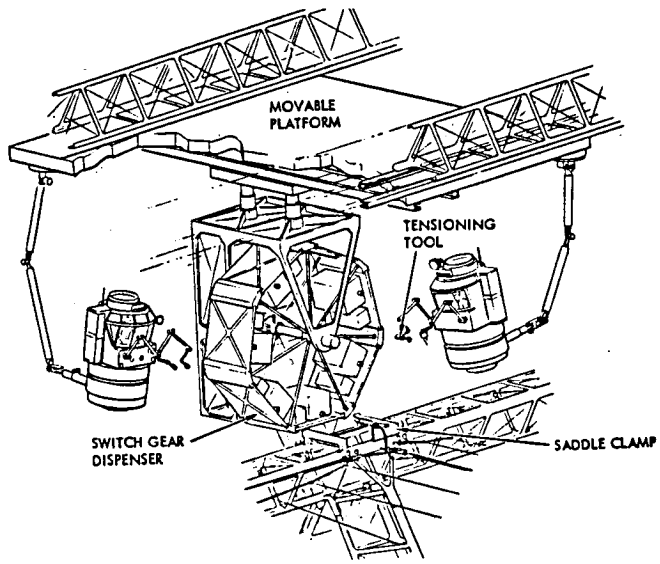

Figure 4.4-32. Switchgear Installation

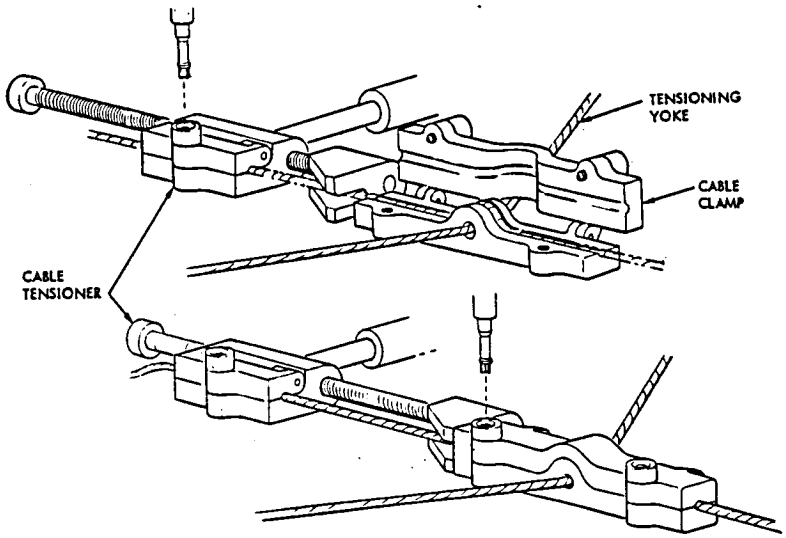

Figure 4.4-33. Cable Tensioning Device

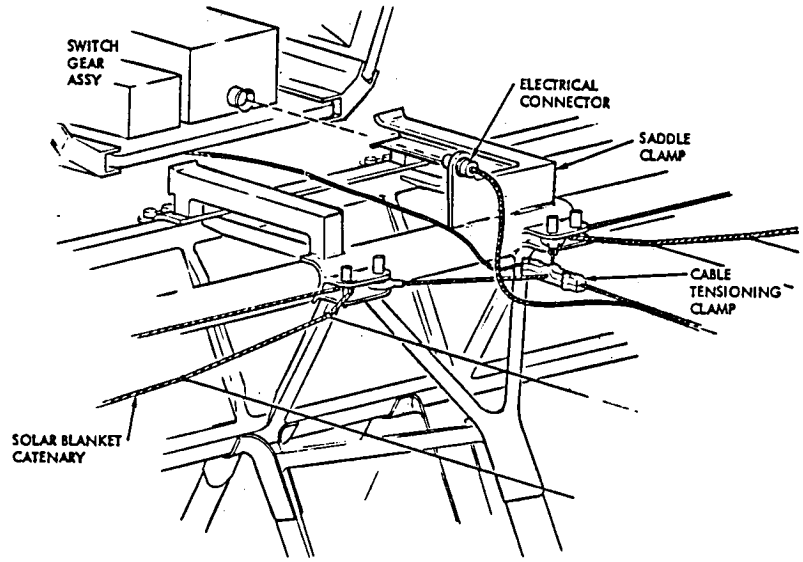

Figure 4.4-34. Switchgear Installation Detail

After the cables have been attached and tensioned and the switchgear assembly installed, secondary feeders must be secured to alternate crossbeams. This process (Figure 4.4-35) utilizes the same gantry previously described. The aluminum feeder roll is mounted on the brackets which are attached to the magazine. As the gantry traverses laterally from one installation point to the next, the feeder is unrolled and welded to insulation mounts which have been installed at the tribeam fabrication facility.

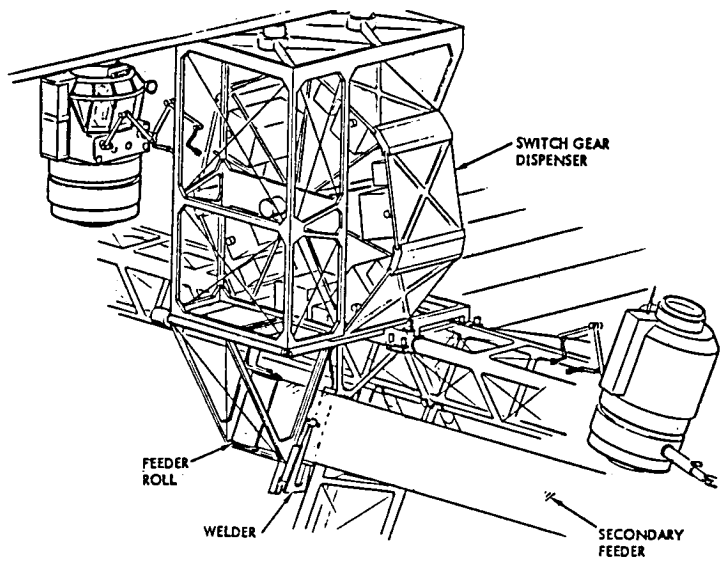

Figure 4.4-35. Secondary Feeder Installation

Antenna Construction

General. The sequence followed in constructing the rotary joint (slip ring) and the antenna supporting structure (Figures 4.4-4 through 4.4-9) was discussed earlier. The overall satellite construction concept requires separation of the SCB from the location in which the antenna will be constructed. A substantial portion of the antenna fabrication operation entails preparation of the RF elements wherein 6993 subassemblies are assembled into 777 mechanical modules. Additionally, 135,684 kliptems must be installed in the mechanical modules. This operation was described in some detail in SD 78-AP-0023-5, Satellite Power Systems (SPS) Concept Definition Study, Final Report Volume V of April 1978. The assembly concepts identified in that report are generally still valid; the notable exception being separation of the SCB from the antenna assembly location. The RF assembly process is extensively automated and requires specialized equipment. In the above referenced report which reflected the Rockwell Point Design of June 1978, the RF assembly and installation facility was an integral part of the SCB. That is no longer the case. However, it is obviously undesirable to construct an RF assembly facility for each of the 60 satellites. Therefore, a concept involving a mobile RF facility (Figure 4.4-36) has been developed. This facility initially will be parked on an upper deck of the SCB, where RF assembly operations will be conducted, (see Figure 4.4-2, Construction Timeline). After completion of the antenna structure, the facility is transferred to the yoke arms to support RF installation operations. When these operations are completed, the facility is transferred back to the SCB and RF assembly for the next satellite is started. Sufficient facilities for removal and replacement of elements up to the size of a mechanical module remain.

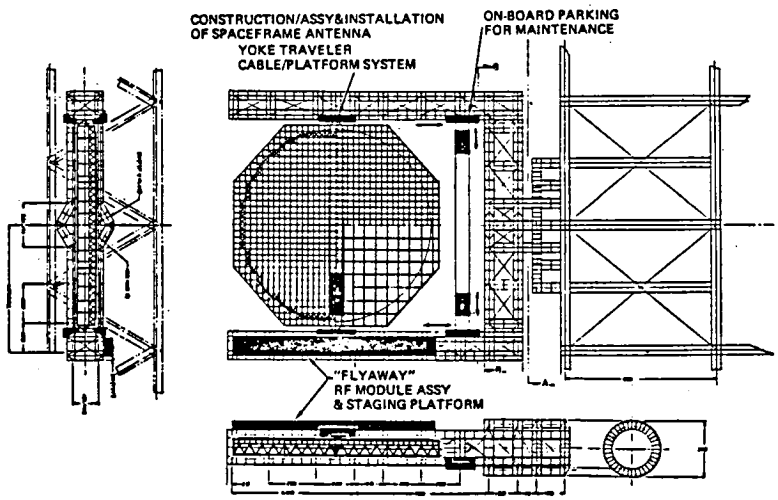

Figure 4.4-36. Antenna Construction Concept "A"

End Mounted Antenna Installation. Three concepts, described below, have been developed for antenna fabrication, RF element installation, and subsequent maintenance activities.

1. Concept A (Figure 4.4-36). This concept utilizes two sets of travelers which move on tracks installed on the yoke arms. Each set consists of two travelers, one on each yoke arm, connected by cables. One set travels on the upper yoke arm surfaces; the other set travels on the bottom of the arms as shown in the figure. Platforms are attached to the cables and can be positioned on the cables as desired. The mobile RF assembly facility is shown in position in the lower yoke arm of the figure. Mobile beam fabricating facilities are parked on the lower traveler cable/platform system.

   Construction of the antenne primary and secondary structure begins at the antenna edge nearest the rotary joint. The lower traveler system fabricates the first structural row (primary and secondary structures) which is secured to the upper traveler system for correct positioning. The second structural row is then fabricated, being connected to the first row during the fabrication process. When the completed structure has progressed to the antenna gimbal plane, the gimbal (or trunnion) interface structure is installed and the partially completed antenna structure connected to the yoke arms by the trunnions joints. At this point, since the structure is attached to the yoke, the upper traveler system can be released from the antenna structure to begin installation of RF elements in that portion of the antenna structure thus far completed. The lower traveler assembly proceeds with the completion of the remainder of the antenna structure.

   Upon completion of the antenna, the RF assembly facility is relocated to the SCB where assembly of RF elements for the next satellite is started. The two traveler cable/platform systems remain in their track on the yoke arms to support antenna maintenance activities after the satellite is operational.

   A perspective of Concept A is depicted in Figure 4.4-37. The traveler set which rides tracks on the upper face of the yoke arms is positioned adjacent to the slip ring, or rotary joint. The platforms which traverse the cables of this set have been positioned and attached to the first structural row of the antenna structure. The other traveler set, which is equipped with cables for securing both primary and secondary structural fabrication equipment, has almost advanced to the gimbal plane of the antenna. The fly away platform used to support assembly and installation of antenna RF elements is shown on the right yoke arm. This facility presently is approximately 1 km in length. It is probable that detailed engineering studies of the equipment and activities required for RF assembly would result in a reduction of facility size.

2. Concept B (Figure 4.4-38). Two sets of gantry platforms, one being the RF assembly facility, have been substituted for the cable/platform arrangement in the previous concept. The structural fabrication concept remains unchanged; the upper gantry holding and positioning structure which has been completed by beam fabrication facilities secured to the lower gantry. Upon structural completion, the RF assembly is utilized for RF installation.

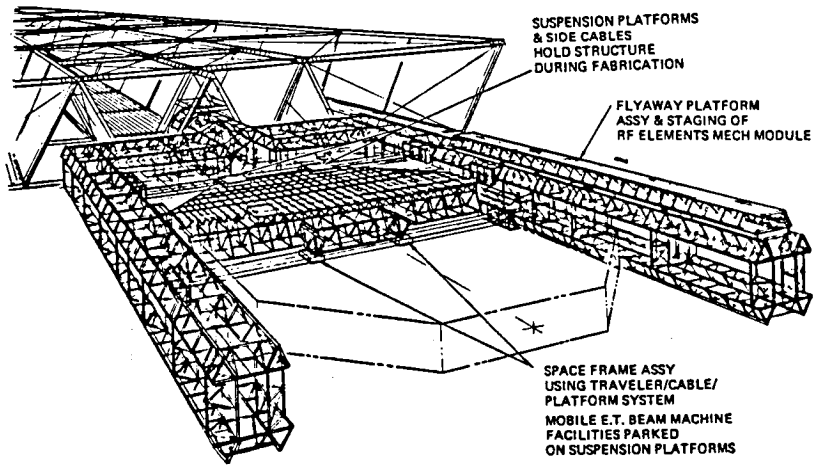

Figure 4.4-37. Antenna Construction Concept "A" (Perspective) Traveler/-Cable/Platform System

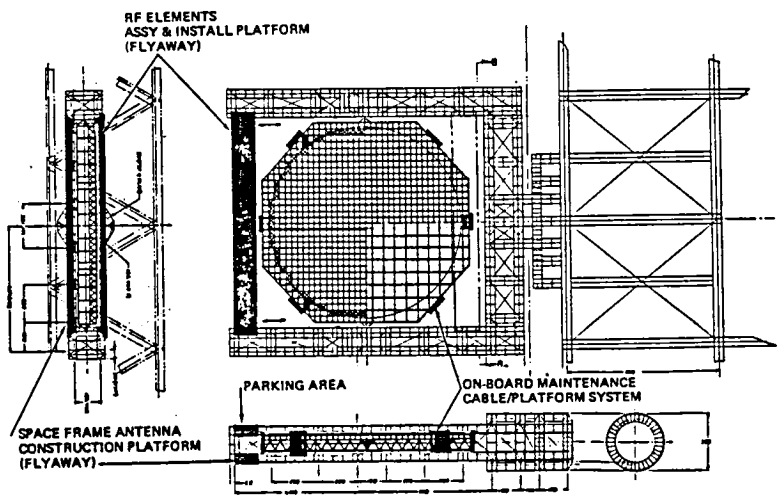

Figure 4.4-38. Antenna Construction Concept "B"

Referring to the plan view of the antenna in Figure 4.4-38, three sets of maintenance platforms have been installed. Each set can traverse opposing sides of the antenna on tracks as shown. The platforms sets are connected by cables which support work platforms and permit their travel across either the face or the rear side of the antenna. These facilities are utilized for final closeout of the overall installation and subsequently for maintenance. The cables will be fabricated from non-conducting material which will not affect the antenna performance.

3. Concept C (Figure 4.4-39). This concept differs from the two preceding concepts in that the initial phase of antenna structural fabrication occurs at the gimbaling center plane, where a diamond shaped girder is constructed, the gimbal interface structure completed, and the trunnion, or gimbal joints installed, securing the girder to the yoke. This operation is accomplished by beam fabricators attached to a cable guideway system on the inner face of the antenna construction/installation platform (ACIP), which moves in tracks on the yoke arm. Upon completion of the central diamond girder the ACIP moves to the next adjacent station to fabricate the next section of the antenna primary and secondary structure. After the antenna structure has been completed, the ACIP is utilized to rig the on-site cable system described in Concept B which is used to install (and subsequently maintain) the antenna RF elements. Assembly of the RF elements takes place on the outer face of the ACIP, which is relocated to the SCB after antenna completion. Provisions for maintenance access to the electrical runs and supporting components on the rear face of the antenna is incorporated within the primary structure.

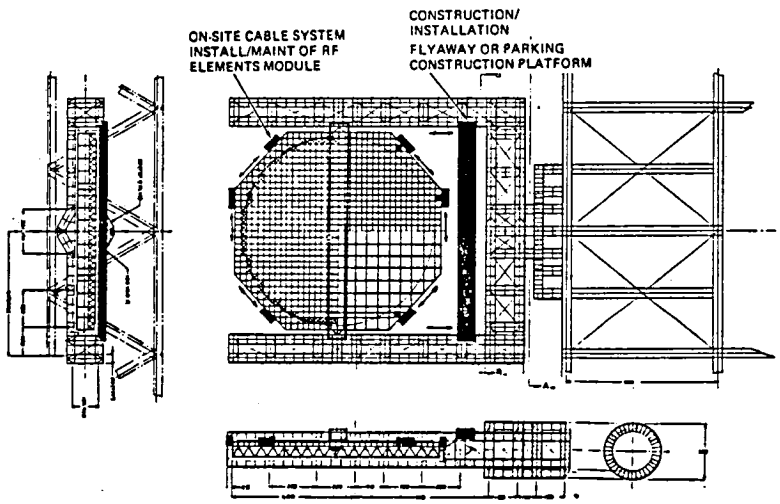

Figure 4.4-39. Antenna Construction Concept "C"

Several other concepts were evaluated. These concepts require utilizing two sets of either gantry platforms or cable-connected travelers for construction and installation operations. By rotating the partially completed antenna 180°, the requirement for gantry/traveler translation to the end of the yoke arms no longer exists and the yoke arms can be reduced to a length just sufficient to accommodate the trunnion joints. Rotation of the antenna also would be required during maintenance to provide 100% accessibility.

Center Mounted Antenna Installation. The general configuration of the three-trough satellite with center mounted antenna is displayed in Figure 4.1-1. The overall timeline for construction of this version differs from the end-mounted configuration primarily in the sequence of events in that the

rotary joint and antenna yoke are constructed after completion of the first wing and before start of the second wing. Additionally, a total of 20 days (vice 10 for the end-mounted version) has been allocated for construction of the rotary joint, supporting structure and antenna frame without impacting the overall 180 day schedule. The antenna yoke (end-mounted antenna) has been replaced by a square structure that completely surrounds the antenna. This structure provides required support for either the gantries or cable-connected travelers which are utilized for both antenna construction and maintenance. An RF assembly and installation platform similar to that described in the above concepts is parked in one side of the square structure which encloses the antenna during RF installation operations; upon completion of these operations it is transferred to the SCB for reuse.

4.5 MASS FLOWS AND TRAFFIC MODEL

Mass flows for both satellite construction and maintenance are contained in Table 4.5-1. A satellite mass of 33.3×10^6 kg was used as a baseline. This includes an allowance for the operational maintenance base and SCB spares as per note (A) of the table.

The satellite construction schedule is shown in the left portion of the table. Although 180 days construction time per satellite has been established, one year has been made available for the first satellite.

Approximately 0.9×10^6 kg of spares must be provided to each satellite on an annual basis. [See Note (B) of the table]. Combining the mass requirements of the satellite construction material, the maintenance base, and spares with the construction schedule and applying the ten percent packaging allowance provides the basis for determining yearly EOTV flights from LEO to GEO in accordance with the payload capacity defined in Note (C) of the table, and for determining yearly HLLV flights required to support the mass flow based on a payload capacity of 227,000 kg.

Satellite construction and maintenance crews must be rotated every 90 days. The portion of the table entitled "Personnel Mass" summarizes the annual POTV flights to GEO [see Notes (C), (D), and (C) of the table], and the HLLV flights required to transport personnel, their consumables, the POTV crew module, and the POTV chemical stages to LEO from the launch site.

On-orbit propellants are required for POTV's and IOTV's. Since the POTV's are refueled in GEO for the GEO-LEO return trip and since a portion of the IOTV's operate exclusively in GEO, propellant for these operations must be transported to GEO via EOTV's. The overall on-orbit propellant requirements, including that required for EOTV flights, are contained in the table, together with the HLLV flights required to deliver the propellant to LEO.

The columns at the right of the table summarize annual and total flights for all vehicles required to support the 30 year satellite construction program. Operational requirements for precursor and EOTV fleet buildup have been added at the bottom of these columns. Establishment of the LEO base and construction of the SCB and precursor test article are supported by the shuttle derived HLLV, since the large HLLV will not be available in that time frame. After the SCB and precursor test article have been completed, an initial fleet of EOTV's will be constructed in LEO, using the SCB as a fabrication fixture. Availability of the HLLV has been assumed for support of this operation.

Since the EOTV's are life limited, a 10 year life being postulated, 26 additional EOTV's will be constructed in GEO at various times during the 30 year program. HLLV and EOTV flights to support this construction have been included but not time phased, since the number of flights required is small compared to the traffic model supporting satellite construction.

It is noted that the total traffic requirements contained in the summary are not exact because of the rounding off process utilized in constructing the table. However, the accuracy is considered to be within 1% and should be sufficient for long range planning.

Table 4.5-1. Space Construction and Operational Scenario (Preliminary)

PROGRAM YEAR	CALENDAR YEAR	SATELLITE CONSTRUCTION SCHEDULE: PER YEAR	SATELLITE CONSTRUCTION SCHEDULE: CUMULATIVE TOTAL	CONSTRUCTION TIME PER SATELLITE (DAYS)	EOTV DELIVERED MASS TO GEO EACH YEAR (INCLUDES 25% GROWTH) (A)	TOTAL CONSTRUCTION MASS TO GEO EACH YEAR (INCLUDES 25% GROWTH)	SATELLITES OPERATIONAL AT YEAR'S END	NUMBER COMPLETED SATELLITE YEARS AT YEAR'S END	EOTV DELIVERED SATELLITE MAINTENANCE MASS DURING YEAR (B)	TOTAL YEARLY MASS TO ORBIT (CONSTRUCTION + MAINTENANCE)	EOTV DELIVERY REQUIREMENTS PER YEAR (CONSTRUCTION + MAINTENANCE + 10% PACKAGE)	EOTV FLIGHTS (C)	HLLV FLIGHTS (C): SCHEDULED EOTV PAYLOAD MASS	HLLV FLIGHTS (C): HLLV FLIGHTS	PERSONNEL MASS: SATELLITE CONST CREW: CREW ROTATION EACH 90 DAYS (600 MEN)	PERSONNEL MASS: SATELLITE CONST CREW: FLIGHTS EACH FOR IOTV AND GROWTH SHUTTLE (D)	PERSONNEL MASS: SATELLITE MAINT CREW: CREW ROTATION EACH 90 DAYS/ SATELLITE YEAR (30 MEN)	PERSONNEL MASS: SATELLITE MAINT CREW: FLIGHTS EACH FOR POTV AND GROWTH SHUTTLE 0.5 FLIGHTS/ ROTATION (D)	PERSONNEL MASS: LEO BASE: CREW ROTATION EACH 90 DAYS (24 MEN)	PERSONNEL MASS: LEO BASE: GROWTH SHUTTLE FLIGHTS	CREW CONSUMABLES (G): SATELLITE CONSTRUCTION CREW: CREW CONSUMABLES AT 0.235×10^6 Kg/CREW ROTATION	CREW CONSUMABLES (G): SATELLITE CONSTRUCTION CREW: EOTV FLIGHTS	CREW CONSUMABLES (G): SATELLITE CONSTRUCTION CREW: HLLV FLIGHTS	CREW CONSUMABLES (G): SATELLITE MAINTENANCE CREW: CREW CONSUMABLES AT 0.01175×10^6 Kg/CREW ROTATION	CREW CONSUMABLES (G): SATELLITE MAINTENANCE CREW: EOTV FLIGHTS	CREW CONSUMABLES (G): SATELLITE MAINTENANCE CREW: HLLV FLIGHTS	CREW CONSUMABLES (G): LEO BASE: CREW CONSUMABLES AT 0.0099×10^6 Kg/CREW ROTATION	CREW CONSUMABLES (G): LEO BASE: HLLV FLIGHTS	TOTAL EOTV FLIGHTS (CONSUMABLES)	TOTAL HLLV FLIGHTS (CONSUMABLES)	ON-ORBIT PROPELLANTS: POTV PROPELLANT GEO - LEO (E)	ON-ORBIT PROPELLANTS: EOTV FLIGHTS FOR POTV PROPELLANT LEO - GEO	ON-ORBIT PROPELLANTS: HLLV FLIGHTS FOR TOTAL POTV PROPELLANT (E)	ON-ORBIT PROPELLANTS: IOTV FLIGHTS IN LEO (CONSTRUCTION + MAINTENANCE)	ON-ORBIT PROPELLANTS: PROPELLANT TO LEO (0.00033 Kg/IOTV FLIGHT)	ON-ORBIT PROPELLANTS: HLLV FLIGHTS - IOTV PROPELLANT	ON-ORBIT PROPELLANTS: IOTV FLIGHTS IN GEO (CONSTRUCTION + MAINTENANCE)	ON-ORBIT PROPELLANTS: PROPELLANT TO LEO AND GEO (0.00033 Kg/IOTV FLIGHT)	ON-ORBIT PROPELLANTS: HLLV FLIGHTS, IOTV PROPELLANT	ON-ORBIT PROPELLANTS: EOTV FLIGHTS, IOTV PROPELLANT	ON-ORBIT PROPELLANTS: EOTV PROPELLANT AT 0.72000 Kg/TRIP (F)	ON-ORBIT PROPELLANTS: HLLV FLIGHTS FOR EOTV PROPELLANTS	SUMMARY: TOTAL POTV FLIGHTS	SUMMARY: TOTAL IOTV FLIGHTS	SUMMARY: TOTAL GROWTH SHUTTLE FLIGHTS	SUMMARY: TOTAL EOTV FLIGHTS	SUMMARY: TOTAL HLLV FLIGHTS	SHUTTLE DERIVATIVES HLLV
1	2000	1	1	360	33.30	33.30	1	0	0.448	33.75	37.13	7	36.19	159	4	40	1	0.5	4	4	0.94	0.2	4.1	.02	0	0	0.04	0.2	0.2	4.3	1.45	0.3	13	194	0.06	0.3	166	0.05	0.2	<0.1	5.53	24	41	360	45	7.5	200.8	
2	2001	2	2,3	180	33.30	66.60	3	1.5	1.343	67.94	74.73	15	77.55	342	4	40	6	3	4	4	0.94	0.2	4.1	.071	0	0.3	0.04	0.2	0.2	4.6	1.53	0.3	13	404	0.13	0.6	342	0.11	0.5	<0.1	11.42	50	43	746	47	15.1	410.7	
3	2002	2	4,5	180	33.30	66.60	5	3.5	3.138	69.74	76.71	15	77.55	342	4	40	14	7	4	4	0.94	0.2	4.1	.165	0	0.7	0.04	0.2	0.2	5.0	1.67	0.3	13	404	0.13	0.6	342	0.12	0.5	<0.1	11.42	50	47	768	51	15.5	413.1	
4	2003	2	6,7	180	33.30	66.60	7	5.5	4.923	71.52	78.67	15	77.55	342	4	40	22	11	4	4	0.94	0.2	4.1	.259	.1	1.1	0.04	0.2	0.3	5.4	1.81	0.4	16	428	0.14	0.6	362	0.12	0.5	<0.1	11.57	51	51	790	55	15.6	415.5	
5	2004	2	8,9	180	33.30	66.60	9	7.5	6.713	73.31	80.64	16	82.72	364	4	40	30	15	4	4	0.94	0.2	4.1	.353	.1	1.6	0.04	0.2	0.3	5.9	1.95	0.4	17	440	0.15	0.7	372	0.12	0.5	<0.1	12.31	54	55	812	59	16.7	442.1	
6	2005	2	10,11	180	33.30	66.60	11	9.5	8.503	75.10	82.61	16	82.72	364	4	40	38	19	4	4	0.94	0.2	4.1	.447	.1	2.0	0.04	0.2	0.3	6.3	2.09	0.4	18	452	0.15	0.7	382	0.13	0.6	<0.1	12.31	54	59	834	63	16.7	443.6	
7	2006	2	12,13	180	33.30	66.60	13	11.5	10.293	76.89	84.58	16	82.72	364	4	40	46	23	4	4	0.94	0.2	4.1	.541	.1	2.4	0.04	0.2	0.3	6.7	2.23	0.4	20	464	0.15	0.7	392	0.13	0.6	<0.1	12.31	54	63	856	67	16.7	446.0	
8	2007	2	14,15	180	33.30	66.60	15	13.5	12.083	78.68	86.55	17	87.89	387	4	40	54	27	4	4	0.94	0.2	4.1	.635	.1	2.8	0.04	0.2	0.3	7.1	2.38	0.5	21	476	0.16	0.7	402	0.13	0.6	<0.1	12.31	54	67	878	71	17.7	474.4	
9	2008	2	16,17	180	33.30	66.60	17	15.5	13.873	80.47	88.52	17	87.89	387	4	40	62	31	4	4	0.94	0.2	4.1	.729	.1	3.2	0.04	0.2	0.3	7.5	2.52	0.5	22	488	0.16	0.7	412	0.14	0.6	<0.1	13.12	58	71	900	75	17.8	475.8	
10	2009	2	18,19	180	33.30	66.60	19	17.5	15.663	82.26	90.49	18	93.06	410	4	40	70	35	4	4	0.94	0.2	4.1	.823	.2	3.6	0.04	0.2	0.4	7.9	2.65	0.5	23	500	0.17	0.7	422	0.14	0.6	<0.1	13.12	58	75	922	79	18.9	503.2	
11	2010	2	20,21	180	33.30	66.60	21	19.5	17.453	84.05	92.46	18	93.06	410	4	40	78	39	4	4	0.94	0.2	4.1	.917	.2	4.0	0.04	0.2	0.4	8.3	2.80	0.5	25	512	0.17	0.7	432	0.14	0.6	<0.1	13.93	61	79	944	83	18.9	505.6	
12	2011	2	22,23	180	33.30	66.60	23	21.5	19.243	85.84	94.42	18	93.06	410	4	40	86	43	4	4	0.94	0.2	4.1	1.011	.2	4.5	0.04	0.2	0.4	8.8	2.94	0.6	26	524	0.17	0.7	442	0.15	0.7	<0.1	13.93	61	83	966	87	18.9	508.2	
13	2012	2	24,25	180	33.30	66.60	25	23.5	21.033	87.63	96.39	19	98.23	433	4	40	94	47	4	4	0.94	0.2	4.1	1.105	.2	4.9	0.04	0.2	0.4	9.2	3.09	0.6	27	536	0.18	0.8	452	0.15	0.7	<0.1	14.00	62	87	988	91	20.0	535.7	
14	2013	2	26,27	180	33.30	66.60	27	25.5	22.823	89.42	98.36	19	98.23	433	4	40	102	51	4	4	0.94	0.2	4.1	1.199	.2	5.3	0.04	0.2	0.4	9.6	3.23	0.6	28	548	0.18	0.8	462	0.15	0.7	<0.1	14.74	65	91	1010	95	20.0	537.1	
15	2014	2	28,29	180	33.30	66.60	29	27.5	24.613	91.21	100.33	19	98.23	433	4	40	110	55	4	4	0.94	0.2	4.1	1.293	.3	5.7	0.04	0.2	0.5	10.0	3.37	0.7	30	560	0.18	0.8	472	0.16	0.7	<0.1	14.74	65	95	1032	99	20.1	540.5	
16	2015	2	30,31	180	33.30	66.60	31	29.5	26.403	93.00	102.30	20	103.40	456	4	40	118	59	4	4	0.94	0.2	4.1	1.387	.3	6.1	0.04	0.2	0.5	10.4	3.51	0.7	31	572	0.19	0.8	482	0.16	0.7	<0.1	14.88	66	99	1054	103	21.1	567.9	
17	2016	2	32,33	180	33.30	66.60	33	31.5	28.193	94.79	104.27	20	103.40	456	4	40	126	63	4	4	0.94	0.2	4.1	1.481	.3	6.5	0.04	0.2	0.5	10.8	3.65	0.7	32	584	0.19	0.8	492	0.16	0.7	<0.1	15.62	69	103	1076	107	21.2	569.3	
18	2017	2	34,35	180	33.30	66.60	35	33.5	29.983	96.58	106.24	21	108.57	478	4	40	134	67	4	4	0.94	0.2	4.1	1.575	.3	6.9	0.04	0.2	0.5	11.2	3.80	0.7	33	596	0.20	0.9	502	0.17	0.7	<0.1	15.62	69	107	1098	111	22.2	595.8	
19	2018	2	36,37	180	33.30	66.60	37	35.5	31.773	98.37	108.21	21	108.57	478	4	40	142	71	4	4	0.94	0.2	4.1	1.667	.3	7.3	0.04	0.2	0.5	11.6	3.94	0.8	35	608	0.20	0.9	512	0.17	0.7	<0.1	16.44	72	111	1120	115	22.2	598.2	
20	2019	2	38,39	180	33.30	66.60	39	37.5	33.563	100.16	110.18	21	108.57	478	4	40	150	75	4	4	0.94	0.2	4.1	1.763	.3	7.7	0.04	0.2	0.5	12.0	4.08	0.8	36	620	0.20	0.9	522	0.17	0.7	<0.1	16.44	72	115	1142	119	22.3	599.6	
21	2020	2	40,41	180	33.30	66.60	41	41.5	37.143	103.74	114.11	22	113.74	501	4	40	158	79	4	4	0.94	0.2	4.1	1.857	.4	8.2	0.04	0.2	0.6	12.5	4.22	0.8	37	632	0.21	0.9	532	0.18	0.8	<0.1	17.25	76	119	1164	123	23.4	628.2	
22	2021	2	42,43	180	33.30	66.60	43	43.5	38.933	105.53	116.08	22	113.74	501	4	40	166	83	4	4	0.94	0.2	4.1	1.951	.4	8.6	0.04	0.2	0.6	12.9	4.36	0.8	38	644	0.21	0.9	542	0.18	0.8	<0.1	17.25	76	123	1186	127	23.4	629.6	
23	2022	2	44,45	180	33.30	66.60	45	45.5	40.723	107.32	118.05	23	118.91	524	4	40	174	87	4	4	0.94	0.2	4.1	2.045	.4	9.0	0.04	0.2	0.6	13.3	4.51	0.9	40	656	0.22	1.0	552	0.18	0.8	<0.1	18.01	79	127	1208	131	24.4	635.1	
24	2023	2	46,47	180	33.30	66.60	47	47.5	42.513	109.11	120.02	23	118.91	524	4	40	182	91	4	4	0.94	0.2	4.1	2.139	.4	9.4	0.04	0.2	0.6	13.7	4.65	0.9	41	667	0.22	1.0	563	0.19	0.8	<0.1	18.01	79	131	1230	135	24.5	659.5	
25	2024	2	48,49	180	33.30	66.60	49	49.5	44.303	110.90	121.99	24	124.08	547	4	40	190	95	4	4	0.94	0.2	4.1	2.233	.4	9.8	0.04	0.2	0.6	14.1	4.79	0.9	42	679	0.22	1.0	573	0.19	0.8	<0.1	18.01	79	135	1252	139	24.5	660.9	
26	2025	2	50,51	180	33.30	66.60	51	51.5	46.093	112.69	123.96	24	124.08	547	4	40	198	99	4	4	0.94	0.2	4.1	2.327	.5	10.3	0.04	0.2	0.7	14.6	4.93	1.0	43	691	0.23	1.0	583	0.19	0.8	<0.1	18.94	83	139	1274	143	25.6	689.4	
27	2026	2	52,53	180	33.30	66.60	53	53.5	47.883	114.48	125.93	24	124.08	547	4	40	206	103	4	4	0.94	0.2	4.1	2.421	.5	10.7	0.04	0.2	0.7	15.0	5.07	1.0	45	703	0.23	1.0	593	0.20	0.9	<0.1	18.94	83	143	1296	147	25.6	691.9	
28	2027	2	54,55	180	33.30	66.60	55	55.5	49.673	116.27	127.90	25	129.25	569	4	40	214	107	4	4	0.94	0.2	4.1	2.515	.5	11.1	0.04	0.2	0.7	15.3	5.21	1.0	46	715	0.24	1.0	603	0.20	0.9	<0.1	19.01	84	147	1318	151	25.7	694.2	
29	2028	2	56,57	180	33.30	66.60	57	57.5	51.463	118.06	129.87	25	129.25	569	4	40	222	111	4	4	0.94	0.2	4.1	2.609	.5	11.5	0.04	0.2	0.7	15.4	5.36	1.0	47	727	0.24	1.0	613	0.20	0.9	<0.1	19.01	84	151	1340	155	26.7	720.3	
30	2029	2	58,59	180	33.30	66.60	59	57.5	51.463	118.06	129.87	25	129.25	569	4	40	230	115	4	4	0.94	0.2	4.1	2.701	.5	11.9	0.04	0.2	0.7	16.1	5.50	1.0	48	739	0.24	1.0	623	0.21	0.9	<0.1	19.70	87	155	1362	159	26.7	722.0	
31	2030	1	60	180	33.30	33.30	60	59.5	53.253	86.55	95.21	18	93.06	410	2	20	238	119	2	2	0.47	0.1	2.1	2.797	.5	12.3	0.04	0.1	0.6	16.5	4.93	1.0	43	547	0.18	0.8	462	0.15	0.7	<0.1	14.45	64	139	1009	141	19.6	535.0	
						1998		915	819.4	2817.4	3100	600	3102	13,666	122	1220	3661	1831	122	122	28.67	6.1	125	43.04	8	190	1.22	6.1	15.0	322	108.22	21	951	17,322	5.71	25	14,613	4.84	21	1	469.1	2064	3051	31,935	3173	637	17,049	0

(A) SATELLITE MASS, 26,416 + 25% GROWTH = 33.02
OPER MAINT BASE, 0.122×10^6 + 25% GROWTH = 0.15
SCB SPARES, 0.100×10^6 + 25% GROWTH = 0.13
33.30×10^6 Kg TOTAL EOTV DELIVERED MASS FOR CONSTRUCTION OF EACH SATELLITE

(B) SATELLITE MAINTENANCE MASS (SPARES), 0.716 + 25% GROWTH = 0.895×10^6 Kg/SATELLITE YEAR

(C) EOTV PAYLOAD CAPACITY = 5.17×10^6 Kg. HLLV PAYLOAD CAPACITY = 0.227×10^6 Kg

(D) ONE POTV FLIGHT REQUIRED FOR 60 CREWMEN ROUND TRIP (LEO-GEO-LEO), ONE GROWTH SHUTTLE (CREW MODULE) REQUIRED FOR 60 MAN CREW TO LEO

(E) 35,475 Kg PROPELLANT (INCLUDING TANKAGE AND PACKAGING) DELIVERED TO GEO FOR ONE POTV GEO-LEO TRANSFER. 67,720 Kg PROPELLANT DELIVERED TO LEO VIA HLLV FOR EACH POTV ROUND TRIP

(F) 737,000 Kg (INCLUDING TANKAGE AND PACKAGING) REQUIRED FOR ONE EOTV LEO-GEO-LEO TRIP

(G) 391.6 Kg (INCLUDING 10% PACKAGE) PER EACH CREWMAN ROTATION (90 DAYS)

PRECURSOR						
LEO BASE (5 MODULES)						5
SCB MASS (5.3×10^6 Kg)						53
PRECURSOR TEST ARTICLE (5.4×10^6 Kg)						55
6 EOTV'S + PROP (11.62×10^6 Kg)						
12 CREW ROTATIONS AT 360 PER CREW					51	
CREW CONSUMABLES (1.69×10^6 Kg)			72			16
EOTV CONST						
EOTV BUILDUP (26.3×10^6 Kg TO GEO)				5	116	
EOTV PROP - 5 FLTS (3.69×10^6 Kg)					16	
TOTAL	3051	31,935	3245	642	17,232	129

4.6 CREW SIZE ESTIMATES

4.6.1 ORBITAL PERSONNEL REQUIREMENTS

An initial evaluation of total personnel requirements for orbital operations was conducted as part of Task 2.2.5. The evaluation was confined to crews required for satellite construction and maintenance, and for routine operations of the LEO facility. Although HLLV concepts under consideration may require more than one LEO facility because of launch window constraints, only one facility was considered for this first estimate. Crew sizes utilized for satellite maintenance and for the LEO base were those contained in Volume V of Satellite Power Systems (SPS) Concept Definition Study, final report (SD 78-AP-0023-5). The satellite construction crew size, including SCB support personnel, has been revised to reflect the new satellite configuration and further updates may be required. Therefore, a crew size of 600 has been assumed as a representative figure. These crew sizes are summarized below:

Satellite Construction and SCB Support	600
Satellite Maintenance	30
LEO Base (less EOTV Construction)	2+

Radiation exposure is considered the limiting factor for defining crew continuous on-orbit stay time per tour and lifetime allowable number of tours. For this analysis, each crew is rotated every 90 days and a maximum of five orbital tours per man was postulated, with a minimum of six months between tours. This is well below the limits of Table 4.6-1. Figure 4.6-1 contains a crew utilization timeline which is compatible with these exposure criteria. It is noted that four months of the interval between orbital tours are allocated to training other crews and to preparation for the next tour. Effective utilization of orbital crews between tours (particularly if the six months ground tour is increased) requires more detailed study, since orbital crews outnumber launch site personnel by a considerable margin, making a man-for-man relief unfeasible.

HLLV pilots have not been considered in this analysis. Their exposure time per mission is limited and confined to LEO, and shielding is provided by the HLLV. Therefore, there should be no constraints on the number of missions per pilot.

Required crew rotations to support construction of 60 satellites total 120, which results in 24 crews or 14,400 men. Applying a 20% attrition factor (resignations, etc.) raises this figure to 17,280. Similarly, 3,660 maintenance crew rotations at 30 men per crew and including attrition generate a requirement for 26,352 men. An additional 691 men are needed to operate one LEO facility for 30 years. Figure 4.6-2 shows manpower requirements for those three operations over a 30 year period. The slope of the curves are based on an interval of six months between orbital tours. Any increase in this interval will affect portions of the slope but will not change the final cumulative figures, providing the five tours per crew are maintained.

Table 4.6-1. Allowable Times Due to Radiation Doses in GEO

	PER MONTH	PER QUARTER	PER YEAR	PER CAREER
EVA (1 GM/CM^2)	(Hrs)	(Hrs)	(Hrs)	(Hrs)
BONE MARROW	500	700	1500	8000
SKIN	150	210	450	2400
EYES	92.5	130	280	1500
TESTES	130	180	380	2000
CABIN (2 GM/CM^2)	(Days)	(Days)	(Days)	(Days)
BONE MARROW	250	350	750	4000
SKIN	150	210	450	2400
EYES	92.5	130	280	1500
TESTES	86.5	120	253	1333
EYES LIMIT EVA TO ~35 DAYS/YEAR (8 HRS/DAY)				
TESTES LIMIT CABIN OCCUPANCY TO ~8 MONTHS/YEAR				

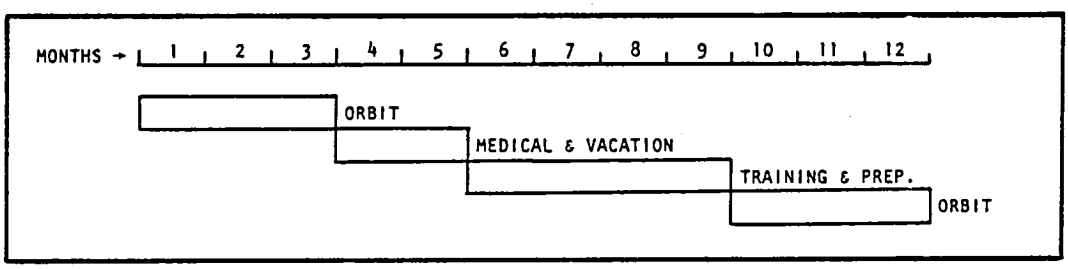

Figure 4.6-1. Crew Utilization Timeline

4.6.2 LAUNCH SITE PERSONNEL REQUIREMENTS

Launch site activities comprise, in broad terms, receiving and processing material destined for launch to LEO, personnel processing and administration, and launch site operations involving HLLV loading, launch, recovery, and refurbishment. Estimates of manpower required to support material processing have been developed and fall into four categories: (1) material receiving and unloading, (2) warehouse operations, (3) MW antenna RF element fabrication and assembly, and (4) payload preparation. All estimates reflect single shift operations and do not include security forces.

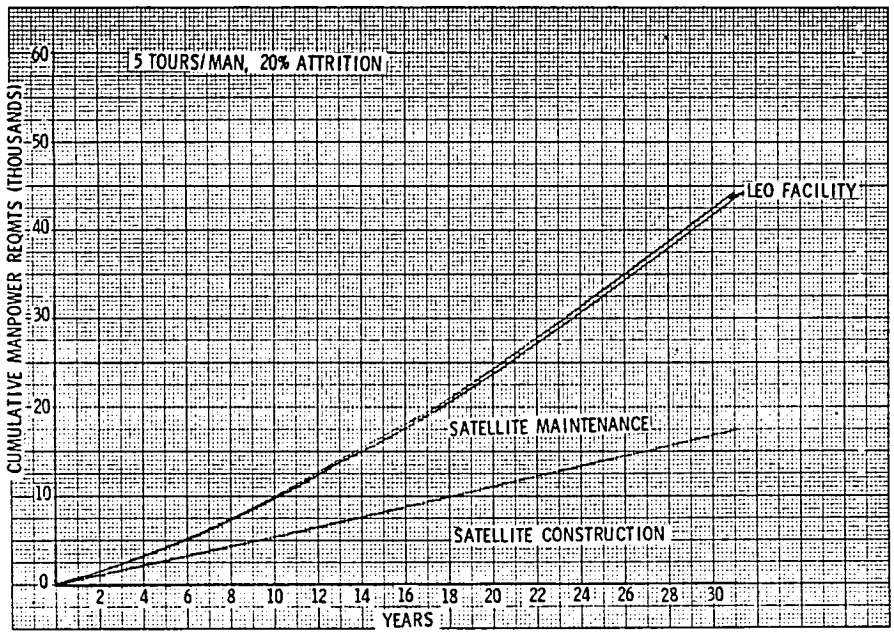

Figure 4.6-2. Cumulative Manpower Requirements - Orbital Operations

Material Receiving

Volume V of the final report of Satellite Power Systems (SPS) Concept Definition Study, (SD 78-AP-0023-5), dated April, 1978 contains an analysis of railroad car requirements for transporting material for satellite construction and maintenance and for EOTV construction. The peak annual traffic totaled 5,849 cars per year by the end of the 30 year program. The new program of a total of 60 satellites and revised EOTV fleet requirements reduced this to about 1,400 cars per year. This translates into an average of about 6 cars per day (5 day week) which must be off-loaded. Based on consulation with representatives of Santa Fe Failroad, and the size of railroad cars (high volume) selected for the SPS, it was estimated that a 4 man crew could unload one car in the average time of 3 hours, or 2.6 cars in an eight hour shift. Therefore, 10 men will be required to process the average traffic of 6 cars per day.

Warehouse Operations

Warehouse area required to support material flow was developed in the above referenced final report and totals about 170,000 square meters. A warehouse complex satisfying this requirement was postulated and consists of two adjacent 3 story buildings connected by platforms and ramps. Each building measures 168×168 m by approximately 20 m high. The crew required to operate this warehouse was estimated and is listed below:

Function	No.
Superintendent	1
Superintendent's staff	4
Warehouse manager/building	2
Warehouse manager's staff/building	6
Floor supervisor × 6 floors	6
Floor supervisor assistants × 6 floors	12
Area foreman - 2/floor × 6 floors	12
Crew - 20/floor × 6 floors	120
Data processing - 2/floor × 6 floors	12
Total (1 Shift)	175

RF Element Assembly

Microwave antenna subarrays (less klystrons and control electronics modules) will be fabricated and assembled at the launch site. All subarrays, are of identical dimensions, measuring approximating 11×10×0.26 m. Each subarray is composed of varying numbers of power modules which reflect ten different sizes. There are about 136,000 power modules per satellite which are assembled into 6,993 subarrays, resulting in 10 different internal subarray configurations, i.e., number of power modules per subarray.

The metal stock from which the power modules are fabricated is shipped to the launch site RF assembly facility in flat sheets. There, the sheets are cut to the proper size, formed, and assembled into subarrays. This process is largely automatic and requires ten fabrication and assembly lines because of the ten different power module and subarray configurations. A single floor assembly facility measuring 155 m wide and 100 m long will provide space for ten assembly lines 10 m wide and allow adequate space between lines.

Peak satellite construction (2/year) generates a peak annual requirement for 13,986 subarrays, or an average of about 6 subarrays per line per day (5 day week). This figure varies for different lines because the number of subarrays in each configuration is not the same. Facility manpower requirements for a single-shift operation are as follows:

Supervision	12
Incoming material flow	5
Completed subarray outflow	10
Assembly line - 10 men each × 10 lines	100
	127

Payload Preparation

In determining payload preparation requirements, an HLLV launch rate of 3 per day was utilized as a planning basis. Additionally, it was assumed that six completed payloads would be available in a standby area, and that three payloads would be in work at any one time.

Each payload covers a floor area of 41.5 m by 8 m, totaling 332 m^2. Three single-shift days have been allowed for preparation of a payload. Since three payloads are in work, three crews are required. However, to support a launch rate of 3 flights per day, three payloads must be delivered daily and packaging of three more started the following day. This equates to a total of 9 crews. It is estimated that 14 men and a foreman will be required to process one payload in the time allocated. This results in a total requirement of 135 men for 9 crews plus one overall supervisor.

4.7 EOTV FLEET REQUIREMENTS AND CONSTRUCTION CONCEPTS

A study was conducted to compare various EOTV construction concepts. The study assumed an EOTV life of 10 years, which translates into approximately 25 round trips between LEO and GEO. Ten EOTV's are required to transport construction material for one satellite to GEO. Because of the time required for EOTV transit, loading, and maintenance, each EOTV is limited to one trip per satellite - i.e., no "doubling up". EOTV's must be replaced at approximately 11 year intervals, or 25 round trips.

In addition to satellite construction, maintenance material must be delivered to each satellite on an annual basis, (approximately 1×10^6 kg per satellite year).

The bottom line of Figure 4.7-1 shows the EOTV total fleet requirements by year to transport both construction and maintenance mass to GEO. It is noted that EOTV's sufficient to support initial satellite construction are required at time zero. Since satellite construction ceases after 30 years, the requirement drops significantly to reflect only maintenance mass for the completed satellites. The downward trend is caused by decommissioning (or otherwise disposing of) satellites when they attain their design life of 30 years.

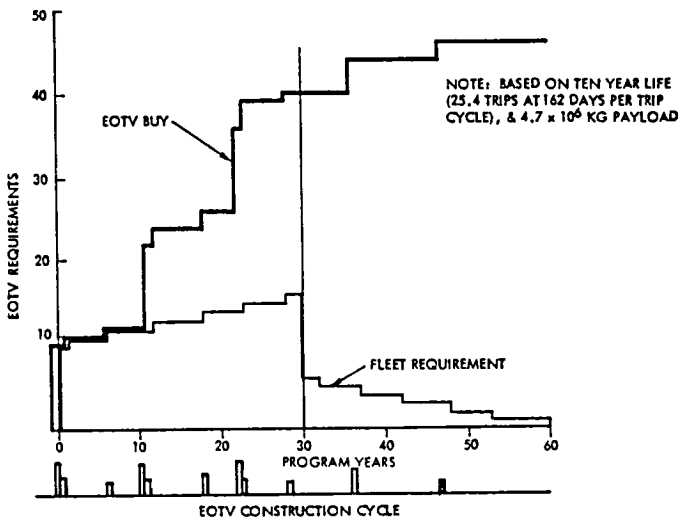

Figure 4.7-1. EOTV Requirements Overview

Because of EOTV life, program buy requirements exceed fleet size by a substantial margin. The top line shows these requirements. EOTV replacements fall into a total of seven build cycles (excluding initial build) as shown on the horizontal bar at the bottom of the figure. Five of these cycles occur during the first 30 years.

4.7.1 EOTV CONSTRUCTION TIMELINE

The EOTV consists of only 4 bays. Therefore, a total build cycle of seven days has been postulated. Much of the operation can be conducted in parallel as shown in Figure 4.7-2. It is estimated that an EOTV can be constructed in 11 days, including 2 days for facility preparation (i.e., loading beam machines, solar blanket dispensing, etc.). The time allocated for the designated activities is consistent with that allocated to satellite construction for similar activities.

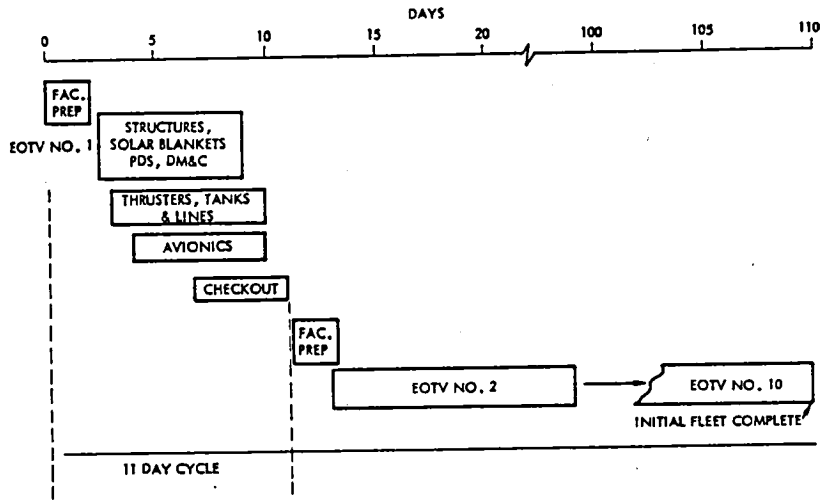

Figure 4.7-2. EOTV Construction Timeline

4.7.2 EOTV CONSTRUCTION CONCEPTS

Three potential options for constructing the EOTV's have been identified. These are:

Option 1 - Construct and maintain EOTV's in LEO with an integrated facility.

Option 2 - Construct EOTV's in LEO, but place the fixture in GEO during periods of non-building. Maintain the EOTV's in GEO except for the five EOTV build cycles, when maintenance also would be conducted in LEO. Maintain a permanent LEO facility for crew/cargo processing.

Option 3 - Transfer the fixture to GEO. Build and maintain all EOTV's in GEO. Maintain a permanent LEO facility for crew/cargo processing.

These options are depicted in Figure 4.7-3. It is noted that in each case, the fixture and initial EOTV are constructed in LEO.

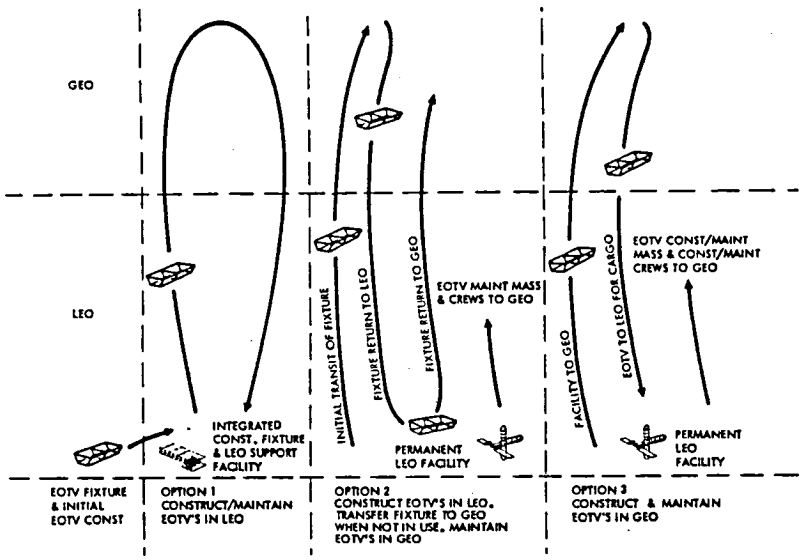

Figure 4.7-3. EOTV Construction Options

In Option 1, no EOTV construction/maintenance crews or material are transported to GEO. Option 2 requires transportation of maintenance crews and material to GEO for 27 of the 30 program years. The other 3 years are spent in LEO, constructing EOTV's (5 build cycles). In Option 3, construction/maintenance crews and material must be transported to GEO. Additionally, each constructed EOTV must return to LEO for initial loading, a loss of about 140 days.

4.7.3 30 YEAR PROPELLANT REQUIREMENTS

Figure 4.7-4 shows a comparison of options 1, 2 and 3 relative to additional propellants required over a 30 year period and resultant additional HLLV flights to carry the propellant to LEO. An additional option, 2A, has been added. This option entails constructing EOTV's in the nominal LEO orbit of 500 km and transferring the facility to a 556 km orbit between EOTV build periods to reduce stationkeeping propellant requirements. The total propellants over a 30 year period, including ΔV requirements for 5 orbital changes, is somewhat less than that required to maintain the facility permanently at 500 km.

The data displayed on the figure indicate that severe propellant (and HLLV) penalties are associated with Options 2 and 3.

Options 1 and 2A are essentially the same relevant to propellant usage, the difference being reduction of HLLV flights by one in favor of Option 2A, although operationally Option 2A is slightly more complex. However, based on these comparisons, Option 2A appeared to be the preferred concept.

ITEM / CONSTRUCTION ORBIT	OPTION 1 LEO	OPTION 2 LEO/GEO	OPTION 2A LEO/LEO	OPTION 3 GEO
• FACILITY STATION KEEPING - LEO	622,000 KG	KG	411,040 KG	- KG
• FACILITY STATION KEEPING - GEO	-	5,940	-	6,600
• PROPELLANT FOR FACILITY TRANSFER TO GEO	-	587,500	-	117,500
• PROPELLANT FOR FACILITY TRANSFER TO LEO	-	587,500	-	-
• PROPELLANT FOR EOTV CONST MAT'L TO GEO	-		-	4.84×10^6
• PROPELLANT FOR EOTV MAINT MAT'L TO GEO	-	20.8×10^6	-	22.5×10^6
PROPELLANT	622,000 KG	22×10^6 KG	411,040 KG	27.5×10^6 KG
HLLV FLTS	3	98	2	123
• HLLV FLTS-EOTV MAINT CREWS - 2 HLLV'S PER ROTATION	-	108	-	120
• HLLV FLTS-EOTV CONST CREWS - 5 BUILD CYCLES AT 5 HLLV'S EACH	-	-	-	25
TOTAL HLLV FLTS	3	206	2	268

OPTION 1. CONSTRUCT AND MAINTAIN EOTV'S IN LEO (500 KM). STORE CONSTRUCTION FACILITY IN LEO (500 KM) WHEN NOT IN USE
OPTION 2. CONSTRUCT EOTV'S IN LEO (500 KM) - TRANSFER CONSTRUCTION FACILITY TO GEO FOR STORAGE WHEN NOT IN USE MAINTAIN EOTV'S IN GEO.
OPTION 2A. CONSTRUCT EOTV'S IN LEO (500 KM) - TRANSFER CONSTRUCTION FACILITY TO HIGHER LEO (556 KM) FOR STORAGE WHEN NOT IN USE
OPTION 3. CONSTRUCT AND MAINTAIN EOTV'S IN GEO. STORE CONSTRUCTION FACILITY IN GEO WHEN NOT IN USE

Figure 4.7-4. EOTV Construction Orbit 30-Year Propellant Requirements

4.7.4 EFFECTS OF EOTV LIFE EXTENSION

The preceding study was based on a ten year EOTV life and a payload of 4.7×10^6 kg. The current EOTV has a payload capability of 5.17×10^6 kg for a 120 day transit time from LEO to GEO. Assuming a 30 year life, no EOTV replacements would be required under normal conditions. Referring to Table 4.4-1, by the end of the fifth program year, about 17 annual EOTV flights will be scheduled. For a turnaround time (LEO-GEO-LEO plus loading, unloading and maintenance) of 161 days, each EOTV can make about 2.27 trips per year, resulting in a fleet requirement of 8 EOTV's. This increases to 9 EOTV's by the fourteenth year, and increases incrementally to a total of 12 EOTV's at the end of 30 years. This compares with a total program buy of almost 50 EOTV's (Figure 4.7-1) having a 10 year life and slightly less payload capability.

4.7.5 RECOMMENDED CONSTRUCTION SCENARIO

Since this study was conducted, a change in the overall orbital scenario has occurred as a result of conversations between NASA and Rockwell representatives. The current concept, described in Section 3.0, consists of utilizing the SCB to construct approximately 6 EOTV's in LEO. The last EOTV would remain secured to the SCB and provide the ΔV requirements for transit to GEO, where satellite construction would be implemented. EOTV maintenance can still be accomplished by the LEO facility. Additional EOTV's, when required, would be constructed in GEO, utilizing the SCB as a fixture.

Satellite Maintenance Concept

The permanent satellite maintenance base is located on the first frame which is adjacent to the rotary joint since the bulk of the maintenance activity is anticipated to be on antenna components. (For a center mounted antenna configuration the base would be located on one of the two center frames).

Antenna. Klystron maintenance is anticipated to be a major portion of the overall maintenance effort. The population of approximately 136,000 klystrons is life limited and also can be expected to experience a high number of random failures. Currently, mean-time-to-failures (MTTB) of over 150,000 hours are being projected for TWT's, which are somewhat similar to klystrons. The primary life limiting factor is the cathodes. Even if klystrons reflecting SPS requirements can be developed with similar MTTF's, a virtually total replacement would be required over a thirty year period. An alternative would be to develop a klystron design which would permit changing the cathodes without removing the klystron.

Because of the thermal interface between the klystrons and heat pipes, it is not clear at present as to what constitutes an LRU. Preferably it would consist of a klystron cathode or klystron, but could be a power module or higher assembly. Regardless of LRU definition, means for removal and replacement will be provided by the gantries or cable-mounted platforms (see Antenna Construction described earlier in this section) which provide access to both sides of the antenna. These platforms will be equipped with the special equipment needed to perform maintenance on both the face and the underside of the antenna. Since shutdown will be required during maintenance, it is anticipated that degradation to a predetermined point would be tolerated and that a non-operating period of some days might be required for complete restoration of functions.

Power Distribution (PDS). The components comprising the PDS (e.g., switchgears) generally are more reliable and fewer in number than the klystrons, but random failures can be expected. (PDS elements on the back side of the antenna are accessible to the antenna gantry.) Because of the locations of these components in the bottom crossbeams of the troughs, the distance of a failed component from the maintenance base could approach 16,000 meters for an end-mounted antenna configuration. Removal and replacement of PDS components, then, will require either an extensive track system or a free flying facility with the capability of an MMM plus space for components. Since maintenance operations would be sporadic and would occur at various locations, a free flying concept appears to be preferable to an extensive track system which would have to provide access to every crossbeam throughout the length of the satellite, as well as to other areas.

A version of the free flying concept could consist of an arrangement similar to the vehicle shown in Figure 4.4-31, but somewhat smaller. The MMM would be equipped with special grabber arms for attaching to a 2 meter beam (Figure 4.7-5) and providing a measure of stability during the operation. Sections of the solar array will be deactivated during maintenance periods. However, temperatures of 125°C or higher may be encountered at the bottom of the trough. Dependant on detailed design characteristics and the type of

materials used in MMM construction relating to thermal control, it may be necessary to work from the underside of the crossbeam rather than the top. This would slightly restrict the access, but the operations still could be accomplished.

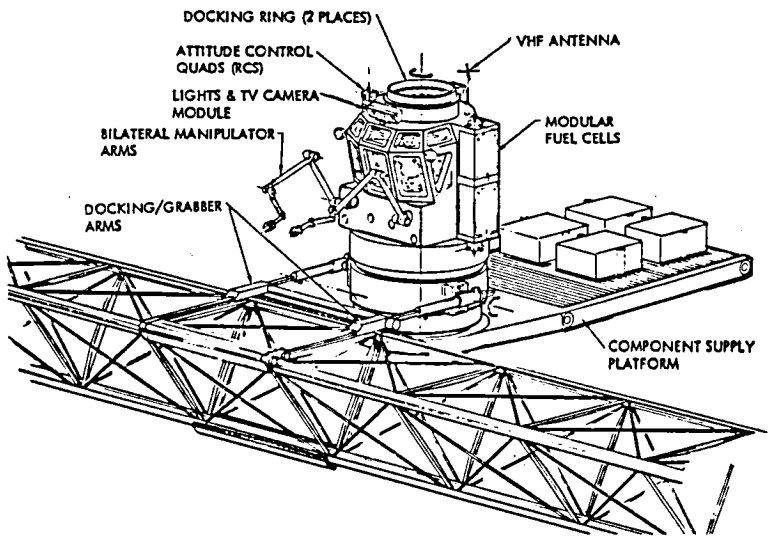

Figure 4.7-5. Manned Work Module Free Flying or Stationary

Solar Blanket/Reflector. The design and sizing of these elements are predicated on the degradation expected over thirty years, including meteoroid penetration. To effectively immobilize a large section of solar blanket would require some kind of catastrophic event (e.g., large meteor, collision, etc.). The isolation, removal and replacement of small solar blanket sections with the many interconnects does not appear feasible at this time. Replacement of an entire 25×750 meter strip by utilization of free flyers also does not appear practical. The alternative of using permanently installed equipment mounted on tracks or cables would require an installation in each bay of each trough, totaling 60 sets; most of these installations probably would not be used during the satellite life because of the low probability of catastrophic events. Therefore the current design accepts the predicted degradation and does not provide for blanket strip replacement.

The same rationale applies in general to the reflector sheets which are considerably larger. However, in the event of a large perforation or tear in the reflector, it may be possible, by use of free flyers, to treat the edges of the perforation in some manner to avoid propagation.

Attitude Control. Servicing and maintenance of the reaction control system, including thruster replacement will be accomplished by the same type of vehicle (beam grabbing MMM) utilized for the PDS.

Conclusions. With the exception of solar blanket and reflector replacement maintenance of the satellite subsystems is feasible. Partial or complete satellite shutdown will be required for conducting maintenance in some areas. More detailed design information for both satellite subsystem installations and manned manipulators will be required before maintenance operations can be defined in any great detail, timelines established, and satellite downtime assessed.

5.0 RESOURCES AND MANUFACTURING

5.0 RESOURCES AND MANUFACTURING

5.1 SATELLITE REQUIREMENTS

5.1.1 MATERIALS

The SPS satellite (Rockwell Point Design of June 1978) will require substantial quantities of diverse materials. This study was conducted to ascertain whether a problem existed in the procurement of the various materials, and if so, which materials presented potential problems, what was the magnitude of the problems, and what might be some possible solutions. Consequently, the productive capacity of the United States for these materials was determined, and the potential impact of SPS satellite construction on this capacity assessed. Data sources are listed in Table 5.1-1.

Table 5.1-1. Key Data Sources

1.	THE WORLD ALMANAC - 1978
2.	STATISTICAL ABSTRACTS OF THE UNITED STATES - 1976
3.	MINERAL FACTS AND PROBLEMS (1970) U.S. DEPT. OF INTERIOR
4.	UNITED STATES MINERAL RESOURCES, U.S. DEPT. OF INTERIOR (1973)
5.	CHEMICAL INFORMATION SERVICE S.R.I.
6.	SOCIETY OF THE PLASTICS INDUSTRY
7.	TYCO LABORATORIES, INC. - SAPHIKON DIVISION
8.	UNION CARBIDE CORP. - ELECTRONICS DIVISION
9.	UCLA REFERENCE LIBRARY
10.	CHEMICAL ENGINEERING
11.	LIBRARY OF CONGRESS
12.	AVIATION WEEK & SPACE TECHNOLOGY
13.	CHEMPLAST INC.
14.	ALUMINUM COMPANY OF AMERICA REPORT
15.	MODERN PLASTICS

Ground Rules

The "productive capacity" of the United States for any given material is elastic and continuously changing. It can be expected to change substantially by the year 2000. Even though some production data are approximations (±20%) they never-the-less would provide a valid basis for a rough-order-of-magnitude (ROM) analysis to ascertain if and where potential problems might exist. In some instances the peak annual production figures over a several year span were used as surrogates for production capacity when those data were unavailable.

The capability of the United States to produce the raw materials formed the basis of the analysis. One exception was aluminum because of the diverse sources of bauxite.

The basic analysis was confined to the material requirements of one SPS satellite. However, the results were extrapolated to a construction rate of 4 per year in the analysis and conclusions.

In the case of gallium arsenide and gallium aluminum arsenide, the two gallium requirements were combined as were also those for arsenic. The aluminum requirement was included with that of basic aluminum.

The SPS requirement for sapphire was primarily in the form of ribbon. However, total industrial sapphire production was examined to ascertain the breadth of synthetic sapphire production technology.

Water was identified as the heat transfer medium in the heat pipes. Its availability was judged to be obvious.

Those materials that exceeded 1% of the productive capacity of the United States were examined in greater depth.

Material Requirements - Rockwell Point Design

Figure 5.1-1 shows the basic materials and their quantities (in millions of kilograms) necessary for construction of one satellite. These weights were used in determining the impact of satellite construction on national productive capacity for these materials. It is noted that since this study was completed, NASA redirection resulted in a new satellite concept in which the structure is constructed of composites. Availability of composites is discussed later. The remainder of the materials are representative of the requirements for the new configuration (Reference concept).

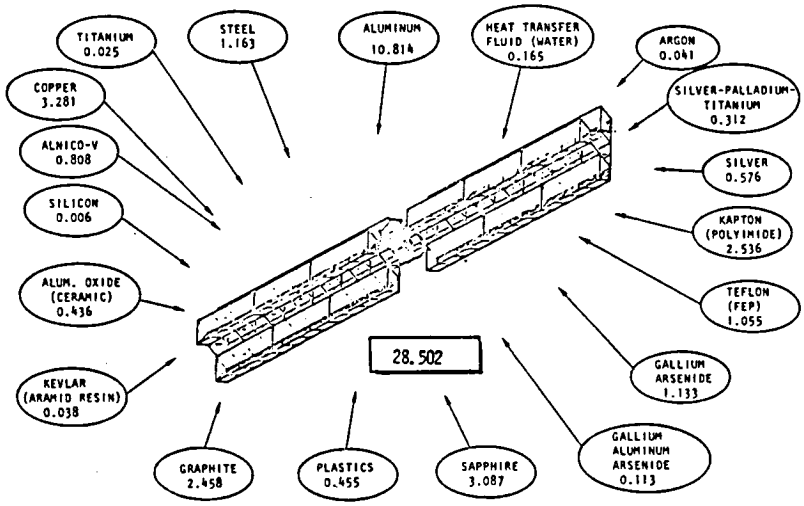

Figure 5.1-1. SPS Material Requirements (Millions of Kilograms)

The impact of the material requirements of one satellite on the United States productive capacity for the respective materials is shown in Table 5.1-2. In the case of cobalt and silver whose annual productivity could present problems, the data also show the material requirements in relation to government stockpiles.

Table 5.1-2. Summarized Data

MATERIAL	REQUIREMENT AS % OF U.S. PRODUCTION
1. ALUMINUM (INCLUDES NOs 5 & 13)	0.24%
2. STEEL	0.001%
3. TITANIUM (INCLUDES No. 17)	0.015%
4. COPPER	0.23%
5. ALNICO-V	
54% IRON 24% COBALT	0.0005%
AS % of U.S. STOCKPILE	1.0%
AS % OF U.S. CONSUMPTION	2.5%
14% NICKEL 8% ALUMINUM	0.73% INCLUDED IN NO. 1
6. SILICON	0.005%
7. ALUMINUM OXIDE (FROM BAUXITE)	0.022%
8. KEVLAR/RESIN (ARAMID)	1.7%
9. GRAPHITE (SYNTHETIC + NATURAL)	0.94%
10. PLASTICS	0.003%
11. SAPPHIRE (SYNTHETIC)	
INDUSTRIAL	3400%
RIBBON	97,000%
12. GALLIUM ALUMINUM ARSENIDE	
13. GALLIUM ARSENIDE	
GALLIUM	4000%
ARSENIC	3.6%
ALUMINUM	INCLUDED IN NO. 1
14. TEFLON (FEP)	40%
FLUORINE	0.49%
15. KAPTON (POLYAMIDE)	140%
16. SILVER (INCLUDES NO. 17)	
ANNUAL PRODUCTION	82%
STOCKPILE	4.5%
17. SILVER-PALLADIUM-TITANIUM	
SILVER 96.6%	INCLUDED IN NO. 16
PALLADIUM 1.7% U.S.	3000%
WORLD	11.0%
TITANIUM 1.7%	INCLUDED IN NO. 3
18. ARGON	0.16%
19. HEAT TRANSFER FLUID (WATER)	

Those materials whose requirements by 1 SPS would exceed 1% of the current United States national productive capacity are tabulated below. The associated comments describe the status of the material's anticipated availability.

1. COBALT : No U.S. mining - all imported - over 70% from Zaire. U.S. government stockpile could supply SPS requirements.

2. KEVLAR : Dupont aramid fiber. Productive capacity is being expanded. Should not present substantial problem.

3. SAPPHIRE : Raw material Al_2O_3 plentiful. Requires large amounts of electric energy. Production appears readily expandable.

4. GALLIUM : Alcoa study* projects potential 1995 Ga production capability in U.S. at 2.6 times 1 SPS satellite requirement.

5. ARSENIC : U.S. production currently at half of capacity. Production slack could satisfy SPS demand.

6. TEFLON : Raw materials present no problem. Production facilities would need to be expanded. Dupont's patents expiring. Competition likely.

*Survey of availability and economical extractability of gallium from earth resources. Alcoa, 1 October 1976

7. KAPTON : Dupont polyamide. Raw materials available. Production facilities would need to be expanded.

8. SILVER : Annual production varies considerably, but SPS would require major portion of production unless withdrawn from stockpile.

9. PALLADIUM: Although only a small quantity is required by SPS, it vastly exceeds U.S. production. Major supplier is USSR. U.S. stockpile would be significantly impacted (-14%).

The scheduled satellite production rate would exacerbate possible material production problems. However, the twenty-plus years prior to the construction of the first SPS satellite (~2000) provides ample time for either expansion of problem material production capacity or the development of substitute materials that would be more readily available and/or more efficient. Most of the plastic materials shown had not been developed twenty years ago. Consequently, these or superior materials that would be developed in the ensuing years would actually be used in construction of the SPS satellite, so that this analysis may be viewed as a "worst-case analysis".

Composites

Based on revised SPS designs, composites will be substituted for half of the aluminum initially assumed to be required. The initial aluminum requirements were estimated to be 6.738×10^6 kg without 25% growth (SD 78-AP-0016-1A). This is equivalent to $6.738 \times 10^6 \times 2.2045 \times 1.25 = 18.567 \times 10^6$ lb, including 25% growth factor. If half of this were composite, then 9,284,000 lb of composites per satellite would be required.

The basic constituents of composites are:

Graphite - approximately 30% by weight	2,785,000 lb
Glass fibers - approximately 15% by weight	1,393,000
Resin - approximately 55% by weight	5,106,000
	9,284,000 lb

Although these data are highly normalized, they are judged to be indicative of composite composition.

The graphite used in composites is produced synthetically. The U.S. productive capacity in 1976 for synthetic graphite was 573,000,000 lb. Avco Corporation's Specialty Materials Division recently announced construction of a new graphite fiber facility[1]. It alone is expected to produce on the order of 10 million lb of graphite fibers by the mid-to-late 1980's, or almost 2 times the SPS annual requirement. All indications are that the SPS graphite requirements could be readily met from U.S. productive capacity.

In 1977 the U.S. produced 3,388,937,000 lb of fiber glass, up 21% from 1976. The SPS requirements constitute less than 0.1% of U.S. productive capacity and so should present no availability problems.

[1]Chemical Engineering, 23 October 1978, pages 95,96

The resins planned for in the satellites are thermoplastics. These can be reused upon heating. Typical of these plastics are the polysulfones. Based on chemical industry projections[1], the excess capacity of polysulfone will be 17.0 million pounds in 1981, or 3.3 times that required per SPS. Consequently, availability of the resin portion of the composites should present no special problems.

Conclusion

While construction of one SPS would not present major material problems, construction of 60 would. At a construction rate of 2/year, requirements for palladium - which is primarily obtained from the USSR, with South Africa as a lesser secondary source - would almost equal 25% of current world production. While the requirements for silver would also approximate 25% of world production, the silver supply is vastly more expandable than the palladium supply. Curtailment of cobalt supplies from Zaire would necessitate development of substitutes for the Alnico V.

Consequently, possible substitutes for Alnico V, silver and palladium are being investigated.

Extrapolation of Alcoa study projections to 2000 indicates that sufficient gallium could be available from annual U.S. Bauxite processing for 2 satellites per year.

Materials Requirements (Reference Configuration)

Since the materials analysis for the Rockwell Point Design of June 1978 was conducted, a coplanar satellite configuration (Figure 4.4-1) reflecting revised program ground rules has been developed. Accordingly, the materials and resource availability analysis has been updated and expanded to include the ground receiving station (rectenna). The results are summarized in the following sections.

Satellite. Table 5.1-3 indicates the materials requirements for one satellite. The primary structure which supports the solar converter and antenna is now comprised of graphite impregnated composites. The total weight of the composites is 1.028×10^6 kg of which 30% by weight (0.309×10^6 kg) is graphite, 15% (0.154×10^6 kg) glass fibers and 55% (0.565×10^6 kg) is resin. The secondary structure/mechanisms are considered to be largely aluminum, weighing 1.769×10^6 kg.

Power Distribution and Conditioning. This category includes the power conditioning equipment and conductors in both the solar array and the antenna. Also included are the power-transmitting slip rings. The total weight of power distribution and conditioning equipment, etc., amounts to 8.884×10^6 kg, or 19.585×10^6 lb.

The reflectors consist of aluminum coated 0.5 mil Kapton. The total weight is 1.29×10^6 kg of which 1.283×10^6 kg is Kapton.

[1]Materials Engineering, January 1978

Table 5.1-3. Material Requirements for Main Satellite System Elements

MATERIAL	STRUCTURE/ MECHANISMS x 10^6 KG	CONCENTRATORS x 10^6 KG	SOLAR BLANKET x 10^6 KG	POWER DISTR. & COND. x 10^6 KG	POWER MODULE (KLYSTRONS) x 10^6 KG	TOTAL WEIGHT KG x 10^6	TOTAL WEIGHT LB x 10^6
ALUMINUM	1.769	0.013	0.013	6.824	0.346	8.965	19.768
ALUMINUM OXIDE					0.531	0.531	1.171
ARSENIC			0.465			0.465	1.025
COBALT					0.242	0.242	0.533
COPPER			0.476	0.839	2.550	3.865	8.520
GALLIUM			0.432			0.432	0.952
GLASS FIBER	0.154				0.024	0.178	0.392
GOLD			1.640			1.640	3.615
GRAPHITE	0.309				0.048	0.357	0.787
IRON					0.545	0.545	1.201
KAPTON		1.283	1.219				5.517
NICKEL					0.141	0.141	0.311
PLASTIC				0.681		0.681	1.501
RESIN	0.565				0.088	0.653	1.440
SAPPHIRE			2.700			2.700	5.952
SELENIUM			(34 KG)			(34 KG)	(75 LB)
SILVER			0.172	0.006		0.178	0.392
STEEL				0.506	0.690	1.196	2.637
TEFLON			0.915			0.915	2.017
TIN			0.488			0.488	1.076
TITANIUM				0.028		0.028	0.062
ZINC			(11 KG)			(11 KG)	(24 LB)
SUBTOTAL	2.797	1.296	8.518	8.884	5.205	26.700	58.873
OTHER (ACS & THERMAL)						6.318	13.931
					TOTAL WEIGHT	33.018	72.804

The solar blankets consist of a variety of materials as listed in Table 5.1-4. The total amounts are factored, based on the work completed under Arthur D. Little Contract with NASA (NAS9-15294).

Table 5.1-4. Solar Blanket Material Mass

MATERIAL	AMOUNT REQUIRED 10^6 kg	AMOUNT REQUIRED x 10^6 lb
ALUMINUM	0.008	0.018
GALLIUM	0.432	0.952
ARSENIC (99.999%)	0.465	1.025
SELENIUM (00.999%)	34 kg	75 lb
ZINC (99.999%)	11 kg	24 lb
ALUMINUM (99.999%)	0.005	0.011
SILVER	0.172	0.379
GOLD	1.640	3.615
TIN	0.488	1.076
SAPPHIRE (Al_2O_3)	2.700	5.952
COPPER	0.476	1.049
TEFLON	0.915	2.017
KAPTON	1.219	2.687
TOTAL	8.518	18.781

The composition of the remainder of the elements listed in Table 5.1-3 is self explanatory.

Ground Receiving Station. Key elements of the ground receiving station that might impact resource availability consists of the site and facilities requirements, the rectenna support structure, and the power collection system requirements. Other elements such as conversion stations, the grid interface and the operations requirements are basically identical to those required by conventional power generating systems and are not anticipated to impose significant resource requirements. Likewise, the control system, while unique to the GRS concept, is not anticipated to require either unusual types or large quantities of natural resources.

Site and Facilities. The ground receiving station will require an area of approximately 35,000 acres. The rectenna field will occupy approximately 25,000 acres with a surrounding buffer zone of 10,000 acres. The land will need to be cleared and leveled and a rainfall run-off system would need to be constructed. Several alternative layouts were examined, however, the amount of excavation and concrete was found to be relatively insensitive to the layout alternatives. Concrete footings (2 parallel rows) would need to be poured for each row of antenna panels. Concrete requirements for GRS rectenna panel footings and for the water channels were translated into the constituent materials (see Table 5.1-5).

Table 5.1-5. Cement/Aggregate Requirements

CEMENT	949,000 TONS
SAND	2,827,000
ROCK (APPROX. 1" - 1-1/2")	3,695,000
WATER	606,000
	8,077,000 TONS
REINFORCING ROD	19,000 TONS

It was assumed that the access road between panels would consist of a 6 inch deep layer of gravel. The gravel requirements for the access roads would be 9,791,000 yd^3 or approximately 13,707,000 tons. Requirements associated with construction of 10 miles of access roads and 23 miles of perimeter roads plus 20 miles of access railroad, and 25 miles of perimeter railroad were not considered to impose abnormal requirements on natural resources or production capacities.

Rectenna Support Structure. The rectenna support structure consists of steel hat sections, I beams, tube braces, fittings and hardware along with miscellaneous items. The total weight of steel required for rectenna support was calculated to be 1666.7 kg or 3674 lb per panel, or a total of 967.5×10^6 kg or 2132.9×10^6 lb for the 580,500 panels in the rectenna array.

Power Collection. The power collection occurs in the panel array elements mounted on the rectenna panels. The elements consist of three 0.5" layers of a dielectric (plastic compound) that separates four layers of 0.0039 inches of copper, clad to 0.001 inches of Mylar. Interspersed within

each panel are 735 diodes, or a total of 426.67×10^6 diodes in the total array of 580,500 panels. The one ounce diodes consist of 44% tungsten, 40% copper, 15% gallium arsenide and 1% gold and other exotic materials. Consequently, the total material requirements for the power collection portion of a single rectenna are itemized in Table 5.1-6. Miscellaneous materials such as copper wiring, J-boxes, etc., were not considered to severely impact either material availability or production capacity.

Table 5.1-6. Diode Materials per Rectenna

MATERIAL	AMOUNT REQUIRED	
	$kg \times 10^6$	$lb \times 10^6$
PLASTIC DIELECTRIC	169.96	374.68
MYLAR	11.32	24.95
COPPER (COATED OR MYLAR)	46.13	101.70
DIODES		
TUNGSTEN	5.32	11.73
COPPER	4.84	10.67
GALLIUM ARSENIDE	1.81	4.00
GOLD/EXOTICS	0.12	.27

Materials Availability. A review of materials required for construction of the satellite and the ground receiving station identifies several potential problem areas of material availability. Table 5.1-7 summarizes eight materials that can pose limitations on SPS requirements. The availability of these materials (excepting gold and tungsten) is discussed earlier in this section (Material Requirements, Rockwell Point Design).

Table 5.1-7. Significant SPS Resource Needs

COBALT:	0.242 10 kg REQUIRED. IMPORTS FROM PRIMARY SOURCE - ZAIRE - SUSCEPTIBLE TO INTERRUPTION
GALLIUM:	1.31×10^6 kg
GOLD:	1.70×10^6 kg
KAPTON:	2.51×10^6 kg
SAPPHIRE:	2.71×10^6 kg
SILVER:	0.18×10^6 kg
TEFLON:	0.92×10^6 kg
TUNGSTEN:	5.32×10^6 kg

Considerations on the availability of gold and tungsten follow:

Gold. The 3,750,000 lb of gold required exceeds recent U.S. annual gold production. Approximately 45% of the gold produced in the U.S. is obtained as a by-product from other metal production, primarily copper. In 1977, approximately 75,000 lb of gold were produced domestically, at a value of $148 per

troy ounce. With gold currently selling at about $240 per troy ounce, some increased production can be expected, but far short of the SPS requirements. The U.S. Treasury stockpile currently contains approximately 18.5 million lb of gold. Thus, the SPS requirement would constitute approximately 20% of our gold reserve. A substitute material will likely need to be developed to replace the gold requirements of the solar blanket.

Tungsten. The 11,730,000 lb of tungsten required by the SPS constitutes approximately 14% of the annual world production, or 50% more than the total U.S. production of tungsten in 1974. The total annual U.S. consumption of tungsten is on the order of 15 million pounds. U.S. Government stockpiles contain about 110 million pounds of tungsten or 9.4 times the SPS requirement. Consequently, the tungsten requirement of the SPS could present a major problem. Use of alternative materials for the tungsten in the panel diodes should be investigated.

Summary. The above analyses have been based on the construction of one SPS. A construction rate of two SPS per year, for even several years, could substantially compound the material resources availability problems described. A list of data sources used in this analysis was presented in Table 5.1-1.

5.1.2 MANUFACTURING

An investigation of manufacturing capabilities required to support a satellite construction rate of two per year was conducted. The investigation was confined to high usage material, which included LSI components, klystrons, heat pipes, and aluminum.

The following sources were contacted:

Rockwell International (Autonetics Strategic Systems Division): LSI Components

Varian Associated: Klystrons

Hughes Electron Dynamic Division: Heat Pipes

Kaiser Aluminum and Alcoa: Aluminum rolls

Quantitative data were obtained from these sources, excepting the aluminum companies. Both of these companies stated that the projected production (previous baseline of 4 and ultimately 5 satellites per year) was within existing plant facilities; however new stamping equipment conforming to the desired configuration of the aluminum rolls would be required. These data are included as a matter of interest; the aluminum structure has been replaced by composites, which reduce significantly requirements for aluminum.

Table 5.1-8 summarizes the remainder of the data received. Since GaAlAs solar cells manufacturing processes are still being developed, solar cell data are not included.

Table 5.1-8. Manufacturing Implications

ITEM	PEAK ANNUAL QTY	NEW FACILITIES (m^2)	FACILITY/EQUIPMENT COST
KLYSTRONS	300,000	190,520	$\$309\times10^6$
HEAT PIPE	8.7×10^6	8,000	9.6×10^6
ELECTRONICS (LSI COMPONENTS)	1,500,000	NONE	19.4×10^6
NOTE: SINGLE SHIFT OPERATIONS ASSUMED			

6.0 SPS PROPELLANT ANALYSIS

6.0 SPS PROPELLANT ANALYSIS

6.1 REQUIREMENTS

The propellants of concern in this analysis are LOX, LH_2 and RP. Three vehicles utilized during the satellite construction phase generate requirements for these propellants; growth shuttle, personnel orbital transfer vehicle (POTV) and the HLLV. These vehicles are described in detail in Volume IV of this report. The propellant requirements per flight for each of these vehicles will be identified and then factored to reflect the estimated average flights per year to arrive at the annual propellant requirements per vehicle type. These data will then be combined to obtain the total average propellant requirements in support of the SPS.

6.1.1 GROWTH SHUTTLE

The propellant requirements for the Growth Shuttle were obtained from the Rockwell Shuttle Growth Study final report (SD N-SR-0008) dated May 1977. The concept selected was that identified in the study as the LRB (Liquid Rocket Boosters), SSME-35, requiring a total propellant weight (LOX plus LH_2) of 1.36×10^6 kg. This configuration can place 233,000 lb of payload into a 160 nmi, 28.5° orbit.

Assuming a 6 to 1 oxidizer fuel ratio, propellant requirements per flight are:

LOX	1,161,000 kg
LH_2	193,000 kg

The average number of growth shuttle flights required per year (see Section 5.4) in support of the SPS will be about 106. Thus, assuming a 5% boil-off loss, the average yearly requirements would be:

LOX	129,200,000 kg
LH_2	21,500,000 kg

6.1.2 POTV

The POTV was designed to carry 60 passengers from LEO (28.5° incl.) to GEO. A cargo canister which carries consumables for the 90 day orbital stay is shipped to GEO via EOTV. The total propellant required to deliver the POTV to GEO is 32,250 kg. The vehicle is refueled in GEO for the return trip, which requires the same amount of propellant. The round trip propellant requirements are:

LOX	55,280 kg
LH_2	9,220 kg

The annual average of POTV flights is approximately 100. Applying this and a boil-off factor of 5% results in the following annual average requirement.

LOX	5,804,400 kg
LH_2	968,100 kg

6.1.3 HLLV

The HLLV consists of a two-stage vehicle with a 225,000 kg payload capability. The first stage utilizes LOX/RP and carries additional propellant which is fed to the second stage during the parallel burn. The second stage engines are powered by LOX and LH_2. Total propellant requirements for one flight are:

LOX	4,709,000 kg
LH_2	381,000 kg
RP	926,000 kg

For the annual average of about 560 flights, and including boil-off, the average annual requirements are:

LOX	2769×10^6 kg
LH_2	224×10^6 kg
RP	519×10^6 kg

6.1.4 INTERORBITAL TRANSPORT VEHICLE (IOTV)

The IOTV is utilized both at LEO and GEO to transfer cargo. An estimated 28,970 sorties will occur during the 30 years of the program. Each sortie will average:

LOX	257 kg
LH_2	43 kg

Factoring in the annual average of 966 sorties, total requirements, including 5% boil-off, are:

LOX	260,675 kg
LH_2	43,615 kg

6.1.5 SPS AVERAGE ANNUAL PROPELLANT REQUIREMENTS

Based on the preceding data, the average propellant requirements per year during the entire program are summarized as follows:

Vehicle	LOX (kg)	LH_2 (kg)	RP (kg^6)
Growth Shuttle	129.2×10^6	21.5×10^6	
POTV	5.8×10^6	0.97×10^6	
HLLV	2769×10^6	224×10^6	519×10^6
IOTV	0.26×10^6	0.044×10^6	
	2904.3×10^6	246.5×10^6	519×10^6

The daily requirement (365 days) is:

LOX	7.96×10^6 kg	(17.5×10^6 lb)
LH_2	0.675×10^6 kg	(1.49×10^6 lb)
RP	1.42×10^6 kg	(3.13×10^6 lb)

6.2 UNITED STATES PRODUCTION OF O_2, H_2 AND RP

In 1973, the United States production of these fluids were:

O_2	14.76×10^9 kg
H_2	6.12×10^9 kg
RP	40.52×10^9 kg

The SPS average annual requirements as a percent of 1973 production are:

O_2	19.7%
H_2	4%
RP	1%

Assuming a 5% annual growth in productive capacity, by 1993 the percent of United States production would be:

O_2	9.9%
H_2	2%
RP	0.5%

It is noted that the listed SPS requirements are average. However, referring to Table 4.4-1, the intensity of the traffic model increases somewhat throughout the 30 year program, primarily because of the increasing amount of satellite maintenance mass as additional satellites become operational. For comparison with the above tabulated data, the propellant requirements during the 30th year are:

LOX	3700×10^6 kg
LH_2	300×10^6 kg
RP	648×10^6 kg

6.3 POWER REQUIREMENTS FOR PROPELLANT PRODUCTION

Assume that the hydrogen is produced through the G.E. solid polymer electrolysis process, considerable oxygen is produced simultaneously, but the quantity of oxygen is insufficient to meet the demand. The balance of oxygen requirements are assumed to be provided by the liquefaction of air.

6.3.1 POWER REQUIREMENTS FOR HYDROGEN PRODUCTION

The solid polymer process requires 22.1 kWh to produce 1 lb of hydrogen and 8 lb oxygen. To produce the 1.49×10^6 lb of H_2 required per day would require:

$$1.49\times10^6 \times 22.1 = 32.929\times10^6 \text{ kWh/day}$$

Assuming steady 24 hour operations, this would require a power level of 1.37×10^6 kW or a 1.37 gigawatt facility.

The electrolytic production of hydrogen would simultaneously produce 8 lb of O_2 for every lb of H_2, so $(8\times1.49\times10^6) = 11.92\times10^6$ lb of O_2 would be obtained per day from the H_2 production, or 68% of the daily requirement. An additional 5.58×10^6 lb O_2 would be required per day.

6.3.2 POWER REQUIRED FOR HYDROGEN LIQUEFACTION

Liquefaction of gaseous hydrogen requires on the order of 2.0 kWh per lb. Consequently, to liquify 1.49×10^6 lb of GH per day would require 2.98×10^6 kWh. Assuming 24 hours per day production, a power level of 124,167 kW or 0.124 GW is required.

6.3.3 TOTAL POWER REQUIREMENT: HYDROGEN PRODUCTION AND LIQUEFACTION

The total power level required to meet the LH_2 demands of the SPS would be:

Production	1.370 GW
Liquefaction	.124 GW
	1.494 GW

6.3.4 POWER REQUIRED TO PRODUCE BALANCE OF OXYGEN REQUIREMENTS

It is assumed that the balance of LO_2 requirements would be met by the liquefaction of air. The energy required is 0.411 kWh per lb of LOX. Consequently, to produce the 5.58×10^6 lb of O_2 shortfall from H_2 production would require: $0.411\times5.58\times10 = 2.29\times10^6$ kWh. Again, assuming a 24 hour production facility, a power level of 95,558 kW or 0.096 GW would be required.

6.3.5 POWER REQUIRED TO LIQUIFY GASEOUS O_2 OBTAINED BY ELECTROLYSIS

Approximately 0.281 kWh would be required to liquify each pound of gaseous oxygen. Thus the 11.92×10^6 lb of GO_2 obtained by electrolysis would require 3.35×10^6 kWh, or, for 24 hour operations, a power level of 139,163 kW of 0.14 GW.

6.3.6 TOTAL POWER REQUIRED FOR SPS LOX/LH_2 PRODUCTION

The SPS LOX/LH_2 requirements would require electric power generation facilities on the order of:

LH_2 + GO_2	1.49 GW
LO_2 (Balance)	.10 GW
LO_2 (Electrolysis)	.14 GW
	7.71 GW

To generate this power would require 2 large nuclear reactors.

6.4 CONCLUSIONS

- The requirement for LOX for SPS missions could present problems although these would be relatively minor if adequate lead time were available for facility construction/expansion. LH_2 and RP could be supplied by anticipated growth of production capacity.
- Raw materials are available (i.e., coal, air, water).
- Because of the large energy requirements of the production processes, the unit costs would be substantially increased over current costs (depending on the processes selected and the source(s) of the energy requirements.
- To produce the LOX/LH_2 requirements for SPS transportation the equivalent power output of two large nuclear generators would be required.

7.0 SPACE ENVIRONMENT

7.0 SPACE ENVIRONMENT

7.1 PLASMA ENVIRONMENTS AND EFFECTS

The plasma environments in geosynchronous earth orbit (GEO) have been measured for over six years, although our understanding of the phenomena involved is still being expanded. The highest voltages recorded are in the 19- to 20-kilovolt range, but there are theoretical reasons for believing that equilibrium voltages of ~30 kilovolts can occur. The equilibrium voltage, for spacecraft surfaces not exposed to sunlight and having poor secondary electron emission characteristics, is ~2.5 E_o where E_o is the mean electron energy of a quasi-Maxwellian energy distribution

$$N_e\ (\geq E) = N_o\ e^{-E/E_o}$$

In this expression N_o is the density of electrons present where N_e ($\geq$E) is the density of electrons with energies $\geq$E. Values of $E_o \lesssim 12$ kilovolts are theoretically possible based upon the dynamics of the geomagnetic tail (where the energetic plasmas are produced).

The charging currents measured in GEO have typically been ≤ 1 nA/cm^2, although there are theoretical reasons for believing that the upper limit can be a few (3 to 5) nA/cm^2. The charging current is the difference between the primary electron current and the primary positive ion current plus any secondary electron losses from the spacecraft. When uncharged the primary electron current is ~43 times as great as the primary positive ion current. As the spacecraft becomes negatively charged, the primary electron current decreases exponentially while the primary positive ion current increases linearly (see Figure 7.1-1). These different behaviors are due to the fact that the charging plasma is moving relative to the spacecraft, with the electron motion being subsonic (thermal velocity > directed velocity) while the positive ion motion is supersonic (directed velocity > thermal velocity). When the primary electron current and the primary positive ion current are equal, the spacecraft charging stops (unless previously stopped by secondary electron processes). At this point the equilibrium voltage has been reached. However, if electrical discharges (usually between conducting and non-conducting portions of the spacecraft surface) take place before the equilibrium voltage has been reached, the voltage drops to some low value, only to begin increasing again, leading to a second discharge, etc. It is these discharges which can cause trouble, since the energy accumulated over a period of a few moments can be released in $\lesssim 1$ μs. If the energy released as a result of these discharges can find its way (via conduction or radiation) to sensitive electronic circuits, it can upset them, causing anomalous switching, bit errors in computer or communication signals, etc.

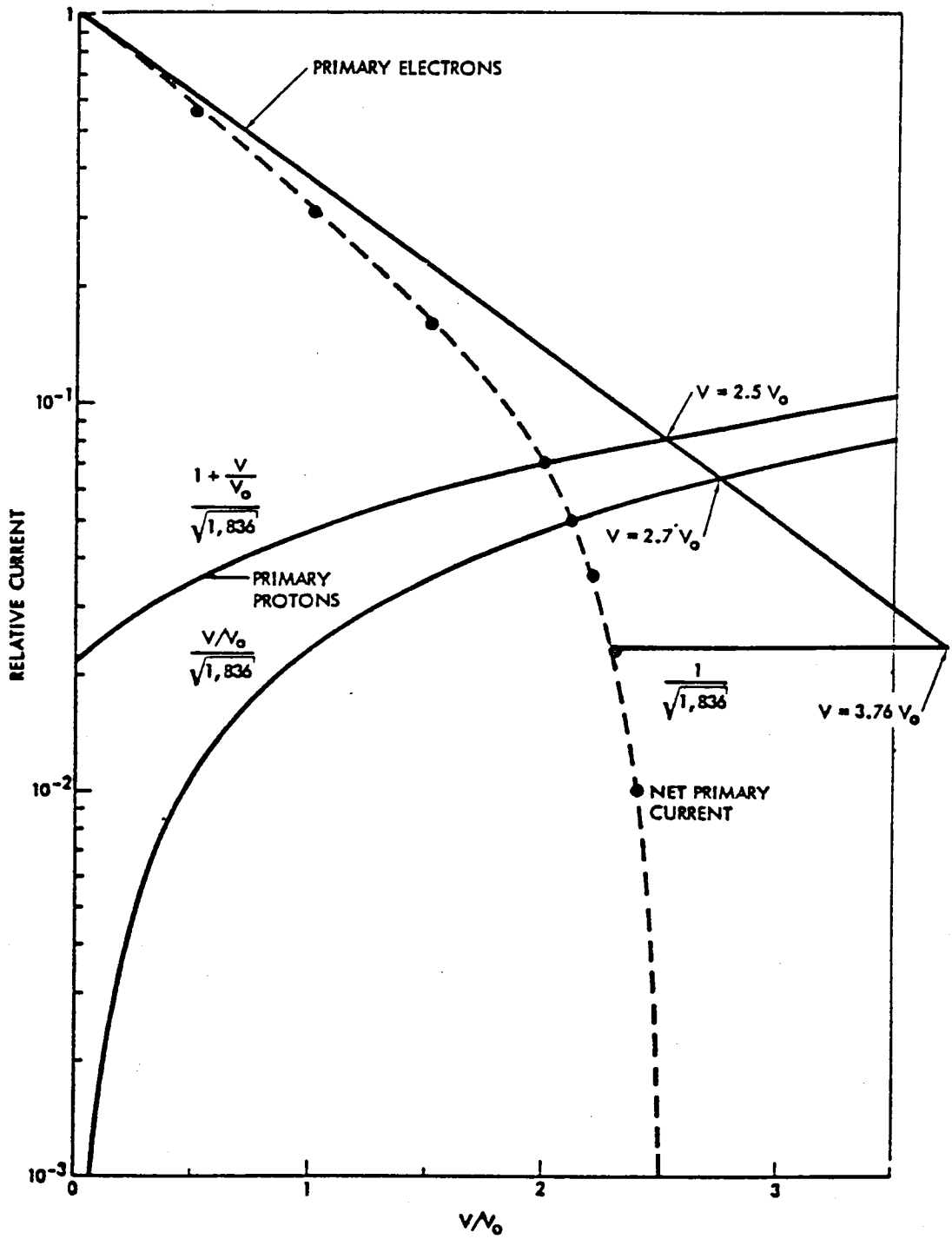

Figure 7.1-1. Net Primary Current as a Function of Spacecraft Voltage/Plasma Temperature Ratio

The energetic plasma responsible for spacecraft charging is produced in (by compressional heating) and projected toward the earth from the geomagnetic tail. The plasma continues its motion as an entity until it encounters its equal (in energy density) in the geomagnetic field). When the plasma has approached the earth (from the anti-solar side) sufficiently close that the energy density of the geomagnetic field equals the energy density of the plasma (which is largely due to its directed motion), the geomagnetic field tears the plasma apart, sending the electrons into the midnight-to-dawn quadrant and the positive ions (largely protons) into the dusk-to-midnight quadrant. There are two important consequences of this interaction of the energetic plasma and the geomagnetic field. First, the high-energy density (but lower probability) plasmas can approach to within ~3 R_E of the orbit of the earth, while the low-energy density (but high probability) plasmas are limited to higher altitudes. Second, most of the observed spacecraft charging events take place in the midnight-to-dawn quadrant because that is where the electrons are pushed by the geomagnetic field—and it is the electrons which are responsible for spacecraft charging.

The consequence of this behavior is that the orbital transfer vehicle (OTV) will not encounter the high-energy plasmas responsible for spacecraft charging below ~3 R_E (measured from the center of the earth). Above this altitude, the probability of encountering such plasmas increases rather rapidly with altitude (Figure 7.1-2), while the charging current density will decrease (Figure 7.1-3). The plasma temperature and, therefore, the equilibrium voltage it will produce, are expected to be relatively independent of altitude. At GEO the measured parameters (~10% probability, $\leq$1 nA/cm , and $\lesssim$20-kV equilibrium potential) are expected; the altitude dependencies of the various parameters have only been obtained theoretically.

There are two major effects of concern when the OTV encounters high-temperature (keV) plasma in the altitude region 3 R_E to 6.6 R_E (GEO). The first effect is the decrease in available power due to neutralizing currents from the plasma reaching exposed solar cell power leads. The second effect is high voltages which result from charge accumulation on spacecraft surfaces. Fortunately the size of the OTV acts to protect it, so only edges and corners will be subject to the full force of these effects.

For any plasma, a fundamental quantity is the Debye length. This length is the distance which the effects of an electrical disturbance are decreased by a factor, e. The solution to the Poisson equation for an isolated charge, q, in a plasma is

$$v(r) = \frac{q\, e^{-r/T_D}}{4\pi\varepsilon_o r}$$

where r is the distance from the charge, ε_o is the permittivity of free space ($8.854\ 10^{-12}$ farad/m), and v is the potential. It is seen that at a distance $r = T_D$ (the Debye length), v has been reduced by a factor of e. In the expression

$$T_D = \frac{1}{e}\sqrt{\frac{\varepsilon_o kT}{N}}$$

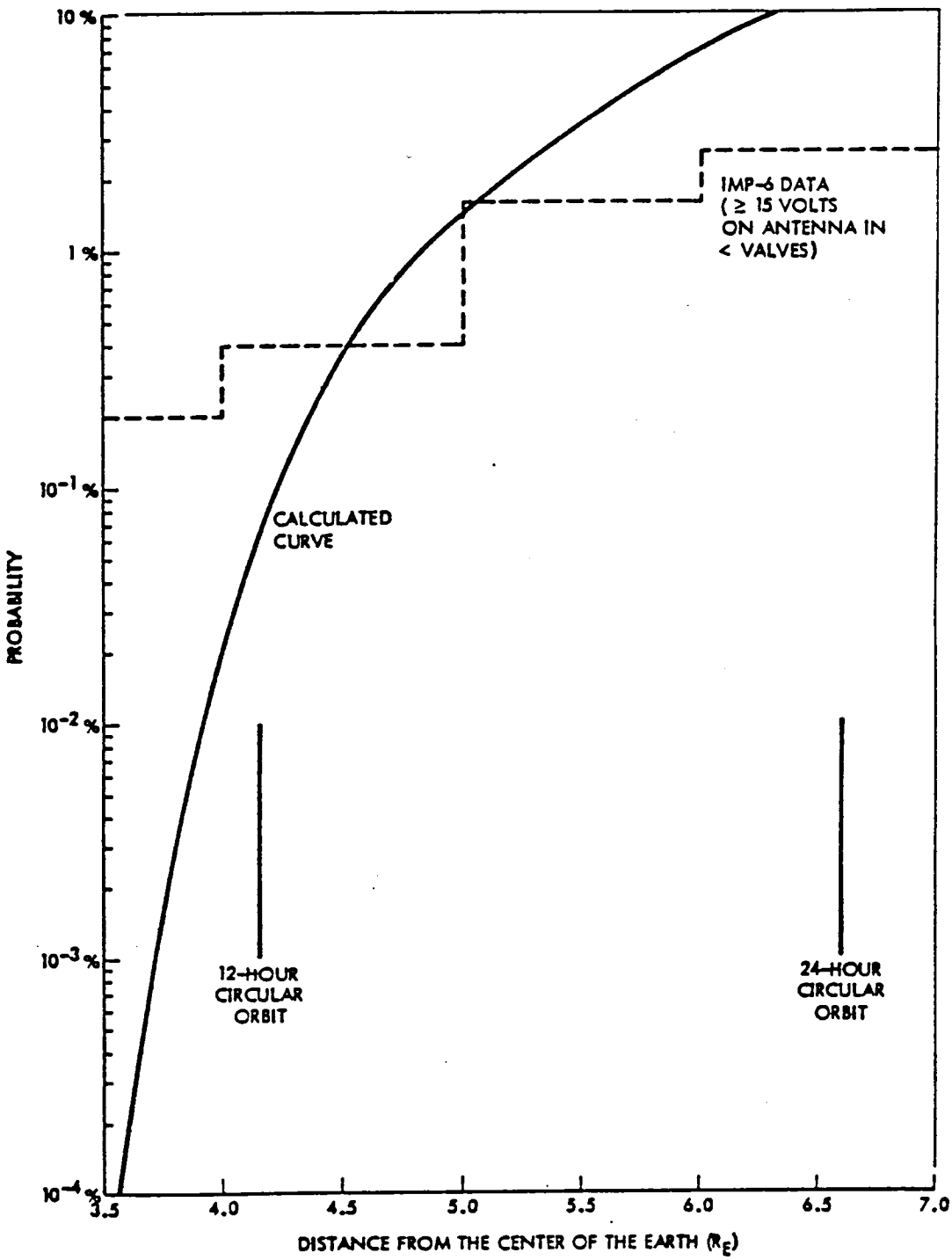

Figure 7.1-2. Comparison of Calculated Hot Plasma Probability Curve with IMP-6 Data

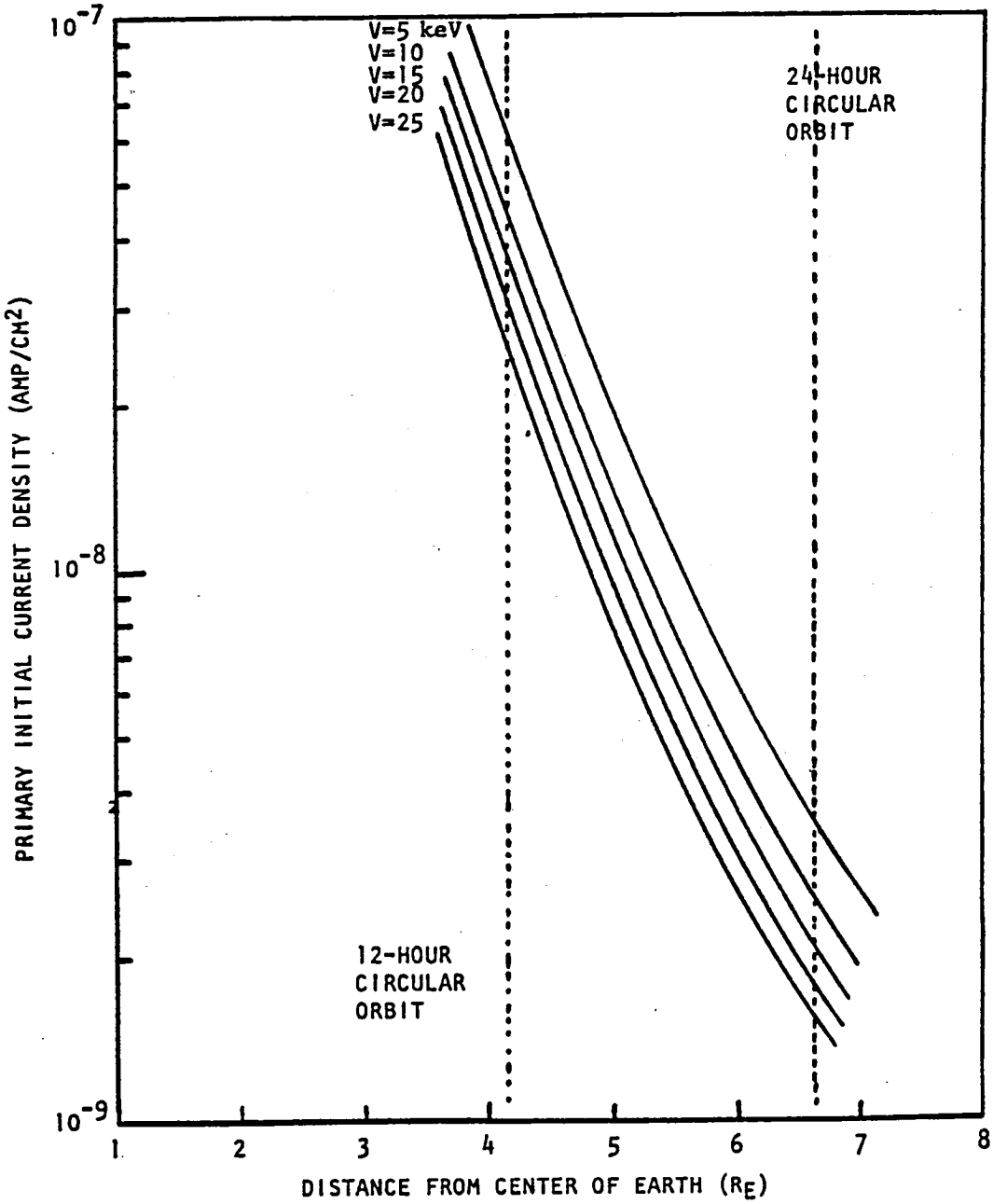

Figure 7.1-3. Calculated Primary Initial Current Density as a Function of Altitude (λM = 0 deg)

where e = electronic charge (1.6×10^{-19} coulomb)
k = Boltzmann's constant (1.38×10^{-23} J/°K)
T = absolute temperature of the plasma (°K)
N = density of electrons in the plasma (m^{-3})

For a plasma temperature of 5 keV, which is relatively typical value for the hot plasma that produces charging (producing an equilibrium voltage of ~12.5 kV), kT is 8×10^{-16} J. For 5 keV plasma

$$\lambda_D = \frac{5.4\times10^5}{\sqrt{N}} \text{ meters}$$

At geosynchronous orbit, N is $\sim10^6$ e/m^3, leading to a Debye length of ~540 m. At lower altitudes, N will be larger so λ_D will be smaller. Thus, to a first approximation, only the outer $\lesssim$540 m of the OTV will be exposed to the high-temperature plasmas. If the OTV is basically a conducting plane, the effect acts to reduce but not eliminate charging effects in the middle of the spacecraft. However, if the OTV is an open-gridded structure in three dimensions, the inside volume will be protected provided the spacing betweeen grid members is $\lesssim$540 m.

For those portions of the spacecraft not thus protected, the two effects previously mentioned—current losses from exposed conductors and spacecraft charging—must be considered. The current losses will be relatively small because the electron density in the plasma is small (~10 e/m^3). For exposed conductors with voltages (relative to spacecraft ground) less than the plasma temperature (a few kilovolts), the current losses will be on the order of a few nA/cm^2. Since solar cells with a 10-percent efficiency generate 10 mA/cm^2, the current losses will at most be a fraction of a percent even at kilovolt voltages. The charging phenomenon is potentially more serious, since the sudden release of electrical charge at high voltages can adversely affect sensitive electronic circuits. While power circuits should be immune from these effects, control, computer, and communications circuits (which operate on currents in the $\leq$ microamp region) are vulnerable. The recommended procedure is to insulate and RF-shield those sensitive circuits very well—basically an extension of current practice to prevent EMI effects. If each sensitive electronic "black box" can tolerate a 10-kV, 1-J discharge to any point on the box or any cable which leads into the box (which is equivalent to 10 m^2 of multi-layer insulation discharging at one time), it should be safe from effects due to spacecraft charging. While this is more severe than requirements specified for smaller spacecraft (~10 kV, few millijoule discharges), the larger size of the OTV may lead to larger discharges. The suggested requirements are therefore beleived to be conservative, but not excessively so.

The OTV may face another plasma problem—current losses from exposed high-voltage conductors in low-altitude earth orbits. The plasma responsible is the ionosphere. While the plasma temperatures are only a fraction of an eV (typically 1000°K to 1500°K), the plasma density is quite high at altitudes in the vicinity of 250 nmi—on the order of 10^6 electrons/cm^2 (10^{12} electrons/m^3). For this reason, the Debye length is quite small—on the order of a few millimeters—at that altitude. The combination of high density and relatively low temperature leads to appreciable neutralizing currents on the order of a

μA/cm for ~0 V, rising rapidly as the potential of the exposed conductor increases. Fortunately, space charge effects act to limit the current to <100 percent of that produced by the solar cells if the voltage of the exposed conductors is not too high. The curves shown in Figures 7.1-4, 7.1-5, and 7.1-6 are extrapolations of calculations by Kennerud. The calculations assume that 10 percent of the solar array consists of exposed high-voltage leads. The effect of the solar panel area is essentially a square root dependence in the plasma-dominated region. The altitude dependence is essentially that of the electron density. The curves have been plotted as percentages of generated power (~10 W/ft^2 or ~100 W/m^2). For those situations in which the curves are >100 percent, obviously more power will be lost than can be generated. However, for large solar panel arrays (≳10 ft^2), this situation is not expected to occur at voltages ≲ ±16,000 V.

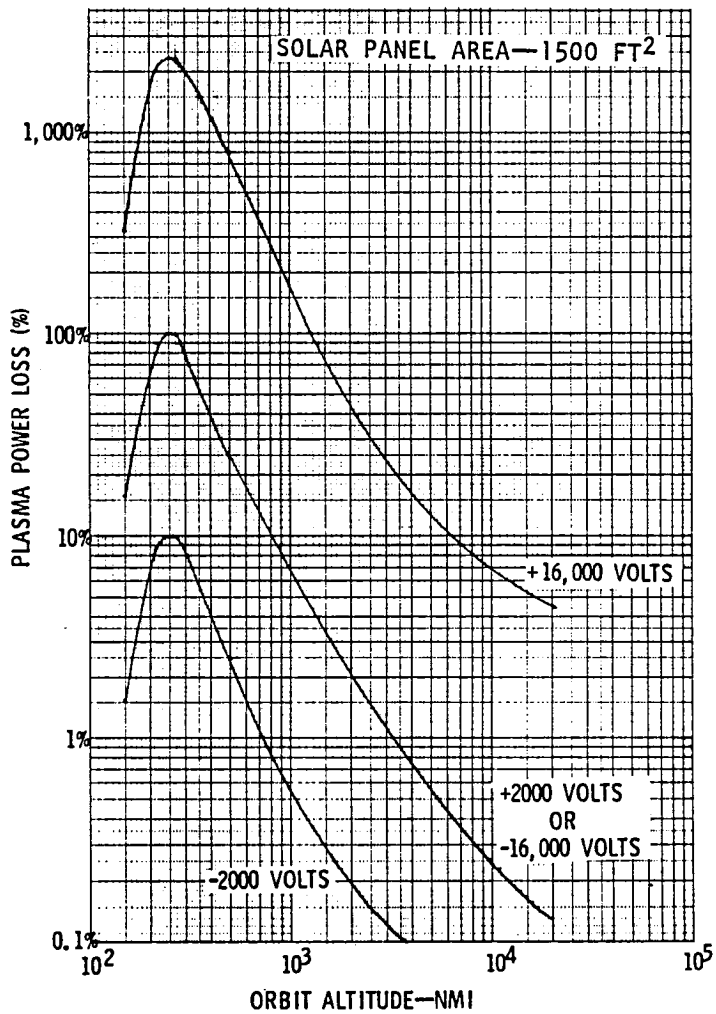

Figure 7.1-4. Calculated Plasma Power Loss as a Function of Altitude and Voltage for a 1500-ft^2 Solar Cell Array

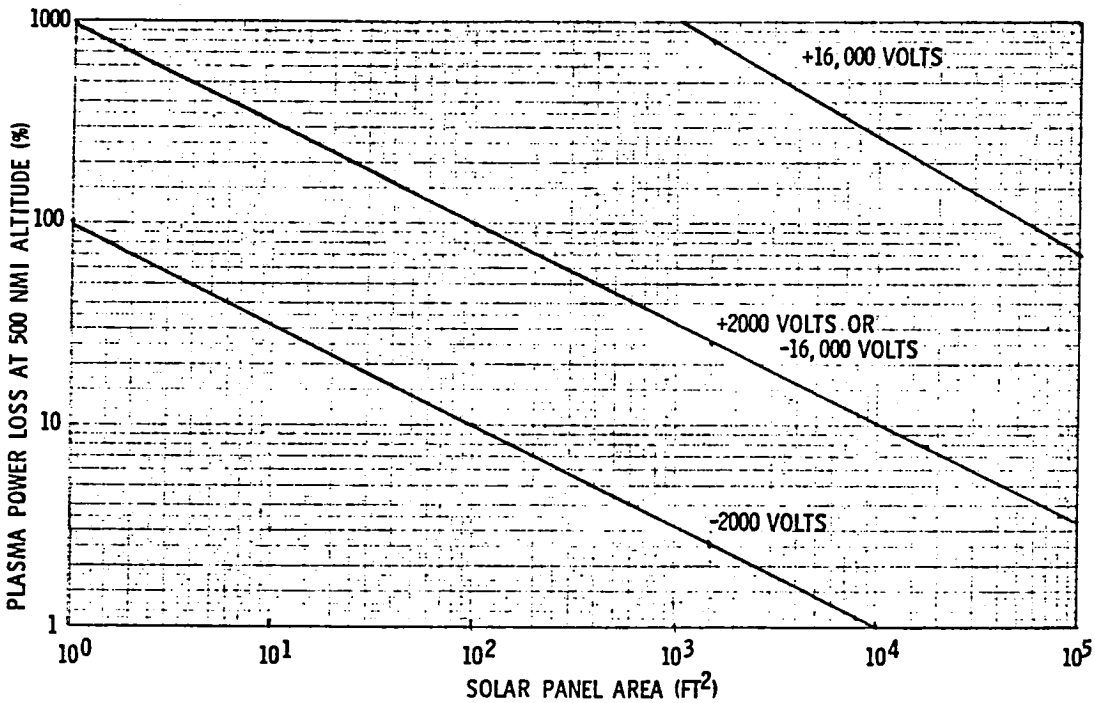

Figure 7.1-5. Calculated Plasma Power Loss as a Function of Solar Cell Panel Area and Voltage at an Altitude of 500 NMI

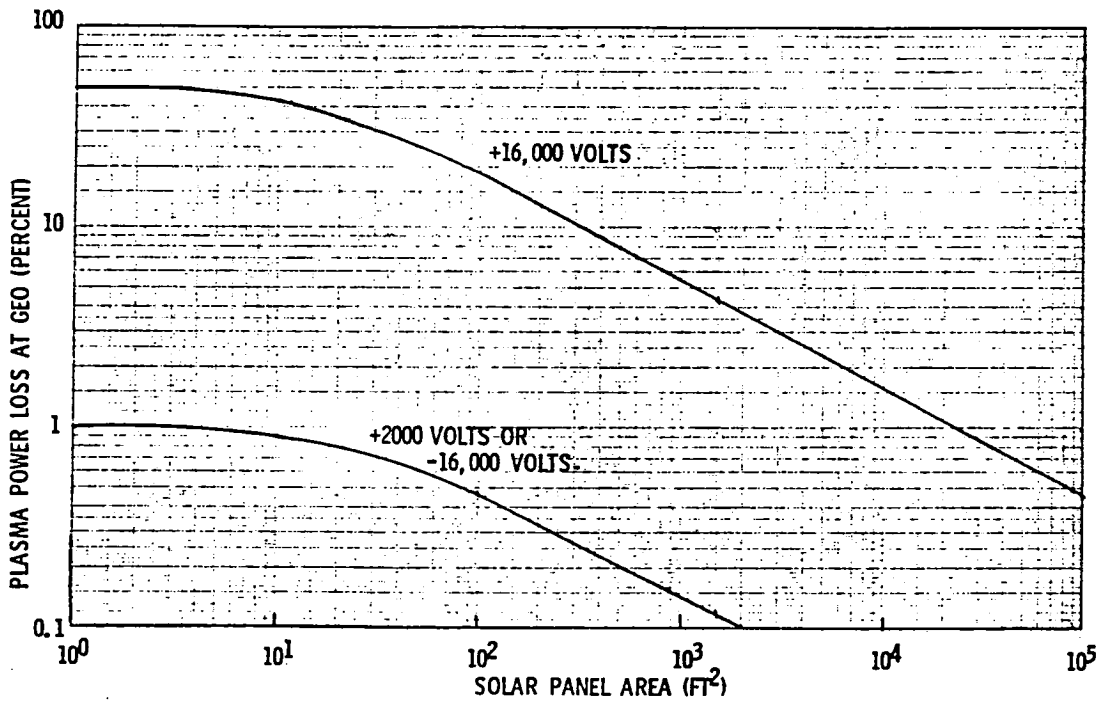

Figure 7.1-6. Calculated Plasma Power Loss as a Function of Solar Panel Area and Voltage at Geosynchronous Altitude

There is evidence that these calculations may be optimistic. Experimental work by Stevens et al. at NASA-Lewis, carried out in vacuum chambers at ~5×10^{-5} torr, showed that negative voltages $\gtrsim |600|$ volts resulted in discharges on their test solar cell panel. At positive voltages the plasma leakage currents increased linearly with voltages above ~300 V. The plasma densities were 2×10^{3} and 2×10^{4} e/cm^{3} for these tests. One possible explanation for the discrepancy between experiments and calculations might be the ambient pressures involved (and the corresponding molecular densities). The 5×10^{-5}torr used for the tests corresponds to an altitude of ~110 km, while the pressure at the peak of the ionosphere (250 nmi ≈ 460 km) is ~1.5×10^{-8}torr, over three orders of magnitude lower. Such a low pressure will not support a discharge; therefore, it has been assumed that Kennerud's calculations are basically correct. These calculations show that for large space structures the power losses (percentage-wise) should not be excessive provided the voltage is negative and not too high ($\lesssim$ a few thousand volts). Additional information relating to charging effects is contained in the Appendix.

7.2 NUCLEAR RADIATION ENVIRONMENTS AND EFFECTS

The nuclear radiation environments expected for the OTV are dominated by the earth's Van Allen belt even though solar flare particles become an increasingly important factor as GEO is approached. The radial dependence of Van Allen dose rates for 0° inclination orbits averaged over 24 hours is shown in Figure 7.2-1. The energy spectra of the electrons and protons become softer with altitude, so shielding plays an increasing role as altitude increases. One problem is that the Van Allen models and the data from which they were derived do not extend to zero energy, 40 keV being the minimum for electrons

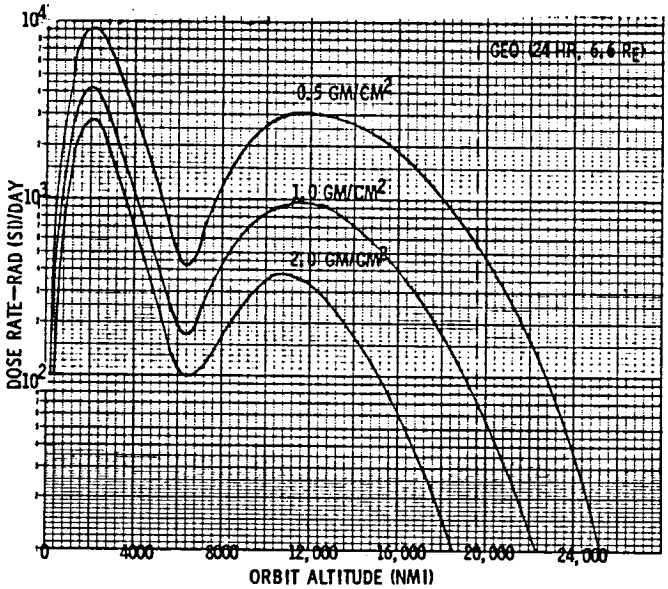

Figure 7.2-1. Time-Averaged Van Allen Dose Rates as a Function of Altitude and Shielding

while proton energy spectra extended down to 0.4 MeV. The cutoff energies for 2-mil SiO_2 solar cell coverslides are ~80-keV electrons and ~0.44-MeV protons. For shielding less than 2 mils (~1.3×10^{-2} g/cm^2) large uncertainties are introduced. While the dose vs. shielding thickness curve for GEO shows a flattening below ~2 mils (Figure 7.2-2), it is not certain that this is the case for other altitudes.

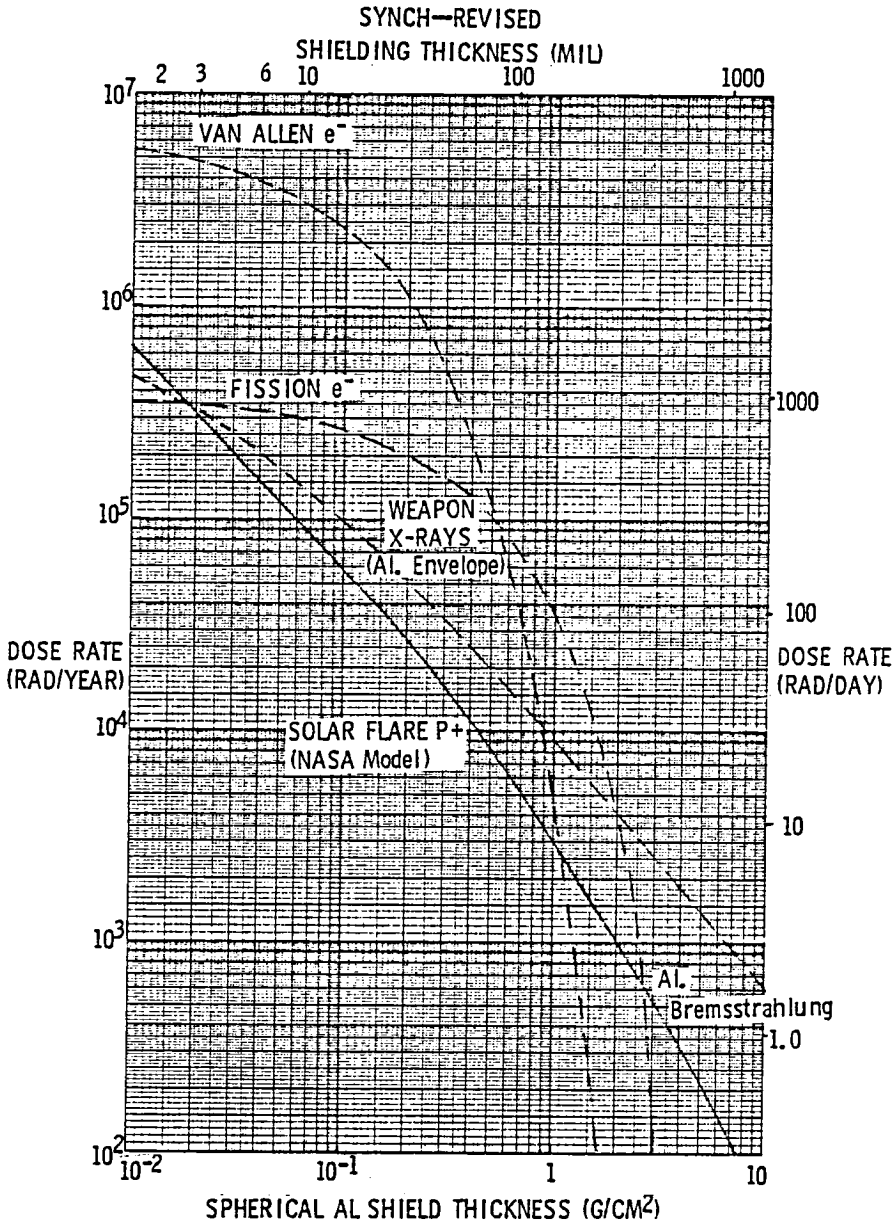

Figure 7.2-2. Nuclear Radiation Dose Rates as a Function of Shielding Thickness at GEO

It is not possible to treat both solar cells and other semiconductor electronic components the same way when considering the effects of nuclear radiation, because the charge carriers have to travel farther (and thus remain mobile longer in the conduction band) in solar cells than in other semiconductor components. For this reason, solar cells are more affected by displacement damage while ionization damage (which decays with time) is less important. For other components, which operate in the <μsec time region, the opposite is true. Therefore the flux-to-dose conversion factors which are largely based upon ionization radiation damage work fine for conventional semiconductor electronic components, but underestimate the effects of protons on solar cells. The usual practice, rather, is to calculate an equivalent 1-MeV electron fluence when dealing with solar cells. As for flux-to-dose conversion, particle fluence to 1-MeV equivalence curves are used. These are essentially identical to the flux-to-dose curves for electrons (normalized at 1 MeV), but are much higher for protons. For example, while a 10-MeV proton produces ~30 times the dose of a 1-MeV electron, it produces ~3000 times the solar cell degradation. Therefore, recourse must be made to the particle spectra.

The Van Allen particle integral spectra at GEO are shown in Figure 7.2-3. In common with the Van Allen particle spectra at all altitudes, they exhibit an $e^{-E/Eo}$ behavior, where E_o is an altitude-dependent characteristic energy. For protons, E_o has approximately an L^{-5} behavior (L = McIlwain parameter, $L = R_E$ at the geomagnetic equator, $R_E = L\cos^2\lambda_M$ at other altitudes) while for electrons, L has a behavior more like $L^{-1.3}$. Thus, at low altitudes the

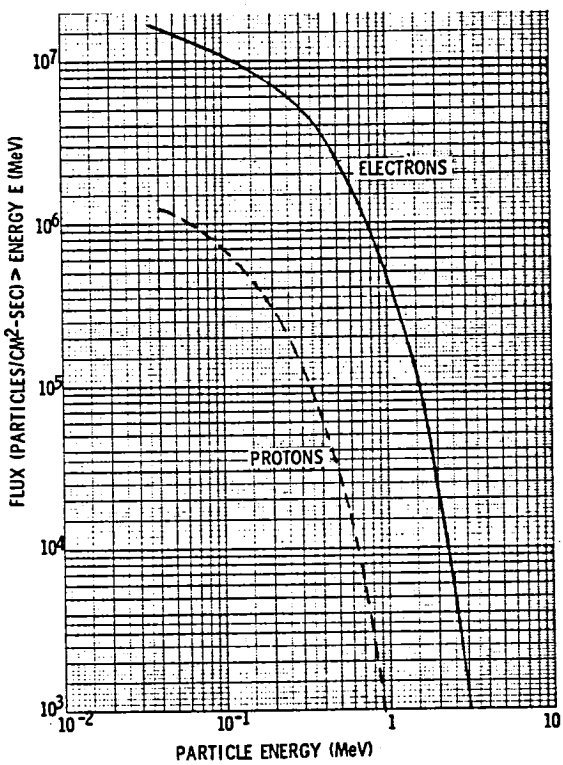

Figure 7.2-3. Van Allen Particle Fluxes in GEO (time averaged)

proton energy spectrum is quite hard (energies >100 MeV) while the electron spectrum is still relatively soft (energies <10 MeV). This is partially offset by the greater penetrating capability of electrons, as compared with protons of the same energy (Figure 7.2-4). The dose rate and the solar cell damage rate are dominated at low altitudes by protons. At high altitudes, e.g., GEO, electrons produce the greater dose rate and Van Allen protons are not an important factor in the solar cell damage rate. A few mils thickness of the solar cell coverslides will stop the Van Allen protons at GEO but not the electrons.

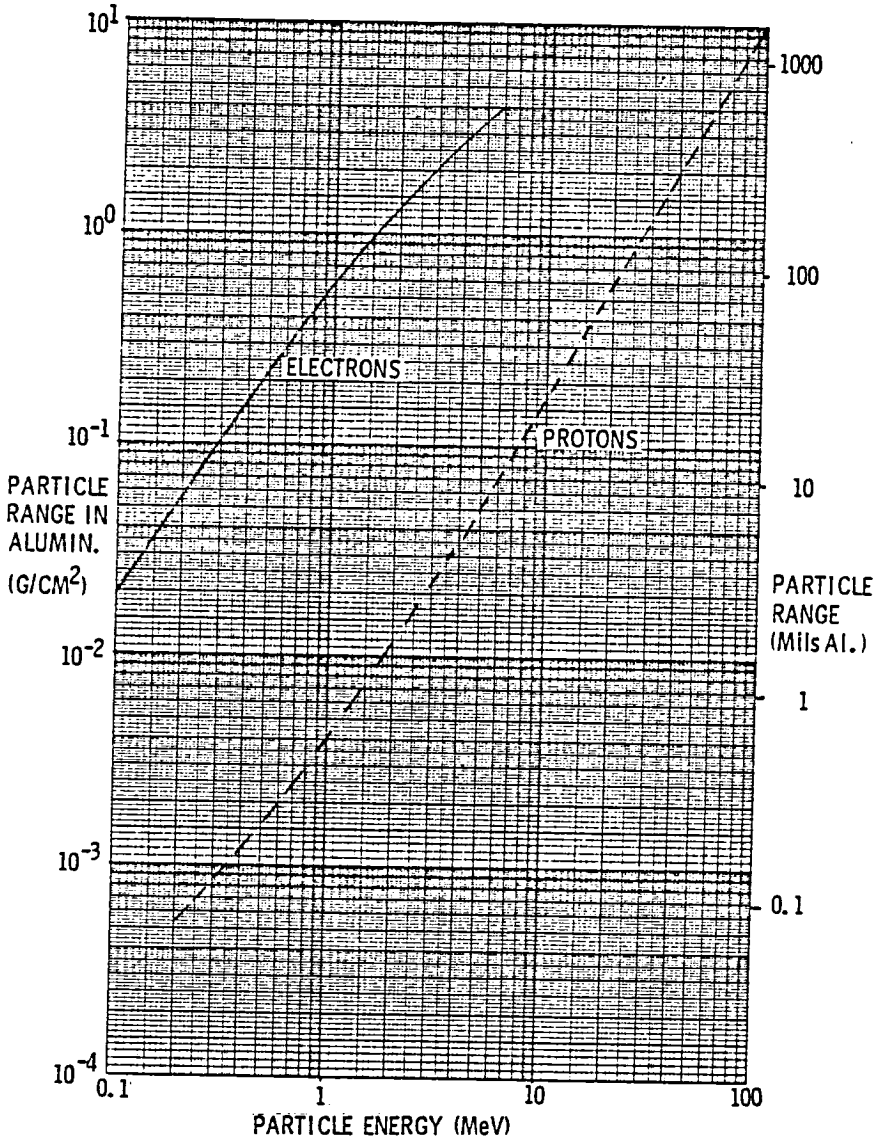

Figure 7.2-4. Range-Energy Relationship for Protons and Electrons in Aluminum

Unfortunately, there is another source of protons with which all radiation-sensitive spacecraft components must cope—solar flare particle events. While these events are relatively rare—especially large events—they can produce proton fluences $>10^9\ cm^{-2}$ above 100 MeV. While the geomagnetic field protects spacecraft at altitudes $\lesssim$500 nmi and at magnetic latitudes $\lesssim$45 degrees from almost all solar flare protons, for altitudes $\gtrsim$10,000 nmi and magnetic latitudes $\gtrsim$45 degrees, the free-space environment is little attenuated.

While solar flare particle events come in various sizes, it is customary to use the NASA model event as representative of the annual radiation environment expected from this source (the August 1972 event was almost that size). The time-integrated proton fluence as a function of energy for the NASA model is

$$\phi_p(>E) = 1.45\times10^{12}\,E^{-1.2} \qquad 1\leq E\leq 10 \text{ MeV}$$

$$= 7.08\times10^{11}\,e^{-P(E)/67} \qquad 10\leq E\leq 30 \text{ MeV}$$

$$= 5.28\times10^{11}\,e^{-P(E)/73} \qquad E>30 \text{ MeV}$$

where $$P(E) = \frac{1}{Ze}\sqrt{E\,(E+2m_oc^2)}$$

In the above equations, $\phi_p(>E)$ is the proton fluence > proton energy (MeV) in protons/cm^2, Ze = 1 for protons, and m_oc^2 = 931 MeV (proton rest energy). There is a solar flare alpha particle model also, but it adds $\lesssim$10 percent to the proton radiation dose and damage. The NASA model solar flare proton integral energy spectrum, calculated using the above equations, is shown in Figure 7.2-5.

Combining the Van Allen belt and solar flare particle event environments to obtain the expected Si solar cell radiation degradation effected on a low-thrust trajectory between LEO and GEO can be time-consuming with the results being dependent on mission duration and solar cell shielding. Such calculations have been carried out by Rockwell, Boeing, and others. A combination of the results yields the curves shown in Figure 7.2-6, after adjusting for differences in the LEO altitudes. It is seen that both solar cell coverslide thickness and mission duration are important; a long-duration mission with thin coverslides will almost totally degrade the solar cells so that their output will be <20 percent of their BOL (beginning of life) power. For large space structures such as the OTV the coverslide mass may be an important fraction of the spacecraft weight, so thick coverslides mean a long-duration mission. Very careful tradeoffs need to be done in this area. Annealing the solar cells once GEO has been attained should also be considered, but it is not certain how much of the radiation-produced degradation can be reversed in this way. (Annealing data are conflicting and apparently dependent upon many parameters.)

The nuclear radiation shielding requirements for sensitive electronics and man depend upon the environment and the radiation tolerance of the sensitive components. The GEO environment as a function of dose was shown in

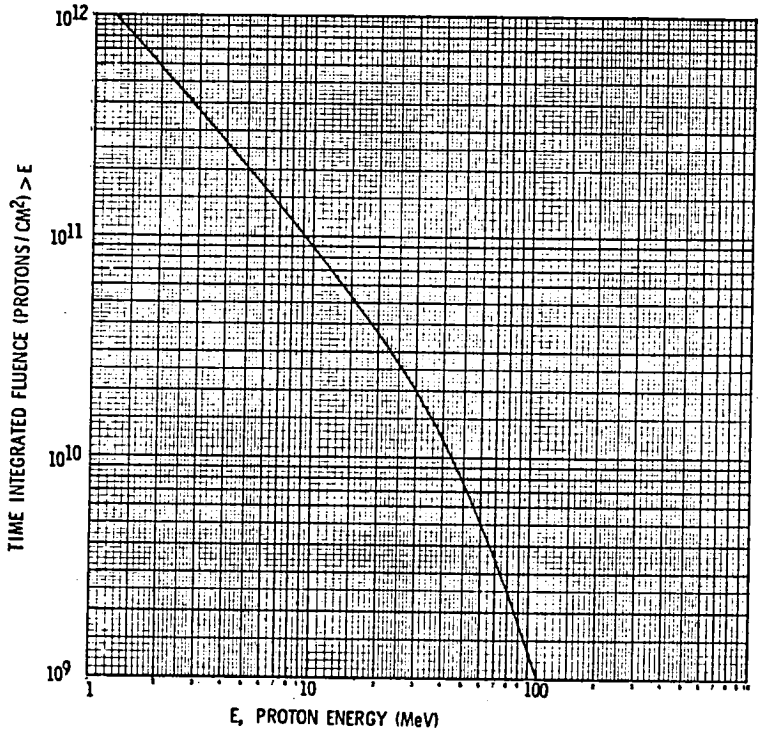

Figure 7.2-5. NASA Model Solar Flare Proton Integral Energy Spectrum

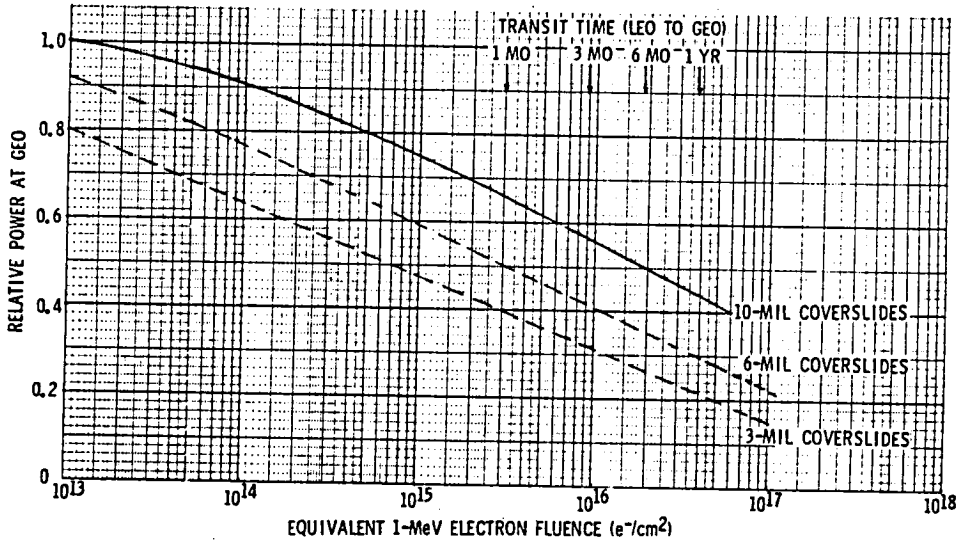

Figure 7.2-6. Calculated Si Solar Cell Degradation Factors for Low-Thrust Trajectories from LEO (500 nmi) to GEO

Figure 7.2-2. By comparing this figure with Table 7.2-1, which lists the approximate nuclear radiation hardness for various types of electronic components, the approximate shielding required for one year in GEO is immediately apparent. Since dose is a linear function of time (to a first approximation), the time-shielding relationship can be obtained. For example, bipolar transistors can tolerate ~10^5 rad before failing (failure is a relative term since a transistor whose current gain decreased by a factor of 2 might work fine in a digital circuit but be useless in an analog circuit—so the numbers in Table 7.2-2 can vary by at least +/- a factor of 3 depending on circuit design), which means that they can survive for one year in GEO behind 0.5 g/cm^2(~75 mil) of aluminum, for two years behind 0.6 g/cm^2 (if no fission electrons), ten years behind 1 g/cm^2, etc. Similar conclusions can be drawn for each of the component types shown in Table 7.2-1.

Table 7.2-1. Approximate Nuclear Radiation Tolerance of Various Electronic Component Types

Type	Approximate Tolerance (rad)
N MOS (STD)	3×10^3
C MOS (STD)	5×10^3
P MOS (STD	3×10^4
SCR	1×10^4
Bipolar	1×10^5
TTL (STD)	2×10^5
Crystals	5×10^5
P MOS/SOS	1×10^6
ECL	2×10^6
Solar cells	$\gtrsim1\times10^7$
TTL (hard)	~1×10^8

Table 7.2-2. Calculated EVA Duration for 28° Inclination Circular Orbits

Altitude		0.2 g/cm^2	0.35 g/cm^2	0.55 g/cm^2
km	(nmi)	EVA Duration (hr/mo)		
300	(162)	108	134	218
350	(189)	61	84	134
400	(216)	34	51	85
450	(243)	19	31	53

Elaborating somewhat, radiation effects on electronics generally fall into three categories—total dose, dose rate, and neutrons. The data presented in Figure 7.2-2 and Table 7.2-1 refer to total dose, which is cumulative (the component keeps working until the critical total dose has been received and then stops working). If nuclear weapon detonations take place, dose rate and neutron effects also come into play. Dose rate effects are transient in that

the electronic component functions as before once the radiation environment has ceased. For nuclear detonations, X-ray dose rates $>10^{10}$ rad/sec for $<10^{-6}$ sec are possible, which drives all semiconductor electronic components into saturation. If current limiters (resistors and ferrite cores) are used, this causes no damage. Dose rate effects are chiefly due to X-rays, which can be shielded out by a few mils of high Z-material (e.g., Ta). Neutron effects are cumulative, but are not generally significant at $\lesssim 10^{12}$ m/cm^2. If a nuclear detonation is close enough to produce $>10^{12}$ m/cm^2, the dose rate effects (due to X-rays) and total dose effects (due to trapped fission electrons) will probably damage the electronic components more than the neutrons.

It should be mentioned that at normal operating temperatures (~300°K) some annealing takes place in electronic semiconductor components. Thus, 10^5 rad received over the period of a few years may not disable a component which could not survive 10^5 rad received within a day. The extent of this annealing is subject to some controversy, so the usual practice is to treat it as an unknown safety factor.

Another uncertainty in calculating shielding requirements for sensitive electronic components is that in the environment itself. Various models have been developed to fit the Van Allen belt data. The extremes are designated by the suffixes "HI" and "LOW" (e.g., AE6-HI and AE6-LOW for the electron evironments). The differences between HI and LOW environments are significant only for high altitudes ($\gtrsim 3$ R_E) and for high energies ($\gtrsim 1$ MeV for electrons, ≥ 10 MeV for protons). This effect is shown in Figure 7.2-7 for the GPS orbit. This is approximately what would be expected for an OTV spiraling outward from LEO to GEO. As can be seen from Figure 7.2-4, the effect shows up for components shielded by $\gtrsim 0.5$ g/cm . The curves of Figures 7.2-1 through 7.2-4 are estimated time-averaged values which lie close to (but below) the HI environments.

The shielding required for humans is a separate problem because humans cannot tolerate nearly as much nuclear radiation as electronic components (450 rad over the entire body in a period of ≤ 1 week will kill 50 percent of the humans thus exposed). In addition, various parts of the human body have differing tolerances for nuclear radiation; the skin, eyes, blood-forming organs, and reproductive organs have been designated as the "critical organs" and separate radiation dose limits have been designated for each. In practice, the skin is usually the limiting factor because it has effectively no protection while the eyes (0.3 cm), reproductive organs (3.0 cm), and blood-forming organs (5.0 cm) are protected by the thickness of tissue indicated. Additionally, the eyes are localized and can be protected by local "spot" shielding. EVA suits are typically a few tenths of a g/cm^2 in shielding effectiveness, so the tissue shielding for the other critical organs is more important than the EVA suit shielding; if the EVA suit were several g/cm^2 thick, the blood-forming organs become the limiting factor.

The human dose limits are:

- One month 75 rad
- One quarter 105 rad
- One year 225 rad
- Lifetime 1200 rad

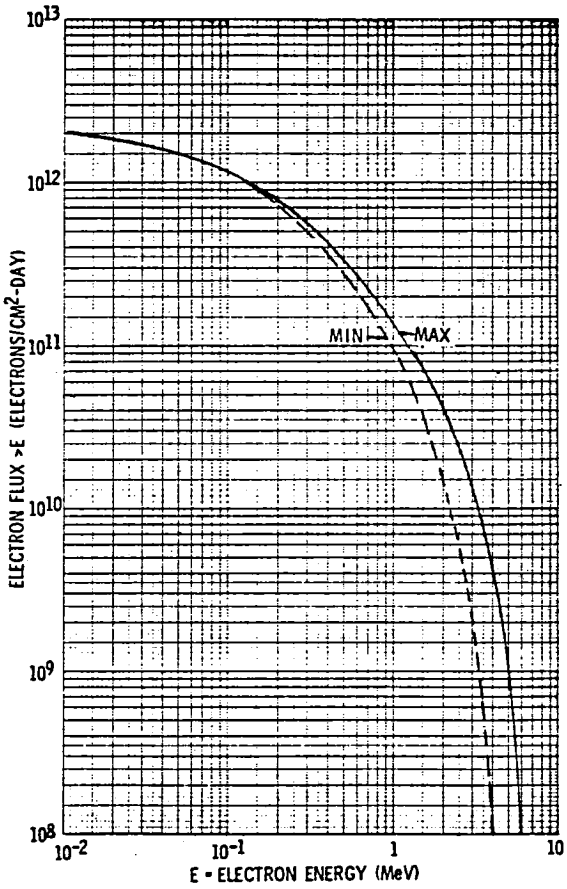

Figure 7.2-7. Relation between Maximum and Minimum Electron Integral Spectra (4.15 R_e, $i = 63°$, $\varepsilon = 0$)

A comparison of the dose limits with the dose rates (Figure 7.2-1) makes it apparent that EVA is possible only at low altitudes ($\lesssim$300 nmi), or in thick ($\geq$ a few g/cm^2) space suits. Low-altitude EVA is preferred to heavy space suits, except in emergencies.

The dose received in LEO is largely confined to a region between 15 and 60 degrees south latitude, 90 degrees west and 60 degrees east longitude called the South Atlantic anomaly. Thus, equatorial LEO orbits will receive appreciably (a factor of ~10) less dose than 28-degree inclination orbits at altitudes $\lesssim$500 km, but this advantage vanishes for altitudes $\gtrsim$900 km. For orbit inclinations $\gtrsim$30 degrees, the effects of the South Atlantic anomaly are rather uniform—all orbits at any altitude spend $\gtrsim$15 percent of their time in the anomaly. If EVA can be avoided when the spacecraft is in the anomaly, the duration of EVA which can be allowed before dose limits stop it can be increased.

The dose in rads is somewhat dependent upon the material involved—tissue rads are approximately equal to silicon rads for electrons and protons (X- and γ-rays) but is approximately a factor of 4 higher for protons because of the hydrogen in tissue. The biological dose unit rem is somewhat suspect because of the uncertainties in the RBE (relative biological effectiveness) or

QF (quality factor) which relate rads to rem. The ERD (effective residual dose) which takes account of biological recovery is even less well established and is treated somewhat like annealing in semiconductor electronic components (as a safety factor of uncertain magnitude).

Calculations have been carried out of the LEO EVA in space suits of various thicknesses. The results, shown in Figure 7.2-8, are for 28-degree inclination, 0 eccentricity orbits, and are based upon a skin dose of 75 rad in one month. Space suit thicknesses are from 0.2 g/cm^2 (about the thickness of space suits used in the past) to 1 g/cm^2 (maximum which probably could be tolerated since 1 g/cm^2 = 2 lb/ft and a space suit 1 g/cm^2 would probably weigh >50 lb). The advantage of low-altitude orbits is apparent from this standpoint. However, atmospheric drag probably precludes orbits below ~400 km (~216 nmi) for large spacecraft (e.g., OTV).

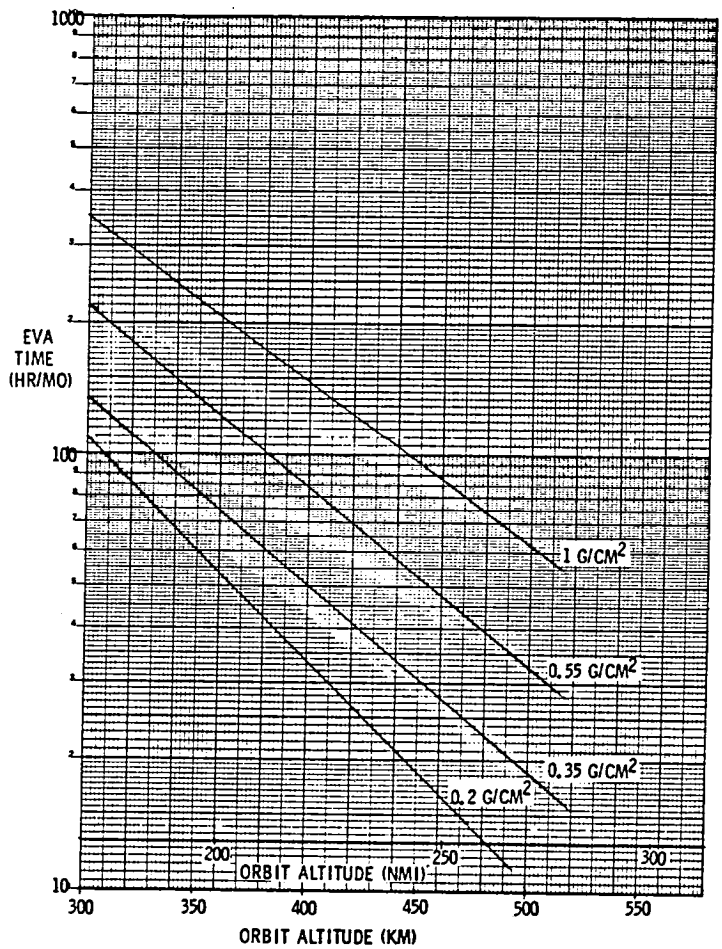

Figure 7.2-8. EVA Time allowed at Leo as a Function of Space Suit Shielding

If EVA lasts more than 30 days, the times shown in Figure 7.2-8 do not apply directly. For example—for a three-month period the total allowable skin dose is 105 rad, an average of 35 rad/month. This is approximately one-half the 75 rad/month allowed for any 30-day period. Thus, by stretching the activties requiring EVA from one month to three months, the total EVA hours will be increased only by about 50 percent from the values shown in the figure (but the EVA hours/month will be approximately halved). For one year, the total EVA hours will be three times the hours shown, but the monthly average will be one-fourth those shown, etc.

7.3 METEOROID ENVIRONMENT AND EFFECTS

The meteoroid environment expected in earth orbit is a combination of stream and sporadic particles. The stream meteoroids occur at well-known dates during the year, and are named for the stellar constellations from which they appear to be coming (lyrids, perseids, taurids, geminids, etc). The sporadic meteoroids come at random times. Both types of meteoroids have particle densities on the order of 0.5 g/cm and average velocities, relative to the earth, of ~30 km/sec (the velocity of the earth in its orbit). The particle fluxes are given in the form of mathematic equations by Weidner in various NASA handbooks. The equation for particles with masses between 10^{-6} grams and 1 gram is

$$\log \phi = -14.37 - 1.213 \log m$$

where ϕ is in particles/m^2 - sec > mass, m

m is the particle mass in grams

This near-earth meteoroid flux is modified in two ways by the presence of the earth. The effects of the earth gravitational field, which attracts meteoroids, is taken into account by a defocusing factor, G_E. The formula for G_E is

$$G_E = 0.565 + \frac{0.435}{r} \quad (r \text{ in earth radii})$$

where r is the distance from the center of the earth. For GEO, G_E is ~0.631. The second effect of the earth is to shield out some of the meteoroids. This body shielding factor, δ, is a simple solid angle calculated from the formula

$$\delta = \frac{1+\cos\theta}{2}$$

where $\sin\theta = \frac{R}{R+h}$

where R is the radius of the earth and h is the altitude above the surface of the earth in earth radii (h = r - 1). For GEO, $\delta \simeq 0.994$. At lower altitudes δ decreases while G_E increases, δ approaching 0.5 at the surface of the earth while G_E approaches unity. There, the altitude dependence of the meteoroid flux is small. While the meteoroid flux shown in Figure 7.3-1 was calculated for GEO, it is approximately correct for lower orbits as well.

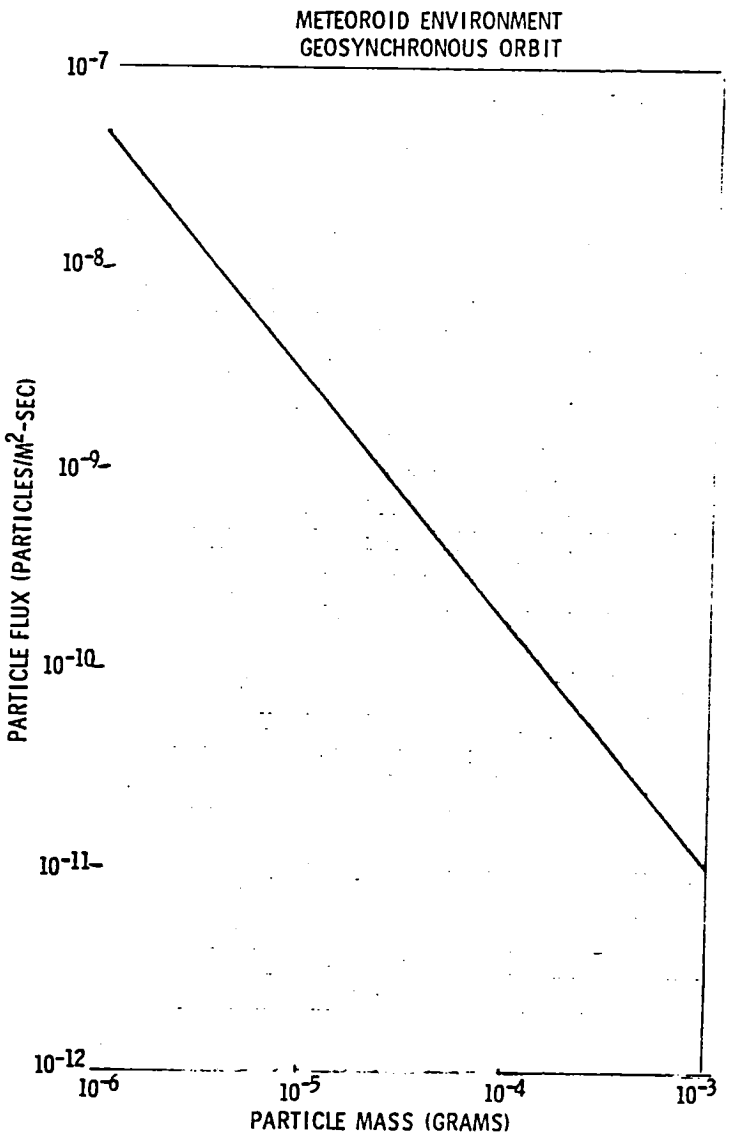

Figure 7.3-1. Time-Averaged Meteoroid Flux at Geosynchronous Orbit

The major effect of the meteoroids on spacecraft is to produce holes in them. The penetrating ability of meteoroids may be calculated from any of a number of equations; the following equation was used here.

$$t = \frac{1.75\ F_F P_P^{0.133} V_P^{2/3} m_P^{0.367}}{H_t^{1/4}\ P_t^{1/6}}$$

where
- P_P = density of the particle (g/cm^3)
- P_t = density of the shield (g/cm^3)
- V_P = velocity of the particle (km/sec)
- m_P = mass of the particle (grams)
- F_F = penetration factor (= 1.8 for hard Al)
- H_t = Brinell hardness of the shield (= 120 for hard Al)
- t = single sheet shield thickness just penetrated

The relationship between meteoroid mass and single sheet aluminum thickness, calculated using the above equation is shown in Figure 7.3-2 for Pp = 0.5 g/cm^3 and V_P = 30 km/sec. If multiple sheets are used, the total thickness needed to

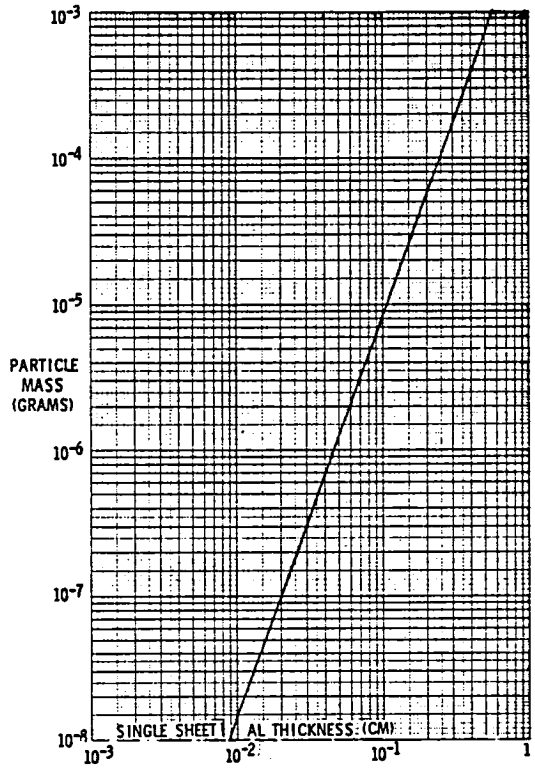

Figure 7.3-2. Relationship between Meteoroid Mass and Average Single Sheet Aluminum Thickness just Penetrated

stop a meteoroid of a given mass is reduced, provided the multiple sheets are sufficiently separated. The amount of reduction in t can be as much as a factor of 5.

For a large spacecraft, such as the OTV, the area exposed is sufficiently great that meteoroid hits will occur rather frequently. For example, if a single sheet 5×10^{-6} cm (20 mils) can just be penetrated by a 1.2×10^{-6} gram meteoroid, and the flux of such particles is $\sim4\times10^{-8}$ particles/m^2-sec, the probability that a 1-m^2 surface will be penetrated in a year (3.1×10^7 sec) is ~1.2. In this way the curve of Figure 7.3-3 was generated, which shows that any extended body will be hit several times each day. Even though Figure 7.3-3 was generated for GEO, it is approximately true at all orbit altitudes. In particular the solar cells of the OTV will suffer repeated hits, so it is important to design the solar cell strings such that a hit on one cell will not disable the entire string.

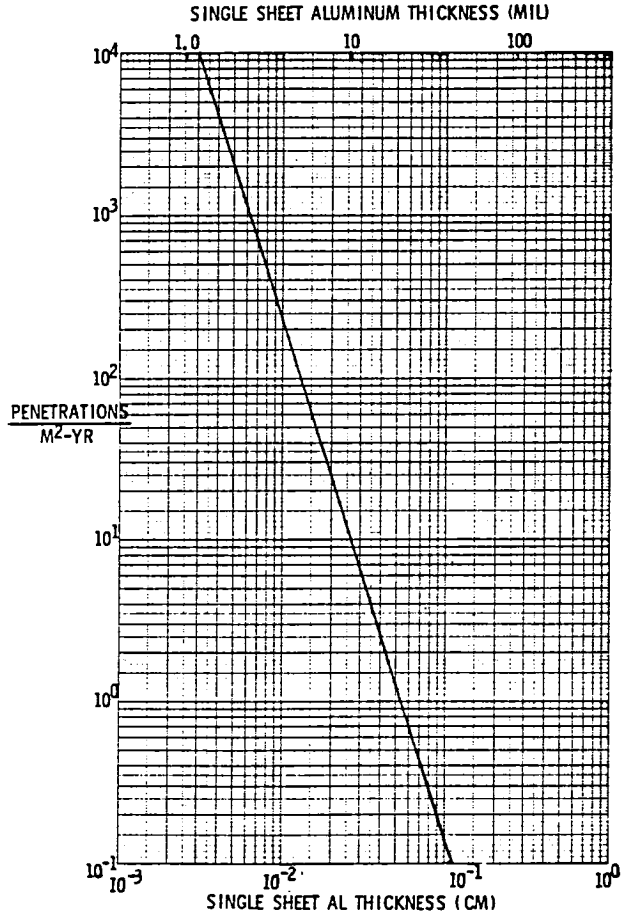

Figure 7.3-3. Average Number of Meteoroid Penetrations (per m^2) expected Each Year in Geosynchronous Orbit

8.0 SATELLITE CONTROL

8.0 SATELLITE CONTROL

8.1 INTRODUCTION

A projection of the electrical energy demands over the next 30 to 50 years, coupled with reasonable assessments of known or developable energy sources, indicates that a shortage of electrical energy will occur about the turn of the century. Recognizing the criticality of such a shortage, the Department of Energy (DOE) is currently evaluating alternative power generation concepts. One of these candidate concepts is the Satellite Power System (SPS).

The satellite power system consists of a large solar power collecting and conversion satellite, located in a stable geosynchronous equatorial orbit (GEO), that transmits this energy in microwave form to a dedicated collecting/conditioning ground receiving station located at designated sites throughout the United States. Each of the orbiting satellites transmit (beam) the microwave power to a single, specific, rectenna location. The ultimate SPS program may consist of as many as 60 of the satellite/rectenna combinations.

The power levels considered during the evaluation of the various satellite systems have ranged from 5-10 GW with the final selected baseline system sized to 5 GW nominal at the utility interface. It is apparent that, with this power level, both the satellite and the rectenna must be very large and encompass a large number of complex operational system activities.

It was the intent of this study to identify and analyze the operating functions of the satellite and the rectenna system to determine the control characteristics of a single satellite/rectenna combination and to also consider the relationship with other satellite/rectenna systems in the total program. Because of the level of system and subsystem definition, the scope of this study focused on the identification of probable operating functions in an attempt to determine the existance of critical operation paths, and to determine specific areas where other definitions would be most effective.

The following sections of this report present a short, descriptive summary of the baseline satellite and ground receiving station (GRS) considered in the analysis, summary descriptions (scenarios) of both the satellite and GRS operation as well as recommendations for future extension/expansion of the system control study.

The majority of the work leading to this report was accomplished by IBM Federal Systems Division personnel under contract (M7M8BNS-890163M) to Satellite Systems Division of Rockwell International.

8.2 SCOPE

The scope of the study has been limited to the outlining and identification of major operations areas for both the satellite and ground based functions with a possible regional control center located at the ground station.

Satellite/ground functional analysis is constrained to startup and nominal operations because of the limited time and because of the limited subsystem/system data available. The satellite functions identified and evaluated primarily address the major subsystems to generate and transfer the energy obtained during the primary satellite mission. The ground portion of this study included the space-ground interface, the primary rectenna, GRS-utility interfaces, the GRS control center, and (if required) a regional control center(s). Emphasis is on all but the regional control center. Figure 8.2-1 illustrates the various elements of the SPS system and their relationships/interfaces with each other.

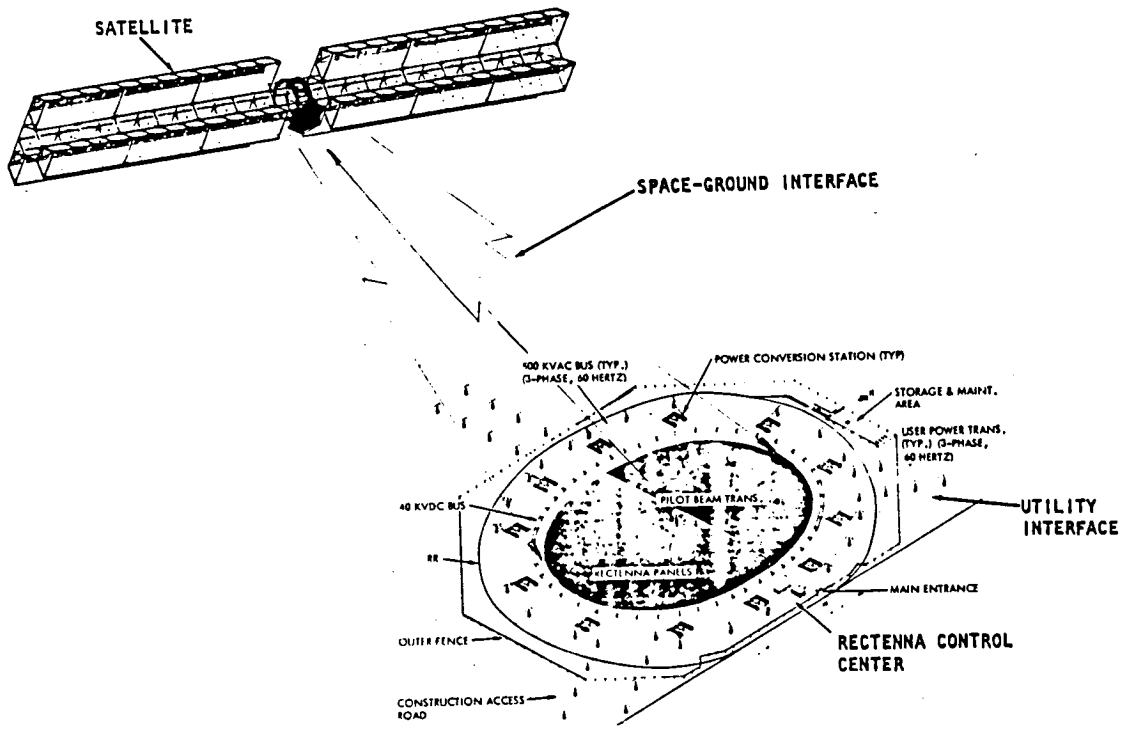

Figure 8.2-1. SPS System

8.3 APPROACH

Satellite control is functionally analyzed from two perspectives: 1) nominal satellite and antenna control, and 2) startup and shutdown operations. These are then considered in a logical time/subsystem ordered sequence to facilitate development of a comprehensive operations scenario.

A chronological sequence is followed from pre-start and startup to steady-state functions. Subsystems are considered as they logically become involved in providing any necessary support, e.g., command/control, communications, information processing, power conversion, distribution, switching, environmental control, etc. Since startup operations are critical to establishing systems operations within the bounds established by the effects of large power transients, to establish accurate beam pointing, and to produce minimum utility power transients, these functions are scrutinized more closely than are the steady-state operations.

Overall functional flows and system performance information is not included pending more detailed subsystems designs. Nevertheless, these preliminary scenarios provide some significant cross-checks to concept feasibility by helping identify any conflicts or lack of identified support requirements (space or ground). These studies also provide a basis for future functional flow chart definition, help identify, to the subsystem designers, those areas requiring increased definition, and help clarify, to program management, how the system may be cohesively integrated into operational reality.

8.4 SYSTEMS

The Satellite Power System (SPS) major elements consist of a power satellite placed in a geosynchronous, equatorial, orbit and a dedicated companion element, the GRS, located at a selected site within the continental United States. The nominal power output of the SPS is pegged at 5 gigawatts (5 million kilowatts) although, because of various system constraints and/or losses may actually produce between 4-5 gigawatts.

This section provides a summary description of the baseline satellite and GRS considered during the control analysis.

The baseline satellite configuration used during this study activity is shown in Figure 8.4-1. Subsequent satellite configuration did not substantially modify the baseline data, nor did they significantly alter any assumed operations.

8.4.1 SATELLITE SYSTEM DESCRIPTION

System capabilities constrain operations so that an understanding of the satellite subsystems is essential to an operations analysis. Further, some subsystem elements are more critical than others and require added attention during the analysis.

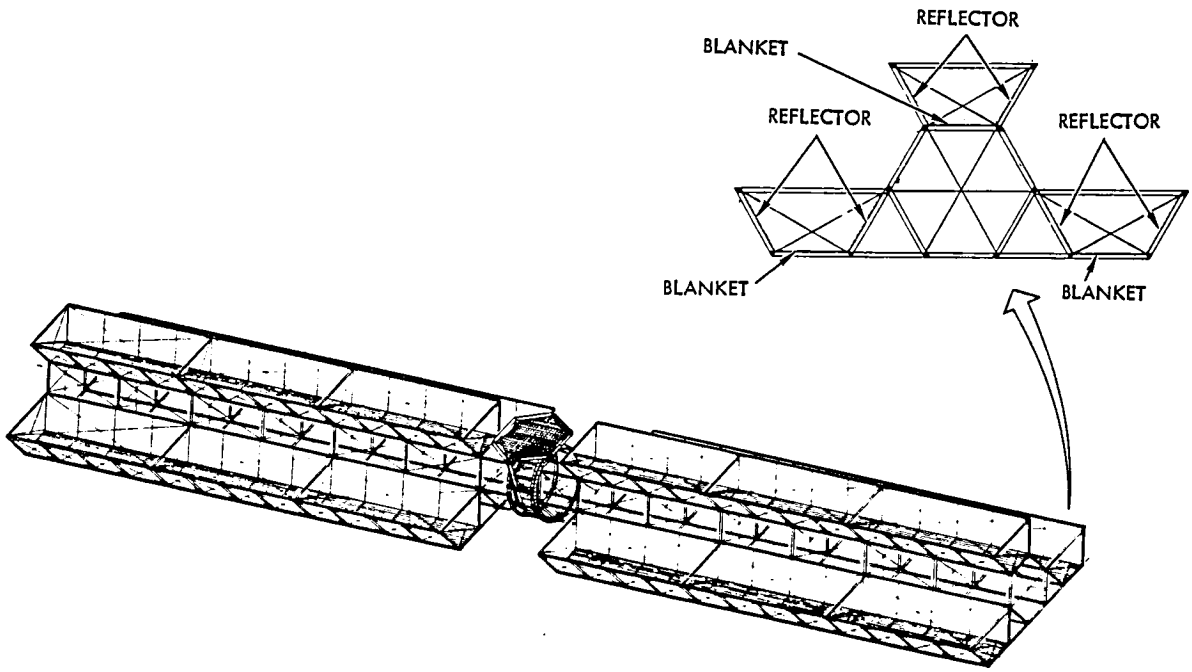

Figure 8.4-1. Baseline Satellite

The ground control facility is used to monitor and control the satellite from the ground. Included in this activity is the activities associated with telemetry, tracking, communications, monitoring of microwave beam characteristics, computing gross plan corrections, and providing frequency standard signals for the satellite. Concurrently, the ground control facility will control and monitor the collected electrical power through required conversion(s) and distribution to the designated utility interfaces.

Overall System

Seven subsystems comprise the satellite (Figure 8.4-2). Attitude control directly affects power generation efficiency and includes satellite-rectenna pointing. Power generation, distribution and transmission are dominant mission functions, while thermal control is essential to dissipation of the large amounts of waste heat. Coordination of satellite operations is performed by the Information Management and Control Subsystem (IMCS) as shown in Figure 8.4-3.

All subsystems support the mission functions of power generation, distribution and transmission. Electrical power output from the solar panels is fed via switch gears into feeder busses and then into main distribution buses to the antenna (Figures 8.4-4 and 8.4-5). Power is also distributed to batteries so that critical functions, such as IMCS and thermal support, can be provided through solar eclipses. The microwave power transmission subsystem (MPTS) (Figure 8.4-6) consists of dc-to-microwave conversion devices which feed an array antenna. Phasing control is maintained by use of a pilot beam originating at the GRS and received at the satellite antenna.

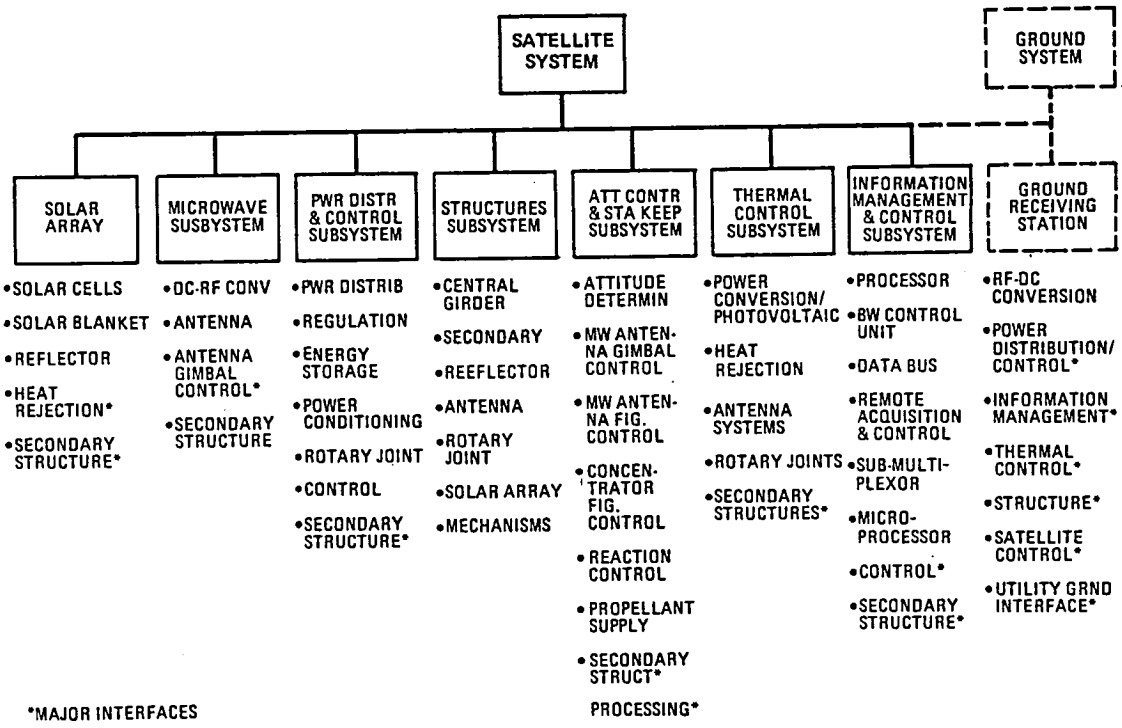

Figure 8.4-2. Total System

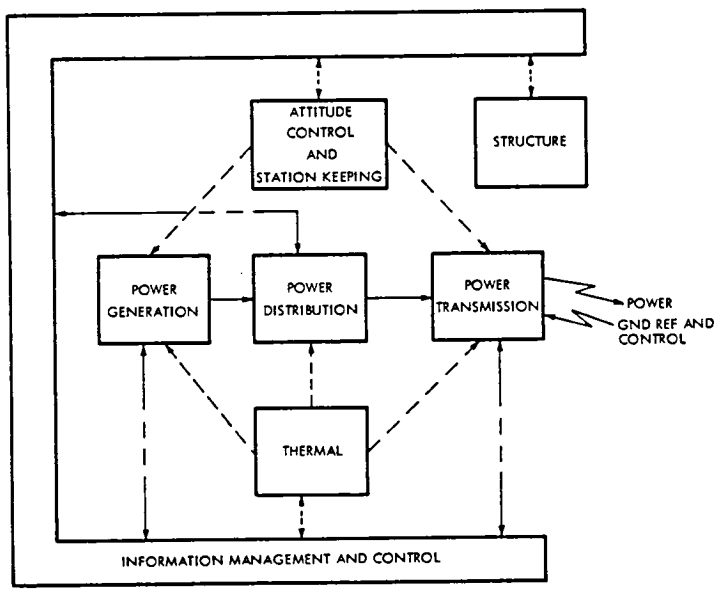

Figure 8.4-3. Key Subsystem Relationships

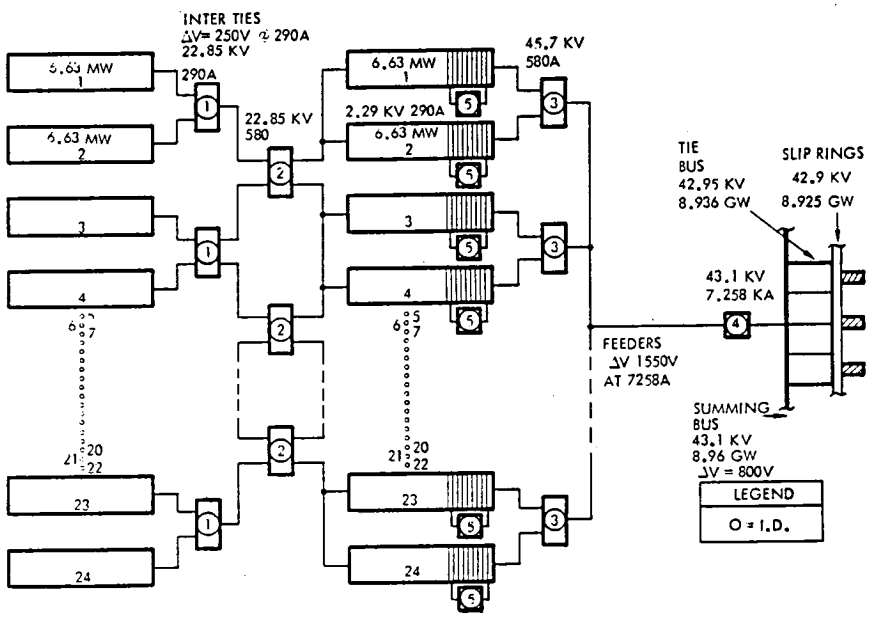

Figure 8.4-4. Power Generation

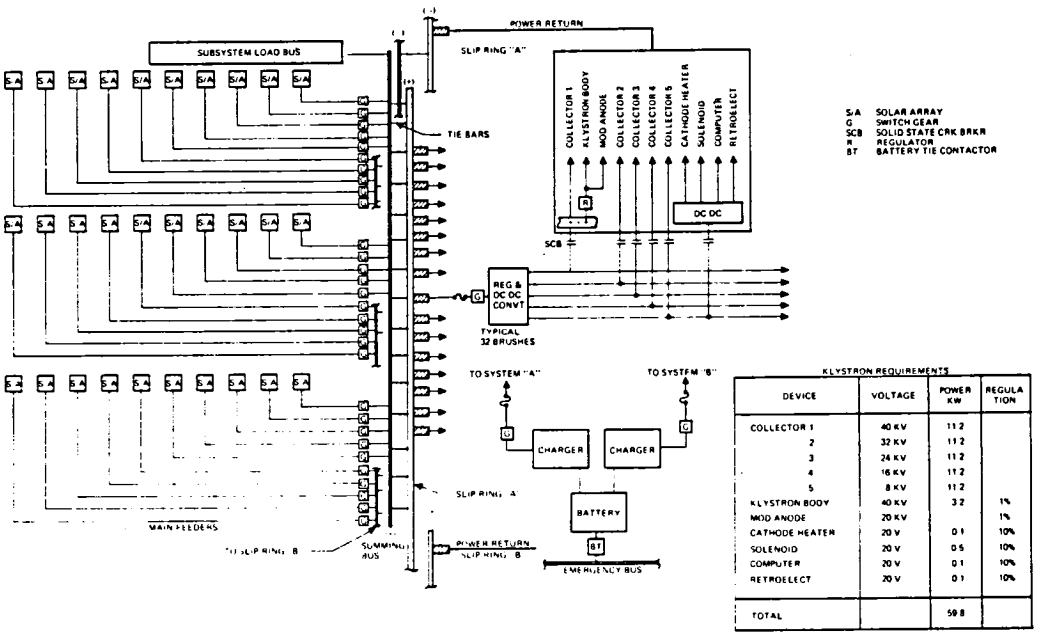

Figure 8.4-5. Power Distribution

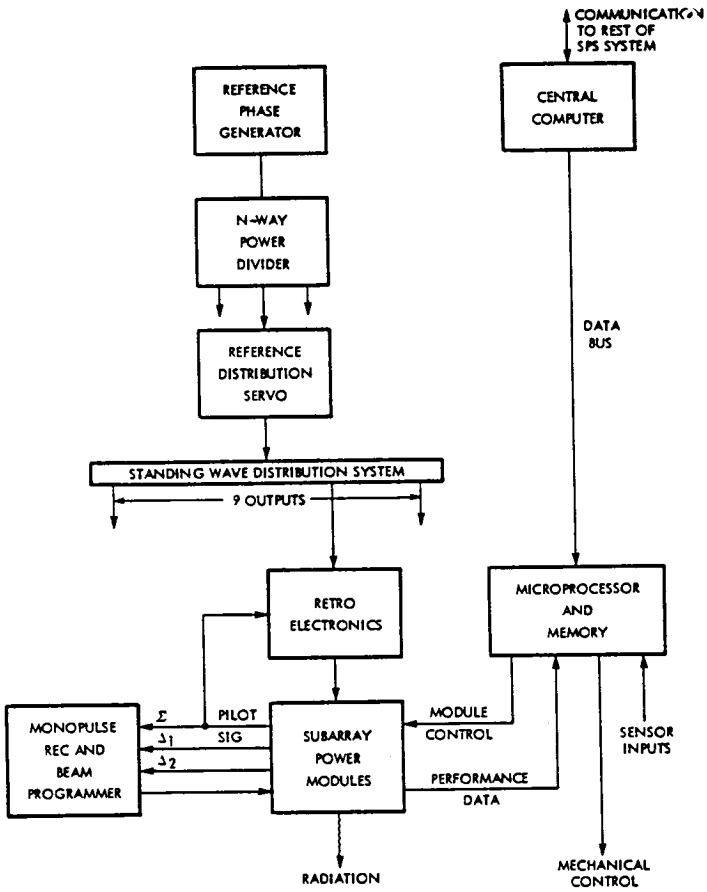

Figure 8.4-6. Microwave Power Transmission

Subsystem Considerations

Microwave control and solar eclipses are two major areas of consideration because they are critical to SPS operations. Beam control is initiated from the GRS through the pilot beam, which is used in a conjugation scheme (Figure 8.4-7) to provide phase control signals for fine pointing. The involvement of ground support coupled with the large number of measurements are commands on the antenna (Table 8.4-1) suggests the need for the operations analysis to focus on antenna functions. Solar eclipses occur during the spring and autumn and can last for up to 1.2 hours. These cause power outages which complicate operations (Figure 8.4-8).

8.4.2 GROUND SYSTEM DESCRIPTION

System capabilities constrain operations so that an understanding of the ground subsystem concept is essential to an overall operations analysis. Emphasis has been given to satellite system definition over the past 2 years so that ground-based systems definition is sketchy in some areas and totally unknown in other areas.

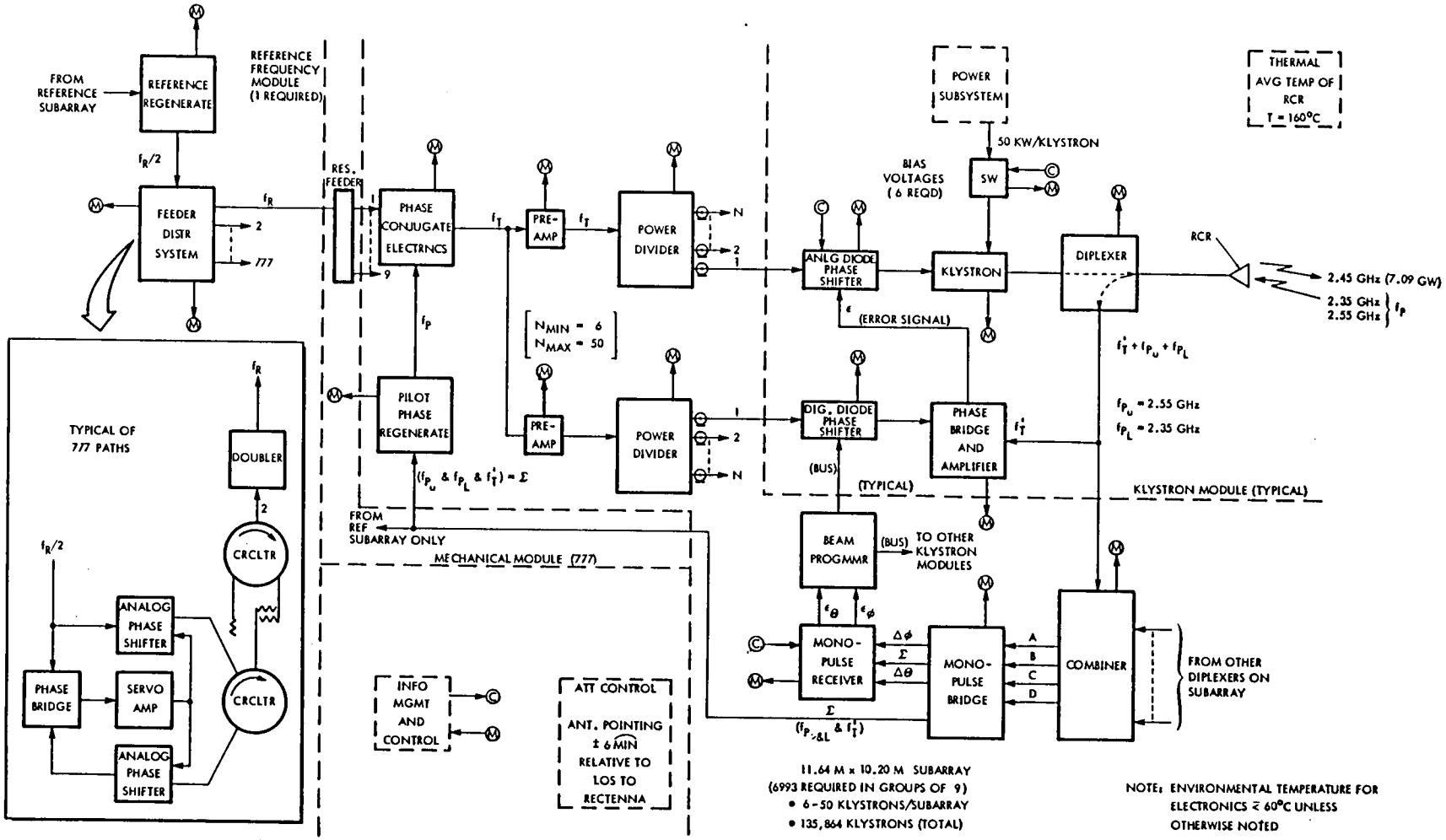

Figure 8.4-7. Beam Generation and Control

Table 8.4-1. Measurements and Controls

SUMMARY MEASUREMENTS				
	ANALOG	DIGITAL	EVENT	TOTAL
MICROWAVE ANTENNA	6×10^6	1×10^6	2.1×10^6	$>9\times10^6$
OTHER SUBSYSTEMS				
STRUCTURE	35	35	35	>100
ATT. CONTROL & STATIONKEEPING	900	800	1,000	~3,000
POWER DISTRIBUTION	1,000	100	2,000	~3,000
INFORMATION MANAGEMENT	-	~19,000	-	~19,000
THERMAL	16,000	-	-	16,000
LIFE SUPPORT	TBD	TBD	TBD	TBD
SAFETY AND SECURITY	TBD	TBD	TBD	TBD

SUMMARY CONTROLS			
	PROPORTIONAL	EVENT	TOTAL
MICROWAVE ANTENNA	$<13.6\times10^6$	30×10^4	$<44\times10^4$
OTHER SUBSYSTEMS			
STRUCTURE	~35	~35	<100
ATT. CONTROL & STATIONKEEPING	~100	>300	<500
POWER DISTRIBUTION	-	>300	>300
INFORMATION MANAGEMENT	-	>3,000	>3,000
THERMAL	-	TBD	TBD
LIFE SUPPORT	TBD	TBD	TBD
SAFETY AND SECURITY	TBD	TBD	TBD

ANTENNA SUMMARY BREAKDOWN					
	MEASUREMENTS			CONTROLS	
	ANALOG	DIGITAL	EVENT	EVENT	PROP.
REFERENCE FREQUENCY MODULE	32			6	
FEEDER DISTRIBUTION	13,986			1,554	
SUBARRAYS	223,776	41,958	104,895	13,986	
POWER MODULES	3,260,736	271,728	1,358,640	135,864	
POWER DISTRIBUTION	2,717,378	679,320	679,418	135,962	135,692
TOTALS	6,215,908	992,466	2,142,953	287,274	135,692
		9,351.867			

The earth-based power receiving element, the rectenna, has been conceptually defined and some hardware technology investigations have been completed. But, the control center which is generally acknowledged to be necessary to satellite-GRS operations has not been conceptually designed. In addition, if many solar power satellites are deployed, some designers believe that regional control centers may be required to coordinate satellite logistics and utility power distribution.

This study utilizes the current Rockwell GRS-utility interface concept which has resulted from earlier studies. General assumptions are made as to the architecture of GRS and regional control centers. Several GRS

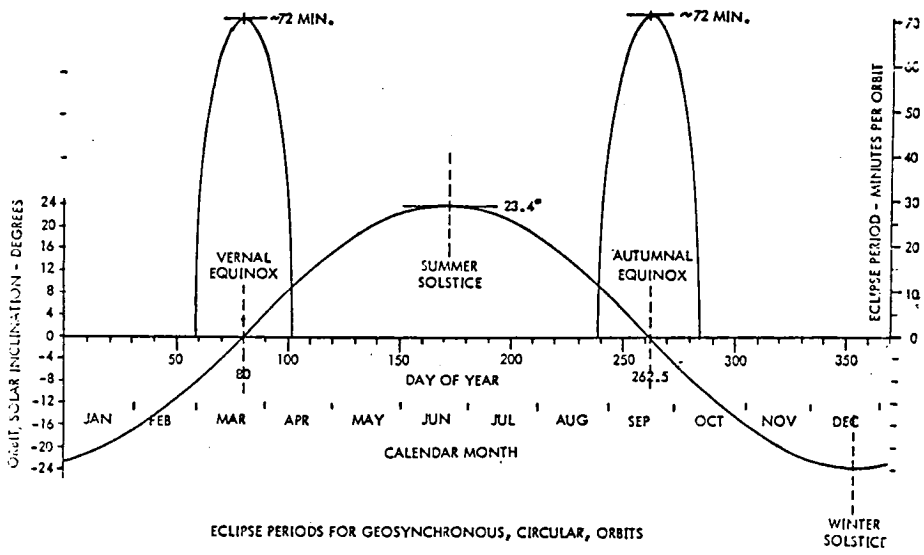

Figure 8.4-8. Power Outages due to Solar Eclipse

are assumed to be under the control of a regional control center. The GRS may be geographically widely separated, e.g., several hundred miles apart. The regional center also might be collocated with a GRS control center, or might be independently sited on the basis of utility switching center locations, or its location may be determined by other criteria.

The functional allocations assumed are that power routings are established within the GRS/utility interfaces. Operational procedures are assumed to be established within the GRS control centers. Also, operational requirements including scheduling, logistics and related requirements are established at the regional level.

GRS-Utility Interfaces

The GRS and utility interfaces are designed to effectively emulate existing power generation sources, such as hydro-electric, thermal or nuclear plants which are presently used. The fact that the electrical power is first converted from solar sources in space is irrelevant to the utility companies. The rectenna receiving panels, which cover 30 to 40 square miles, are treated as if they are merely another type of power source.

Redundancy of operation and flexibility in power distribution interconnections are the keynotes of the concept shown in Figure 8.4-9. Over 1,000 rectenna 'voltage strings' may be connected to each of the feeder lines. These may be selected in groups of up to 55 feeder lines with up to 16 groups of these lines. A number of groups may be interconnected as in the illustrated concept. Each panel is connected by motor operated disconnects which must accommodate 10 to 20 kilowatts each at high voltage, e.g., 40,000 volts direct current (dc). Thus, a large number of motor operated disconnects may be required on the feeder lines alone, e.g., perhaps several hundred thousand or more.

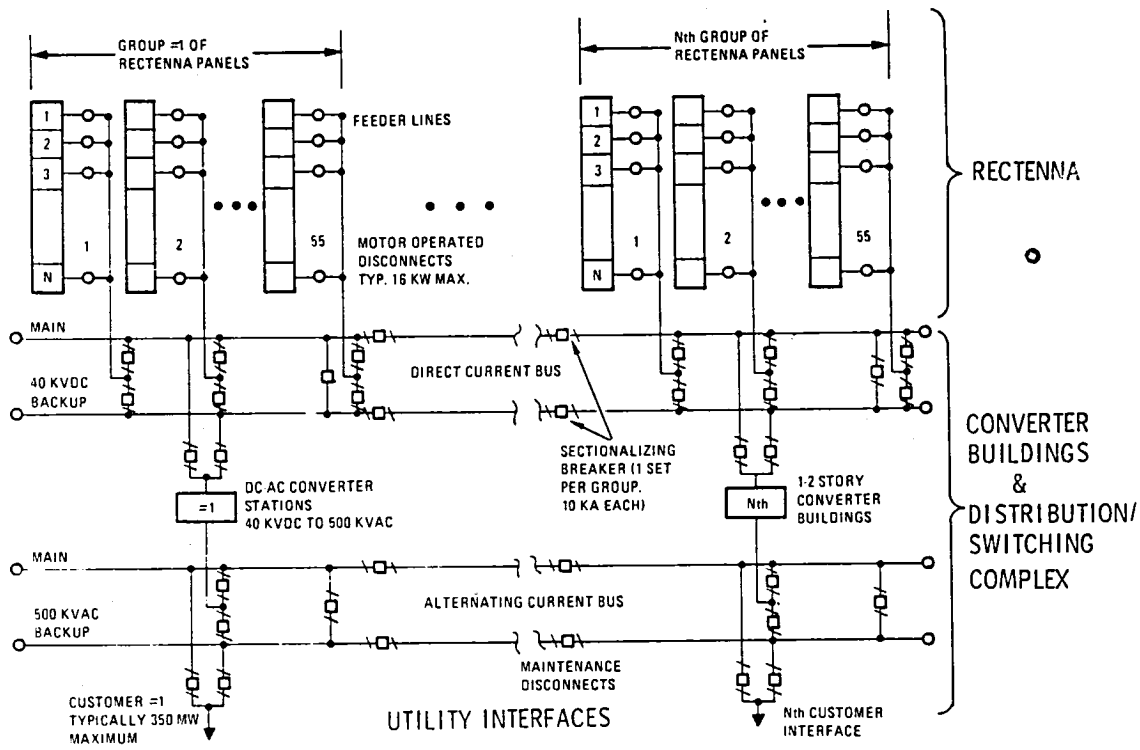

Figure 8.4-9. Rectenna Panels and Power Distribution Interfaces to Utility Customers

Each of the feeders of each group may be connected to a dual redundant dc bus which consists of main and transfer buses. The feeders connect to the dc buses via dual 40,000 volt direct current breakers which may have to conduct several hundred amperes each. The buses, in turn, are connected together by 40 kilovolt dc breakers which must handle current loads of 10 thousand or more amperes. Each of the groups of power panels are protected by dual 40 kV dc, sectionalizing breakers.

The dc buses feed into dc-to-ac (alternating current), (or dc-to-dc), converter stations. Each input line is provided breaker protection. For the dc feeder groups, an identical number of converter stations are provided. Each station converts several million or more watts of electrical power to 60 cycle ac and from 40 kV dc to 500 kV ac or dc. Each station will probably consist of a large building, perhaps 1-2 stories high by several hundred feet on a side. Advanced technology may allow solid state conversion techniques to be applied which would reduce both building size and system complexity. An advanced technology converter station presently operational at Newhall, CA., may provide some insight as to station sizes, problems, and concepts.

In this SPS concept a dual ac output bus is provided. The groups of feeder lines essentially emulate a multi-generator power station. The groups may be isolated to provide dedicated service to special customers whose applications may impose unique load surges or line noises. In this event,

each converter station could supply hundreds of megawatts of electricity at 500,000 volts ac. If dc power is required for the using utility, the converter station(s) would incorporate the additional rectification needed.

It is evident from this brief description that the size and complexity of The GRS imposes instrumentation and control demands similar to that of the satellite (Table 8.4-2). Over 390,000 rectenna panels are to be installed. A like number of motorized disconnects are needed. Temperature, voltage, and current measurements are anticipated on the panels to monitor conditions and outputs.

Table 8.4-2. Preliminary Instrumentation and Control Requirements

DEVICES		NUMBER
RECTENNA PANELS • TEMPERATURE • VOLTAGE • CURRENT	GREATER THAN	390,000
MOTOR OPERATED DISCONNECTS • 40 kV dc @ 0.3 AMPS • SWITCH POSITION • TEMPERATURE • COMMAND VERIFICATION	GREATER THAN	390,000
SWITCHGEAR (SWITCH POSITION, CURRENT, TEMPERATURE, ETC.)		
• 40 kV dc @ 400 AMPS		1,760
• 40 kV dc @ 10,000 AMPS		16
• 500 kV ac @ 700 AMPS		32
• 500 kV ac @ 800 AMPS		16
• 500 kV ac @ 10,000 AMPS		TBD
CONVERTERS		
• 40 kV dc-TO-500,000 VOLTS ac @ 800 AMPS		16
• 40 kV dc-TO-LOW VOLTAGE		TBD

The hundreds of thousands of motor operated disconnects will require computer control. In turn, the instrumentation and measurements subsystem (IMCS) must provide necessary command verification, switch position, and perhaps other information, e.g., temperature.

Thousands of switchgears are also needed to provide the breaker and contingency isolation protection needed to achieve a reliable consumer power system. Position, temperature, and reset controls must be provided. Although maintenance disconnects may be manual or motorized, the IMCS may be required to monitor conditions in either case to automatically establish system status, reserve capacity and provide configuration and safety protection.

Finally, the converter stations are expected to be complex advanced technology high-power-level facilities. The IMCS requirements resulting are anticipated to be so extensive that the ground-based IMCS should be of the same order of magnitude as that utilized on the satellites. The spaceborne electronics technology approach may be transferrable to the ground systems to

meet the instrumentation and control challenges. Reduced unit costs may result because space qualification will be unnecessary. But this could be offset by unique terrestrial environmental requirements of humidity, dust, wind loads, rain, snow, ice, or lightning.

Ground Control Facility

The ground control center at the GRS site will control the uplink pilot beams, provide status and control of the GRS power distribution network and utility interfaces, as well as provide primary satellite control support. It is anticipated that it will be located at the GRS site in a separate building which also would house administrative personnel, management and maintenance workers, as well as displays, computers and controls.

The computer architecture concept is shown in Figure 8.4-10 and projects the use of multi-processing units which interface to the satellite through communications processors and to control/status operations through a common bus and terminal equipment. Real time displays and related keyboard control/ entry equipment would be incorporated into the design.

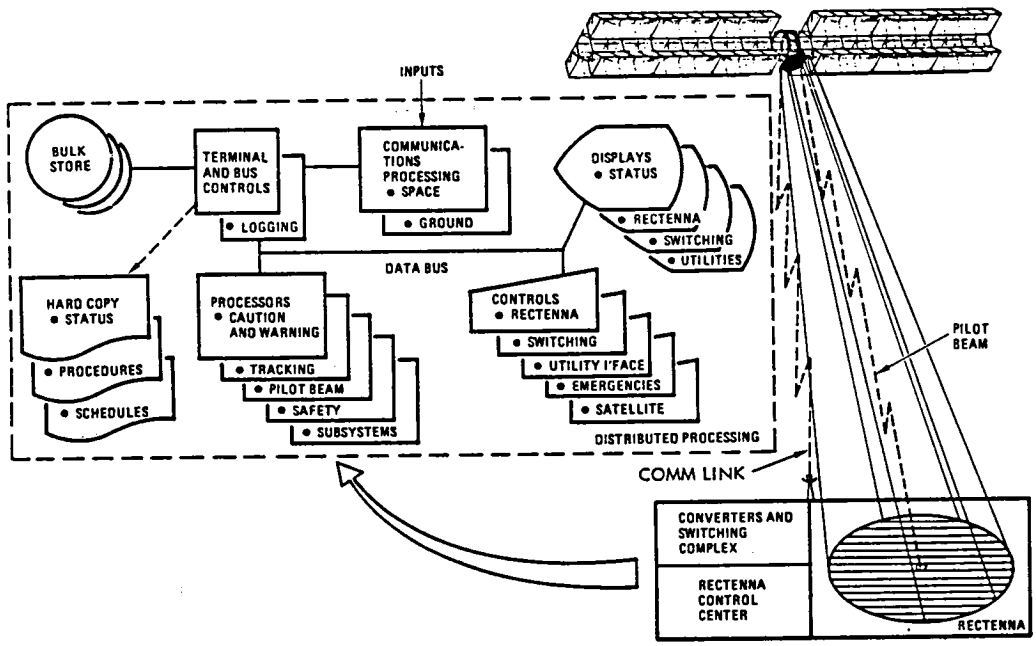

Figure 8.4-10. Ground Receiving Station - Rectenna Control Center Concept

The center's functions and their allocations are beyond the scope of this introductory study. Some of the basic functions anticipated include:

- Operating system
- Data base control
- Data logging/storage

- Pilot beam control
- Satellite status monitoring
- Satellite control
- Power beam monitoring
- Rectenna site safety
- Intrusion control
- Telemetry control
- Rectenna power distribution
- Converter station status/control
- Emergency shutdown
  - Satellite
  - Rectenna
- Utility interface control/monitoring

Regional Control Center

A conceptual regional control center is shown in Figure 8.4-11. It would be differentiated from the ground control facility by a higher functional level. Whereas the local centers are procedurally implementing controls based on instrumentation and telemetry inputs, the regional center accepts computer data from the various local centers and then establishes a schedule of GRS of satellite support requirements. The local centers could then define a compatible procedural performance of, say, logistical, maintenance, power distribution or load shifting requirements.

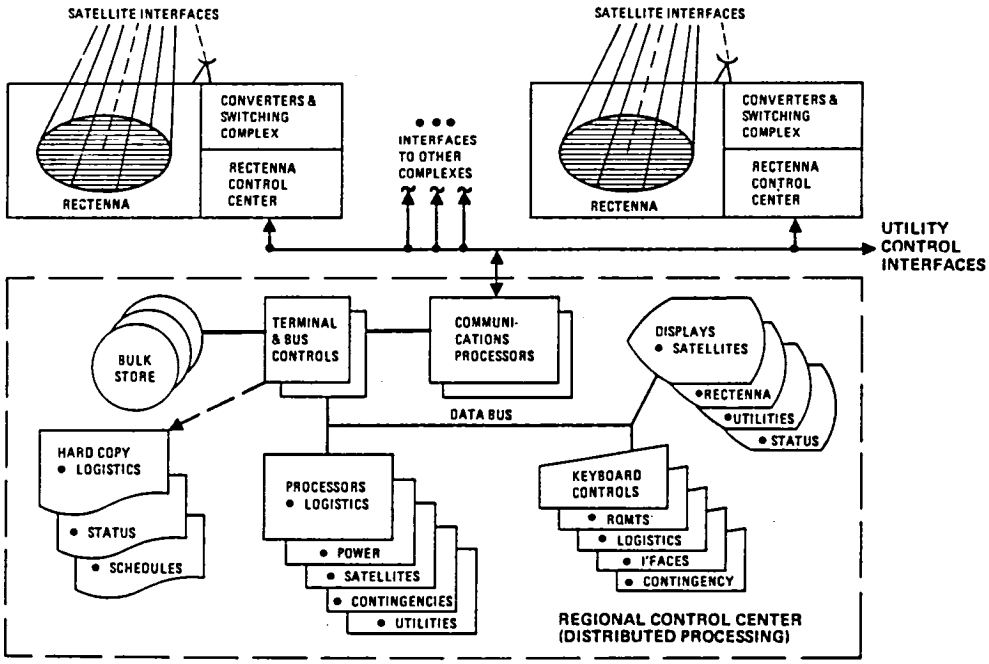

Figure 8.4-11. Regional Control Center Concept

This regional center has only been conceptually postulated and has not received further study consideration or design definition. Future studies should examine the need and functional allocations of such a center. It may evolve as the only effective interface to coordinate the SPS ground power sites and the existing utility networks. Analysis also might show that this function is best served by integrating the regional functions into existing utility network command/control centers. However, the unique satellite support aspects of the SPS system may require a contrary conclusion. Regional control may be needed to effectuate logistical, ephemeris and satellite resupply support among the various anticipated functional needs.

A generalized multi-processing architecture is shown in Figure 8.4-11 as one concept for meeting support demands. Again, a separate study is needed to define architecture and performance requirements as well as functional and siting needs. A centralized dedicated control architecture may be adequate with use of large computers. Or perhaps only partial support is needed at a utility network command center using multi-programming.

8.5 OPERATIONS

The SPS has at least three distinct time phases of operations. These time phases are (1) Test and Evaluation (T&E), (2) Initial Operational Capability (IOC) including start-up, and (3) Final Operational Capability (FOC). As the SPS capability passes through these time phases, there will be an evolutionary change from semi-automated control and validation to a more automated system. The ultimate level of automation will reflect the highest degree of system performance commensurate with required safety standards.

It is assumed that the initial test phase (e.g., T&E) has been successfully completed and that start-up procedures are to be initiated.

Initial discussions will address the satellite with ground operations considered later. This section will conclude with a brief discussion of expected nominal operational requirements.

8.5.1 SATELLITE OPERATIONS

The operations analysis begins with preliminary preparations for power generation and traces the power flow, enabling commands and system controls across the satellite-rectenna/control center interfaces. The satellite is assumed to have been assembled and to have completed basic individual subsystems checkout. At this point it is expected to be ready for startup operations during which each subsystem is brought on line and integrated with other elements in logical order.

Start-up

Start-up operations are divided between the non-rotating portions of satellite and its rotating antenna.

Non-Rotating. Five major areas of satellite operations have been identified as follows:

- Status checking of all system components
- Attitude control to enable solar power conversion
- Power generation by the solar blankets
- Power distribution to the antenna rotary joint
- Voltage regulation to account for losses and aging

Status. Prior to start-up, all satellite subsystems must be checked for ready status. These include structure, attitude control, solar blankets, power distribution, thermal control and the information management and control system. A status check command or request would be expected to be received from the rectenna control center indicating that the ground systems are ready for operations and that status of the satellite must now be checked. If the satellite is manned, this request might be a simple voice communications or a digital message displayed on a screen.

The IMCS is a central element in the checkout of all satellite subsystems. It is assumed to already by in an "on" status since it is required at all times for satellite operations, such as attitude control. However, it may be in a standby mode with only essential support functions operative. Control support to power generation, distribution, and microwave transmission may be in an "off" or standby status. Whatever the existing IMCS configuration and operational condition, the IMCS must be checked out. IMCS operative portions are placed into automatic sequencing checks and non-operating portions are brought on line and similarly status checked.

After IMCS checkout is complete, measurements data are accepted from the attitude control, structural, thermal, solar blanket and power distribution subsystems, and verified. These include temperatures, positions, pressures, voltages, etc. Next, limited control actions are issued to the various subsystems to check control loops and operating modes. Even though measurements and controls, as compared to the antenna, are relatively limited on the satellite, they still represent a hundred thousand or more data points which are sampled a number of times. Similarly over ten thousand control points are exercised. Such checkout sequences will be automatically implemented with human monitoring of test results on board the satellite in its master control center and/or on the ground in the rectenna control center. The time duration of such status checks may well be established by subsystem stabilization time constants rather than the actual time to automatically sequence through the various functions.

Attitude Control. Once all systems are checked out, the satellite must, concurrently, be oriented to its solar inertial attitude for power generation. For example, it may have been allowed to drift several degrees in attitude during the time since completion of assembly and basic checkout. Such drift errors must be corrected prior to initiation of power generation. Since stationkeeping is included in this function, the geographic location of the satellite centroid must be verified in relation to the rectenna location. Any undesirable drift must be eliminated and the satellite's longitude location refined.

The physical pointing angle of the microwave antenna is also controlled by this subsystem. Once the satellite achieves its proper solar orientation and longitude location with residual drift errors eliminated, the antenna gimbal drives are controlled to bring the antenna within boresight of the rectenna. This is likely to be a process that will take a significant period of time because of the large masses involved. Both support from the rectenna site to assist boresighting, and power support from the solar blankets to the gimbal drives will be required.

Solar Blankets. The solar blankets are brought on line by closing switchgears between pairs of adjacent bay segments, each of which are 25×750 m and provide 250 amps nominal at 22.5 kV. Each bay has 22 segments if located in either of the lower troughs and 24 segments if located in the upper trough. The two segments are connected to the first switchgear so that either one can be connected to corresponding segment pairs in the second panel, thus providing flexibility for current control and panel outages. Paired segments from the first panel nominally provide 500 amps to the 2nd bay panels which are connected in series by a second set of switchgear to achieve the required voltage level of 45 kV. Bay segment pairs are sequentially brought on line from all 18 bays in each wing of the satellite until the power demands are met.

Power Distribution. Bay bus switchgears isolate each bay segment pair from the bay buses. As each bay panel pair is connected, it is tied to the main buses through closure of the related switchgear. During this connection process, bus temperatures and current measurements must be monitored to detect any shorts throughout the vast bus runs of the satellite so that controlled emergency disconnects can occur under IMCS or local breaker control to avoid catastrophic effects. Nominally, 215,000 amps at 42 kV are fed into two antenna slip rings for transmission to Earth. During the startup sequence (as well as during nominal operations) it will be necessary to monitor ground power flows because of their possible influence on satellite procedures.

Voltage Regulation. Voltage regulation is obtained by selectively shorting module segments within the 2nd (series) panel. During the solar blanket connection process, voltage levels of each bay segment pair are monitored continuously to assure proper matching between outputs and the main antenna summing bus.

Antenna. Antenna startup operations are divided into status checking, power distribution, power storage, pointing initialization, thermal stabilization, acquisition of the rectenna and fine pointing including focus.

Status. The electronic and pointing status of the microwave antenna must be verified prior to power distribution for space-ground transmission. For example, the previously verified boresight of the antenna to the rectenna may have drifted so that updating may be required. This type of boresight support, from the rectenna control center, may be required on a continuous basis.

Concurrently with boresight verification, the power distribution, thermal and phase control electronics must be checked. The switchgears on the antenna must be verified for proper positioning and functioning. The ability of the thermal control system to provide both heating and cooling is confirmed. Finally the phase control electronics are activated to ensure that all components

are properly functioning. The reference phase generator is energized and the reference distribution servos are exercised to confirm that they are operating properly. Retro-electronics are activated so that the pilot beams from the rectenna can be received and processed through the monopulse receiver subsystem. The beam programmers are also checked through use of built-in test procedures.

Power Distribution. If the satellite is experiencing a solar eclipse, internal battery power is utilized to energize the satellite emergency distribution buses. The main power module switchgears are opened while switches at the subarray, mechanical module and bus levels may be left closed to provide power to antenna electronics for checkout and thermal stabilization.

If the satellite is leaving an eclipse, antenna electronic phase control must be reactivated and power fed to the klystrons for transmission to Earth. The satellite's power distribution system is reenergized and stabilized; the antenna ring brush switchgears are closed, allowing power to be distributed to the 32 dc-dc central converters. These provide the 60 kW to each klystron collector at 5 voltage levels. Five-pole switchgears are then closed allowing the power to enter the primary and secondary feeders, where additional sets of 5-pole switches determine whether 1 or both secondary feeders may be activated (redundantly). In the same manner, the 5-pole switchgears at the mechanical and power module levels are sequentially closed until power flows through the klystrons and is transmitted to Earth.

Power Storage. Prior to the satellite entering an eclipse, the batteries are checked and brought up to full storage capacity to ensure IMCS, thermal, attitude control, communications, and other vital functions when photovoltaic power is lost. Closed loop control of the charging process is maintained through the IMCS until the batteries are fully charged.

When the satellite enters the eclipse, the photovoltaic supply buses are shut down and the emergency buses provide subsystem power. Prior to this time, the klystron power modules are switched off. Non-essential subsystems are shut down or placed in a standby mode to preserve power during the up to 1.2 hours eclipse time. Rectenna control center support is used to update orbit predictions for eclipses and generally support scheduling of satellite operations prior to predictable power outages.

Initialization. Initialization of antenna operations begins with activation of the reference frequency module and computation of coarse phase angles by the beam programmers, which command the digital diode phase shifters. Pilot signals are fed through the retro-electronics to initiate the phase conjugation process. Cathode heater power was applied during initial startup to bring the klystrons up to a stabilized temperature for accurate phase control. This heater power is maintained through all eclipses and other scheduled standby situations.

Under IMCS control, the amount of power fed to the klystron is increased while monitoring phase and pointing stability. All scheduled klystrons are brought on line simultaneously with this gradual process to first establish pointing and then the required power levels. Klystron operation is carefully monitored and local arc detection circuits/circuit breakers disconnect any power module which malfunctions.

Thermal Stabilization. Thermal stabilization of klystron cathode temperatures is extremely important to accurate phase control and fine pointing. Phase control and fine pointing are achieved using pilot beam and reference phase comparisons through the monopulse bridge and monopulse receiver. Phase error signals are provided to the beam programmer for correcting the coarse phase angle which was computed at startup. The klystron output phase is also fed back into a phase bridge. Thus, individual klystron manufacturing irregularities and aging differences are automatically accounted for.

During eclipses when excessive cooling could occur, the battery storage subsystem provides cathode heating capability to prepare the system for restart as the satellite emerges from the eclipse.

Conversely, antenna array temperatures on the back side where control electronics are mounted must remain less than 60°C. The IMCS continuously monitors component temperatures and adjusts power levels or heater input power (if required) to maintain required temperatures consistent with the passive heat pipe cooling system used on the antenna.

Phasing. Once the MPTS acquires the rectenna by locking on the pilot signals, the antenna must also be phased (focused) so that all down-linked power remains within the confines of the rectenna and is within given safe power levels. The beam programmer computes a phase gradient to be applied across each subarray. This, in turn, is locked to the reference phase which is generated at the reference subarray.

After lock-on to the rectenna is achieved, phase gradient corrections begin to achieve the required beam pattern. Signal strength is also monitored at the rectenna and transmitted to the satellite to provide independent confirmation of beam location and focus.

8.5.2 GROUND OPERATIONS

The organization of the ground operations scenario parallels that of the satellite scenario. Operations begin with status confirmation and proceed to startup and steady-state phases. The satellite and ground systems are assumed to have been completely assembled, integrated, manned, checked out and placed in standby status.

Display and Control Thermal - Human Interface

The SPS ground system requires a high degree of adaptability in its ground operations center to meet the varying demands of the system. The operating scenario discussed herein has been oriented towards providing a basic representational understanding of the operator-machine interfaces.

In the initial system startup, man will interface with the system primarily in order to validate or stop system operations. The basic information that will be presented to the human will involve status and operational checks of all ground subsystems and a count-down to system startup. In addition, status summaries of all satellite subsystems will also be presented. The system initiation sequence will involve the utilization of both voice and displayed messages. These will be properly validated and authenticated.

The focal point of human decision making and control is the display and control terminal. Augmenting this interface are:

- Communications
  - voice
  - teletype
  - computer-to-computer
  - written with manual transmission
- Management
  - organization
  - operating policies and rules
- Manual Operations
  - space/ground on-site

Prior to startup of the satellite or GRS, the configuration and status of the local control center must be determined by operations personnel. Displays will be assigned to various functions, e.g., communications, computer operations, satellite and rectenna. Each of these consoles might be sequenced through various types of display formats and information content to assess the status of:

- Display electronics
- Keyboard functions
- Related data buses and external communications
- Supporting computer(s) and software
- Data files
- Operating modes

Upon system startup all power levels, beam focusing, beam dispersion, etc., will be monitored and checked to assure that they are within predetermined levels. For elements of the system that will require switching or shut down faster than human reaction time, the system will operate in an automated mode in order to prevent damage to any system elements and to maintain safety requirements. When time and policy permit, human intervention will be able to start, stop, validate, override or branch any machine function.

Upon receipt of a requirements schedule and startup command from a higher echelon of authority, i.e., regional control center director, the aforementioned make-ready status assessment would be performed. Next the GRS control center is ready to extend its information input and command authority to other interfaces, i.e., GRS and satellite.

Satellite Interfaces

Communications, telemetry, command and pilot beam control interfaces to the satellite must now be exercised to insure control integrity. Voice, telefax and teletype links to and from the satellite are exercised with test messages to insure functional readiness. Satellite computer (and backup primary instrumentation) data telemetry streams would be sampled to confirm

high speed downlink digital data functions as well as reported subsystem status. Ground-based pilot beam transmitter status is next checked. This scenario assumes that a spaceborne crew has completed satellite assembly, checkout and placed the satellite into a standby systems mode, i.e., only computer controls, communications and environmental systems activated.

The GRS pilot transmitters are now activated and radiated power and pointing angles are verified. On the satellite, pilot receivers are turned-on in response to enabling commands from the GRS control center. Down-link telemetry further verifies reception of the pilot beam signals and bore-sight.

Those elements of the detailed schedule of required operations, logistical support and power demands, which are needed by the spaceborne control center, are transmitted by high speed uplinks. This data is assumed to be prepared in the regional control center on a generalized basis, and is refined to a detailed schedule at the ground control facility.

GRS-Utility Interfaces

The GRS and its utility interfaces must be configured to receive the power which is converted and transmitted from the satellite. Rectenna panel status must be checked through instrumentation inputs related to temperature, mechanical integrity and electrical continuity. Maintenance status must be reviewed to ascertain which panels are inoperative and to reroute any affected interconnections. Personnel must be notified and cleared from exposed areas within the rectenna site.

Power distribution to the utility interface is next configured. Feeder lines and bus switches are configured to route the scheduled power to the proper customer interfaces. The various groups of panels are appropriately interconnected on the dc buses to provide the required degree of isolation. All bus connections, including backups, and breakers are checked. Orders are automatically issued to yard crews to establish correct switch positions for manual maintenance disconnect switches.

Status and control is next sequenced to dc-to-ac converter subsystems. The huge size, redundancy needs and system complexity of the converter stations dictate that they incorporate their own dedicated computerized controls. Within this assumption it is also presumed that digital data buses connect converter and rectenna control centers so that converter station ready-status is automatically determined. Status is, of course, displayed to rectenna center control personnel who may sequence their displays to examine in increased depth any specific areas of concern.

Converter stations are sent enabling commands to allow local control to turn on electronics to standby mode. Automatic sequencers and input power detectors are assumed to switch each converter station to operating mode as power is received from the satellite.

Finally the ac bus switches are monitored for their status and appropriate commands are issued to establish the required distribution configuration. At

this point, the ground systems are checked out and placed in standby or operating mode as appropriate.

Next, regional control center and the utility distribution network control centers are sent standby status signals. Similarly, the satellite is also sent pre-start "make ready" warning signals and appropriate enabling commands. Encryption is utilized for communications and command to insure security against intrusions or takeover.

Satellite Pre-start "Make Ready"

The ground control facility is assumed to control the satellite through the master control center which is located on the satellite. Control is effected through the satellite's distributed computer control and information management system. This results in a higher level of control on the ground, i.e., enabling and scheduling of spaceborne activities in contrast to direct telemetered control. Only in contingency situations involving critical subsystems would direct preemptive control links be provided to the ground center.

Nevertheless, the spaceborne computerized control system must be polled to determine subsystem status. The ground center would also be expected to issue enabling commands, adjustments to performance levels, requests for specific pointing angles, system configurations, etc. Status polling would include structure, attitude control, solar panel confitions, power distribution, environmental control, and the spaceborne information management and control system. The latter would include operating modes of the various distributed computers, data bus ready condition, terminal equipment, software configuration, and data base contents. Any updates to the data bases would be provided from the ground control center. Such updates might include maintenance schedules, logistics planning, control system parameters, ephemeris updates, etc.

Status pre-start operations would also include providing to the satellite systems various ground-based systems status data. This might include pilot beam status and pointing parameters to facilitate acquisition and boresight.

Status checking would include issuance of enabling commands to the satellite IMCS to begin automatic sequencing checks. These would also bring non-operating segments on line to achieve the required configuration of the various subsystems. When checkout is complete, a formal data logging command would be issued to record a sequential subsystems summary of satellite status into the ground center logs.

Where questionable status exists in various areas, the ground center might command pre-stored limited control actions on the satellite to test, debug or verify system conditions. Prestart status and configuration operations involve hundreds of thousands of control and data points, requiring significant processing time even with automatic sequencing. Satellite attitude refinement may involve long time delays and the integration of space-ground prestart operations may amplify any such time delays. Special studies are needed to quantify these potential impacts on SPS operations.

Satellite Startup

Startup control functions for satellite power production and transmission are automatically sequenced by the spaceborne computers. The ground control center does not play a direct role unless the onboard control system fails. In this event, direct ground control would be limited to performing emergency shutdown using separate control links in critical systems' areas.

Whether this would be implemented through separate, direct telemetry command links, which bypass the onboard IMCS, is undetermined. Special operations impact and design feasibility studies are needed in this area to clarify this situation.

The ground control center would monitor startup sequencing in order to provide any necessary ground support to the satellite. This includes antenna boresighting, pilot beam control and initiation of power reception, conversion and distribution to the utility customer interfaces. Special coordination functions may be needed from the ground center to avoid power surges and to provide load leveling. Emergency shutdown of satellite operations may also be required if a major ground system failure occurs.

Ground center support to satellite startup will generally parallel satellite systems sequencing. This begins with attitude control. The satellite may have drifted in attitude or geographical position. Ground center support to boresight and ephemeris updates based on precision observations are major elements of this type of ground support. This may include revised satellite antenna gimbal angles to be inputted into the spaceborne data base. Attitude, stationkeeping and boresight functions are expected to be long term repetitive operations which extend into steady state operations.

Once boresight is achieved, the solar panels can be brought on line. This is a complicated operation which is automatically sequenced by onboard computers. Ground center personnel would merely issue enabling commands once prerequisite spaceborne functional modes and system configurations are achieved and verified. Similarly, power distribution from the solar panels to the antenna is automatically implemented by onboard computers. This is also true of the voltage regulation process. Operations are only monitored on the ground. Preemptive ground support is required only if the onboard IMCS fails.

Antenna operations do require additional ground support because of boresight, alignment, and pilot beam functions. The mechanical pointing status of the antenna is verified during the earlier status checking phase. However, this must be continuously rechecked during startup to insure safety and efficiency of power transmission.

Subsequent to boresight confirmation, enabling commands are sent to the satellite to turn on the reference phase frequency generator and related retro control electronics. This enables processing of the received pilot signals and initiation of power transmission. Earlier data base updates insure insertion of the correct data to the beam programmers.

Power beam monitors are located throughout the GRS site to provide an independent assessment of power beam pointing. Outputs of these monitors are computer polled and processed. Any residual pointing errors are translated into phase angle corrections and telemetered to the satellite for use by the beam programmers within the retro-electronic control system. Beam location and drift rate are monitored for possible emergency shutdown of satellite operations if error boundaries are exceeded.

If the satellite startup is coincident with termination of a solar eclipse, the ground center must confirm that battery recharging operations are initiated. If the satellite is projected to enter an eclipse, battery status must be verified. Use of klystrons for power transmission requires ample power for thermal stabilization, i.e., cathode heating, during eclipse periods.

Two operational considerations must be investigated which relate to klystron activation. If all klystrons are powered up simultaneously there will be possible power surges injected into the utility network. Simultaneous klystron energization is assumed to begin at low levels with power output gradually raised so that the ground power station can gradually come on-line to full power output to the utility network. Coordination between the rectenna, regional and utility network control center is needed to ensure smooth load time history changes.

If klystrons are activated to full power with a given number of klystrons activated at a time, the impact on rectenna power output must be ascertained. Problems may result in coordination of panel grouping, conversion and distribution. Unstable beam patterns, if resulting, could cause power output transients to utility customers, distribution surges with undesired bus breaker activations, and unstable dc-to-ac conversion processes.

In any event, power startup operations between space and ground systems must be closely coordinated to ensure smooth power delivery. Excessive transients in the satellite and rectenna/utility interfaces must be avoided. The rectenna control center will automatically monitor the thousands of power conversion, distribution and control points to effect adjustments or emergency shutdown as needed. Any unusual situations will be displayed to rectenna center operations in real time. Emergency conditions must be relayed to any regional and utility network command centers.

Nominal Operations - Satellite

At this point, the satellite has reached stabilized power production and transmission of that power to the rectenna. Power demands are constantly monitored at the GRS and transmitted to the satellite so that system surges can be mitigated and scheduled maintenance can be planned. For example, as midnight is reached at the users' locations, power demands reduce. Solar blankets, antenna components or other related power production elements are removed from the line for replacement or repair on a progressive basis to avoid future unscheduled shutdowns.

Satellite and GRS status are constantly monitored so that any unscheduled power production or distribution changes can be accommodated. Constant communications, voice, data, and commands, are required between the satellite and the ground control center to achieve effective coordination.

Progressive maintenance inspections are performed on the satellite to insure reliable operation. The IMCS is constantly monitoring the status of components. As out-of-tolerance conditions are noted, the affected element is scheduled for repair or replacement before failure. As a statistical basis is developed for predicting problem conditions, inspections and replacements are pre-scheduled at convenient times before the problem occurs. The ground control center is expected to provide some support through logistical scheduling and data base maintenance.

Scheduled outages occur during solar eclipses. These time periods can be utilized for minor repairs and replacements. Prior to each eclipse, coordinated planning occurs between the satellite and ground control center crews to develop a master maintenance schedule. Since an eclipse may last for a maximum of 1.2 hours, careful planning is needed to capitalize on this time for component replacements. Once replacement parts are installed and safe conditions are verified, selective activation of the affected subsystems is implemented to checkout replaced parts in preparation for startup subsequent to the eclipse.

Nominal Operations - Ground

In this phase the satellite and GRS have reached stabilized power conversion and transmission to the utility network. The ground center will receive periodic updates of scheduled power requirements from the utility network control center. These load schedules are translated by the ground center into satellite power output schedules which take into account RF transmission, rectenna conversion, dc-to-dc conversion efficiencies, and related factors. This scheduling facilities matching of generated power to load levels.

If for some reason the entire utility network or a dedicated customer drops off the line, the SPS power output may be shutdown, adjusted, or switched to other loads. The ground center must accommodate these and other contingencies such as problems in rectenna dc-to-ac conversion and distribution. Emergency shutdowns or load adjustments require authenticated commands, rather than enabling messages, to be transmitted to the satellite.

Progressive maintenance schedules and procedures are prepared by the ground center for rectenna, converter and distribution maintenance. Similar schedules and procedures are prepared for the satellite. However, those related to the GRS will be detailed whereas those for the satellite would be at a higher level. The onboard system and control center personnel would convert such inputs from the GRS center into the required detailed form.

Satellite tracking and ephemeris refinement functions are performed by the supporting rectenna satellite tracking subsystem. Eclipse and related systems schedules are then prepared based on these schedules, which include space-ground system startup, shutdown and logistical support.

Several other safety, security, and environmental monitoring functions are performed during startup and steady-state operations. Safety will be of continuous concern. Prior to startup, maintenance and other types of workers must be evacuated from exposed radiation or high power switching areas.

Equipment must be properly configured and adjusted to avoid or investigate accidents or incidents. Particularly close monitoring must be maintained and safety shutdown possibilities must be preserved during startup due to the presence of rapid and large power transients. Required safety functions must be defined along with supporting caution and warning instrumentation and controls.

Security perimeters must be defined so that the GRS site, control center and switching yards are protected from intruders. This includes personal, command and other forms of physical intrusion. Accidental or intentional intrusion of people must be presented by automatic detector, entry controls and guard personnel. Command links must be encrypted and physically protected from accidental or intentional interference or takeover. Arrangements must be made with appropriate authorities to avoid beam interruption by over-flights which might cause power transients in various portions of the rectenna, confuse beam location monitoring equipment, or interrupt the pilot beam.

Environmental monitoring will also take place during all phases of system operation. For example, radio receivers which are located within the neighborhood of the GRS, e.g., 30 miles radius, will scan the radio spectrum for possible interference to radio, television and other forms of radio frequency interference (RFI). Inputs to the GRS control center may allow identification of malfunctioning SPS equipment to resolve any RFI problems. The SPS system design must minimize environmental impacts to acceptable community levels. Electromagnetic interference (EMI) must also be monitored.

Regional Control Center

As stated previously it is uncertain whether a regional center is required to coordinate several rectenna sites. It may be that coordination of each rectenna only with its respective utility network center is needed. Even these separate centers might be eliminated if they could be integrated into a single location by the utility company. Design trade studies are needed to investigate these possible ramifications.

In this preliminary study, a regional control center is assumed. Its primary purpose is development of schedules for required operations, while the rectenna center would define the procedural accommodation of such requirements.

The regional center would maintain archival records of system problems and recommended schedules for logistical resupply and maintenance. It would also review past history for unique needs or difficulties in the SPS-utility interfaces, load leveling, contingency outages, etc. Based on these experiences, operational directives could be developed to impose policy, procedural and contingency response requirements. These could ensure improvements in overall system safety, efficiency, coordination of operations, and power output-to-load matching.

Scheduling of requirements for GRS site and satellite maintenance could also be the function of the regional center. These would be based on site

operational logs and would be provided to GRS and onboard satellite control centers, where they would be translated into detailed schedules and procedures.

8.6 COMMUNICATIONS IMPLICATIONS

While communications have not been specifically studied in this preliminary analysis, a number of implications have been drawn. The satellite must maintain continuous contact with the ground control center. This includes voice, data, video, and commands in both directions. In addition, the dual uplink pilot beams from the rectenna are crucial to acquisition and fine pointing (within 0.02 degrees). The high EMI environment in the near vicinity of the satellite imposes difficult conditions for communications. This requires primary emphasis and special design considerations.

Intra-satellite communications are highly dependent upon optical data buses to avoid the EMI problem.

Space-ground communications may have to be encrypted to avoid command intrusions and interference. Data compression may be required if data traffic becomes too heavy due to large data base updates, significant amounts of video traffic, or excessive interference.

8.7 CONCLUSIONS AND RECOMMENDATIONS

From the previous discussion it may be concluded that there are no operational 'show stoppers'. The basic need is to identify in greater detail the operating characteristics of the various equipment utilized on the satellite and in the ground system with particular emphasis on activation and stabilization times, intervals, and sequences. These being required before detailed functional flow diagrams (FFD) can be prepared.

Another highly important study detailing communications requirements and constraints must also be initiated before overall system FFD's can be prepared.

Future activities required to prepare data necessary for further detailing of the FFD's include the following:

1. Early development of segment specifications and interface requirements. In addition, each of the segment relationships to possible environmental impacts must be ascertained.

2. Study is required of high level ground control system operations. This would include analysis of all control functions that would be required by each ground segment element. Control and data paths between segments must be defined in order to size total control requirements. This is an essential first step in a ground system architecture development This provides the ability to ascertain critical paths as a preface to doing a failure mode and contingency analysis.

3. Detailed failure mode and effects analysis to determine possible single points of failure that could impact mission essential or safety functions is needed. This failure mode and effects analysis would allow alternate routing or redundant capabilities to be investigated for early determination of related system architecture and design requirements. This would assure early evaluation of possible environmental impact or safety constraints.

4. A major area of concern is the need to develop an early man/machine interface concept design in order to provide for an evolutionary transition from a semi-automated control system during the Test and Evaluation (T&E) phase to a mixed man/machine automated operation during Initial Operating Capability (IOC) to a highly automated capability for the Final Operating Capability (EOC) stage. A significant aspect of an evolutionary approach is that where a function has gone from semi-automated to fully automated, the ability to manually intervene to override a function may be needed. Provisions must be made to provide for changes in control architecture during evolution, provide for system malfunctions and to support system test and training.

5. Segments that will require dedicated control functions to be performed include the large dc-to-ac converter installations. This will require large scale monitoring and switching functions within each converter building. All ground segments will require data exchanges including, operational readiness, configuration selection, ascertainment of redundant paths and definition of schedules.

6. The need for a regional control center must be clarified. If it is needed, should it be located at a rectenna site, be separately located but central to several GRS, or should it be located with a utility network control and distribution center? A related question is the allocation of functions. Those functions which have been postulated for regional control, coordination, requirements definition and logistical support, must be corroborated. Also, control architecture issues of distributed versus centralized control should be resolved.

7. It is known that some sort of ground and satellite control center is needed such as the GRS control center, which must be defined. Its functional definition is essential to any follow-on operational analysis and SPS economic and feasibility study. Its control architecture must be similarly clarified, especially the control interfaces to the utility network and the satellite. A vital question to be addressed is the degree of direct ground control to be allocated to the ground center.

9.0 LASER ENVIRONMENTAL IMPACT

9.0 LASER ENVIRONMENTAL IMPACT

9.1 INTRODUCTION

Satellite Power Systems (SPS) are currently under consideration by NASA as civilian electric power sources. Power derived from the continuous solar flux is converted to electricity via photovoltaic cells, beamed to earth as microwave radiation, and then converted back into electricity for distribution by commercial electric power grids. Due to concerns about the environmental implications and potential biological hazards of long-term, low-level microwave radiation, alternate power beaming approaches are being considered, in this case lasers.[1,2]

The primary emphasis of this effort is on the environmental impact of space-to-earth power transmission using lasers. Before this is undertaken, it is necessary to define the laser system and the complementary ground based receptor. Estimates of the relevant efficiencies for laser power generation, atmospheric transmission, and receptor electrical conversion will enable a comparison with the microwave based SPS. Ancillary issues, such as laser beam spreading, safety and security, mass and volume estimates, and technology growth projections, must be considered to fully bound the operational limits and characteristics of the laser-SPS system. This section summarizes the study performed to define the laser-SPS concept, to address important ancillary issues, and to assess the environmental impact of space-to-earth power transmission using lasers. The concluding paragraphs of this section summarizes important findings and recommend further study in the areas of advanced laser development and atmospheric effects of laser power transmission. Proponents of a newly suggested concept, (the free-electron laser), have suggested its use in space-based power transmission schemes; for this reason, a cursory review of this laser is included.

The two major guidelines have been followed in this study. Specifically, (1) the operational attitude and orbit to be considered will be Geosynchronous Equatorial Orbit (GEO) with laser-beam pointing at typical U.S., midlatitude receptor sites, and (2) the individual subsystems or cluster power sources of the laser SPS will be capable of being grouped at a single location in GEO and operated as a single laser-beam generator capable of consuming, as input power, the entire power output of the baseline photoelectric power source (9.4 GW). Slant ranges to typical receptor sites in the U.S. from a laser in GEO at an altitude of 35,786 km will be taken to be 42,700 km. The zenith angle of the laser beam pointing at earth, θ, is taken to be 50°.

The terms of efficiency, scalability, reliability, and atmospheric propagation, two molecular-gas electric-discharge lasers (EDL's) have been suggested for their potential in space-to-earth power transmission systems, namely, the CO and CO_2 lasers. Both types have received extensive support in terms of high-power military applications, and both are documented by a large quantity

of published and unpublished literature. Based on the present evaluation of CO and CO_2 EDL's for operation in space, the laser-SPS system efficiency, defined as the ratio of power available at the user grid to power produced by the solar photovoltaic array, is largest for the CO EDL system. Furthermore, the laser system mass is lowest and the environmental impact is less if a CO EDL is employed for power transmission rather than a CO_2 EDL.

9.2 CONCEPT DEFINITION

9.2.1 EVALUATION OF ELECTRIC-DISCHARGE LASERS

Closed-Cycle Thermodynamic Models

We shall limit the evaluation to molecular-gas high-power lasers in which the excitation process is an electric discharge and the gas is circulated in a closed cycle. Gas circulation permits removal of waste heat, and closed-cycle operation minimizes the rate of gas consumption, allowing long periods of operation. In general, the laser gas mixture consists of a small amount of lasant, such as CO or CO_2, added to a diluent, such as He, Ne, Ar, N_2, or mixtures thereof.

The most important parameter characterizing a large-scale laser is the total system efficiency,

$$\eta_L = \frac{P_L}{P_{PS} + P_M} , \tag{1}$$

where P_L is the laser power output, and P_{PS} and P_M are the electrical power inputs required by the excitation power supply(ies) and gas compressor motor. The electrical power deposited into the gas, P_E, is related to the electrical power input to the discharge power supplies by

$$P_E = \eta_{PS} P_{PS} , \tag{2}$$

where η_{PS} is the intrinsic power supply efficiency. Similarly, the compressor power, P_c, is related to the electrical power input to the compressor motor by

$$P_c = \eta_M P_M , \tag{3}$$

where η_M is the intrinsic motor efficiency. The most oftenly quoted efficiency in experimental laser studies is the discharge efficiency, η_d, defined as the ratio of laser output power to electrical power deposited into the gas, i.e.,

$$\eta_d = P_L/P_E . \tag{4}$$

Substituting Eqs. (2) through (4) into Eq. (1) and rearranging yields

$$\eta_L = \frac{\eta_d}{(1/\eta_{PS}) + (P_c/P_E)/\eta_M} \quad . \tag{5}$$

Knowing η_{PS} and η_M, and inferring η_d from experimental or theoretical studies of EDL's, only the ratio of compressor power to electrical power deposited into the gas, P_c/P_E, is needed to calculate η_L. This ratio is calculated in the thermodynamic analysis described below.

We follow closely the purely thermodynamic treatments of Monson[2,3] and Burns.[4] Two different closed-cycle laser systems are postulated, and the system efficiency is calculated over a range of realistic parameters. For a CO EDL, a low gas-kinetic temperature is required to achieve lasing on low vibrational quantum number bands and to maximize the discharge efficiency. The former requirement is necessary for efficient atmospheric transmission, since only the shorter wavelength lines are not strongly absorbed. For a CO_2 EDL, gas-kinetic temperatures lower than ambient are required for operation on non-standard lasing transitions, also for reasons of efficient atmospheric transmission. Isentropic expansion in a supersonic nozzle is used to achieve the desired static temperature.

Consider the first thermodynamic cycle shown in Figure 9.2-1. In the plenum, the gas has a stagnation temperature T_{01}, a stagnation pressure P_{01}, and a Mach number of approximately zero. The gas is accelerated through a supersonic nozzle to a Mach number M_1 and a static temperature T_1 at the entrance to a constant-area laser channel. In this region, excitation power P_E is added to the gas by a glow discharge. A certain fraction of this excitation power, η_d, is extracted from the optical cavity as laser power output, P_L. The excitation power that is not extracted remains in the gas and eventually goes into gas heating. Now in this simplified cycle, we consider the particular case where enough power is added to the gas so that the Mach number at the laser channel exit is unity, i.e., the flow is choked. This gives the minimum mass flow and compressor power for any given laser power output and, as such, represents an idealized situation which permits ease of calculation without the complication of additional gas-dynamic parameters. (These conditions will not be realized in any particular device. In such a device the power added must be consistent with the discharge stability limits and the maximum temperature increase allowed is limited by lasing kinetics. The simplications and restructions of the present model yield an upper limit to the predicted performance and, as such, represent an optimistic situation which may only be approached with realistic devices.) Because of heat addition, the stagnation pressure decreases to P_{02} and the stagnation temperature increases to T_{02} at the channel exit. The gas then enters a subsonic diffuser where it is decelerated to approximately zero Mach number, then flows through various ducts where frictional and turning losses drop the stagnation pressure further to P_{03}, subsequently flowing through a compressor which adiabatically compresses the gas back to the original stagnation pressure P_{01} and elevates the stagnation temperature to T_{03}. The power added to the gas is $\eta_c P_c$, where η_c is the compressor adiabatic efficiency and P_c is the power required to drive the compressor. Finally, the gas flows through a waste heat exchanger which reduces the stagnation temperature back to the original value, T_{01}. Q_W is the quantity of heat removed from the gas by a single heat exchanger which must be radiated

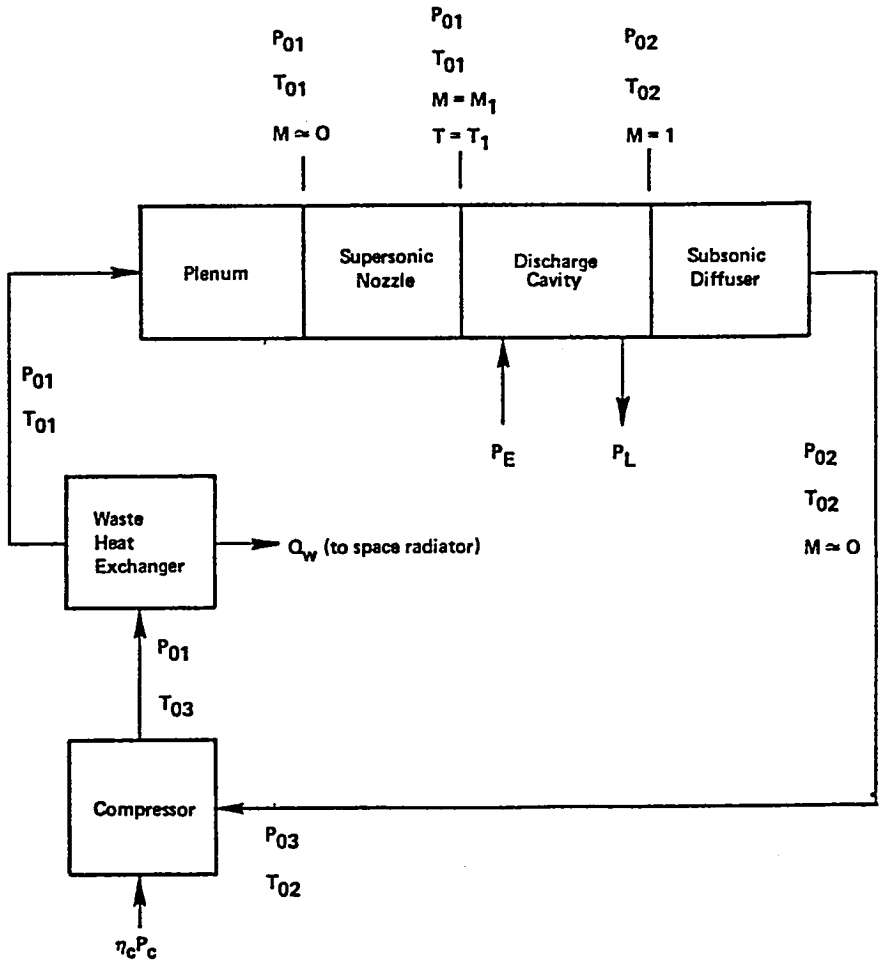

Figure 9.2-1. Single Heat-Exchanger Thermodynamic Cycle for Closed-Cycle EDL Operation

away into space. Note that placing the heat exchanger before the compressor reduces the required compressor power, but at the expense of a much larger radiator area.

The thermodynamic and flow equations that describe the cycle shown in Figure 9.2-1 are now developed. Assuming isentropic supersonic expansion, the static temperature at the entrance to the discharge cavity is

$$T_1 = \frac{T_{01}}{1 + \frac{\gamma-1}{2} M_1^2} . \tag{6}$$

With the assumption of choking at the laser channel exit, the stagnation pressure and temperature ratios follow from standard relations for heat addition in a constant-area duct,[5]

$$\frac{P_{02}}{P_{01}} = \frac{(1 + \gamma M_1^2)}{(\gamma + 1)} \left[\frac{+ 1}{2(1 + \frac{\gamma-1}{2} M_1^2)} \right]^{\frac{\gamma}{\gamma-1}} , \tag{7}$$

$$\frac{T_{02}}{T_{01}} = \frac{(1 + \gamma M_1^2)^2}{2(\gamma + 1)M_1^2(1 + \frac{\gamma-1}{2} M_1^2)} . \tag{8}$$

Monson[2] estimates the pressure drop due to frictional and turning losses between the diffuser and compressor by the quasi-empirical expression

$$\frac{P_{03}}{P_{02}} = \left[\frac{0.75\gamma + 1.25}{\gamma + 1} \right]^{\frac{\gamma}{\gamma-1}} \tag{9}$$

The pressure drop across the heat exchanger is ignored, since it is assumed to be negligible compared with the loss across the laser.

For adiabatic compression, the compressor power is given by the standard expression

$$P_c = \left[\frac{\dot{m} C_p T_{02}}{\eta_c} \left(\frac{P_{01}}{P_{03}} \right)^{\frac{\gamma-1}{\gamma}} \right] - 1 , \tag{10}$$

where $\dot{m}$ is the gas mixture flow rate, η_c is the adiabatic efficiency of the compressor, and C_p is the specific heat at constant pressure. If we assume that the only power lost from the gas is that of the output beam, P_L, and that the specific heat at the laser channel exit equals that at the inlet, then the heat added to the gas by excitation, Q_H, is given by

$$Q_H = \dot{m} C_p (T_{02} - T_{01}) = P_E - P_L = (1 - \eta_d) P_E . \tag{11}$$

The second assumption is not strictly true, since C_p is a function of the rotational and vibrational temperatures of the lasant; however, since the lasant gas comprises a minority fraction of the total gas composition (typically a few percent to 10 percent), this effect is negligible in terms of the gas-dynamic calculation presented here. From Eq. (11), the mass flow rate is

$$\dot{m} = \frac{(1 - \eta_d) P_E}{C_p T_{01} \left(\frac{T_{02}}{T_{01}} - 1 \right)} . \tag{12}$$

Substituting Eq. (12) into Eq. (10) and rearranging gives an equation for P_c/P_E in terms of known efficiences and stagnation states:

$$\frac{P_c}{P_E} = \frac{(1 - \eta_d)(T_{02}/T_{01})}{\eta_c \left(\frac{T_{02}}{T_{01}} - 1\right)} \left[\frac{1}{\left(\frac{P_{02}}{P_{01}} \cdot \frac{P_{03}}{P_{02}}\right)^{\frac{\gamma-1}{\gamma}}} - 1 \right] \quad . \tag{13}$$

Here, the stagnation state ratios depend only on γ and M_1 and are computed from Eqs. (7) through (9). The total laser system efficiency, η_L, is thus obtained by substitution of Eq. (13) into Eq. (5).

Waste heat is removed from the flowing gas by the heat exchanger and subsequently radiated away into space. The required radiator area, $A_r(m^2)$, is given by

$$A_r = \frac{Q_w}{\varepsilon \sigma T_{03}^4} \quad , \tag{14}$$

where ε is the radiator surface emissivity (assumed to be 0.85) and σ is the Stefan-Boltzmann constant (5.6686×10^{-8} $W/m^2-°K$). In Eq. (14), we assume radiation to deep space (sink temperature → 3°K) and ideal heat-exchanger effectiveness. The waste heat, Q_w, is

$$Q_w = P_E - P_L + \eta_c P_c \quad , \tag{15}$$

which may be rewritten in terms of the known and calculated efficiency parameters as

$$Q_w = \left[\frac{1}{\eta_d} - + \eta_M \eta_c \left(\frac{1}{\eta_L} - \frac{1}{\eta_d \eta_{PS}} \right) \right] P_L \quad . \tag{16}$$

The radiator temperature, T_{03}, is simply

$$T_{03} = \frac{T_{03}}{T_{02}} \cdot \frac{T_{02}}{T_{01}} \cdot T_{01} \quad ,$$

where T_{01} is the plenum stagnation temperature, the ratio T_{02}/T_{01} is given by Eq. (8), and the ratio T_{03}/T_{02} is found from the equation

$$\frac{T_{03}}{T_{02}} = \left(\frac{P_{01}}{P_{03}}\right)^{\frac{\gamma-1}{\gamma}} = \frac{1}{\left(\frac{P_{02}}{P_{01}} \cdot \frac{P_{03}}{P_{02}}\right)^{\frac{\gamma-1}{\gamma}}} \quad . \tag{17}$$

The stagnation pressure ratios needed in Eq. (17) were derived previously in Eqs. (7) and (9).

The second thermodynamic cycle, shown in Figure 9.2-2, uses two waste heat exchangers. This cycle is identical to the previous one, except that a second heat exchanger is placed ahead of the compressor to cool the gas back to the initial stagnation temperature, T_{01}. Monson[2] found that this second configuration reduces the compressor power but increases the required radiator

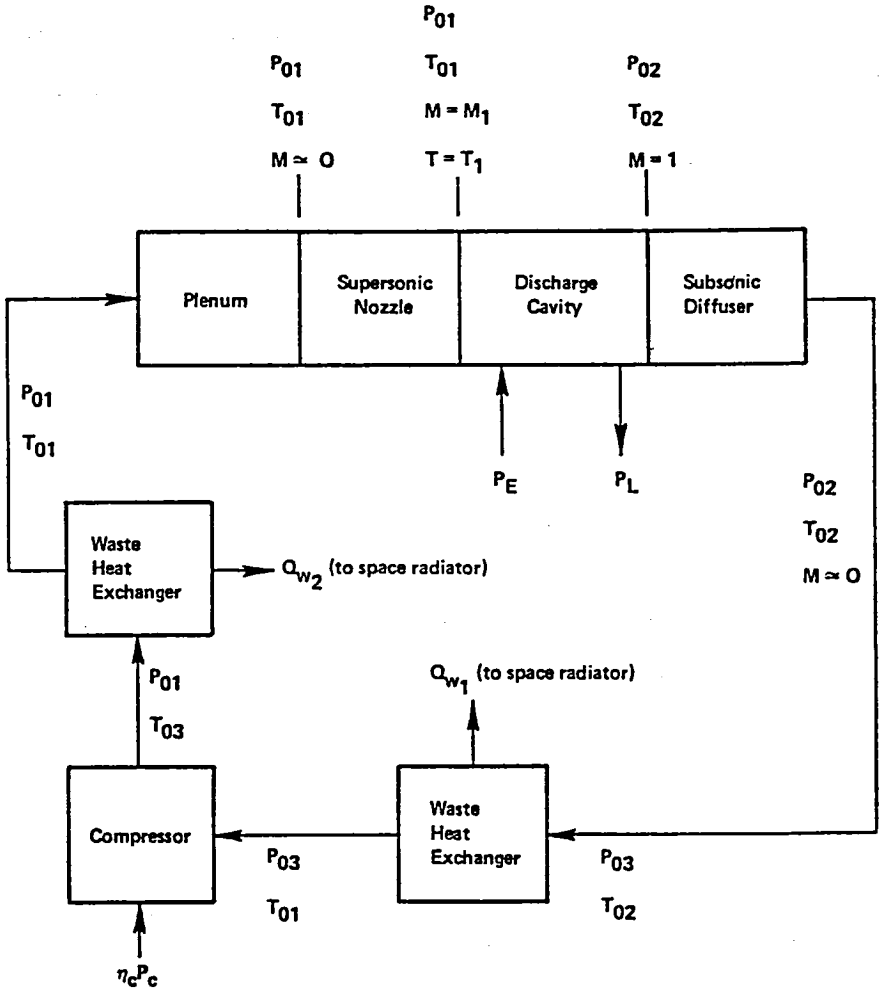

Figure 9.2-2. Dual Heat-Exchanger Thermodynamic Cycle for Closed-Cycle EDL Operation

area. The net result, however, is a reduction in the total system specific mass and an improvement in system efficiency.

The thermodynamic analysis proceeds in an identical manner to that employed for the first cycle. Without showing all of the details, we obtain an alternate expression for the ratio of compressor power to excitation power, namely,

$$\frac{P_c}{P_E} = \frac{(1 - \eta_d)}{\eta_c\left(\frac{T_{02}}{T_{01}} - 1\right)} \left[\frac{1}{\left(\frac{P_{02}}{P_{01}} \cdot \frac{P_{03}}{P_{02}}\right)^{\frac{\gamma-1}{\gamma}}} - 1 \right] . \qquad (18)$$

Substituting Eq. (18) into Eq. (5) yields the appropriate expression for η_L. The stagnation state ratios, T_{02}/T_{01}, P_{02}/P_{01}, and P_{03}/P_{02}, are identical to those employed in the first cycle. The expression for the radiator area is now

$$A_r = \frac{1}{\sigma\varepsilon}\left(\frac{Q_{w_1}}{T_{02}^4} + \frac{Q_{w_2}}{T_{03}^4}\right) \quad , \tag{19}$$

and the waste heat terms are

$$Q_{w_1} = P_E = P_L = \left(\frac{1}{\eta_d} - 1\right) P_L \quad . \tag{20}$$

and

$$Q_{w_2} = \eta_c P_c = \eta_M \eta_c \left(\frac{1}{\eta_L} - \frac{1}{\eta_d \eta_{PS}}\right) P_L \quad . \tag{21}$$

Two different temperatures are associated with the two waste heat sources:

$$T_{02} = \frac{T_{02}}{T_{01}} \cdot T_{01} \tag{22}$$

and

$$T_{03} = \frac{T_{03}}{T_{01}} \cdot T_{01} \quad . \tag{23}$$

T_{01} is again the plenum stagnation temperature, T_{02}/T_{01} is given by Eq. (8), and T_{03}/T_{01} is found by solving the equation

$$\frac{T_{03}}{T_{01}} = \left(\frac{P_{01}}{P_{03}}\right)^{\frac{\gamma-1}{\gamma}} = \frac{1}{\left(\frac{P_{02}}{P_{01}} \cdot \frac{P_{03}}{P_{02}}\right)^{\frac{\gamma-1}{\gamma}}} \quad , \tag{24}$$

where P_{02}/P_{01} and P_{03}/P_{02} are given by Eqs. (7) and (9) as before.

CO_2 Laser Evaluation

Several research groups have suggested using CO_2 EDL's for power transmission. A highly evolved technology base exists, and device scaling to powers of the order of 100 MW is teasonably well assumed. Significant operational experience with closed-cycle systems has been gleaned over the past few years. With CO_2 EDL's, most conceptual systems employ subsonic flow to remove waste heat from the gas mixture; consequently, less compressor power is required as compared with supersonic operation. Advocates of the CO_2 EDL cite this fact as a major advantage and quote rather high laser system efficiencies ($\simeq 25\%$). As discussed in the following paragraphs, this conclusion is inaccurate and

neglects several important physical phenomena.

Under normal circumstances, lasing with the CO_2 molecule can occur between the asymmetric stretch and symmetric stretch modes ($00^01 \rightarrow 10^00$) or the asymmetric stretch and bending modes ($00^01 \rightarrow 02^00$). The laser wavelength is ~ 10.4 μm or ~ 9.4 μm, with the exact wavelength depending upon the details of the respective rotational sublevels. The cogent energy levels are shown in Figure 9.2-3. The 00^01 state is pumped by direct electron impact or by resonant transfer of vibrational energy from N_2. N_2 is usually one gas constituent in a CO_2 EDL. To avoid a cessation of lasing, excess population buildup in the 01^10 level must be removed by collisional relaxation. Helium, also a constituent in CO_2 laser gas mixtures, serves to depopulate this level and to act as the heat transfer medium.

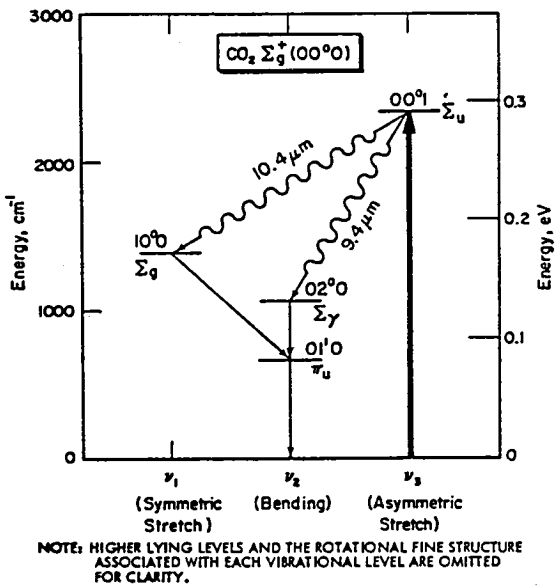

Figure 9.2-3. Energy Level Diagram of the Σ_g^+ Ground State of CO_2

Because the 01^10 state is energetically close to the ground state, it is easily filled by thermal excitation. When this occurs, bottle-necking of the laser transition causes a loss in population inversion and eventually a complete loss in output power. Figure 9.2-4 is a plot of the fractional population of the various CO_2 levels as functions of gas temperature. The two cross-hatched regions identify the conditions under which population inversions on the 9.4- and 10.4-μm transitions are permitted. The two curves denoted by ΔN show the dependence of inversion population on temperature. An inversion cannot be maintained on the $00^01 \rightarrow 02^00$ band (9.4 μm) for temperatures greater than ≃400°K, or on the $00^01 \rightarrow 10^00$ band (10.4 μm) for temperatures greater than ≃700°K. To obtain good discharge efficiencies in large devices, the static temperature of the inlet gas should be much lower, ≃200°K and ≃400°K, respectively.

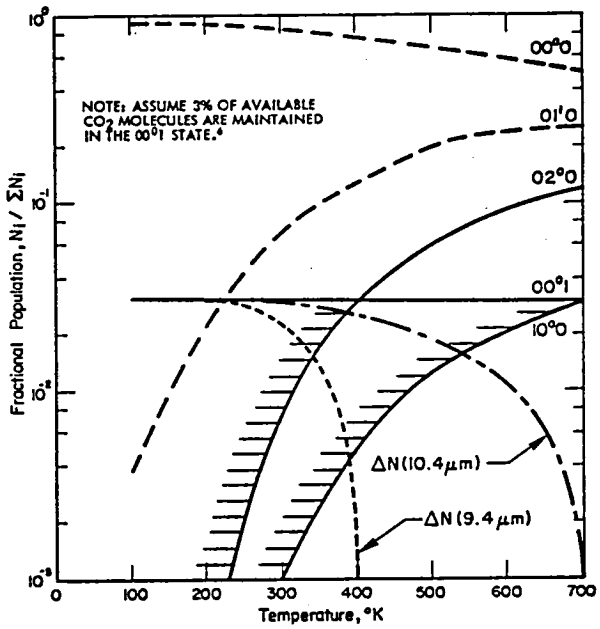

Figure 9.2-4. Fractional Population of the Various CO_2 Levels as Functions of the Gas-Kinetic Temperature

The atmospheric transmission efficiency of any line within the $00^01 \rightarrow 10^00$, 10.4-μm band has been calculated to be very poor. To alleviate this situation various transitions within the $00^01 \rightarrow 02^00$, 9.4-μm band have been suggested. If low-abundance isotopic species of CO_2 are employed as the lasant, a shift in output wavelength occurs and atmospheric absorption features due to natural CO_2 can be avoided.

It is desirable to calculate the maximum theoretical efficiencies for CO_2 lasers operating under these conditions. Using the energy level diagram, Figure 9.2-3, it is straightforward to calculate system quantum efficiencies. The $00^01 \rightarrow 10^00$ transition at 10.4 μm has a quantum efficiency of 40%, while the $00^01 \rightarrow 02^00$ transition at 9.4 μm has a quantum efficiency of 45%. The maximum electric power transfer to the coupled $CO_2(00^01)$-$N_2(v)$ system is about 70%, with the remainder going into ionization, electronic excitation, and translation.[7,8] Hence, the maximum achievable discharge efficiencies are simply

$$\eta_d \ (9.4\ \mu m) = 0.45 \times 0.70 = 0.32,$$

$$\eta_d \ (10.4\ \mu m) = 0.40 \times 0.70 = 0.28.$$

Therefore, if the power required to maintain the closed-cycle flow is small, overall laser systems efficiencies exceeding 20% are reasonable.

As noted above, a static gas temperature as low as 200°K is required for operation of the $00^01 \rightarrow 02^00$ band. Two cooling methods are available for a space-based laser. The laser cycle can be operated subsonic using space radiators to cool the gas emerging from the discharge to ≈200°K before re-entering the

excitation region. Because of the low temperature required, a huge radiator surface area would be necessary. Alternately, high plenum temperatures are permissible to reduce the required radiator area if a supersonic expansion technique is used to obtain the low static gas temperature.

Thermodynamic calculations were performed for such a closed-cycle, supersonic CO_2 laser using the thermodynamic models developed previously and the following plenum stagnation temperature and subsystem efficiencies:

$$P_{01} = 360°K$$

$$\eta_c = 0.85$$

$$\eta_{PS} = 0.9323$$

$$\eta_M = 0.8950 \quad .$$

This procedure permits a direct comparison of CO_2 and CO laser systems efficiencies (see Figure 9.2-11). Using a mixture consisting mostly of He (γ = 1.65), a static gas temperature, T_1, of 200°K requires a flow Mach number of

$$M_1 = 1.57.$$

Under these conditions and with a discharge efficiency of 0.32, the total laser system efficiency for operation on the $00^01 \rightarrow 02^00$, 9.4-μm band is

$$\eta_L = 0.135 \text{ (1 HEX)}$$

$$\eta_L = 0.141 \text{ (2 HEX)} \quad .$$

The total laser system efficiency is defined as the ratio of laser output power to total electrical power required to operate the system. Operation with two heat exchangers affords little improvement in overall system efficiency for these conditions.

To affect maximum atmospheric transmission, lasing on only one specific vibrational-rotational line is being considered. In the analysis above, rotational relaxation effects have been ignored, which leads to an overprediction in the discharge efficiency. Hence, the total system efficiency estimates may be somewhat optimistic.

In this context, the laser would be arranged in a MOPA (Master Oscillator Power Amplifier) configuration in which a small grating-tuned oscillator drives a large power amplifier. The oscillating spectral line is selected by adjusting the grating angle on the oscillator. This technique avoids the use of large, expensive, and delicate gratings with high-power oscillators.

The wavelength range of the two principal lasing bands using several different CO_2 isotopic species is shown in Figure 9.2-5. The line identified by Mevers et al.[11] with the best atmospheric transmittance is the R(20) line of the $00^01 \rightarrow 02^00$ band of $^{12}C^{18}O_2$. The natural abundances of the various

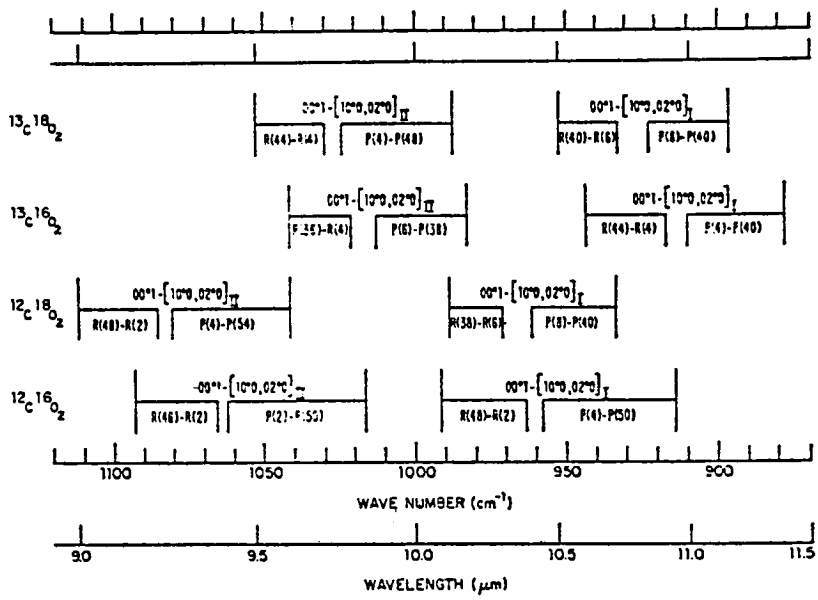

Figure 9.2-5. Comparison of the Frequency/Wavelength Domains of Low-Abundance CO_2 Isotope Lasers with $^{12}C^{16}O_2$

isotopic species of CO_2 are given in Table 9.2-1. If a specific isotopic specie of carbon dioxide is required for acceptable atm ospheric transmission, then some method of isotope separation must be employed. If $^{12}C^{18}O_2$ is chosen as the lasant specie, added expense will be incurred due to the recovery process because of this specie's extremely small abundance. (Actually, only the 0.2% of the ^{18}O is elemental oxygen would require separation; the ^{18}O thus separated would then be reacted with natural carbon, which is 98.89% ^{12}C.) Recall that the separative work is isotope separation, however, is proportional to the isotopic mass difference divided by the abundance-weighted mass. Hence, separation of ^{18}O from oxygen will take far less work than separation of ^{235}U from uranium; thus, the separative cost may not be prohibitive in such a specialized laser application.

Table 9.2-1. Isotopic Species of Carbon Dioxide

SPECIES	NATURAL ABUNDANCE
$^{12}C^{16}O_2$	98.14%
$^{13}C^{16}O_2$	1.105%
$^{12}C^{18}O_2$	0.00041%
$^{13}C^{18}O_2$	0.0000046%

CO Laser Evaluation

The lasing spectra of CO lasers show a characteristic multiline output whose distribution is a function of the gas-kinetic temperature. In large-scale devices, the low gas-kinetic temperature of the lasing medium is achieved by a supersonic expansion. This results in lasing on low v transitions and improved atmospheric transmission. The spectral output above ≈5.4 μm is strongly absorbed by the atmosphere.

The atmospheric transmission efficiency is a sensitive function of the multiline distribution, and any calculation of atmospheric transmission of CO laser radiation must be performed by weighting the line transmittance by the fractional laser power in each line and then summing over all the lines. As shown in Figures 9.2-6 and 9.2-7, the absorption coefficients for the longer wavelength (larger v) transitions are much larger than for the shorter wavelength transitions.[12] Large differences also can exist in the absorption coefficients of adjacent lines. Since a large fraction of the molecular absorption is attributable to the 6.3-μm water band, seasonal variations are pronounced. Due to a significant improvement in atmospheric transmission of the lower v transitions, much effort has been expended in developing laser devices which maximize their power output on such transitions.[13]

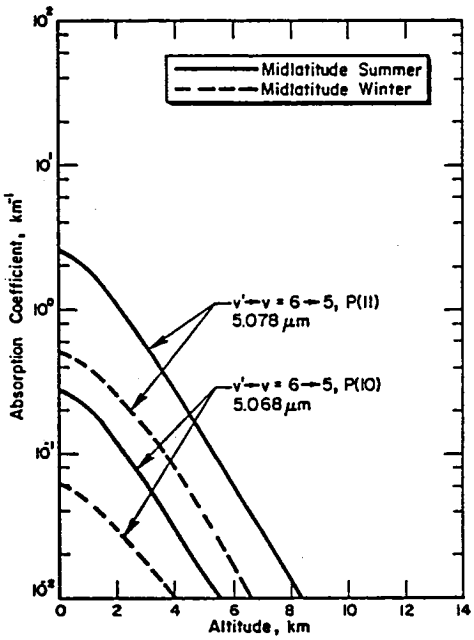

Figure 9.2-6. Absorption Coefficient as a Function of Altitude for Two Adjacent CO Laser Lines[12]

Even at very low temperature many of the CO laser lines do not have satisfactory transmission characteristics. Rice[14] at Northrop Research and Technology Center has developed a technique for redistributing the output line spectra of CO EDL's. An intracavity water vapor cell spoils the gain

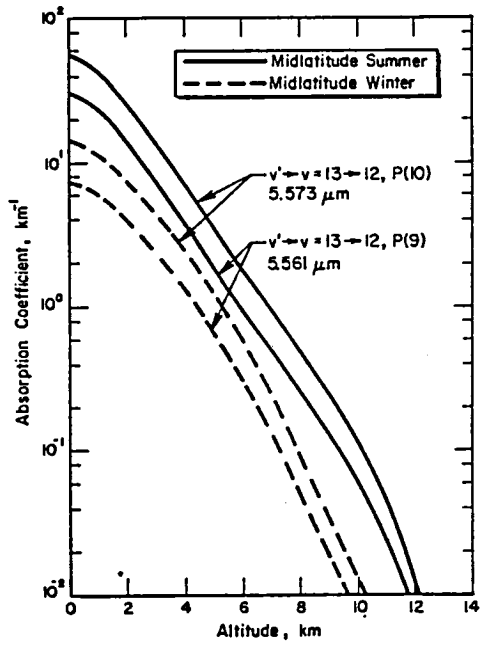

Figure 9.2-7. Absorption Coefficient as a Function of Altitude for Large-v CO Laser Lines[12]

on those lines which are highly absorbed by water, the rotational sublevel populations are redistributed, and positive gain occurs only on those lines unaffected by the absorption. Three spectra from the experiments of Rice are shown in Figures 9.2-8 through 9.2-10. Above each line is the fractional power residing in that line and a relative measure of the atmospheric transmission efficiency (the horizontal propagation distance at sea level for a decrease in intensity by a factor of e using the Midlatitude Winter model). Figure 9.2-8 shows the cw device output without water vapor, and Figures 9.2-9 and 9.2-10 show the effects of increasing vapor pressures in the intracavity cell.

The use of a line selection cell produces a significant decrease in the laser output power. This effect will be less dramatic on large devices having longer gain lengths. Although MOPA configurations are not generally applicable to CO lasers, the development of a special system may be warranted for power transmission. The reason for avoiding CO MOPA's is as follows. The gain on a particular P-branch line is an extremely sensitive function of the gas-kinetic temperature and excitation rates. Thus, it is difficult to ensure proper matching between oscillator and amplifier so that the oscillator lines are indeed amplified and not absorbed. This is further complicated by the cascading nature of the CO transitions. If a line-selected oscillator could be designed in conjunction with a large power amplifier, then the loss is discharge efficiency due to the presence of an intracavity cell would be minimized.

In closed-cycle flow, the compressor power required to circulate the gas is a function of the flow Mach number. Thus, operation at the low gas-kinetic temperatures necessary for efficient atmospheric transmission requires a

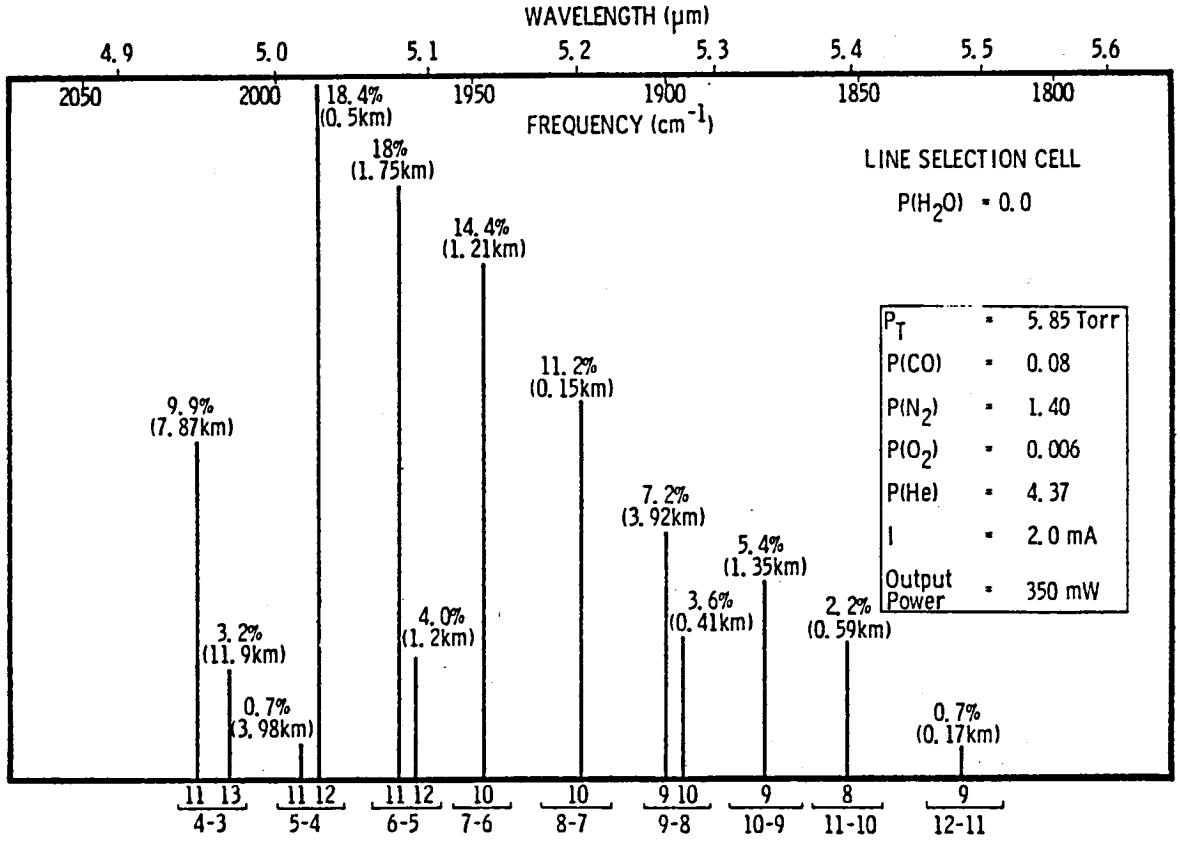

Figure 9.2-8. Output Spectrum of a cw, Cryogenically Cooled (77°K) CO Laser Without Line Selection[14]

substantial fraction of the total power available just to operate the flow cycle. The dependence of total laser system efficiency, η_L, on the discharge efficiency for two thermodynamic cycles is shown in Figure 9.2-11. The shaded region denotes the range of expected performance. To achieve the necessary low static temperature in the discharge cavity, a supersonic expansion of Mach number 3 to 4 is required based on the anticipated plenum stagnation temperature of approximately 360°K. Discharge efficiencies of 0.35 to 0.50 appear possible. Mann[15] has suggested that discharge efficiencies of 0.60 in cw devices may be achievable; however, the best reported[16] performance is 0.39. The thermodynamic cycle with dual heat exchangers affords an improvement in system performance over the cycle with a single heat exchanger. As noted in Figure 9.2-11, the potentially achievable laser system efficiency ranges from 11.5% to 23.4%. In the discussions which follow, we assume best-case performance, i.e., $\eta_L = 0.234$.

Electric Discharge Types

The type of electric discharge employed in conjunction with a molecular-gas laser influences most system parameters (e.g., η_d and η_L) while effecting many ancillary characteristics, such as reliability, serviceability, system

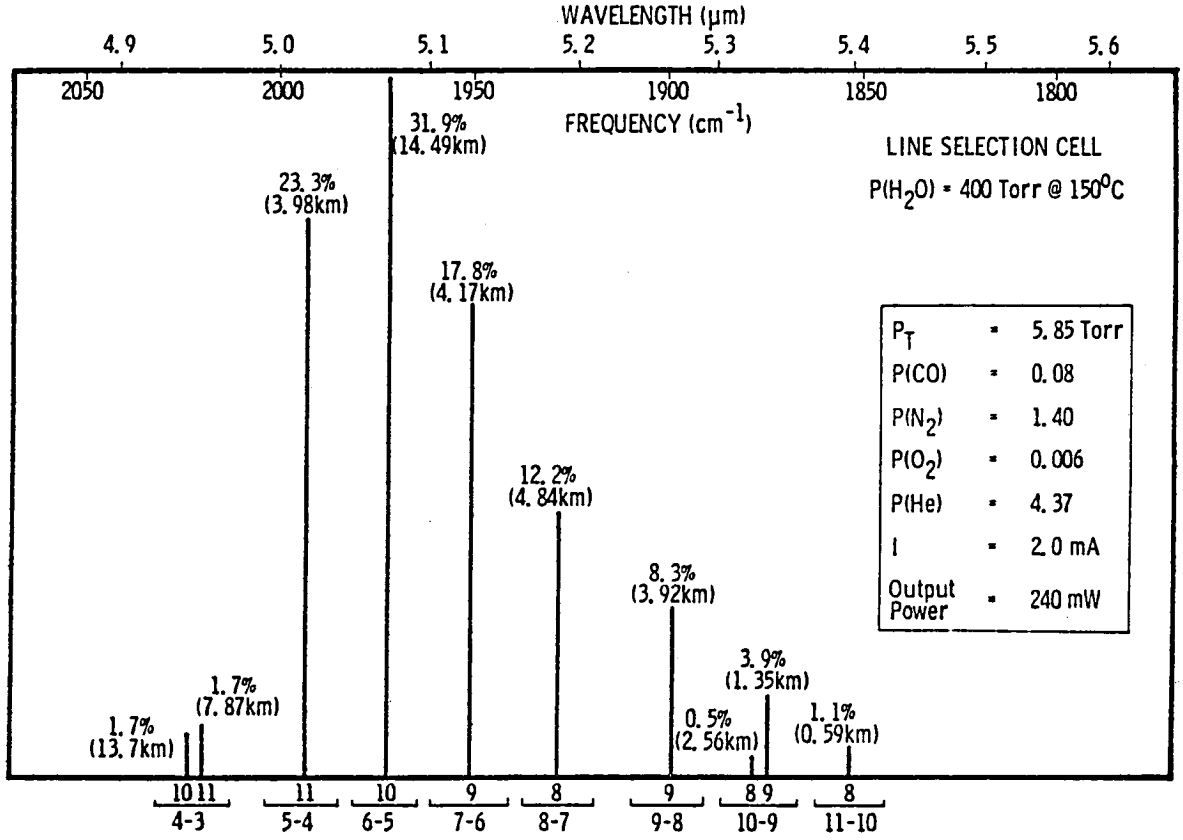

Figure 9.2-9. Output Spectrum of the Same Device Shown in Figure 9.2-8 with an Intracavity Line Selection Cell Filled with 400 Torr H_2O[14]

mass and volume, and scalability. Quantitative characteristics of the various discharge types are listed in Table 9.2-2. Based on our evaluation, the pulser-sustainer type of discharge has many attributes which make it suitable for the present application and deserving of more research support.

Molecular-gas electric-discharge lasers operate at maximum discharge efficiency only within a certain range of the parameter E/N (electric-field strength divided by the neutral species concentration). This range depends only upon the gas mixture composition. With a self-sustained glow discharge, the rates of electron production (e.g., ionization) and electron destruction (e.g., recombination, attachment, etc.) are electron-temperature dependent and adjust themselves until equality is reached. This may lead to discharge operation outside the range of optimum E/N and a concomitant loss in discharge efficiency. The CO EDL is a particularly good case in point, since the optimum E/N is lower than that required to maintain ionization in the plasma. To alleviate this situation, various non-self-sustained discharge schemes have been developed in which the ionization "source" and sustainer electric field are separate. The rates of ionization and electron-impact excitation are effectively decoupled, allowing independent control of E/N; hence, maximum discharge efficiency can be obtained.

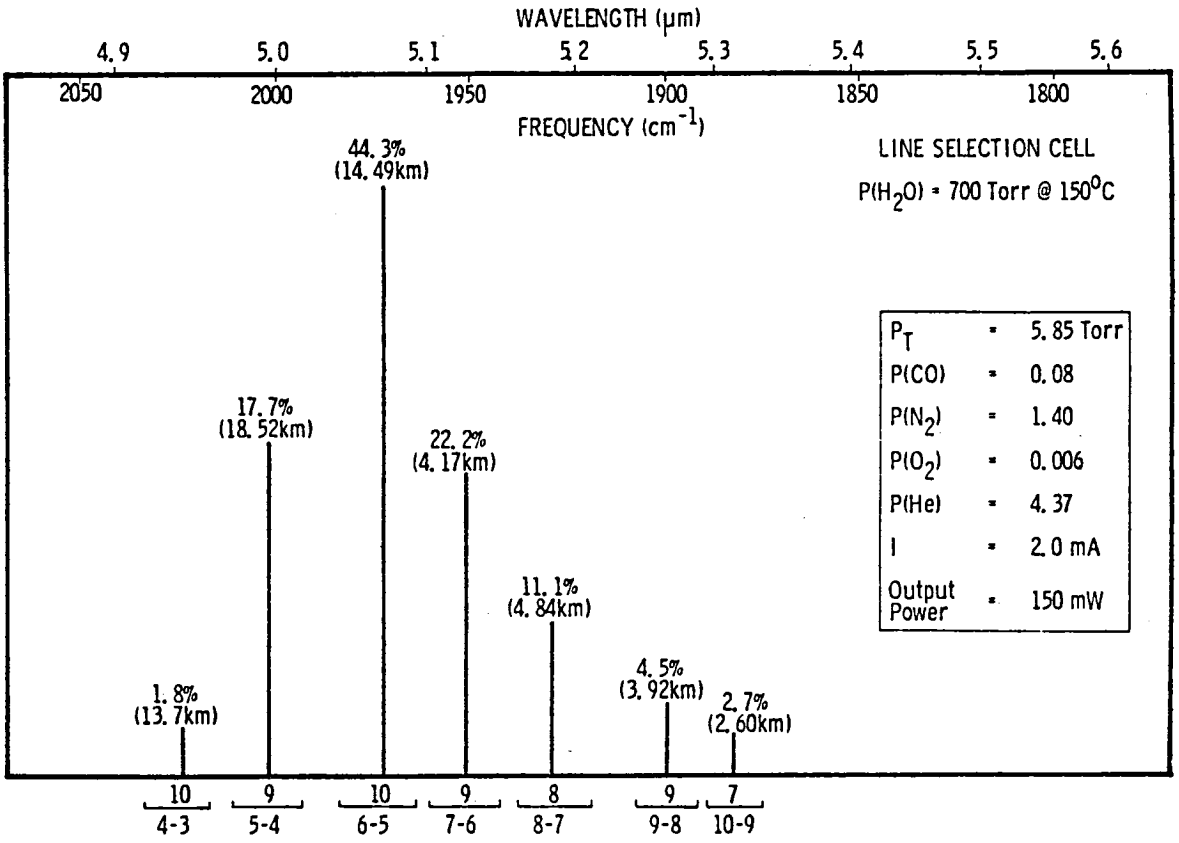

Figure 9.2-10. Output Spectrum of the Same Device Shown in Figure 9.2-8 With an Intracavity Line Selection Cell Filled with 700 Torr H_2O[14]

The utilization of a non-self-sustained discharge with a CO_2 EDL is less critical. However, for both types of molecular-gas lasers, the specific power loading, $P_E/\dot{m}$ (kW/kg/sec or kJ/kg), and volumetric power density, $\langle jE \rangle$ (W/cm^3), are improved when a non-self-sustained discharge is employed. [Here, j is the discharge current density (A/cm^2), E is the electric field strength (V/cm^2), and the other terms were defined previously.]

The pulser-sustainer, or "POKER", discharge was originally investigated by Reilly[17] in conjunction with a subsonic pulsed CO_2 laser. Later, Hill[18] applied the technique to a cw CO_2 laser by superimposing a train of high-voltage breakdown pulses upon the low-voltage dc sustainer field. Although interest in the pulser-sustainer CO_2 laser has waned in the United States, Soviet researchers are actively pursuing this technique in conjunction with subsonic[19-24] and supersonic[25] devices. Their stated intent is the development of non-electron-beam cw gas lasers for industrial materials processing applications.

Research on pulser-sustainer discharges applied to supersonic-flow CO lasers has been conducted at the Air Force Weapons Laboratory[26] and at NASA Ames Research Center.[27,28] The later experiments of Monson[28] are particularly

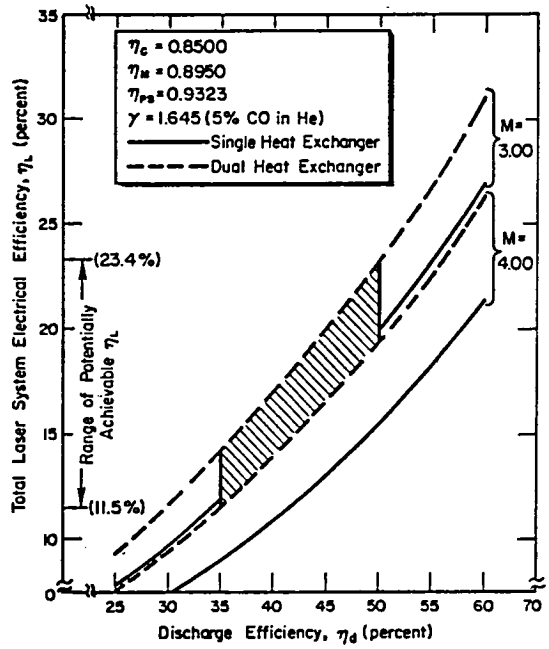

Figure 9.2-11. The Dependence of the Total Laser System Efficiency, η_L, on the Discharge Efficiency Using the Thermodynamic Models of a Closed-Cycle EDL

Table 9.2-2. CW Discharge Characteristics

Discharge Type	Characteristics: Advantages	Characteristics: Disadvantages	Suitability: CO	Suitability: CO_2
Self-sustained discharge	Simple, reliable, highly evolved technology; scaling behavior well understood	Low to moderate discharge efficiency; low specific and volumetric power loadings	No	Yes
Non-self-sustained discharge				
(1) Electron-beam-sustained discharge	Improved discharge efficiency; high specific and volumetric power loadings, scaling behavior understood	Poor reliability, x-ray hazards, complex maintenance; e-beam transmission foil blow out leads to a loss of lasant gases	Yes	Yes
(2) Pulser-sustainer discharge	Less complicated and smaller than e-beam sustained devices; comparable volumetric and specific power loadings may be possible with further research; promises to be more reliable.	Scalability to large devices not demonstrated, discharge efficiencies comparable to e-beam-sustained devices not yet achieved; technology not highly evolved.	Yes	Yes

significant since they indicate discharge performance comparable to electron-beam-stabilized discharges with device scale-up. The pulser-sustainer type of discharge avoids many of the complicatons inherent in electron beams. Furthermore, electron-beam-stabilized cw gas lasers are limited in scalability by transmission foil heating. The capacity to remove heat from the e-beam transmission foil "window" limits the maximum e-beam current density to ~1 mA/cm^2, which imposes limits on the maximum discharge gap. Research funding devoted to pulser-sustainer lasers has amounted to only a minute fraction of that directed toward e-beam devices. Therefore, the scalability limits of the former technique are not known.

9.2.2 TRANSMITTING OPTICS

The three types of optical systems most appropriate for the present application are the prime focus, the on-axis Cassegrain, and the minimum-length off-axis paraboloid section systems. Simplified representations of these configurations are shown in Figure 9.2-12. Because of the power densities involved, only reflective, metal-surface optics can be realistically considered.

Although the prime-focus system is the simplest of the three configurations, beam spread due to diffraction becomes significant when the diameter of the central obstruction is greater than about 10% of the mirror diameter. This is shown in Figure 9.2-13, where the fraction of energy collected within the first dark ring of the classical Airy diffraction pattern is plotted as a function of the central obscuration ratio, ε, which is defined as the ratio of obscurred diameter to overall mirror diameter. Since the required mirror diameter is estimated to be 25 m, it will be exceedingly difficult to reduce the laser (obscuration) diameter to 2.5 m or less. The minimum-length, off-axis paraboloid section system cannot be made as short as the on-axis Cassegrain system, but it does circumvent the difficulties associated with beam obscuration. One inherent disadvantage, however, is the difficulty of optical figuring large-area off-axis mirror sectors. From the standpoint of size, optical stability, and diffraction efficiency, the Cassegrain system is the best choice.

The major disadvantage of the Cassegrain system as a transmitting telescope of high-power laser radiation is that the secondary (smaller) mirror is subject to large incident power densities, which will require some form of active cooling. The sizing of the Cassegrain laser transmitter was performed considering the effects of diameter on diffraction efficiency, beam spread, and power density loading.

In the design of a large-aperture space based laser transmitter, the surface reflectivity and incident power density dictate the method of cooling. The primary mirror designs of Berggren and Lenertz[29] employ a coated metal reflecting surface on low-thermal-expansion glass or ceramic material, and a graphite-epoxy composite supporting structure of matching low-expansion characteristics. The primary mirror is radiatively cooled and can dissipate the absorbed power associated with a maximum laser power density of 10 W/cm^2 in addition to the solar heat load. Because the average incident power density on the primary mirror of the laser-SPS transmitter is $\simeq$20 W/cm^2, active cooling appears Uecessary to maintain optical figure control. Beryllium or beryllium/copper alloys are of interest because of their low density and desirable

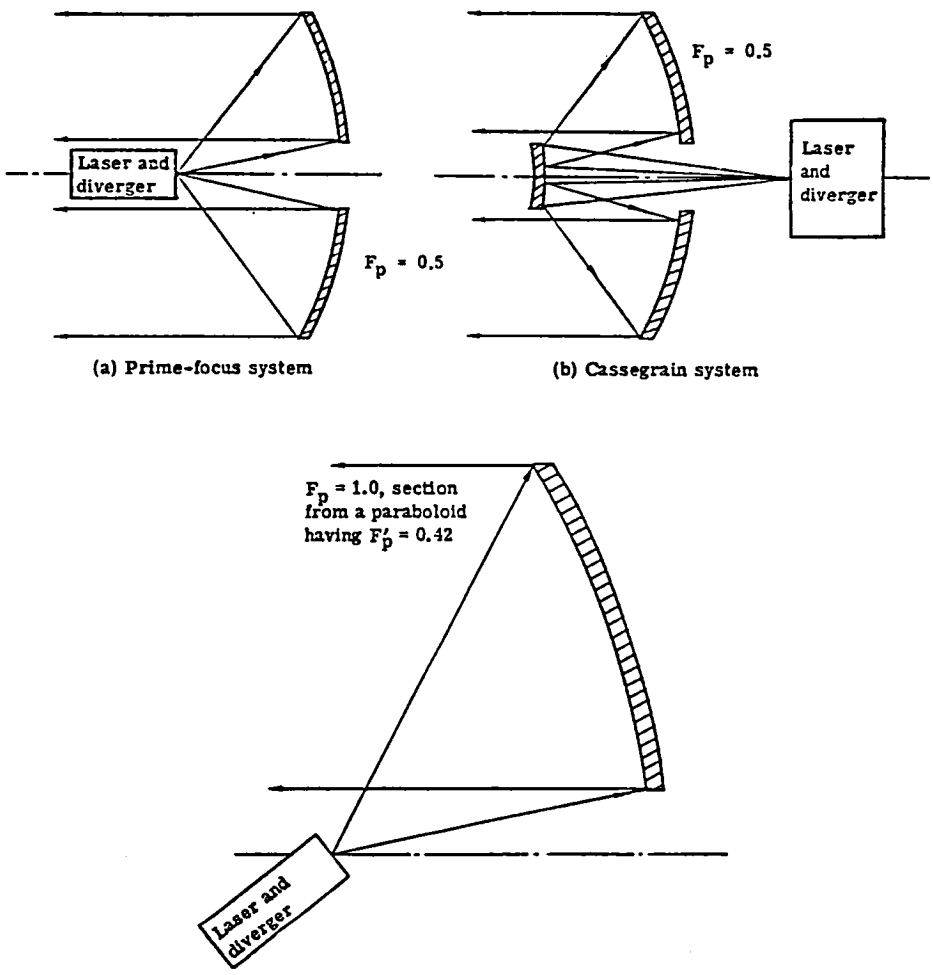

Figure 9.2-12. Principal Optical System Candidates for a Space Based Laser Transmitter.[29] F_p is the Focal Length of the Primary Mirror

thermophysical properties.[30,31] The infrared reflectivities of state-of-the-art Be[32] and BeCu[33] mirrors at 10.6 μm are 0.985 and 0.975, respectively. (The reflectivity changes little in going from 10.6 μm to 5 μm.) Due to the laser power levels involved, however, considerable heat is generated in the mirror even for these high values of reflectivity. Furthermore, Be or BeCu mirrors are not ideal reflectors of the solar spectrum, thus aggravating the heat loading problem. The authors of Ref. (29) showed that the heat loading is significantly reduced when the front surface is overcoated with UHV-deposited silver,[34,35] which has a high reflectance from ultraviolet through infrared wavelengths. The best reflectivity (at 10.6 μm) achieved with Ag overcoated metal mirrors is quoted[36] as 0.9938, which is the reflectivity value adopted for the primary mirror considered here. Only minimal, low-pressure cooling will be required for the primary mirror. Alternately, heat pipe

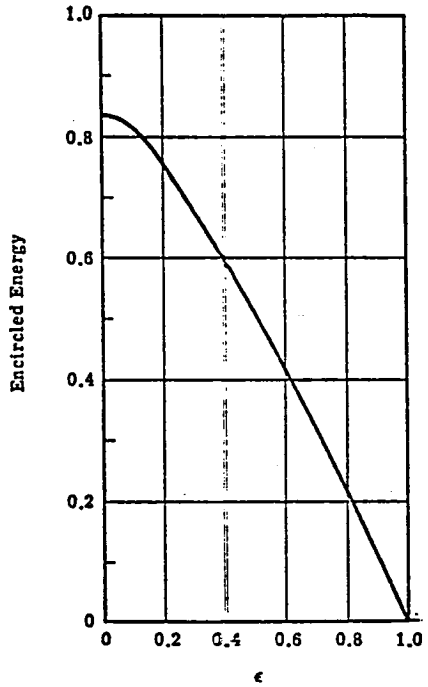

Figure 9.2-13. Fractional Energy with the First Airy Pattern Dark Ring as a Function of the Central Obscuration Ratio, ε.[29]

structures may be desirable for mirror cooling; power densities up to 350 W/cm^2 absorbed by a copper optic were successfully transported without heat pipe "dry out" in the experiments of Ref. (37). At ≈20 W/cm^2, optical distortion can be minimized by judicious heat pipe design.

Because of the very large power densities incident upon the secondary mirror, high-pressure high-flow-rate cooling will be necessary. Oxygen-free, high-conductivity (OFHC) copper mirrors are the optimum choice under these conditions due to their high damage threshold. The best quoted reflectivity, again at 10.6 μm, of state-of-the-art diamond turned OFHC Cu mirrors is 0.9932.[38] Enhanced-reflectivity dielectric coatings are not usually employed because their thermal diffusivities are considerably less than that of the bulk substrate. Absorbed heat simply cannot be dissipated fast enough and the damage threshold is reduced accordingly. Optical Coating Laboratory, Inc. (OCLI), however, has developed[39] a proprietary dielectric coating having a 10.6-μm reflectivity $\geq$ 0.998 and a damage threshold in excess of 10 kW/cm^2. If this technology can be extended to large-diameter mirrors, then the secondary Cu mirror should be coated to enhance its reflectivity.

Preliminary specifications of the transmitting optical system are given in Table 9.2-3. Sensing and correcting the optical figure of the large mirror is necessary to permit near diffraction limited performance of the optical transmitter and to affect maximum laser power interception by the receptor. Within the limitation imposed by the optical round-trip duration (0.285 sec), active alternation of the beam phase can be employed to correct for defocusing

Table 9.2-3. Transmitting Optical System Specifications

Optical configuration -- Cassegrain telescope

Primary mirror:

- Composition -- Be or BeCu/Ag overcoated
- Reflectivity -- 0.9938
- Diameter, D_p = 25.0 m
- Average incident power density -- ≈20 W/cm^2
- Thermal heat load (laser only) -- 1.3 kW/m^2
- Cooling method -- conduction plus radiation

Secondary mirror:

- Composition -- Cu/OCLI coating
- Reflectivity -- 0.998
- Diameter, D_s = 2.00 m
- Average incident power density -- ≈3 kW/cm^2
- Thermal heat load (laser only) -- ≈64 kW/m^2
- Cooling method -- conduction

Central obscuration ratio, $\varepsilon = 0.08$

Mirror figure control -- Deformable surface

Transmitter efficiency -- 0.992

Pointing accuracy -- 2×10^{-7} rad [Ref. (29)]

effects caused by atmospheric turbulence and thermal blooming. Only those physical mechanisms having characteristic time scales in excess of the round-trip duration are subject to compensation.

A number of coherent optical adaptive techniques (COAT) have been designed to optimize the laser power delivered to a target for a wide variety of scenarios. In the multidither techniques, widely reported in relation to high-energy laser programs, individual segments of a mirror are periodically displaced by small amounts and each segment is "tagged" by a different oscillation (dither) frequency. The energy received at the target is related to the phase of each displacement and an appropriate correction signal is developed for each segment. The energy can be measured at the receiver or a small corner cube can be used to reflect energy to a detector at the transmitter. The principal difficulty with this approach in connection with a 25-m space based mirror is in extending the multidither technique to a large number of measurement points and the associated computer/control logic processing requirements. Other problems, associated with the optical transit time and the multiline laser spectral output, also exist for this approach.

The approach of Berggren and Lenertz[29] is perhaps the simplest and most effective; a coherent source is located at the receptor and an interferometer, located at the transmitter, then measures the reverse beam as focussed by the large primary mirror providing the correction signals for focus and figure

control. System considerations for implementation of this approach were briefly reviewed in Ref. (29).

The primary mirror will probably be an assembly of semi-rigid faceplates rather than a large thin plate or membrane because of the necessity for active cooling. Three different types of control will be utilized in applying the correction: actuators will be employed for (1) position control of individual segments, (2) faceplate figure control, and (3) support (truss) control. Control logic and actuator technology amenable to the present application is highly advanced.[29]

9.2.3 ATMOSPHERIC TRANSMISSION

The attenuation of laser radiation passing through the earth's atmosphere is termed linear attenuation if the processes responsible are independent of the beam intensity. In general, molecular scattering, molecular absorption, aerosol scattering, and aerosol absorption contribute to linear attenuation.[40] To calculate the transmittance of any single laser line in propagating from outside the earth's atmosphere to a terrestrial receptor site, the attenuation coefficient due to each of the above processes must be known at a sufficient number of points along the beam path. This implies the necessity for local atmospheric data as well as basic physical parameters related to absorption and scattering.

For the various line wavelengths associated with CO and CO_2 lasers in the infrared, attenuation via molecular absorption is of primary importance. Molecular (Rayleigh) scattering has a wavelength dependence approximately proportional to γ^{-4}, and the molecular scattering coefficient depends only on the number density of molecules in the radiation path. Thus, molecular scattering is only significant for visible wavelength lasers and is completely negligible for CO and CO_2 lasers. Aerosol scattering and absorption are also generally insignificant attenuation processes for CO and CO_2 laser wavelengths propagating in clear air. Under hazy or overcast conditions, aerosol attenuation becomes significant, especially at lower altitudes. There is evidence, however, that multi-megawatt infrared lasers may be capable of hole-burning in various types of light clouds or fog.[41] The effects of different meteorological conditions, viz., different aerosol distributions, are considered in results which follow.

The calculational procedure employs two standard-atmosphere models (Midlatitude Summer and Winter),[42] as given in Tables 9.2-4 and 9.2-5. Absorption coefficients for each laser line transition are calculated for the various atmospheric layers using the High Resolution Absorption Coefficient Code (HIRACC).[43] Absorption parameters of the atmospheric species required by HIRACC are obtained from the AFGL line parameter tape.[44] The most recent version (October, 1978) of this line parameter listing has been acquired for these calculations. The atmospheric species of importance, in general, are H_2O, CO_2, O_3, N_2O, CO, CH_4, and O_2; with the exceptions of H_2O and O_3, all species are considered to be uniformly mixed in the abundances given in Table 9.2-6. In addition to the column densities (molecules/cm^2) along the respective atmospheric layer, HIRACC also requires pressure and temperature data, as shown in Tables 9.2-4 and 9.2-5, for use in the calculation of absorption line broadening.

Table 9.2-4. United States Standard Model Atmosphere: Midlatitude Summer

MIDLATITUDE SUMMER					
Ht. (km)	Pressure (mb)	Temp. (°K)	Density (g/m^3)	Water Vapor (g/m^3)	Ozone (g/m^3)
0	1.013E+03	294.0	1.191E+03	1.4E+01	6.0E-05
1	9.020E+02	290.0	1.080E+03	9.3E+00	6.0E-05
2	8.020E+02	285.0	9.757E+02	5.9E+00	6.0E-05
3	7.100E+02	279.0	8.846E+02	3.3E+00	6.2E-05
4	6.280E+02	273.0	7.998E+02	1.9E+00	6.4E-05
5	5.540E+02	267.0	7.211E+02	1.0E+00	6.6E-05
6	4.870E+02	261.0	6.487E+02	6.1E-01	6.9E-05
7	4.260E+02	255.0	5.830E+02	3.7E-01	7.5E-05
8	3.720E+02	248.0	5.225E+02	2.1E-01	7.9E-05
9	3.240E+02	242.0	4.669E+02	1.2E-01	8.6E-05
10	2.810E+02	235.0	4.159E+02	6.4E-02	9.0E-05
11	2.430E+02	229.0	3.693E+02	2.2E-02	1.1E-04
12	2.090E+02	222.0	3.269E+02	6.0E-03	1.2E-04
13	1.790E+02	216.0	2.882E+02	1.8E-03	1.5E-04
14	1.530E+02	216.0	2.464E+02	1.0E-03	1.8E-04
15	1.300E+02	216.0	2.104E+02	7.6E-04	1.9E-04
16	1.110E+02	216.0	1.797E+02	6.4E-04	2.1E-04
17	9.500E+01	216.0	1.535E+02	5.6E-04	2.4E-04
18	8.120E+01	216.0	1.305E+02	5.0E-04	2.8E-04
19	6.950E+01	217.0	1.110E+02	4.9E-04	3.2E-04
20	5.950E+01	218.0	9.453E+01	4.5E-04	3.4E-04
21	5.100E+01	219.0	8.056E+01	5.1E-04	3.6E-04
22	4.370E+01	220.0	6.872E+01	5.1E-04	3.6E-04
23	3.760E+01	222.0	5.867E+01	5.4E-04	3.4E-04
24	3.220E+01	223.0	5.014E+01	6.0E-04	3.2E-04
25	2.770E+01	224.0	4.288E+01	6.7E-04	3.0E-04
30	1.320E+01	234.0	1.322E+01	3.6E-04	2.0E-04
35	6.520E+00	245.0	6.519E+00	1.1E-04	9.2E-05
40	3.330E+00	258.0	3.330E+00	4.3E-05	4.1E-05
45	1.760E+00	270.0	1.757E+00	1.9E-05	1.3E-05
50	9.510E-01	276.0	9.512E-01	6.3E-06	4.3E-06
70	6.710E-02	218.0	6.706E-02	1.4E-07	8.6E-08
100	3.000E-04	210.0	5.000E-04	1.0E-09	4.3E-11

Table 9.2-5. United States Standard Model Atmosphere: Midlatitude Winter

MIDLATITUDE WINTER					
Ht. (km)	Pressure (mb)	Temp. (°K)	Density (g/m^3)	Water Vapor (g/m^3)	Ozone (g/m^3)
0	1.018E+03	272.2	1.301E+03	3.5E+00	6.0E-05
1	8.973E+02	268.7	1.162E+03	2.5E+00	5.4E-05
2	7.897E+02	265.2	1.037E+03	1.8E+00	4.9E-05
3	6.938E+02	261.7	9.230E+02	1.2E+00	4.9E-05
4	6.081E+02	255.7	8.282E+02	6.6E-01	4.9E-05
5	5.313E+02	249.7	7.411E+02	3.8E-01	5.8E-05
6	4.627E+02	243.7	6.614E+02	2.1E-01	6.4E-05
7	4.016E+02	237.7	5.886E+02	8.5E-02	7.7E-05
8	3.473E+02	231.7	5.222E+02	3.5E-02	9.0E-05
9	2.992E+02	225.7	4.619E+02	1.6E-02	1.2E-04
10	2.568E+02	219.7	4.072E+02	7.5E-03	1.6E-04
11	2.199E+02	219.2	3.496E+02	6.9E-03	2.1E-04
12	1.882E+02	218.7	2.999E+02	6.0E-03	2.6E-04
13	1.610E+02	218.2	2.572E+02	1.8E-03	3.0E-04
14	1.378E+02	217.7	2.206E+02	1.0E-03	3.2E-04
15	1.178E+02	217.2	1.890E+02	7.6E-04	3.4E-04
16	1.007E+02	216.7	1.620E+02	6.4E-04	3.6E-04
17	8.610E+01	216.2	1.388E+02	5.6E-04	3.9E-04
18	7.350E+01	215.7	1.188E+02	5.0E-04	4.1E-04
19	6.280E+01	215.2	1.017E+02	4.9E-04	4.3E-04
20	5.370E+01	215.2	8.690E+01	4.5E-04	4.5E-04
21	4.580E+01	215.2	7.421E+01	5.1E-04	4.3E-04
22	3.910E+01	215.2	6.338E+01	5.1E-04	4.3E-04
23	3.340E+01	215.2	5.415E+01	5.4E-04	3.9E-04
24	2.860E+01	215.2	4.624E+01	6.0E-04	3.6E-04
25	2.430E+01	215.2	3.950E+01	6.7E-04	3.4E-04
30	1.110E+01	217.4	1.783E+01	3.6E-04	1.9E-04
35	5.180E+00	227.8	7.924E+00	1.1E-04	9.2E-05
40	2.530E+00	243.2	3.625E+00	4.3E-05	4.1E-05
45	1.290E+00	258.5	1.741E+00	1.9E-05	1.3E-05
50	6.820E-01	265.7	8.954E-01	6.3E-06	4.3E-06
70	4.670E-02	230.7	7.051E-02	1.4E-07	8.6E-08
100	3.000E-04	210.2	5.000E-04	1.0E-09	4.3E-11

Table 9.2-6. Abundance of Uniformly Mixed Gases in the Atmosphere[42]

Constituent	Molecular Wt.	ppm by Vol.	$(cm\text{-}atm)_{STP}$ in vertical path from sea level	$(cm\text{-}atm)_{STP/km}$ in horizontal path at sea level
Air	28.97	10^6	8×10^5	10^5
CO_2	44	330	264	33
N_2O	44	0.28	0.22	0.028
CO	28	0.075	0.06	0.0075
CH_4	16	1.6	1.28	0.16
O_2	32	2.095×10^5	1.68×10^5	2.095×10^4

Because of the low density of the high-altitude layers, multiple layers were homogenized to form single layers of greater depth. A spline fitting and integration procedure was used to evaluate the species column densities, and a weighting function was calculated for each sub-layer to give the homogenized temperature and pressure. For altitudes below 9.5 km, HIRACC runs were performed for each 1-km layer; above 9.5 km, the homogenized layers correspond to the following heights: 9.5 to 14.5 km, 14.5 to 24.5 km, 24.5 to 52.5 km, and 52.5 to 80 km. In addition to reducing the number of required computer runs, these regions roughly bound the troposphere, stratosphere, and mesosphere.

Note that atmospheric absorption calculations for both CO[12,45,46] and CO_2[47] laser lines have been performed previously. New calculations are necessary in light of revised absorption parameters and improved precision in the laser line wavelengths. Also, the atmospheric absorption of certain laser lines, especially the isotopic CO_2 laser lines, has not been calculated with sufficient spectral resolution to yield accurate transmittance values for propagation through the earth's entire atmosphere.

The meaningful calculation of atmospheric absorption requires an accuracy in the precision of each laser line wavelength to $<0.01\ cm^{-1}$. Considerable care has been exercised to obtain the best measurements of line wavelengths; for the CO laser, the data for Rao[48] were used, while for the low-abundance isotopic species of CO_2, the data of Freed et al.[9,10] were employed.

Attenuation due to aerosol absorption and scattering is calculated using the U.S. continental aerosol models developed by McClatchey et al.[42,49] The two aerosol models used here are for clear and hazy meteorological conditions, corresponding to 23-km and 5-km-horizontal visibility at sea level. The aerosol size distribution function for both models is the same at all altitudes and is similar to Deirmendjian's model "C", except that the large particle cut-off is extended from 5 μm to 10 μm. The real and imaginary parts of the aerosol refractive index and the total aerosol particle concentration were adjusted to fit experimental data for clear air and selected wavelengths at each altitude. The clear and hazy models are identical above 5 km in altitude.

Below 5 km, the aerosol particle concentration in the hazy model increases exponentially to a value corresponding to a ground visibility of 5 km at $\gamma = 0.55$ μm.

For CO laser lines, aerosol absorption and scattering coefficients as functions of altitude were obtained from Ref. (12). Analogous data for the P- and R-branch transitions in the $00^01 \rightarrow 0.2^00$ band of $^{12}C^{18}O_2$ have not been compiled. As shown by Figure 9.2-14, it would be inaccurate to assume that the aerosol extinction coefficients for these lines are similar to those for the "standard" CO_2 laser lines near 10.6 m since considerable structure exists in this spectral region. For these reasons, aerosol effects have not been included in the $^{12}C^{18}O_2$ transmission efficiency calculations; however, the decrease in transmission efficiency of the $^{12}C^{18}O_2$ laser lines due to aerosol attenuation is approximately equal to that calculated for the CO laser lines because of similar extinction coefficients (see Figure 9.2-14).

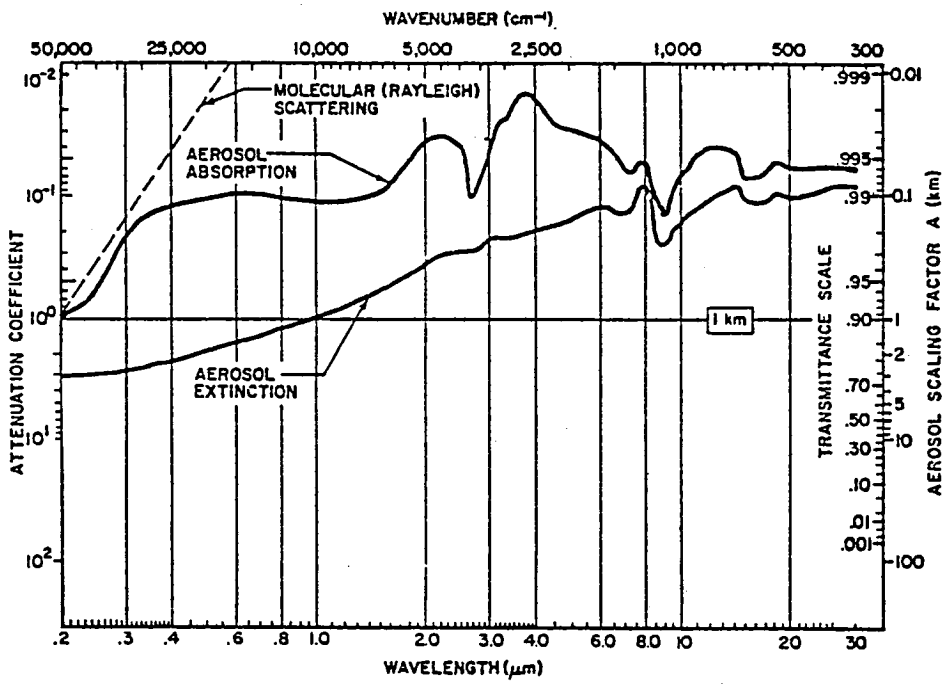

Figure 9.2-14. Clear Air Aerosol Absorption and Extinction Coefficients as Functions of Wavelength for Sea Level Transmission[49]

Results of the HIRACC runs are given in Tables 9.2-7, 9.2-8, and 9.2-9. Transmission efficiencies were calculated for P- and R-branch midrotational transitions of isotopic CO_2 (those lines capable of the largest discharge efficiency) and for the CO spectra shown in Figures 9.2-9 and 9.2-10. Transmission efficiencies for CO-laser lines of importance are also isted individually in Tables 9.2-8 and 9.2-9. Most of the CO radiation absorption occurs at the lower altitudes and it is highly inadvisable to place a CO-laser receptor site at an elevation less than 0.5 km. A significant improvement in CO-laser

Table 9.2-7. Atmospheric Transmission Efficiencies for $^{12}C^{18}O$ Laser Transitions Using the Midlatitude Summer Model and θ = 50°. Aerosol Attenuation is Not Included.

Transition	λ, μm	ν, cm^{-1}	Transmission Efficiency: Typical Location (0.5 km elevation)	Transmission Efficiency: Mountain-top Operation (3.5 km elevation)
$00^01 \rightarrow 02^00$				
P(22)	9.369	1067.3589	0.8081	0.8604
P(20)	9.355	1068.9425	0.6838	0.8060
P(18)	9.341	1070.5071	0.6217	0.7665
R(18)	9.124	1095.9645	0.9911	0.9937
R(20)	9.114	1097.1507	0.9885	0.9926
R(22)	9.105	1098.3174	0.9767	0.9908

Table 9.2-8. Atmospheric Transmission Efficiencies for CO Laser Transitions Using the Midlatitude Summer and Continental Aerosol Models for a Zenith Angle θ = 50°.

Transition	ν, cm^{-1}	Transmission Efficiency: Typical Location (0.5km elevation) Molecular Absorption Only	Typical Location (0.5km elevation) Clear (23km Visibility)	Typical Location (0.5km elevation) Hazy (5km Visibility)	Mountain-top Operation (3.5km elevation) Molecular Absorption Only	Mountain-top Operation (3.5km elevation) Clear (23km Visibility)	Mountain-top Operation (3.5km elevation) Hazy (5km Visibility)
4→3 P(10)	2025.0794	0.5975	0.5673	0.5046	0.9479	0.9350	0.9315
P(11)	2020.9975	0.5692	0.5406	0.4811	0.9535	0.9405	0.9370
5→4 P(9)	2003.1656	0.8479	0.8056	0.7176	0.9832	0.9700	0.9664
P(11)	1995.1054	0.5627	0.5347	0.4765	0.9712	0.9582	0.9546
6→5 P(10)	1973.2960	0.9571	0.9101	0.8121	0.9979	0.9846	0.9811
7→6 P(9)	1951.4557	0.4632	0.4406	0.3936	0.9083	0.8964	0.8931
8→7 P(8)	1929.5860	0.8146	0.7754	0.6936	0.9720	0.9593	0.9559
9→8 P(9)	1900.0429	0.9684	0.9230	0.8267	0.9921	0.9794	0.9760
10→9 P(9)	1874.4518	0.9178	0.8749	0.7852	0.9906	0.9781	0.9747
Spectrum #1 (Fig. 10)	2025.0794-1882.0272	0.8231	0.7828	0.6988	0.9745	0.9616	0.9581
Spectrum #2 (Fig. 9)	2025.0794-1852.7092	0.7405	0.7044	0.6291	0.9633	0.9506	0.9472

Table 9.2-3. Atmospheric Transmission Efficiencies for CO Laser Transitions Using the Midlatitude Winter and Continental Aerosol Models for a Zenith Angle $\theta = 50°$

Transition	ν, cm^{-1}	Transmission Efficiency					
		Typical Location (0.5km elevation)			Mountain-top Operation (3.5km elevation)		
		Molecular Absorption Only	Clear (23km Visibility)	Hazy (5km Visibility)	Molecular Absorption Only	Clear (23km Visibility)	Hazy (5km Visibility)
4→3 P(10)	2025.0794	0.8804	0.8360	0.7436	0.9832	0.9698	0.9662
P(11)	2020.9975	0.8649	0.8214	0.7309	0.9867	0.9733	0.9697
5→4 P(9)	2003.1656	0.9702	0.9218	0.8211	0.9958	0.9824	0.9788
P(11)	1995.1054	0.8644	0.8214	0.7320	0.9917	0.9783	0.9747
6→5 P(10)	1973.2960	0.9870	0.9385	0.8375	0.9989	0.9856	0.9820
7→6 P(9)	1951.4557	0.8059	0.7667	0.6849	0.9702	0.9574	0.9540
8→7 P(8)	1929.5860	0.9287	0.8839	0.7907	0.9625	0.9500	0.9466
9→8 P(9)	1900.0429	0.9850	0.9388	0.8409	0.9944	0.9817	0.9782
10→9 P(9)	1874.4518	0.9758	0.9302	0.8348	0.9964	0.9838	0.9804
Spectrum #1 (Fig. 10)	2025.0794-1882.0272	0.9417	0.8956	0.7995	0.9884	0.9754	0.9718
Spectrum #2 (Fig. 9)	2025.0794-1852.7092	0.9063	0.8621	0.7698	0.9836	0.9706	0.9671

transmission efficiency is realized by high-altitude receptor operation, while for the $00^0 1 \rightarrow 02^0 0$ R-branch lines of $^{12}C^{18}O_2$, little improvement is to be gained.

For the CO laser lines, the transmission efficiency improves during the winter because of a decrease in humidity. At an elevation of 0.5 km, the yearly average transmission efficiency for CO-laser spectrum #1 (best case) is 84%. Mountain-top reception at an elevation of 3.5 km increases this value to 97%. For spectrum #2, the corresponding values are 78% and 96%. These results are for receptor sites which are not subject to persistent overcast conditions. Hazy or overcast conditions have less of a degrading effect on transmission efficiency as the receptor-site elevation is increased.

The yearly average transmission efficiency for the 9.114-μm $^{12}C^{18}O_2$-laser line to an elevation of 0.5 km is estimated to be 93% for clear air conditions (aerosol attenuation included). Mountain-top reception at an elevation of 3.5 km increases this value to about 98%. Transmission efficiencies for the CO_2 laser lines were only computed using the midlatitude summer model since these conditions represent worst-case performance (aerosols neglected).

9.2.4 RECEPTOR CONCEPTS

Table 9.2-10 lists the various candidate receptor concepts for the conversion of laser light into electricity. Only those concepts applicable to infrared light conversion are considered. Many of the schemes are in the exploratory or research development phase, and the quoted efficiencies may be only theoretical predictions. The basic characteristics and limitations will be delineated for each concept.

Mercury-cadmium-telluride and lead-tin-telluride photovoltaic cells designed specifically for power conversion have been proposed.[50] The conversion efficiency for CO_2 laser radiation conversion into electricity has been estimated as high as 50 percent. Large arrays of these devices would be expensive and their lifetime and weatherability are uncertain. Cooling requirements may also present undue complications.

The tuned optical diode[51-53] is the infrared-light analog of the microwave rectenna diode. Proposed devices are extremely fragile, they must be configured in a close packed array to affect maximum conversion, and no satisfactory method of heat removal from the contact junction has been proposed. Hence, their power handling capability is limited and experimental efficiencies of these devices have not been determined.

Four heat engine concepts are potentially suitable for laser power conversion. The boiler heat engine relies upon absorption of the incident radiation and conduction of the resulting heat to the working fluid. The laser[51,54-57] and photon[51,48-60] engines both utilize absorption of concentrated incident radiation in the working gas. The lack of appropriate window materials presents a difficult problem.

Another class of heat engines developed some years ago has proved capable of very-high-temperature operation by using a device called the energy

Table 9.2-10. Candidate Receptor Concepts for Conversion of IR Radiation into Electricity

Conversion System	Type	Wavelength, μm	Efficiency	Development Stage	Limitations
Photovoltaic cells					
HgCdTe	Semiconductor	4-18	0.50	Research	Expensive; degradation by the terrestrial environment
PbSnTe	Semiconductor	4-13	0.50	Research	
Tuned Optical Diode	Semiconductor	?	?	Research	Fragile; limited power handling capability
Heat Engines					
Boiler	Mechanical	uv through ir	0.40	Advanced	———
Laser	Mechanical		0.50	Exploratory	Window Strength
Photon	Mechanical		0.60-0.75	Research	Lack of high-temperature materials; window strength
Energy Exchanger/ Binary Cycle	Mechanical		0.73	Research	Scaling Uncertain
TELEC	Thermoelectronic	Near to mid ir	0.42	Research	Scaling Uncertain

exchanger,[61] which is related to principles initially developed by Claude Seippel[62] of Brown Bovari. Energy is directly exchanged between high-temperature and low-temperature fluids so that the wall temperature of the machine sees only an average. Operation above normal material temperatures is thus achievable. By extension of the basic principle, this energy exchange can be made highly efficient if an acoustic velocity match between the hot and cold fluids is maintained. This is accomplished using high and low molecular-weight fluids as the hot and cold working fluids, respectively, permitting temperature ratios as high as 10. Because of the high temperature in the driver side of the energy exchanger, the circulating power fraction becomes very small since the work available per unit of mass flow is correspondingly large. Hertzberg[60] has investigated the use of an energy exchanger in conjunction with his photon engine concepts.

The energy exchanger/binary cycle concept developed by Lockheed[63] uses a high-temperature Brayton cycle coupled to a bottoming Rankine cycle. The efficiency has been calculated to be 73%; however, the necessary high temperatures in the primary loop require the use of a liquid alkali as the working fluid, which may present difficulties in materials selection.

The TELEC (Thermo-Electronic Laser Energy Converter) is a plasma device in which the laser radiation is absorbed via inverse bremsstrahlung. The resulting energetic electrons diffuse out of the plasma and, because the anode and cathode electrodes have different areas and temperatures, more electrons are collected by the cathode (larger area) producing a net transport of current in an external circuit. Theoretical predictions of the efficiency of the TELEC cell for conversion of 10.6-μm laser light into electricity yielded values in excess of 42%,[64,65] although experimental results, both at Lewis Research Center[66] and Ames Research Center,[67] have fallen far short of this prediction. Device scaling may improve this situation. Window limitations pose a severe problem for this device since the incident laser power density must sustain the plasma (power density $\geq 10^4 W/cm^2$) and the cell vapor (e.g. Cs) may condense on the surfaces of the cooler optical windows.

Two receptor concepts, as selected from Table 9.2-10, appear sufficiently advanced and workable for the conversion of 5-μm or 9-μm laser radiation into electric power. These are the boiler heat engine and the energy exchanger/binary cycle heat engine. The receptor design will depend upon the available power density at the focal spot and constraints imposed by high-temperature materials.

Since both concepts utilize thermal absorption, concentrated laser radiation must be employed to obtain the high temperatures needed for efficient operation. If concentrating optics are to be avoided, then the ground based laser spot should be reduced to the limitations imposed by diffraction, turbulence, thermal blooming, pointing accuracy and jitter. Concentrating optics are undesirable from two standpoints. First, environmental degradation of the reflecting surface will cause power losses and a concomitant decrease in system efficiency. Second, large-area precision optics will be expensive, especially if a high mirror figure is required to obtain very large power densities in the conversion device.

For any heat engine receptor concept, the absorbing surface should possess a high absorptance but a small hemispherical emittance at the characteristics operating temperature. In this manner, re-radiation losses due to greybody radiation to the ambient environment can be minimized. Cuomo et al.[68] have demonstrated a device consisting of a dense forest of aligned metal whiskers whose diameter is of the order of the incoming radiation and whose spacing is several wavelengths. Using tungsten, they obtained an absorptance greater than 98% with normal incidence light over a large wavelength range (0.5 - 40 μm) and a hemispherical emissivity of less than 0.26 at 550°C. The possible degradation of these structures under the combined effects of prolonged, intense laser radiation and terrestrial weather must be evaluated before their usefulness as an absorbing surface can be determined.

Another concept for maximizing the absorption of incoming radiation while minimizing thermal losses is shown in Figure 9.2-15. Re-radiated energy can only escape through the entrance aperture, which purposely subtends a small solid angle. Convective losses due to internal air heating can be minimized by purging with dry air. Most importantly, this concept does not employ high quality optical surfaces and, as such, is not subject to environmental degradation. Hence, the absorbing sphere concept is preferred provided that the focal spot size at the receptor is small enough to obtain the large radiation power density necessary for high-temperature (i.e., high thermal-efficiency) operation. Using a receptor aperture of approximately 30 m in diameter, the average incident power density on the internal (absorbing) surface is estimated to be roughly 35 kW/m^2. High-temperature operation should be possible if the material chosen for the internal wall possesses a large infrared absorptance and is compatible with the working fluid.

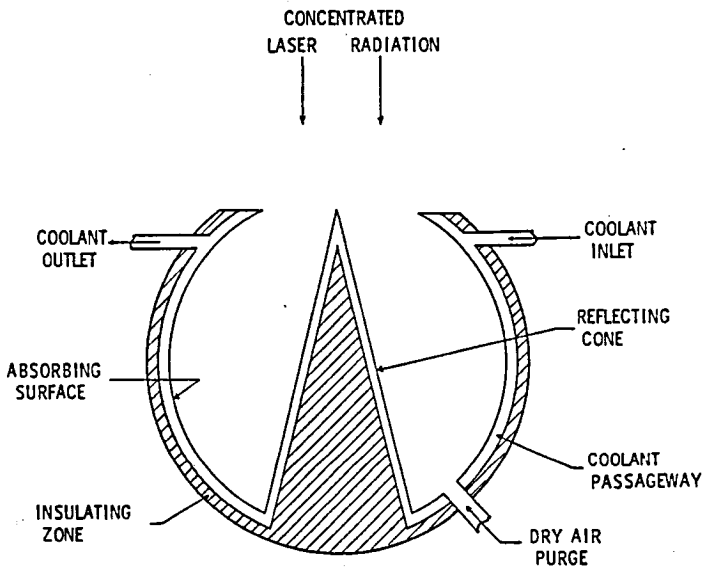

Figure 9.2-15. Absorbing Sphere Concept

9.2.5 SYSTEM CHAIN EFFICIENCIES

The efficiency chain of a single transmitting laser system is shown in Figure 9.2-16. Each laser transmitter chain will contain two sub-chains. The electric discharge will require a total power given by P_{PS}, while the gas compressor (subsystem) power requirement is designated by $P_{c_{elec}}$. Initial system designs utilize a total of 20 or 24 laser transmitters, each radiating power by switched in or out of the system as circumstances warrant. The receptor efficiency includes the thermodynamic efficiency of the electrical generating plant and losses of incoming laser radiation at the absorbing surface. A wire loss, τ, of 2% per chain is assumed. The efficiencies of each component of the laser-SPS system are subject to modification as refined data or calculations become available.

It is assumed that 9.4 GW is available at the rings, which is divided equally between either 20 or 24 independent laser systems. The electrical, mechanical, and thermal power distribution for a single transmitter chain is given in Table 9.2-11. Efficiencies used in the calculations are as follows:

$$\eta_d = 0.50$$

$$\eta_L = 0.2337$$

$$\eta_M = 0.8950$$

$$\eta_{PS} = 0.9323.$$

These values were derived using a two-heat-exchanger thermodynamic cycle employing a subsonic diffuser. The plenum stagnation temperature, T_{01}, and Mach number, M_1, were chosen to be consistent with the requirement $T_1 < 100°K$. In this thermodynamic cycle, $T_{01} = 360°K$ and $M_1 = 3.00$. The calculated radiator area is consistent with the space allowed on the current Rockwell microwave-based SPS design. A single-side radiator area of 80,000 m^2 is available per laser system if the microwave transmitters are replaced by laser transmitters.

9.2.6 CONCEPT DEFINITION SUMMARY

The atmospheric transmission efficiency for an isotopic CO_2 EDL has been shown to be larger than for a line-selected CO EDL. Because the total laser system efficiency which is potentially attainable with a CO EDL is substantially larger, then the efficiency of the overall laser-SPS system is largest for the CO EDL. If the laser-SPS system efficiency is defined as the ratio of power available at the user grid to power produced by the solar photovoltaic array (taken from the rings), then values of 14% and 10% are estimated for the CO and CO_2 EDL's, respectively, for propagation to 0.5-km-elevation receptor sites. For mountain-top receptor sites, the laser-SPS system efficiency improves to about 16% for the CO EDL, whereas only a very small improvement is realized for the CO_2 EDL. These values consider seasonal variation in the transmission efficiency. Furthermore, all laser-SPS systems studies, including this one, project smaller total system specific masses (laser system mass per unit radiant output power) for the CO EDL compared with the CO_2 EDL.

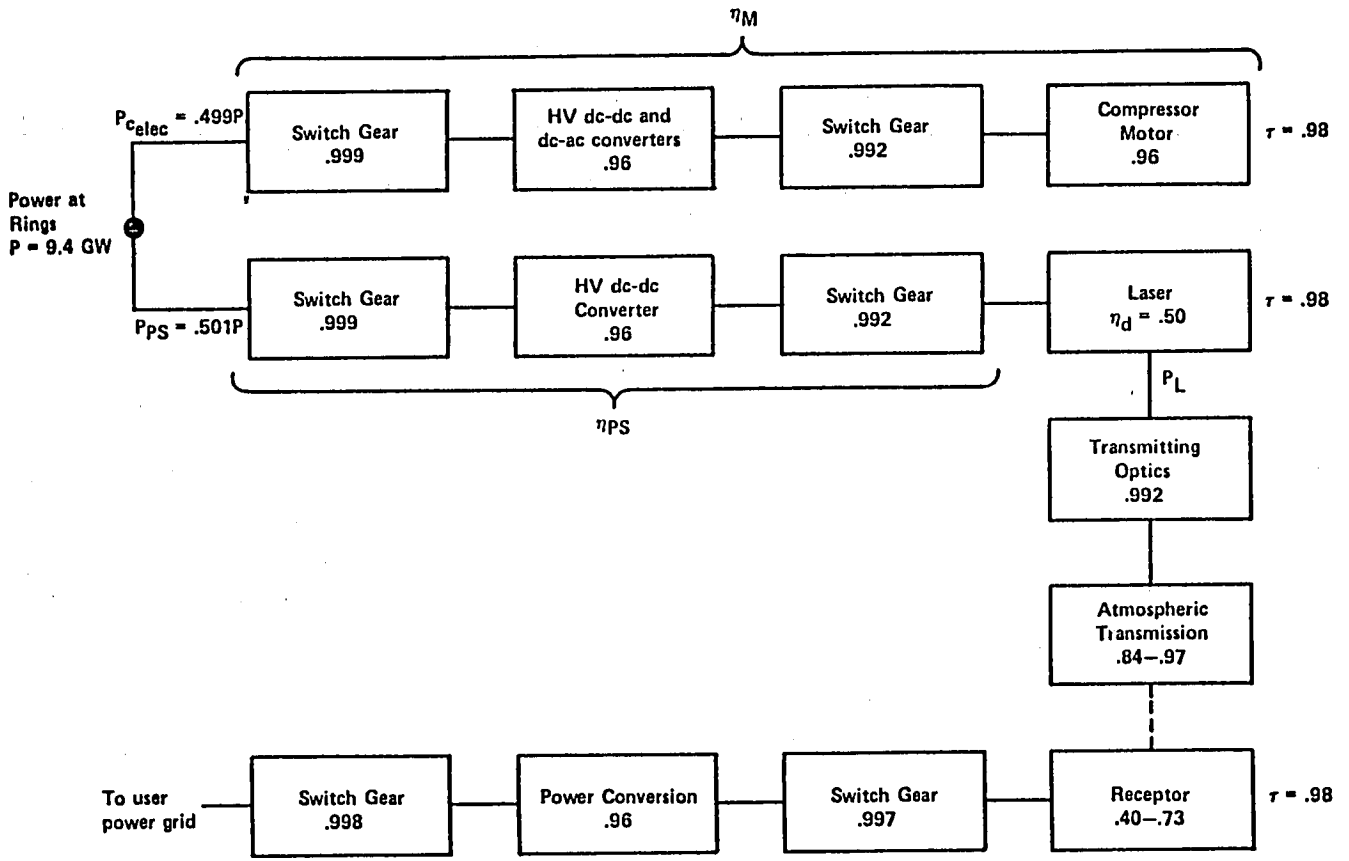

Figure 9.2-16. Laser-SPS System Chain Efficiencies

Table 9.2-11. Electrical, Mechanical, and Thermal Power Distribution for a Laser SPS Employing a Supersonic CO EDL

Parameter	Number of Independent Laser Systems	
	20	24
Total Power Input per System	470.0 MW_e	392.0 MW_e
Laser Output Power, P_L	109.8 MW	91.61 MW
Compressor Mechanical Power, $P_{c_{mech}}$	209.7 MW_m	174.9 MW_m
Compressor Electrical Power, $P_{c_{elec}}$	234.3 MW_e	195.4 MW_e
Discharge Electrical Power, P_E	219.7 MW_e	183.2 MW_e
Discharge Power Supply Power, P_{PS}	235.7 MW_e	196.5 MW_e
Waste Heat Power, Q_w	288.0 MW_{th}	240.3 MW_{th}
Space Radiator Area, A_r	78,830 m^2	65,750 m^2

For these two reasons, we have chosen the CO EDL laser as the baseline system for the environmental impact studies. Various receptor conversion schemes were examined and two heat engine concepts were identified as prime candidates for further investigation. Therefore, the concept definition can be summarized as follows:

- Supersonic, closed-cycle flow, CO electric-discharge laser with line selection,
- Pulser-sustainer type of laser discharge,
- Total of 20 or 24 independently controllable laser systems and optical transmitters, each with an output power of $\simeq$ 100 MW,
- Adaptive, on-axis Cassegrain optical transmitter,
- Heat engine receptor (either advanced Brayton cycle or Lockheed energy exchanger with binary cycle),
- High-elevation receptor site preferred.
- Operation with closely packed receptor-device clusters located at a common site feasible, with the exact number of receptors per site depending upon the desired power-plant electrical rating.

9.3 ANCILLARY ISSUES

9.3.1 LASER BEAM SPREADING

Analytic calculations of laser beam propagation show that beam spreading due to atmospheric turbulence is negligible compared with spreading due to diffraction and pointing inaccuracies at the laser transmitter. Although the angular divergence attributed to turbulence is much larger than the divergence due to diffraction and pointing inaccuracy, the turbulence induced spreading only occurs during the final 30 km of beam path, whereas the diffraction and pointing spreading occurs along the entire path (42,700 km). If laser line selection is employed, then molecular and aerosol absorption is weak and thermal blooming is not a problem. Note that for earth-to-space laser power transmission, however, small beam perturbations attributable to turbulence and nonlinear effects near the transmitter produce significant beam wandering at the target because of the long optical "lever arm" involved. Due to the proximity of these effects to the receptor, beam spreading is much less severe for space-to-earth propagation.

In the sections which follow, beam spreading and required receptor size are calculated for two analytically tractable laser beam intensity distributions which bound the range of expected profiles. These intensity distributions are the uniform or constant-intensity profile and the Gaussian profile. Diffraction effects are considered initially, and the effects of pointing inaccuracies and turbulence are then calculated. Finally, thermal blooming is shown to be insignificant for worst-case propagation conditions. It is assumed that the receptor axis coincides with the laser beam axis such that the minimum focal spot size is intercepted. Hence, the receptor views the laser source at a zenith angle (θ) of 50°.

Uniformly Illuminated Transmitter Aperture

If the primary mirror of the Cassegrain optical transmitter, an annular aperture, is uniformly illuminated by the laser, then the normalized intensity at the receptor due to diffraction only is[69]

$$I(x) = \frac{1}{(1-\varepsilon^2)^2}\left[\frac{2J_1(x)}{x} - \varepsilon^2\,\frac{2J_1(\varepsilon x)}{\varepsilon x}\right]^2, \qquad (25)$$

where

$$\times\ x = (2\pi/\lambda)\ (D_p/2)\ (r/R), \qquad (26)$$

and

$J_1(x)$ = first-order Bessel function of the first kind

ε = transmitter obscuration ratio (D_s/D_p)

D_p = primary mirror diameter

r = radius at the receptor

R = range to the receptor.

For $\varepsilon < 0.1$, Eq. (25) simplifies to

$$I(x) \simeq [2J_1(x)/x]^2 \ . \tag{27}$$

The fractional power intercepted within a radius r_0 is given by

$$F(r_0) = 2\int_0^{x(r_0)} \frac{J_1^2(x)}{x}\, dx \ , \tag{28}$$

which can be analytically solved to yield

$$F(r_0) = 1 - J_0^2[x(r_0)] - J_1^2[x(r_0)]. \tag{29}$$

Gaussian Intensity Distribution

The time-average intensity distribution at the receptor for a Gaussian-profile transmitted beam is[70]

$$\langle I(r)\rangle = \frac{P_T \eta_T}{\pi a^2} \exp(-r^2/a^2), \tag{30}$$

where P_T is the transmitted optical power, η_T is the atmospheric transmission efficiency and a, the beam radius at the 1/e-intensity points, is

$$a^2 = (\theta_d^2 + \theta_p^2)R^2 + \theta_t^2 \bar{R}^2 \ . \tag{31}$$

θ_d, θ_p, and θ_t are the divergences due to diffraction, pointing jitter, and turbulence, respectively, and R is the distance from the receptor for which turbulence contributes to beam spread. The half-angle diffraction divergence is

$$\theta_d^2 = \beta^2 \frac{\lambda^2}{(2\pi)^2 a_0^2} + \frac{a_0^2}{R^2}\left(1 - \frac{R}{f}\right)^2 \ , \tag{32}$$

where the parameter β is used to characterize the beam quality of the optical transmitter in terms of its far-field or focused beam radius being a specified number (β) times the diffraction limited radius. The quantities a_0 and f are the 1/e beam radius at the transmitter and the optical system focal length, respectively. Setting f equal to infinity corresponds to a collimated beam, while setting f equal to R corresponds to best focus at the receptor. The latter condition applies here, so Eq. (32) reduces to

$$\theta_d = \beta \frac{\lambda}{2\pi a_0} \ . \tag{33}$$

The divergence due to turbulence is

$$\theta_t = \frac{\lambda}{\pi \zeta} \ , \tag{34}$$

where ζ, the turbulence coherence length, is given by Fried and Mevers[71] for propagation down through the atmosphere as

$$\zeta = 0.114(\lambda\cos\theta/5.5\times10^{-7})^{3/5} \quad . \tag{35}$$

The coherence length is related to the integral of the refractive index structure constant, C_n^2, over the propagation path. The distance from the receptor for which turbulence effects cause beam spreading can be approximated by

$$\tilde{R} = h_t \sec\theta \quad , \tag{36}$$

where h_t is the altitude where C_n^2 experiences an abrupt fall-off in magnitude. From Figure 9.3-1, $h_t \simeq 20$ km. Finally, the 1/e beam radius at the transmitter is related to the primary mirror diameter, D_p, by the relation

$$D_p = 2\sqrt{2}\, a_0 \quad , \tag{37}$$

which places the 1/e intensity points at the edge of the mirror.

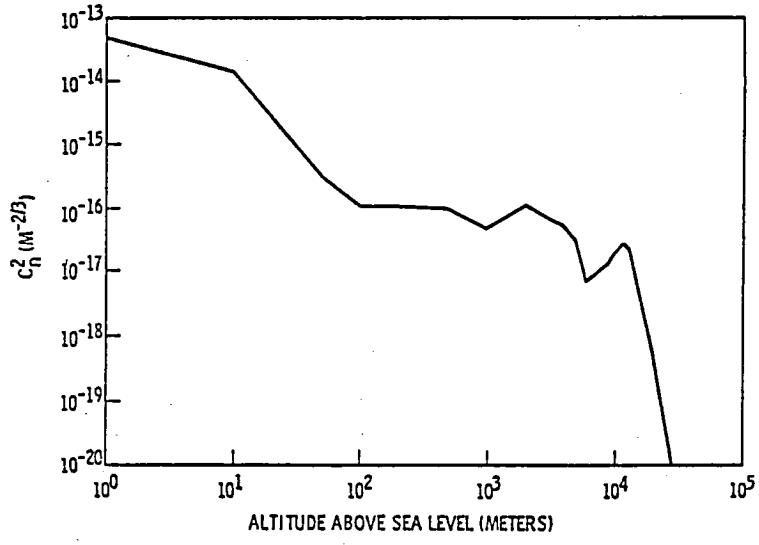

Figure 9.3-1. C_n^2 as a Function of Altitude Above Sea Level, h.[11]

In our case, we have $D_p = 25$ m, $\beta = 1.0$ [Ref. (29)], $\theta = 50°$, $\varepsilon = 0.08$, $\lambda = 5\ 10^{-6}$ m and $R = 4.27\times10^7$ m; hence,

$$a_0 = 8.8388 \text{ m}$$
$$\zeta = 0.3288 \text{ m}$$
$$\tilde{R} = 3.111\times10^4 \text{ m}$$

and the divergences are

$\theta_d = 9.00\times10^{-8}$ rad

$\theta_p = 2.00\times10^{-7}$ rad [Ref.(29)]

$\theta_t = 4.84\times10^{-6}$ rad.

The 1/e beam radius at the receptor is then

a (diffraction only) = 3.844 m

a (diffraction + pointing) = 12.384 m

a (diffraction + pointing + turbulence) = 12.385 m.

Clearly, turbulence-induced spreading is negligible compared with beam spreading caused by diffraction and pointing inaccuracies. Furthermore, if a smaller receptor spot size is required, then better pointing stability is necessary rather than a larger primary mirror since $\theta_p > \theta_d$.

At the receptor, the fractional power intercepted within a radius r_0 is

$$F(r_0) = \frac{1}{P_T \eta_T} \int_0^{2\pi} d\phi \int_0^{r_0} \langle I(r) \rangle dr \quad , \tag{38}$$

which can be simplified to

$$F(r_0) = \frac{2}{a^2} \int_0^{r_0} \exp(-r^2/a^2) r \, dr \quad . \tag{39}$$

Equation (39) is conveniently integrated using a Gaussian quadrature routine.[72]

The percentage of available laser power intercepted by the receptor as a function of the receptor radius is shown in Figure 9.3-2 for several conditions. Considering diffraction spreading only, the two dashed curves show the functional behavior for the uniform or constant-intensity distribution and the Gaussian intensity distribution. These distributions bound the range of expected laser beam profiles, although the Gaussian profile more closely approximates the intensity distribution observed for practical laser devices. The solid curve shows the beam spread of a Gaussian beam including the effects of diffraction, pointing error, and turbulence. A 50-m-diameter receptor will intercept approximately 99 percent of the available power at the ground site. Improvement in the transmitter pointing accuracy could reduce the required receptor diameter to perhaps 30 m.

Thermal Blooming

Thermal blooming is a nonlinear propagation mechanism common to high-power infrared lasers in which self-induced spreading, distortion, and bending of the laser beam occur as a result of molecular and aerosol absorption within the beam path. Absorption leads to heating of the air causing density and, hence,

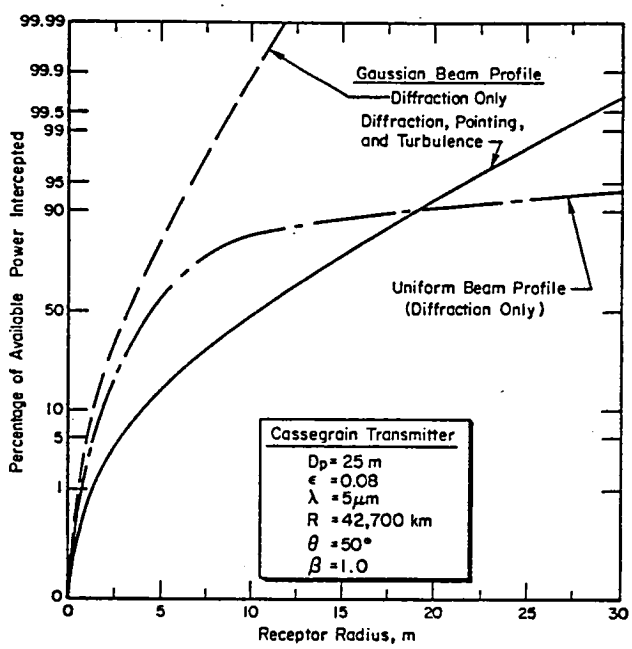

Figure 9.3-2. Percentage of Available Power at the Ground Based Site Which is Intercepted Within a Specified Receptor Radius

refractive index gradients which act as a distributed lens. In general, the explicit determination of the beam phase and intensity distributions at a target illuminated by a remote laser transmitter and separated by an inhomogeneous absorbing medium required numerical solution.[73,74] For the purposes of the present study, however, we wish only to determine the potential impact of thermal blooming on the present space-to-earth power transmission scenario.

There exists a critical distance, z_c, beyond which beam distortion caused by blooming is substantial. For the case of no kinetic cooling of the absorbing medium (a good approximation for CO-laser light absorption), the expression for the critical propagation distance, in meters, is[75]

$$z_c^2 = \frac{\rho(h) C_p v(h) \ (2\pi)^{1/2} (D_p/2)^3}{(-\frac{1}{n}\frac{dn}{dt}) \ 0.96 \ \alpha_t(h) P_T} \ , \tag{40}$$

where ρ is the atmospheric density (g/m^3), C_p is the specific heat of air at constant pressure (0.242 cal/g °K), v is the wind velocity (m/sec), $n^{-1}(dn/dT)$ is the refractive index gradient, and α_t is the total molecular and aerosol absorption coefficient (m^{-1}). Notice that ρ, v, and α_t are functions of altitude, h; hence, z_c is implicitly a function of altitude. The refractive index gradient is also an implicit function of altitude because of the dependence of temperature on altitude. Now in Appendix A of Ref. (11), it was shown that

α

$$\frac{\alpha_t(h)}{C_p\rho(h)} - \frac{1}{n}\frac{dn}{dT} = \frac{n-1}{\rho_0 C_p}\frac{\alpha_t(h)}{T(h)} , \tag{41}$$

where ρ_0 is the sea level density of air in the U.S. standard atmosphere ($1.225\ 10^3 g/m^3$), and

$$(n-1)\times 10^6 = 272.729 + (1.42823/\lambda^2) + (0.02041/\lambda^4).$$

For $\lambda = 5\ \mu m$, $n-1 = 2.73\ 10^{-4}$. Inserting these numerical values and Eq. (41) into Eq. (40), we obtain

$$z_c^2 = \frac{3.544\times 10^5\ v(h)D_p^3 T(h)}{\alpha_t(h)P_T} . \tag{42}$$

The critical propagation distance increases with the square root of wind velocity; the convective dissipation of heated air zones within the beam path is promoted by high wind velocities. Three standard continental wind velocities. Three standard continental wind velocity distributions are shown in Figure 9.3-3.

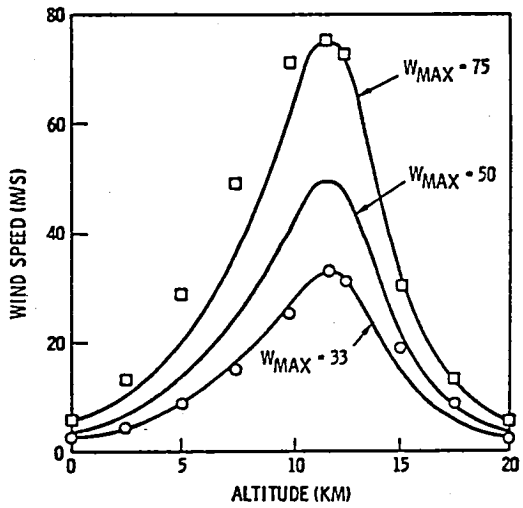

Figure 9.3-3. Continental Wind Velocity Distributions as Functions of Altitude[11]

To insure the absence of thermal blooming, we require $z_c > h$ at all points along the beam path. The largest absorption occurs for the Midlatitude Summer model under hazy conditions, and relatively stagnant air with low surface wind velocity corresponds to the lowest velocity-distribution curve in Figure 9.3-3. Figure 9.3-4 thus shows the dependence of the critical propagation distance on altitude for CO-laser spectrum #1 under worst-case meteorological conditions. For a receptor located at an elevation of 0.5 km, thermal blooming begins about 1 km above the receptor, but little additional beam spreading occurs

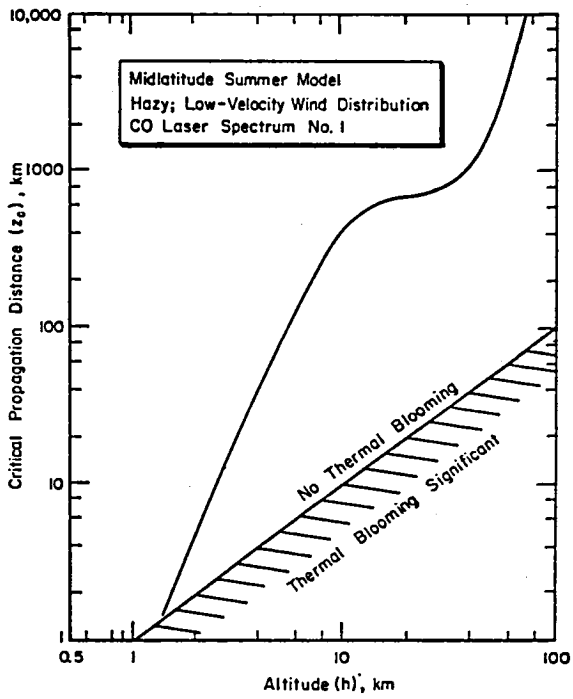

Figure 9.3-4. Critical Propagation Distance for Thermal Blooming as a Function of Altitude

due to the proximity of the absorbing medium to the receptor. Under more typical meteorological conditions or for receptor sites at higher elevations, thermal blooming can be completely ignored. As a corollary to this conclusion, it is evident that line selection at the laser transmitter becomes less critical for high-elevation receptor sites since most of the molecular and aerosol absorption occurs at altitudes less than 3 km.

Any type of coherent adaptive technique (COAT) utilized in conjunction with the Cassegrain laser transmitter will only be able to correct for gross beam wander due to steady-state thermal lensing. Microscopic beam fluctuations (boiling) due to either turbulence or thermal blooming cannot be corrected since they occur on a time scale shorter than the adaptive system response time, which is limited by the round-trip propagation time (0.285 sec). Since we are interested in power rather than information or image transmission, this should pose no problem.

9.3.2 SAFETY AND SECURITY

The transmission air zone associated with all receptor sites must be restricted to all private, commercial, and military aircraft of all types. High-speed jet aircraft probably will not suffer any damage in traversing the beam, with the possible exception of the canopy. The dwell time within the beam and the high infrared reflectivity of aluminum skins combine to yield absorbed fluence levels (J/cm^2) far below those required for damage. Slower, less reflective aircraft could succumb to damage. The principal reason for

restricting all air traffic is the occular hazard presented by an uncontrolled and randomly pointing reflection surface traversing a 100-MW laser beam. Coherent optical adaptive techniques (COAT) have been suggested as a viable solution to sense intruding aircraft and affect beam defocus. The system response time is limited by the round-trip light propagation time, 0.285 sec in this case. In this time, most high-speed jet aircraft would have completely passed through the beam, and to defocus would be useless. Intruding aircraft should be detected by radar as they enter the restricted zone to allow sufficient time for defocus.

Sensing the unintentional loss of pointing accuracy would also be limited by the system response time. The ground distance slewed by the beam in traveling away from the receptor site before complete laser shut-down is a function of the maximum plausible rate of angular beam deflection. Due to the immense size of the proposed SPS, angular beam deflection caused by gross platform motion will occur on a time scale much slower than the laser system response time. The most plausible accident corresponds to complete loss of laser-transmitter phase control. The highly improbable, but worst-case situation, thus involves a slew in the optical pointing vector by about 1.6×10^{-5} rad, representing a maximum shift in the primary mirror phase of 4 wavelengths before laser shut-down. Under these circumstances, all or part of the beam will slew away from the receptor by about 70 m before power-off conditions are achieved. Hence, large slew distances of the focused beam are not possible.

Because of the laser's damage potential to biological entities,[76] it is imperative that adequate safeguards and security exist to prevent sabotage or hostile control. These safeguards would normally take the form of failsafe criteria and automated power-up/power-down sequences, although the satellite could conceivably defend itself against hostile forces in space.

A small percentage of laser power spillover ($\leq$1%) will be unavoidable at the receptor device. Hazards to operating personnel and innocent bystanders exist due to possible specular or diffuse reflections from the spillover region adjacent to the receptor device. Operating personnel will be required to wear protective goggles and clothing when working in this region. An opaque perimeter fence, of appropriate height, will be placed at the boundary where the time-average power density equals the maximum recommended continuous exposure levels for humans. The American National Standards Institute (ANSI) exposure limit for cW infrared lasers is 100 mW/cm^2. This limit was determined for relatively small spot sizes on the skin or eye based on durations in excess of 10 sec. For large-area, long-duration exposure, Sliney et al.[77] recommend an average ocular or wholebody irradiance limited to about 10 mW/cm^2.

The protection radius as a function of perimeter power density is shown in Figure 9.3-5 for the uniform-intensity and Gaussian laser beam distributions. If a maximum permissible exposure limit of 10 mW/cm^2 is adopted and if allowance for the maximum plausible accident is included, a protection radius of 300 to 800 m is appropriate. Note that because the propagation axis is not perpendicular to the earth's surface, an elongated "footprint" will be produced at the receptor site. This effect has been included in these results.

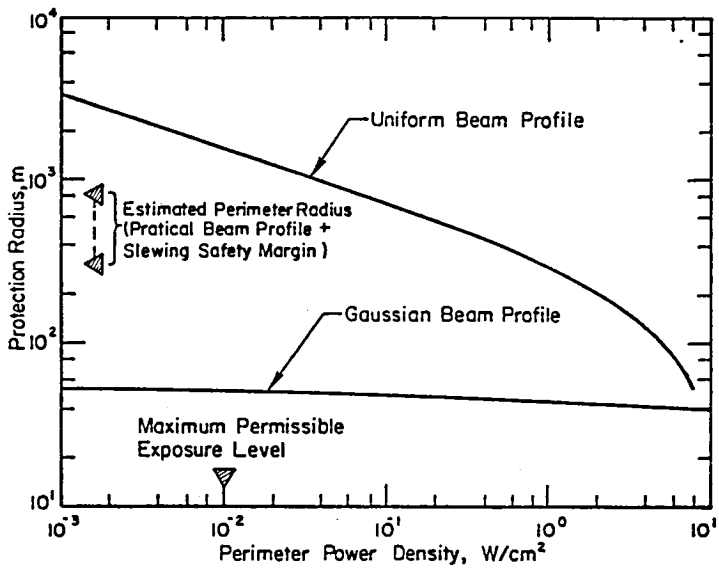

Figure 9.3-5. Receptor Site Protection Radius as a Function of the Perimeter Power-Density Level

The total land area required by the receptor site is estimated to be 0.3 to 2 km^2. Security systems will be necessary at the receptor site to ensure public safety, although security problems will be more manageable due to the small land area involved. Note that if multiple receptor devices are located in close proximity at a common location, the required perimeter radius and land area will increase slowly with the number of devices and not in an additive fashion.

9.3.3 LASER SPS MASS AND VOLUME ESTIMATES

Specific mass estimates for each subsystem are given in Table 9.3-1 along with the source of information. These data were used in conjunction with the power distribution data given in Table 9.2-11 to calculate the laser subsystem and total system masses and the mass per unit of radiated laser power. These results are given in Table 9.3-2. Monson[2] estimated that this latter parameter, the total system specific mass, is lowest for the CO EDL, followed in increasing magnitude by the CO_2 EDL, a direct solar pumped laser (η_L = 0.10), and finally by the CO_2 GDL. Only a direct solar pumped laser having an overall efficiency $\eta_L \gtrsim 0.20$ is capable of improving the total system specific mass. No satisfactory scheme for producing such a laser has yet evolved.

Volume estimates indicate that the multiple-laser-transmitter approach appears viable as a replacement for the microwave transmitters on Rockwell's current SPS system design. Available space-radiator area within the yoke is approximately 1.92 km^2 (one side), whereas the required space radiator area is 1.58 km^2. Ample area exists on the opposite side for heat-load management during periods when one radiator surface faces the sun.

Table 9.3-1. Assumed Subsystem Specific Masses for Candidate Closed-Cycle Lasers

Subsystem Description	Specific Mass	Ref.
Power Sources:		
laser discharge power supply	2.0 kg/kW_e	78
compressor motor and power converter	2.5 kg/kW_e	79
Compressor	0.1 kg/kW_m	80
Waste Heat Exchanger	0.2 kg/kW_{th}	81
Laser Fluid, Ducting, Channel, and Optics	0.7 kg/kW_m	81
Space Waste-heat Radiator	2.0 kg/m^2	81
Transmitting Optics:		
primary mirror	40 kg/m^2	29
secondary mirror	350 kg/m^2	82

Table 9.3-2. Subsystem and Total System Mass Estimates

Subsystem Description	Mass (10^3 kg)/Laser System	
	20 Lasers	24 Lasers
Power Sources:		
laser discharge power supply	471.4	393.2
compressor motor and power converter	585.8	488.5
Compressor	21.0	17.5
Waste Heat Exchanger	57.6	48.1
Laser Fluid, Ducting, Channel, and Optics	146.8	122.4
Space Waste-Heat Radiator	157.7	131.5
Transmitting Optics:		
primary mirror	19.5	19.5
secondary mirror	1.1	1.1
Total Laser System Mass	1,460.9	1,221.8
Total Mass for All Systems	29,218.0	29,323.2
Mass/Radiant Output Power, kg/kW	13.3	13.3

9.3.4 TECHNOLOGY GROWTH

The technology issues which will require considerable research and development in order to realize the performance goals desired for a laser based SPS include the following:

- Scalability by a factor of 1000 in output power beyond that of experimental devices,
- Method of cooling of a large-area transmissive laser window having an incident power ~100 mW.
- Method of gas purification/rejuvenation in a closed-cycle system.

Since these issues may present real impediments to the realization of a laser based SPS, it is imperative that they be resolved before proceeding with any detailed conceptual design.

The technical issue deserving perhaps the greatest attention is the method of coupling the laser flux within the excitation region to the transmitting optics. Two window types are available, viz., aerodynamic and transmissive. Aerodynamic windows have been built for supersonic-flow CO EDL's,[83] and specially designed configurations[84] have been developed in an effort to minimize the required mass flow rate and mass loss, which scale with the window aperture diameter. To our knowledge, however, the design or evaluation of aerodynamic windows for supersonic-flow CO lasers operating in space has not been performed. Therefore, their suitability for use in the present application remains in question. A key issue is the mass loss rate, since large quantities of onboard consumables are highly undesirable.

Regardless of whether the output beam is converging, diverging, or quasi-parallel, any transmissive window will absorb sufficiently to produce a severe volumetric heat loading. Although great advances have been made in the areas of solid-state IR materials[85,86] and coatings,[87] a satisfactory cooling method applicable to large-area transmissive optics subject to power densities ~3 kW/cm^2 has not been devised.[88] Large temperature gradients in laser output couplers employing transmissive optics usually lead to window failure due to thermal-stress fracture.[89] This issue will stringly influence any reliability estimates. It should be noted, however, that single or multiple subsystem failures in one laser transmitting chain will not impede the ability of unaffected chains to function.

9.4 ENVIRONMENTAL IMPACT ASSESSMENT

9.4.1 THERMAL HEATING OF THE ATMOSPHERE

Sources of Waste Heat

Waste thermal power from the laser-SPS will be available to the atmosphere as either sensible or latent heat. Sensible heating of the atmosphere will occur as the result of laser-beam propagation inefficiencies, i.e., aerosol and molecular absorption. As shown by the deposition profiles in Figures 9.4-1 and 9.4-2, most of the direct heating of the atmosphere occurs in close proximity to the receptor due to absorption processes in the lowest atmospheric layers. Mountain-top receptor operation largely mitigates any direct, sensible-heat input to the troposphere. Latent heating of the atmosphere, on the other hand, will occur as the result of waste heat generated by the receptor device and associated electrical power plant. The magnitude of this thermal source depends on the power rating of the plant and its thermodynamic or laser-energy conversion efficiency. Before considering the ramifications of the distributed sensible heat source to local meteorology and the effects of the latent heat source upon the regional ecosystem, we examine the possibility of global climatic change due to laser-SPS proliferation.

Possibility for Global Climatic Change

"Waste" heat is an inevitable consequence of the utilization of most energy sources, and it dissipates in the atmosphere, surface layers of the earth, and surface waters. An estimate of the level at which waste-heat disposal at or near the earth's surface might induce global climatic alternation is not difficult to perform. The average rate of absorption of solar energy is about 250 W/m^2, and simple climatic models suggest that thermal polution sources which increase this value by about 1 percent may produce serious consequences.[90,91] Based on the present laser-SPS design, it would require a proliferation of 200,000 to 400,000 complete satellites to induce this magnitube of waste heat. The quoted range accounts for the possible range in various system powers and efficiencies. To quote Ref. (90):

> Most of the inadvertent climate changes which man might cause represent variations that are comparable to the noise level of the natural variability of the atmosphere, as well as being within the uncertainty range of current modeling techniques.

Meteorological Implications

Direct laser-beam heating of the troposphere is likely to induce local meteorological changes. The effects of heat input from a distributed source (see Figures 9.4-1 and 9.4-2) will differ from effects typically found near conventional fossil-fuel electric power plants.

The nature of the distributed source suggests that significant updrafts will exist in the lower troposphere above the receptor site. Because of

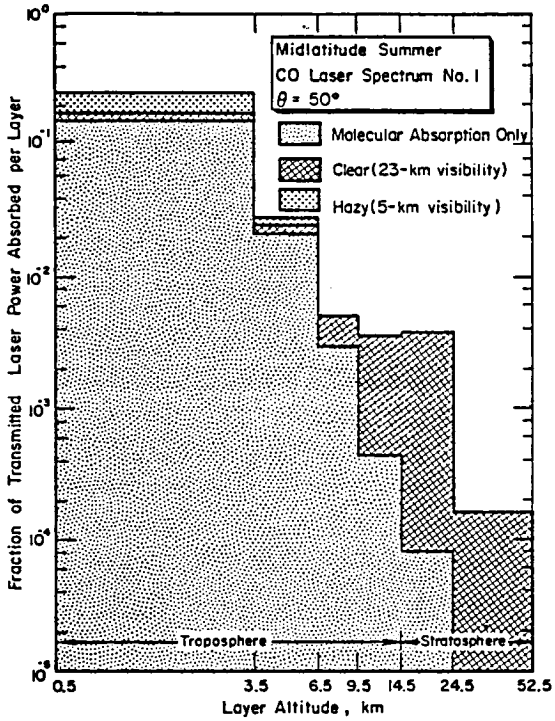

Figure 9.4-1. Fraction of Transmitted Laser Power Absorbed or Scattered by Each Atmospheric Layer (Midlatitude Summer Model)

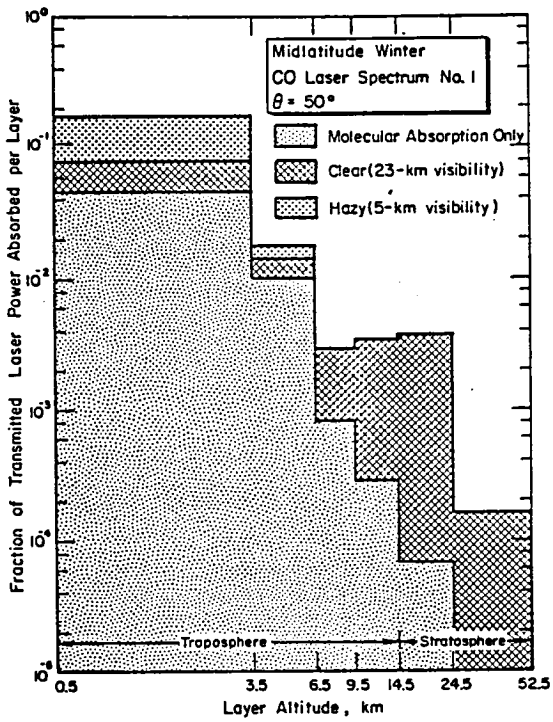

Figure 9.4-2. Fraction of Transmitted Laser Power Absorbed or Scattered by Each Atmospheric Layer (Midlatitude Winter Model)

prevailing winds and the Coriolis effect, the ensuing convective air movement may assume a helical or vortex flow. The turbulence associated with this effect will probably be severe in the lower troposphere, another reason for designating the air zone above the receptor location restricted. It is interesting to compare this "vortex" flow with other naturally-occurring phenomena. For example, the kinetic energy associated with a tornado is ~100 mW.[92] While the estimated kinetic energy associated with laser-heating of the atmosphere is about two orders of magnitude smaller, the effect is certainly not insignificant. There is one outstanding positive benefit to this effect -- the strong convective updraft will promote verticle mixing and waste-heat dispersal more effectively than man-made edifices such as cooling towers. Unlike many cooling towers, which rely upon evaporative cooling, atmospheric disposal of that portion of the plant's waste heat due to laser-beam absorption will not induce cloud generation.

The multimegawatt laser beam will, however, bore holes in ground fogs and light cloud covers.[41] By heating the aerosol droplets, water evaporates leaving the condensation nuclei behind. Reference (41) estimates that power densities of the order of several kW/cm^2 would be necessary to bore through moisture-laden cloud covers; hence, during periods of precipitation or heavy cloud covers, power generation at the affected receptor would terminate and that particular laser beam should be shut off or redirected to an alternate receptor. The power density threshold for boring, I_b (W/cm^2), is[41]

$$I_b \geq \frac{25v}{D} (1 + 1.0\psi L), \tag{43}$$

where v is the wind velocity (m/sec), D is the laser beam diameter (m), ψ is the moisture content (g/m^3), and the L is the cloud or fog thickness (m). In addition to moisture content, increasing wind velocity will also increase the threshold for penetration. The environmental impact of laser hole boring in tropospheric clouds and fogs is believed to be negligible since they will recondense after passing through the beam path. Noctilucent clouds, nucleated ice crystals high in the mesosphere, will be vaporized by a 100-MW laser beam. These formations are so rare in time and space that the environmental consequence of their vaporization is deemed insignificant. Furthermore, since most cloud types in the troposphere and stratosphere will renucleate after passing through the beam, the prospect for changing the continental cloud distribution or albedo is highly improbable.

Aerosol Effects

Aerosols are produced by direct injection from terrestrial sources or by in situ homogeneous or heterogeneous particulate formation. Destruction mechanisms include rainout, washout, and sedimentation. Natural sources for continental aerosols include dust storms (particles $\gtrsim$ 0.6 μm in diameter), photochemical gas reactions involving ozone and hydrocarbons (< 0.4 μm) and various trace gases with ozone and atomic oxygen (various sizes), and volcanic injection of SO_2 which reacts with 0 and H_2O to form heterogeneous sulfate particles (~0.5 μm diameter average). Man-made sources include combustion, both carbon or soot particles and partially or unburned hydrocarbons which react with NO_x to form smog (< 0.4 μm), and SO_2 from industrial polution which also reacts to form sulfate particles.

The concentration of small particles (Aitken nuclei, <0.2 μm diameter) decreases with increasing altitude, consistent with their terrestrial origin. The concentration of large particles (0.2 - 2 μm diameter), however, shows a maximum at about 18 km (the Junge sulfate layer). The formation mechanism involves oxidation of SO_2 to SO_3,[93] reaction of the SO_3 with water to form H_2SO_4,[94] and clustering of H_2SO_4 and H_2O molecules to form prenucleation embryos followed by heteromolecular nucleation.[95] A small concentration of hydrated $(NH_4)_2SO_4$ has been found in stratospheric aerosols, as well as traces of numerous other compounds. The residence times for aerosols in the lower stratosphere (1-3 yr) and upper stratosphere (3-5 yr) are appreciably longer than the lifetime of tropospheric aerosols (6 days - 2 weeks). Exceedingly long residence times (5-10 yr) are experienced by the low concentrations of aerosols in the mesosphere.

As shown in Figures 9.4-1 and 9.4-2, aerosols are the primary absorbers in the stratosphere (aerosol absorption and scattering coefficients are about equal at λ = 5 μm). Because the Junge layer is important to the heat balance in the lower stratosphere and because of the long residence time of stratospheric aerosols,[96-98] the possibility of laser-induced depletion of this layer must be considered. Two processes for decomposition of sulfate aerosols by laser irradiation are possible for laser power densities ~10 W/cm^2. First, absorption of IR radiation is known to preferentially excite certain vibrational modes in polyatomic molecules. Dehydration of cluster molecules is a probable reaction because of the low bond energy of H_2O to the cluster, i.e.,

$$H_2SO_4 \cdot (H_2O)_n \rightarrow H_2SO_4 \cdot (H_2O)_{n-1} + H_2O,$$

followed by V-T collisional relaxation of the reaction products. Second, rapid heating of an aerosol particle exposed to intense IR laser radiation causes internal pressures sufficient for explosive break-up.[99] Since the fundamental constituents of the aerosols remain after passing through the beam, then renucleation will probably occur and depletion of the Junge layer is not believed possible. The irradiated layer volume will be insignificant compared with the whole, and anthropogenic increases in the total mass of sulfate particles will completely outweigh any depletion rate associated with laser-SPS proliferation.

Receptor Thermal Polution

From the geophysical perspective, the exact method of waste heat disposal from the receptor power plant is probably not very important, but persistent local weather and biological effects can be quite different for dry cooling towers, wet towers, or cooling to bodies of water. Poorly sited wet cooling towers can produce unpleasant local modification of fog and drizzle frequencies. Cumulus cloud formation induced by wet cooling towers is fairly common. Increasing the ambient temperature of rivers or estuaries by their use as a source of cooling water for electric power plants is known to alter the local biological ecosystem. The environmental impact of thermal polution from receptors and conventional or nuclear power plants is qualitatively similar and will not be discussed further here.

9.4.2 ENVIRONMENTAL IMPACT ON WILDLIFE

In addition to providing protection to the general public, the perimeter "fence" will protect most indigenous animals from exposure to dangerous irradiance levels; the principal exception is birds. In traversing the primary beam, birds and insects will certainly be incinerated. There is some controversy over the ability of birds to sense the dangerous irradiance levels and to avoid the beam. It is difficult to resolve this point without experimental studies, and studies involving high-power radar transmitters are not applicable to the present problem. It is doubtful that infrared-heat-sensitive insects would be attracted to the laser beam because of the extremely small intensity of side-scattered light. Again, definitive experimental verification is lacking.

9.4.3 LASER-PLASMA INTERACTIONS IN THE IONOSPHERE

Ionospheric Parameters

The properties of the ionosphere, especially the electron density profile, are variable to a great extent with latitude, local time (diurnal variation), season, and solar activity. The ionosphere extends from about 40 km above the ground to an altitude at which H^+ becomes the main ion constituent (~1,000 km). The division of the ionosphere into several regions, C, D. E, and F, are made for conventional, and not necessarily physically compelling reasons.

The C region (~40-60 km) is produced primarily by cosmic rays, and its peak electron density is ~10^2 electrons/cm^3. The D region (~60-85 km) is formed primarily because of photoionization produced by Lyman-alpha (121.6 nm) solar radiation. The steep increase in the electron density in the lower part of the E region (~85-140 km) is due to photoionization by soft x-rays. The F1 (~140-200 km) and F2 (~200-400 km) regions are produced by photoionization by extreme-ultraviolet (euv) solar radiation, principally in the wavelength range 30 nm to 80 nm.

Electron density profiles for the ionosphere at midlatitudes are shown in Figure 9.4-3. The D-layer disappears at night and there is virtually no ionization present below about 80 km. The F1- and F2-layers coalesce in the absence of sunlight. Occasionally, "clouds" of ionization, called sporadic E, are observed at low E-layer altitudes. Ionospheric parameters used in the analyses which follow are given in Table 9.4-1.

Linear and Nonlinear Dissipative Heating

In general, electromagnetic radiation propagating through a cold, anisotropic plasma will lose energy due to linear (ohmic) and nonlinear (anomalous) absorption. For an intense IR laser beam propagating through the ionosphere, the possibility for perturbing the electron concentration, n_e (m^{-3}), or the electron and ion temperatures, T_e and T_i (eV), is examined in an effort to determine the potential environmental impact on the upper atmosphere.

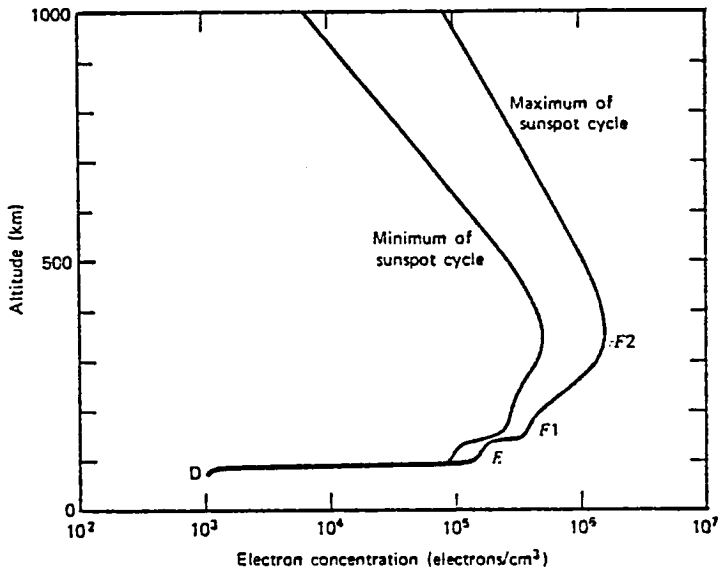

Figure 9.4-3. The Concentration of Electrons in the Earth's Ionosphere for Representative Conditions[100]

Table 9.4-1. Ionospheric parameters.[101,102] *When Two Numbers are Entered, The First Refers to the Lower and the Second to the Upper Portion of the Layer*

Quantity	E Region	F Region
Electron density, $n_e(m^{-3})$	$10^{11} - 2 \times 10^{11}$	$2 \times 10^{11} - 2 \times 10^{12}$
Ion-neutral collision frequency, $\nu_i(sec^{-1})$	$2 \times 10^3 - 10^2$	0.5 - 0.05
Ion-cyclotron frequency, ω_i(rad/sec)	180 - 190	230 - 250
Electron-neutral collision frequency, $\nu_e(sec^{-1})$	$1.5 \times 10^4 - 9.0 \times 10^4$	80 - 10
Electron-cyclotron frequency, ω_e(rad/sec)	6.2×10^6	6.2×10^6
Mean molecular weight, $\bar{M}_g$	28 - 26	22 - 20

Conservation of energy relates the divergence of the Poynting vector $\vec{S}$ to the net dissipation rate within the plasma:

$$\nabla \cdot \vec{S} = -Q = -(Q_L + Q_{anom}) \quad . \tag{44}$$

The dissipation rate Q (W/m^3) is composed of ohmic loss Q_L (linear joule heating) and anomalous loss Q_{anom} due to collisional and Landau damping of plasma waves. The latter quantity is important only when one or more thresholds for excitation of the various plasma instabilities is exceeded. Poynting's vector is related to the electric- and magnetic-field vectors by

$$\vec{S} = \vec{E} \times \vec{H} \quad . \tag{45}$$

The time-average flux of energy is given by the real part of the complex Poynting vector:

$$\vec{S}_{av} = \frac{1}{2} \vec{E} \times \vec{H}^* \ , \tag{46}$$

where * denotes complex conjugate. The laser power density (W/cm^2) is the magnitude of Poynting's vector. The magnitude of the peak electric-field strength, E_0 (V/m), and the laser power density are related by (free-space approximation).

$$S_{av} = |\vec{S}_{av}| = \frac{1}{2} c\varepsilon_0 E_0^2 = 1.327\times10^{-3} \ E_0^2 \tag{47}$$

The linear dissipation term, Q_L, is given by the equation

$$Q_L = \frac{1}{2} \vec{J} \cdot \vec{E} \ , \tag{48}$$

where $J(A/m^2)$ is the current density. For a magnetized plasma,

$$\vec{J} = \sigma_0 \vec{E}_{\parallel} + \sigma_1 \vec{E}_{\perp} + \sigma_2 (\hat{B} \times \vec{E}), \tag{49}$$

where $\vec{B}$ (Weber/m^2) is the earth's magnetic induction, $\vec{E}$ (V/m) is the laser's electric field, $\hat{B} = \vec{B}/|\vec{B}|$, $\vec{E}_{\parallel} = (\vec{E} \ \hat{B})\hat{B}$ is the electric field parallel to $\vec{B}$, and $\vec{E}_{\perp} = \vec{E} - \vec{E}_{\parallel}$ is the electric field perpendicular to $\vec{B}$. The conductivity elements σ_0, σ_1, and σ are called the direct (or longitudinal), Pedersen, and Hall conductivities, respectively. In general, each is of the form

$$\sigma = \sigma^R + i\sigma^I \ , \tag{50}$$

where the real component accounts for attenuation of the EM wave and the imaginary component is responsible for a phase shift. Without showing all of the tedious algebraic details, the real parts of the three conductivities can be obtained from the standard expressions as follows:

$$\text{Re } \sigma_0 \simeq \frac{n_e e^2}{m_e} \frac{\nu_e}{\omega^2} \tag{51}$$

$$\text{Re } \sigma_1 = \frac{n_e e^2}{m_e} \frac{\nu_e \omega_e^2}{\omega^4} \tag{52}$$

$$\text{Re } \sigma_2 = \frac{n_e e}{m_e} \frac{\omega_e}{\omega^2} \tag{53}$$

where n_e is the electron density (electrons/m^3), e is the electronic charge (1.602×10^{-19} coul), m_e is the electron mass (9.1095×10^{-31} kg), $\omega_e = eB/m_e$ is the electron cyclotron frequency (rad/sec), and ν_e is the electron-neutral collision frequency (sec^{-1}). These as well as other cogent parameters are listed in Table 9.4-1. In deriving Eqs. (51) through (53), it is assumed that $\nu_e << \omega_e << \omega$, while the ions are infinitely massive and only the electrons contribute to the conductivity. The laser light angular frequency is given by

$$\omega = 2\pi c/\lambda = 1.885\times10^{15}/\lambda \quad , \tag{54}$$

where λ is expressed in μm. For $\lambda = 5$ μm, $\omega = 3.77\times10^{14}$ rad/sec and the aforementioned assumptions are well satisfied. Using the data in Table 9.4-1, the conductivities are

$$\text{Re } \sigma_0 = 3.0\times10^{-22} - 4.0\times10^{-24} \text{ mho/m}$$

$$\text{Re } \sigma_1 = 8.0\times10^{-38} - 1.1\times10^{-39} \text{ mho/m}$$

$$\text{Re } \sigma_2 = 1.2\times10^{-19} - 2.0\times10^{-18} \text{ mho/m}$$

where the range is taken from the lower E region to the F2 region with maximum n_e. Now we do not know the relative orientations of $\vec{E}$ and $\vec{B}$ a priori, since the propagation path through the geomagnetic field and the laser polarization state are unspecified. Clearly, the maximum ohmic loss occurs when $\vec{E}$ is perpendicular to $\vec{B}$. Equations (48) and (49) are then combined to give

$$Q_L = \frac{1}{2} (\text{Re}\sigma_2) E_0^2 \quad , \tag{55}$$

where secondary terms are ignored since Re σ_1 << Re σ_0 << Re σ_2. For a 100-MW, 5-μm laser beam incident upon the ionosphere at an unspecified angle, the maximum dissipation rate is

$$Q_L = 0.008 - 0.17 \text{ nW/m}^3 \quad ,$$

which occurs about local noon during periods of maximum susspot activity. The range quoted above is for altitudes of 120 km to 340 km, corresponding to the lower E-region during periods of minimum solar activity and to the upper F2-region during periods of maximum solar activity, respectively.

It is informative to compare Q_L with other naturally occurring dissipation rates.[103,104] Above an altitude of about 80 km, the primary dissipative mechanism of the solar flux is O_2 absorption in the Schumann-Ruge continuum (125 -

175 nm), which is the principal source of oxygen atoms in the upper atmosphere. Extreme ultraviolet (euv) radiation (<100 nm) from the sun photoionizes the atomic oxygen and about 160 km, 0^+ is the dominant positive ion. Using data obtained from Figure 9.4-4, the solar-flux dissipation rate due to molecular-oxygen absorption, Q_{SR}, can be computed as

$$Q_{SR} = 970 - 0.26 \text{ nW/m}^3,$$

where the range applies to altitudes of 120 km to 340 km, respectively. Hence, for most of the ionosphere, the energy dissipation rates of naturally-occurring phenomena far exceed the maximum estimated dissipation rate which may be introduced by ohmic heating.

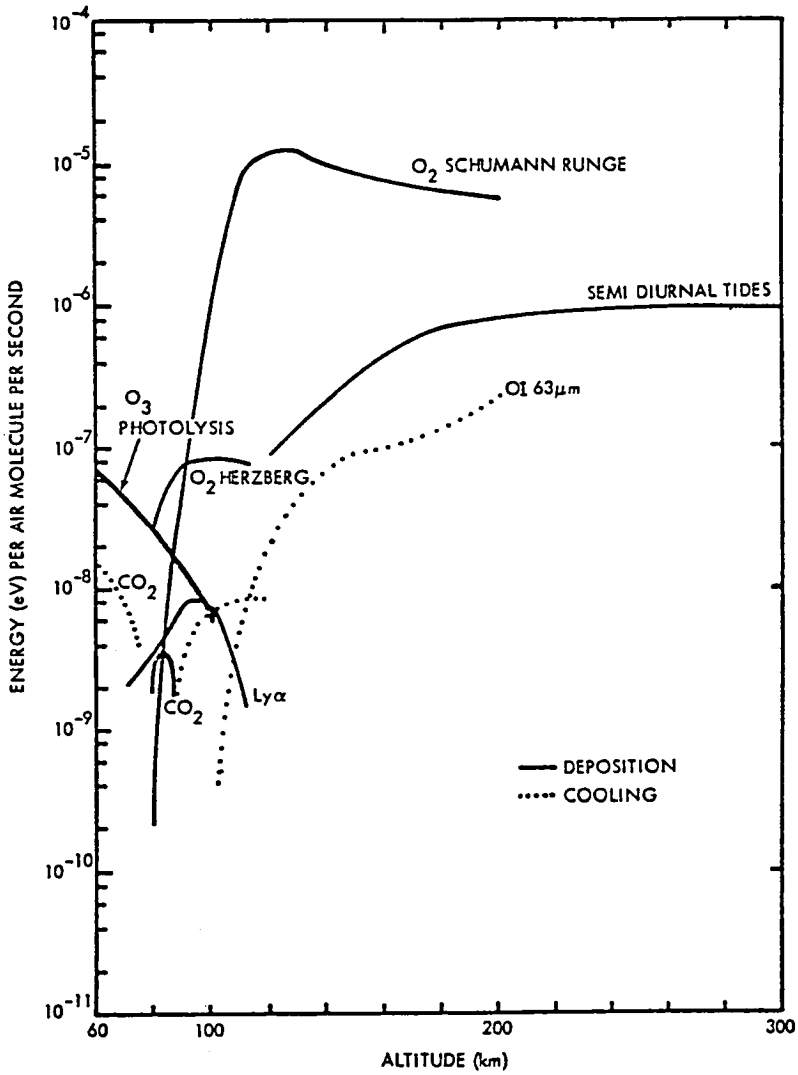

Figure 9.4-4. Altitude Dependence of Energy Absorption and Emission[105]

In the last decade, the subject of radiation induced parametric instabilities has received intensive study. These instabilities have been observed in experiments involving RF heating of the ionosphere by powerful ground based microwave transmitters and in magnetically confined plasma experiments for thermonuclear fusion research. More recently, the parametric excitation of plasma instabilities by intense coherent light has become an exceedingly active field of research, spurred by interest in laser-induced thermonuclear fusion.

These instabilities can lead to anomolous absorption or stimulated backscatter of the incident radiation. Each type of instability is associated with a certain density regime within the plasma and has a characteristic power density (W/cm) threshold for excitation which depends on a number of plasma parameters [see, for example, References (106-110)]. An important characteristic of the plasma is the electron plasma frequency, given by

$$\omega_{pe} = \left(\frac{n_e e^2}{m_e \varepsilon_0}\right)^{\frac{1}{2}} = 56.4\ n_e^{\frac{1}{2}} \quad , \tag{56}$$

where the units of n_e are m^{-3}. According to linear plasma theory, EM radiation having an angular frequency $\omega \leq \omega_{pe}$ will be reflected from the "critical density" layer $\omega_{pe}\ (n_e^c) = \omega$.

A variety of nonlinear processes are known to exist, including the parametric decay and oscillating two-stream instabilities (both important when $\omega \simeq \omega_{pe}$), resonant absorption ($\omega \simeq \omega_{pe}$), and stimulated Raman ($\omega \simeq 2\ \omega_{pe}$) and Brillouin (any $\omega > \omega_{pe}$) scattering. The instabilities may be conveniently thought of as the induced decay of an incident photon into various elementary excitations. Thus, the parametric decay instability corresponds to the decay of a photon into a plasmon and phonon. Further possibilities are photon → plasmon + plasmon, or →plasmon + photon' (SRS), or → photon' + phonon (SBS). Using the peak electron density observed for the F2-region and Eq. (56),

$$\omega_{pe} = 8\times10^7 \text{ rad/sec.}$$

For a 5-μm laser, $\omega = 3.8\times10^{14}$ rad/sed and, hence,

$$\omega >> \omega_{pe}$$

and the laser beam will not be reflected at any electron-density layer. Furthermore, the only instability which can be excited in a greatly underdense plasma ($n_e << n_e^c$) is stimulated Brillouin scattering, which has a power density threshold ($\sim10^{10}$ W/cm^2) far greater than the proposed power density incident upon the ionosphere ($\simeq$18 W/cm^2). Therefore, we conclude that

$$Q_{anom} = 0 \ .$$

For microwave interaction with the ionosphere, $\omega \gtrsim \omega_{pe}$ and anomalous absorption resulting from parametric instabilities is no longer insignificant. In F-layer heating experiments, increased electron temperature and enhanced

airglow were produced at irradiation power densities ~10 $\mu W/m^2$ by ground-based RF transmitters operating at frequencies in the range of a few to 10 MHz [see, for example, References (111-114)]. In the upper ionsophere, dissipative heating produces a spatial redistribution of electrons which is manifested by a depletion in electron density. Field-aligned density irregularities give rise to various scattering phenomena (e.g., spread-F). In the D-region, the increased electron temperature lowers the electron-ion recombination rate, resulting in an increase in electron density. Plasma instabilities also modify the electron energy distribution. The enhanced high-energy tail of the distribution can promote the excitation of various atomic species and a concomitant increase in airglow.

Inverse Bremsstrahlung Absorption

Another method of examining the effect of the laser beam is to calculate the fraction of power absorbed via electron-neutral and electron-ion bremsstrahlung, P_a, given by

$$P_a = P_T \left[1 - \exp\left(- \int_0^\infty k(h)dh\right)\right], \tag{57}$$

where the absorption coefficient as a function of height is[115]

$$k(h) = 1.272\times10^{-37}\lambda^3 n_e^2 T_e^{-\frac{1}{2}} \left[\exp(1.240/\lambda T_e) - 1\right]\xi \ , \tag{58}$$

where k is in units of cm^{-1}, the laser wavelength λ in μm, the electron density $n_e{}^{-3}$, and the electron temperature T_e in eV. The non-hydrogenic correction factor $\xi = \xi(\lambda, n_e, T_e)$, which is close to unity, is plotted in Reference (116). Using the electron density profile shown in Figure 9.4-3 for maximum sunspot activity, the ionospheric absorption fraction is estimated to be

$$P_a/P_T \lesssim 10^{-15} \ ,$$

and thus, is insignificant.

9.4.4 PERTURBATION OF THE PLASMA CHEMISTRY OF THE MESOSPHERE AND THERMOSPHERE

Preliminary examination has revealed that certain reactions in the mesosphere and thermosphere may be induced by the presence of an intense IR-photon flux and chemical reaction channels may be altered. In the upper atmosphere, mid-IR photons have sufficient energy only for vibrational-state photoexcitation and a limited number of charged-species reactions, such as positive- and negative-ion photodissociation and electron photodetachment. Such laser photons have insufficient energy for any photoionization or neutral photodissociation reactions of interest to upper-atmosphere constituents. Multiphoton processes are only important when the collisional or radiative relaxation rate is much longer than the photoexcitation rate.

The environmental consequences of plasma-chemistry perturbations are uncertain. Any mechanism which alters the electron density or the relevant temperatures of the various species (T_e, T_i, T_v) will have some environmental ramifications. The manifestations of these phenomena, such as enhanced airglow and changes in HF communications, are not fully understood. Probably the worst consequence of any space-to-earth power beaming scheme would be depletion of the ozone layer which protects the earth's surface from harmful UV radiation. Most of the ozone is found below an altitude of 50 km. Some depletion above that altitude would have little consequence; however, ozone does not absorb in the mid-IR wavelengths and no direct photodestruction scheme at any altitude was identified in this study. Secondary reaction channels (discussed below) may later the O_3 concentration, but only at high altitudes (>60 km) and only in a localized manner.

Vibrational Photoexcitation

Molecules can be vibrationally excited by a variety of mechanisms, including exothermic chemical reactions, electron impact, V-V energy transfer, and photoexcitation. Sunshine and earthshine are the primary radiation sources for photoexcitation of upper-atmosphere molecules under undisturbed conditions. The earthshine appears to be the most important source of vibrational excitation for wavelengths $\gtrsim$ 5 μm.[117]

Among the molecular species of the upper atmosphere, the metal oxides are most susceptible to this source of excitation, since their band fundamentals tend to fall near the peak of the earthshine irradiance spectrum and collisional quenching of their vibrational states in slow.[117] Because of CO laser spectrum consists of a number of discrete lines, absorption transitions would need to be coincident with the laser lines for significant photoexcitation to occur. While the detailed transition levels of the various metal oxides have not been examined in detail, the concentrations of metal oxides are so low and the laser-beam area is so small that the likelihood of serious ionospheric perturbation is insignificant. Furthermore, almost all of the metal oxides, such as AlO, FeO, etc., reradiate in the infrared and, hence, no visible airglow would be observed.

Charged-Species Reactions

Most of the charged-species reactions of interest to the present discussion are possible only in the D-region. The D-region is the most chemically complex region of the ionosphere. The flux of energetic particles and photons is insufficient to maintain a highly-ionized plasma at the ambient pressure. Hence, the D-region consists of a large concentration of neutral species in which positive and negative ions are the principal charge carriers and complex ion-interchange and electron attachment and detachment reactions occur. Species of importance to D-region chemistry are listed in Table 9.4-2. Schematic representations of the positive- and negative-ion reaction channels are shown in Figures 9.4-5 and 9.4-6. Because solar euv radiation is the primary ionization source, the ionic concentrations show a diurnal time dependence, as shown in Figures 9.4-7 and 9.4-8.

Table 9.4-2. Species of Importance to the Sub-D- and D-Regions[121]

Neutrals	Neutral Excited States	Negatives	Positives
CH_4	$N(^2D)$	CO_3^-	$H^+(H_2O)_{n=1-5}$
CO	$N_2(A^3\Sigma_u^+)$	$CO_3^-(H_2O)$	$H^+(H_2O)(HO)$
CO_2	$O(^1D)$	CO_4^-	$H^+(H_2O)(N_2)$
H	$O(^1S)$	$CO_4^-(H_2O)$	N^+
HNO_2	$O_2(a^1\Delta_g)$	NO_2^-	NO^+
HNO_3	$O_2(b^1\Sigma_g^+)$	$NO_2^-(H_2O)$	$NO^+(CO_2)$
HO		NO_3^- *	$NO^+(H_2O)_{n=1-3}$
HO_2		$NO_3^-(H_2O)_{n=1-5}$	$NO^+(N_2)$
H_2		O^-	NO_2^+
H_2O		O_2^-	N_2^+
H_2O_2		$O_2^-(H_2O)$	O^+
N		O_3^-	O_2^+
NO		O_4^-	$O_2^+(H_2O)$
NO_2		$OONO^-$ *	O_4^+
NO_3		e	
N_2			
N_2O			
N_2O_5			
O			
O_2			
O_3			

*The difference between the designations $OONO^-$ and NO_3^- is explained on page 18A-7.

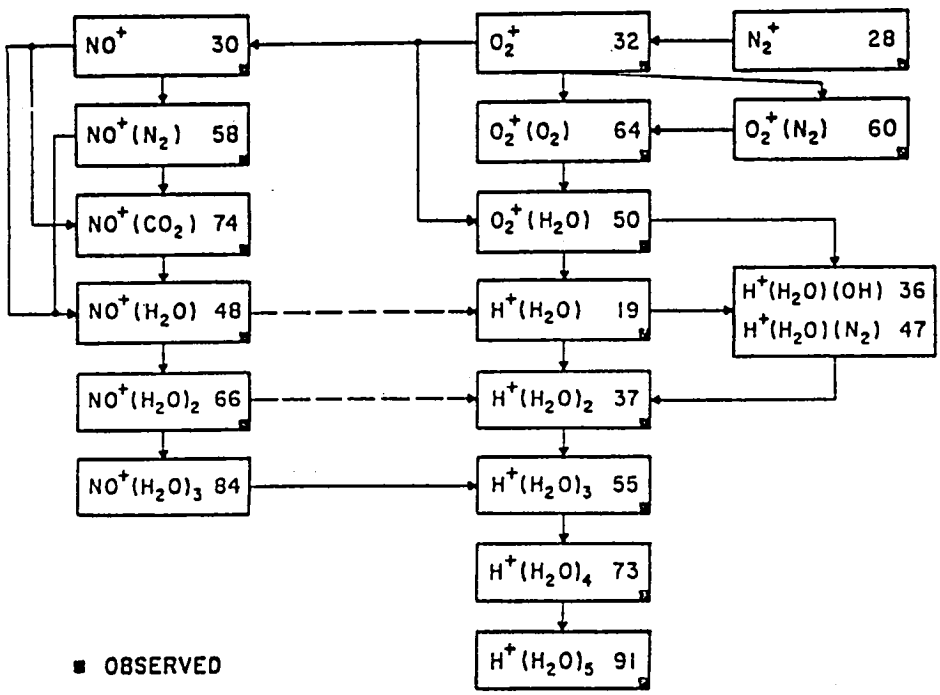

Figure 9.4-5. Schematic Representation of the Formation of Positive Ions in the D-Region.[121] *The Dashed Lines Indicate Possible Reactions*

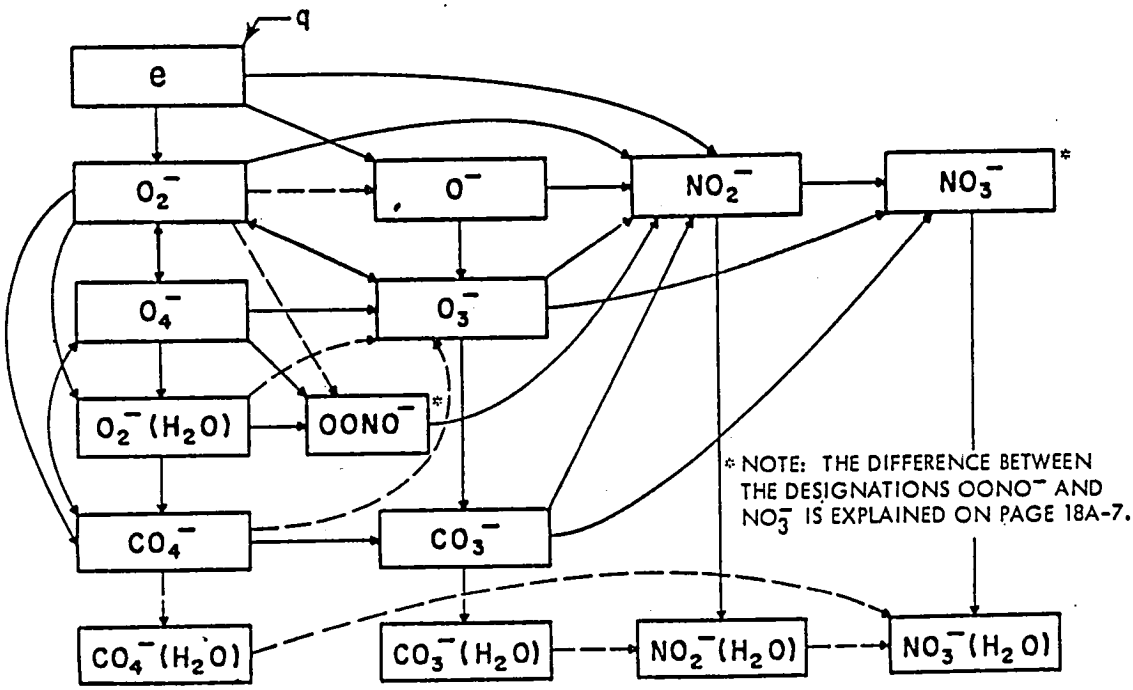

Figure 9.4-6. Schematic Representation of the Formation of Negative Ions in the D-Region.[121] *The Solid Lines Indicate Probable Reactions, on the Basis of Experimental Measurements of the Rate Coefficients*

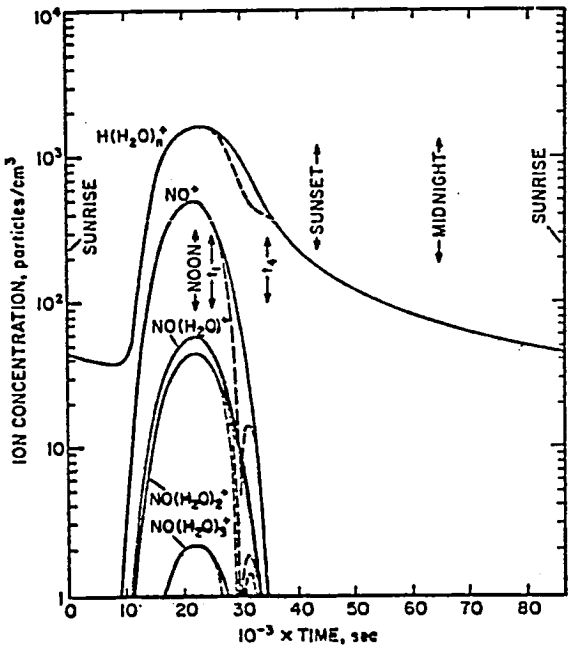

Figure 9.4-7. Calculated Positive-Ion Concentrations in the D-Layer at 70 km for a Day in Which the Noonday Sun is Overhead

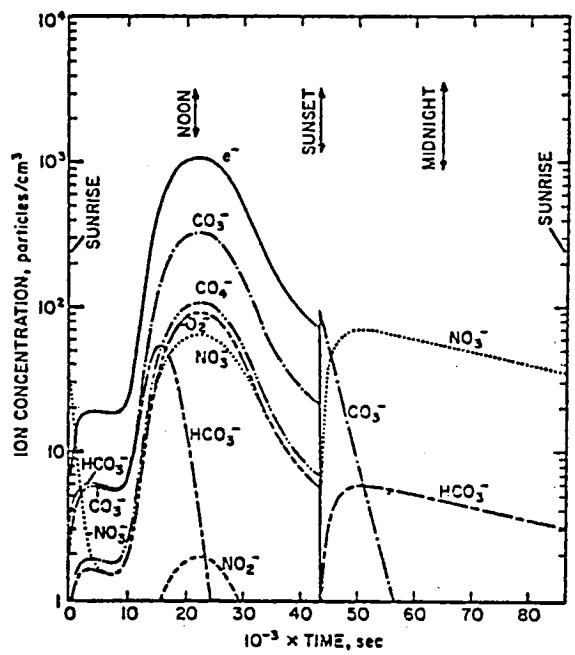

Figure 9.4-8. Calculated Negative-Ion Concentrations in the D-Layer at 70 km for an Ordinary Day in Which the Noonday Sun is Overhead[122]

Photoreactions in the D-region which may be induced by single or multiphoton processes involving an intense photon flux from an infrared laser are listed in Table 9.4-3. The CO laser photons have an average energy of about 0.25 eV; hence, most of these reactions are inaccessible by single-photon processes. If the ionic species process a long V-T relaxation time, however, then photodissociation or electron photodetachment are possible by multiphoton excitation. Again, because the interaction volume is so restricted, significant modification to an appreciable fraction of the D-layer is not believed possible. THis premise should be verified by kinetic modeling which accounts for all plausible processes. Perturbations of this region are known to greatly affect the absorption of HF radio signals and the reflection of LF signals; for this reason, the remote possibility of D-region modification by space-to-earth laser power transmission should be investigated further.

In the E- and F- regions, the only energetically accessible reaction which was identified is

$$O_3^+ + h\nu(\geq 0.32 \text{ eV}) \rightarrow O_2^+ + O \ .$$

The concentration of O_3^+ is so low that the consequences of increasing its photodissociation rate (which is already large because of the solar flux) by laser-power beaming are completely negligible. Furthermore, only shorter-wavelength laser photons have sufficient energy to induce this reaction.

Table 9.4-3. Photoreactions Involving Charged Species Found in the D-Region Which may be Induced by an Intense IR-Photon Flux

Reaction	Photodetachment Threshold or Dissociation Energy, eV
Negative-ion electron photodetachment and photodissociation:	
$O_2^- + h\nu \rightarrow e^- + O_2$	0.46
$O_2^-(H_2O)_n + h\nu \rightarrow O_2^-(H_2O)_{n-1} + H_2O, \quad n = 1\text{-}5$	0.8 - 0.5
$O_4^- + h\nu \rightarrow O_2^- + O_2$	0.54
$CO_4^- + h\nu \rightarrow O_2^- + CO_2$	0.8
Positive-ion photodissociation:	
$H_3O^+(H_2O)_n + h\nu \rightarrow H_3O^+(H_2O)_{n-1} + H_2O, \quad n = 1\text{-}5$	- - -
$NO^+(H_2O)_n + h\nu \rightarrow NO^+(H_2O)_{n-1} + H_2O, \quad n = 1\text{-}3$	- - -

9.4.5 ALTERNATE POWER-BEAMING LASER WAVELENGTHS

The "best" wavelength regime represents several tradeoffs between atmospheric transmission efficiency and potential environmental risks. Based on minimization of molecular absorption and aerosol extinction, several high-transparency windows in the approximate wavelength range of 3.6 to 3.8 μm can be found. Several regions of low molecular absorption exist at shorter wavelengths, but aerosol attenuation is more of a problem (refer to Figure 9.2-14. Furthermore, operation at shorter wavelengths (and larger photon energies) makes an increasing number of plasma reactions energetically accessible, which may have portentous environmental ramifications.

Longer wavelength "windows" are present, e.g., at the 9.114-μm line of isotopic CO_2. The molecular absorption which does occur, however, is distributed such that sensible heating will occur at high altitudes. This is believed to be undesirable from an environmental impact point of view. Laser lines having an absorption coefficient which decreases rapidly with increasing altitude, such as with the line-selected supersonic CO EDL, are less environmentally offensive since sensible heating only occurs in the lower troposphere.

The "window" at ~3.6 to ~3.8 μm possesses considerable fine structure which should be avoided for maximum transmission efficiency. The EF laser has many lines which satisfy this requirement; however, high-power DF laser operation in a closed-cycle system operating at high efficiency is not currently possible. The best prospect for suitable laser development in this spectral range involves electronic-vibrational (E-V) energy transfer schemes [see, for example, References (123-126)]. Much more research is needed before device capabilities compatible with the present power-transmission application can be achieved.

9.4.6 SUMMARY OF ENVIRONMENTAL IMPACT ISSUES

For the baseline laser-SPS concept defined earlier in this study, results of the assessment of environmental impact issues can be summarized as follows:

- Global climatic change resulting from the proliferation of laser-SPS systems is highly improbable,
- Mesoscale weather modifications at receptor locations will be less significant than such phenomena associated with conventional or nuclear electric power plants of comparable power rating,
- Thermal heating of the lower troposphere by the laser beam will promote waste-heat dispersal by verticle mixing, but will also induce severe turbulence which could be hazardous to aircraft intruding into the restricted air zone,
- The environmental impact on certain wildlife, especially birds and insects, is uncertain,
- Laser-plasma interactions in the ionosphere are insignificant,

- Laser-beam perturbation of the plasma chemistry in the mesosphere and thermosphere is believed to be of negligible magnitude and consequence; however, confirming research is needed to substantiate this claim, and
- Serious environmental modifications, such as depletion of the ozone concentration in the stratosphere, are not possible.

9.5 CONCLUSIONS AND RECOMMENDATIONS

The conclusions of this study are as follows:

- Of the current state-of-the art electric-discharge lasers, the supersonic-flow CO EDL is capable of achieving the highest total SPS system efficiency (≈16%), defined as the ratio of electric power available at the user grid to photoelectric power generated onboard the satellite,
- Significant technology improvement is necessary in order to realize a closed-cycle laser device capable of the performance goals required for power transmission,
- Two viable receptor concepts were identified which project laser energy conversion efficiencies of 40 to 73%,
- High-elevation receptor sites are preferred, both from environmental and system efficiency standpoints,
- Safety and security issues present no formidable obstacles to the laser-SPS concept, although societal and political issues may present stubborn impediments, and
- No effects could be found which present a real danager of serious injury to the environment.

In this study, the environmental ramifications of SPS transportation into space have been specifically omitted. This author believes that the environmental impact of laser-SPS operation will be inconsequential compared with laser-SPS transport [see, for example, Reference (127)].

Specific recommendations for continuing work in this area include the following:

- Because of the low system efficiency and large specific mass of the current photovoltaic-EDL SPS concept, NASA should seriously consider any reasonable approaches for an advanced, direct-solar-pumped laser for power transmission, and
- Possible perturbations of the upper-atmosphere plasma chemistry by an intense IR-photon flux should be examined in more detail using state-of-the-art kinetic models to either verify or countermand the assessment of this study.

9.6 REFERENCES

1. J.D.C. Rather, "*New Candidate Lasers for Power Beaming and Discussion of Their Applications*," W. J. Schafer Associated, Inc. (unpublished)

2. D. J. Monson, "*Systems Efficiency and Specific Mass Estimates for Direct and Indirect Solar-Pumped Closed-Cycle High-Energy Laser in Space*," Proc. 3rd NASA Conference on Radiation Energy Conversion (1978)

3. D. J. Monson, "*Potential Efficiencies of Open- and Closed-Cycle CO, Supersonic, Electric-Discharge Lasers*," AIAA J. 14, 614 (1976)

4. R. K. Burns, "*Parametric Thermodynamic Analysis of Closed-Cycle Gas-Laser Operation in Space*," NASA Lewis Research Center Report No. NASA TN D-7658 (1974)

5. M. J. Zucrow and J. D. Hoffman, "*Gas Dynamics*," Vol. I (Wiley, New York, 1976); see especially sections 6-5 and 7-12

6. A. J. DeMaria, "*Review of CW High-Power CO_2 Lasers*," Proc. IEEE 61, 731 (1973)

7. W. L. Nighan and J. H. Bennett, "*Electron Energy Excitation Rates in CO_2 Laser Mixtures*," Appl. Phys, Lett. 14, 240 (1969)

8. W. L. Nighan, "*Electron Energy Distributions and Collision Rates in Electrically Excited N_2, CO_2, and CO*," Phys, Rev. A 2, 1989 (1970)

9. C. Freed, A.H.M. Ross, and R. G. O'Donnell, "*Determination of Laser Line Frequencies and Vibrational-Rotational Constants of the $^{12}C^{18}O_2$ $^{13}C^{16}O_2$, and $^{13}C^{18}O_2$ Isotopes From Measurements of CW Beat Frequencies With Fast HgCdTe Photodiodes and Microwave Frequency Counters*," J. Mol. Spectrosc. 49, 439 (1974)

10. C. Freed, R. G. O'Donnell, and A.H.M. Ross, "*Absolute Frequency Calibration of the CO_2 Isotope Laser Lines*," IEEE Trans. Instrum. Meas. IM-25, 431 (1976)

11. G. E. Mevers et al., "*Analysis and Design of a High Power Laser Adaptive Phased Array Transmitter*," Rockwell International, Autonetics Division Report No. NASA CR-134952 (1977)

12. R. A. McClatchey, "*Atmospheric Attenuation of CO Laser Radiation*," Air Force Geophysics Laboratory Report No. AFCRL-71-0370 (1971)

13. J. W. Baiber and H. M. Thompson, "*Performance of a Large, CW, Pre-excited CO Supersonic Laser*," IEEE J. Quant. Electron. QE-13, 10 (1977)

14. D. K. Rice, "*Spectral Line Selection of Carbon Monoxide Lasers*," Northrop Research and Technology Center Report No. NRTC-74-44R (1974)

15. M. M. Mann, "*CO Electric Discharge Lasers*," AIAA J. 14, 549 (1976)

16. E. L. Klosterman, S. R. Byron, and D. C. Quimby, "*Supersonic Continuous Wave CO Electric Discharge Laser Parametric Investigation*," Mathematical Sciences Northwest Report No. AFWL-TR-76-298 (1977)

17. J. P. Reilly, "*Pulser/Sustainer Electric-Discharge Laser*," J. Appl. Phys. 43, 3411 (1972)

18. A. E. Hill, "*Continuous Uniform Excitation of Medium-Pressure CO_2 Laser Plasmas by Means of Controlled Avalanche Ionization*," Appl. Phys. Lett. 22, 670 (1973)

19. N. A. Generalov, V. P. Zimakov, V. D. Kosynkin, Yu. P. Raizer, and D. I. Roitenbury, "*Method of Significantly Increasing the Stability Limit of the Discharge in Fast-Flow Large-Volume Lasers*," Sov. Tech. Phys. Lett. 1, 201 (1975)

20. A. P. Napartovich, V. G. Naumov, and V. M. Shashkov, "*Plasma Decay in a Glow Discharge in a Constant Electric Field*," Sov. J. Plasma Phys. 1, 449 (1975)

21. A. P. Napartovich and A. N. Starostin, "*Stability of a Glow Discharge With External Ionization*," Sov. J. Plasma Phys, 2, 469 (1976)

22. A. P. Napartovich, V. G. Naumov, and V. M. Shashkov, "*Heating of a Gas in a Combined Discharge in a Flow of Nitrogen*," Sov. Phys. Dokl. 22, 35 (1977)

23. A. P. Napartovich, V. G. Naumov, and V. M. Shashkov, "*Transverse Combined Discharge with a Large Gap*," Sov. Tech. Phys. Lett. 3, 142 (1977)

24. V. G. Naumov and V. M. Shashkov, "*Investigation of a Combined Discharge Used to Pump Fast-Flow Lasers*," Sov. J. Quant. Electron. 7, 1386 (1977)

25. V. G. Naumov and V. M. Shashkov, "*Combined Discharge in a Supersonic Gas Flow*," Sov. Tech. Phys, Lett. 3, 465 (1977)

26. W. M. Moeny and J. P. O'Loughlin, "*POKER-Controlled Pulsed Discharges in Supersonic CO Flows*," Paper NB-5, 30th Gaseous Electronics Conference, Palo Alto, California (October 18-21, 1977)

27. D. J. Monson and G. Srinivasan, "*A Pulser-Sustainer Carbon Monoxide Electric-Discharge Supersonic Laser*," Appl. Phys. Lett. 31, 828 (1977)

28. D. J. Monson, "*Pulser-Sustainer CO Supersonic Laser*," Seminar Presented at Battelle Columbus Laboratories (April 21, 1978)

29. R. R. Berggren and G. E. Lenertz, "*Feasibility of a 30-Meter Space Based Laser Transmitter*," Itek Corporation Report No. NASA CR-134903 (1975)

30. R. R. Altenhof, "*Design and Manufacture of Large Beryllium Optics*," Opt. Engr. 15, 2650 (1975)

31. G. V. Rodkevich and V. I. Robachevskaya, "*Possibilities of Reducing the Mass of Large, Precision Mirrors*," Sov. J. Opt. Technol. 44, 515 (1977)

32. M. D. Guadagnoli and T. T. Sanito, "*Beryllium Mirrors: 10.6-μm Characterization*," Appl. Opt. 14, 2806 (1975)

33. T. T. Saito and L. B. Simmons, "*Performance Characteristics of Single Point Diamond Machined Metal Mirrors for Infrared Laser Applications*," Appl. Opt. 14, 2647 (1974)

34. D. K. Burge, H. E. Bennett, and E. J. Ashley, "*Effect of Atmospheric Exposure on the Infrared Reflectance of Silvered Mirrors With and Without Protective Coatings*," Appl. Opt. 12, 42 (1973)

35. J. Kurdock, T. Saito, J. Buckmelter, and R. Austin, "*Polishing of Supersmooth Metal Mirrors*," Appl. Opt. 14, 1808 (1975)

36. T. T. Saito, "*Machining of Optics: An Introduction*," Appl. Opt. 14, 1773 (1975)

37. D. L. Jacobson, W. Bickford, J. Kidd, R. Barthelemy, and R. H. Bloomer, Jr., "*Analysis and Testing of a Heat Pipe Mirror for Lasers*," J. Energy 1, 306 (1977)

38. T. T. Saito and J. R. Kurdock, "*Diamond Turning and Polishing of Infrared Optical Components*," Appl. Opt. 15, 27 (1976)

39. T. T. Saito, "*10.6 μm Mirror Reflectivities*," Proc. SPIE 65, 118 (1975) and OCLI Technical Information Sheets

40. P. L. Kelley et al., "*Linear Absorption and Scattering in the Atmosphere*," J. Defense Res. 4A, 311 (1975)

41. R. C. Harney, "*Hole-Boring in Clouds by High-Intensity Laser Beams: Theory*," Appl. Opt. 16, 2974 (1977)

42. R. A. McClathchey et al., "*Optical Properties of the Atmosphere (Third Edition)*," Air Force Geophysics Laboratory Report No. AFCRL-71-0497 (1972)

43. S. A. Clough, F. A. Kneizus, and J. H. Chetwynd, "*Algorythm for the Calculation of Absorption Coefficient-Pressure Broadened Molecular Transitions*," Air Force Geophysics Laboratory Report No. AFGL-TR-77-0164 (1977)

44. R. A. McClatchey et al., "*AFCRL Atmospheric Absorption Line Parameters Compilation*," Air Force Geophysics Laboratory Report No. AFCRL-TR-73-0096 (1973). The Computer Tape (Available from NOAA, Ashville, NC) is Periodically Updated with Revised and Refined Data

45. R. K. Long and F. S. Mills, "*Calculated Absorption Coefficients for Low Vibrational CO Laser Frequencies*," Ohio State University Report No. 3271-8 (Also appears as RADC-TR-74-95) (1974)

46. E. L. Harris and W. J. Glowacki, "*Absorption of CO Laser Radiation by Water Vapor Near 5* μm," Naval Ordnance Laboratory Report No. NOL-TR-73-206 (1973)

47. R. A. McClatchey and J.E.A. Selby, "*Atmospheric Transmittance 7-30* μm*: Attenuation of CO_2 Laser Radiation*," Air Force Geophysics Laboratory No. AFCRL-72-0611 (1972)

48. K. N. Rao, "*High Resolution Infrared Spectroscopy: Aspects of Modern Research*," in Physical Chemistry, Series 2, Vol. 3, edited by D. A. Ramsey (Butterworths, Woburn, MA, 1976)

49. R. A. McClatchey and J.E.A. Selby, "*Atmospheric Attenuation of Laser Radiation from 0.76 to 31.25* μm," AFCRL-TR-74-003 (1974)

50. C. N. Bain, "*Potential of Laser for SPS Power Transmission*," PRC Energy Analysis Company Report No. R-1861 (1978)

51. K. W. Billman, "*Laser Energy Conversion*," Astronaut. Aeronaut. 13 (July/Aug.), 56 (1975)

52. A. Javan, "*Optical Electronics*," Second NASA Conference on Laser Energy Conversion, edited by K. W. Billman, NASA SP-395 (1975), pp. 61-66

53. T. K. Austafson, "*Optical Diodes*," ibid., pp. 67-79.

54. M. Garbuny and M. J. Pechersky, "*Optimization of Engines Operated Remotely by Laser Power*," ibid., pp. 173-180

55. R. L. Byer, "*Initial Experiments with a Laser Driven Stirling Engine*," ibid., pp. 181-188

56. G. E. Caledonia, "*Conversion of Laser Energy to Gas Kinetic Energy*," J. Energy 1, 121 (1977)

57. M. Garbuny and M. J. Pechersky, "*Laser Engines Operating by Resonance Absorption*," Appl. Opt. 15, 1141 (1976)

58. A. Hertzberg, W. H. Christiansen, E. W. Johnston, and H. G. Ahlstrom, "*Photon Generators and Engines for Laser Power Transmission*," AIAA J. 10, 394 (1972)

59. W. H. Christiansen and A. Hertzberg, "*Gasdynamic Lasers and Photon Mechines*," Proc. IEEE 61, 1060 (1973)

60. A. Hertzberg, "*High-Power Gas Lasers: Applications and Future Developments*," J. Energy 1, 331 (1977)

61. R. C. Weatherston and A. Hertzberg, "*The Energy Exchanger, A New Concept for High-Efficiency Gas Turbine Cycles*," Trans. ASME Ser. A 89, 217 (1967)

62. C. Seippel, "*Pressure Exchanger*," U. S. Patent No. 2,399,394 (April 30, 1946)

63. _____, "*Laser Power Conversion Systems Analysis*," Lockheed Palo Alto Research Laboratory Presentation to NASA Lewis Research Center on Contract No. NAS 3-21132 (May 30, 1978)

64. L. K. Hansen and N. S. Rasor, "*Thermo Electronic Laser Energy Conversion*," Second NASA Conference on Laser Energy Conversion, op. eit., pp. 133-146

65. E. J. Britt and C. Yuen, Interscoiety Energy Conversion Engineering Conference, Washington, D.C. (1977), pp. 1453-1460

66. R. W. Thompson, E. J. Manista, and D. L. Alger, "*Preliminary Results on the Conversion of Laser Energy into Electricity*," Appl. Phys, Lett. 32, 610 (1978)

67. E. J. Britt, N. S. Rasor, G. Lee, and K. W. Billman, "*A Cesium Plasma TELEC Device for Conversion of Laser Radiation to Electric Power*," Appl. Phys. Lett 33, 384 (1978)

68. J. J. Cuomo et al., "*A New Concept for Solar Energy Thermal Conversion*," Appl. Phys. Lett. 26, 557 (1975)

69. M. Born and E. Wolf, "*Principles of Optics*," 4th ed. (Pergamon, Oxford, 1970), pp. 395-416

70. F. G. Gebhardt, "*High Power Laser Propagation*," Appl. Opt. 15, 1479 (1976)

71. D. L. Fried and G. E. Mevers, "*Evaluation of r_0 for Propagation Down Through the Atmosphere*," Appl. Opt. 13, 2620 (1974)

72. Hewlett-Packard Company, HP-97 Math Pac I, Program MA1-10A

73. P. B. Ulrich et al., "*Documentation of PROP E, a Computer Program for the Propagation of High-Power Laser Beams through Absorbing Media*," Naval Research Laboratory Report No. 7681 (1974)

74. P. B. Ulrich, "*PROP I: An Efficient Implicit Algorythm for Calculating Nonlinear Scalar Wave Propagation in the Fresnel Approximation*," Naval Research Laboratory Report No. 7706 (1974)

75. M. R. Wohlers, "*Approximate Analyses of the Refractive Attenuation of Laser Beam Intensities by Turbulent Absorbing Media*," Appl. Opt. 11, 1389 (1972)

76. D. H. Sliney and B. C. Freasier, "*Evaluation of Optical Radiation Hazards*," Appl. Opt. 12, 1 (1973)

77. D. H. Sliney, K. W. Vorpahl, and D. C. Winburn, "*Environmental Health Hazards from High-Powered, Infrared, Laser Devices*," Arch. Environ. Health 30, 174 (1975)

78. A. I. Gordon, Rockwell International, Space Systems Group, Personal Communication

79. Estimate; see also G. R. Woodcock, "*Solar Satellites -- Space Key to Our Power Future*," Astronaut. Aeronaut. 15, (July/Aug.) 30 (1977).

80. J.D.G. Rather, E. T. Gerry, and G. W. Zeiders, "*Investigation of Possibilities of Solar Powered High Energy Lasers in Space*," W. J. Schafer Associates, Inc. Report No. 77SR-VA-U3 (1977)

81. G. W. Kelch and W. E. Young, "*Closed-Cycle Gas Dynamic Laser Design Investigation*," NASA CR-135130 (1977)

82. Estimate Based on a High-Pressure Water Cooled Cooper Mirror

83. P. I. Shen, "*Supersonic Continuous Wave Carbon Monoxide Laser: Supersonic Channel Alcove and Double Shock Aerodynamic Window Development*," Northrop Research and Technology Center Report No. AFWL-TR-77-105 Vol. IV (1977)

84. R. N. Guile and W. E. Hilding, "*Investigation of a Free-Vortex Aerodynamic Window*," AIAA Paper No. 75-122 (1975)

85. T. F. Deutsch, "*Laser Window Materials -- An Overview*," J. Electron Mat. 4, 663 (1975)

86. J. A. Harrington, D. A. Gregory, and W. F. Otto, Jr., "*Infrared Absorption in Chemical Laser Window Materials*," Appl. Opt. 15, 1953 (1976)

87. J. E. Rudisill, M. Braunstein, and A. I. Braunstein, "*Optical Coatings for High Energy ZnSe Laser Windows*," Appl. Opt. 13, 2075 (1974)

88. G. H. Sherman and G. F. Frazier, "*Transmissive Optics for High Power CO Lasers: Practical Considerations*," Opt. Engr. 17, 225 (1978)

89. V. Biricikoglu, "*Thermal Stresses in Cryogenic Windows*," Appl. Opt. 12, 1831 (1973)

90. W. H. Matthews, W. W. Kellogg, and G. D. Robinson, "*Man's Impact on the Climate*," MIT Press, Cambridge, MA (1971)

91. R. A. Llewellyn and W. M. Washington, "*Regional and Global Aspects*," in Energy and Climate, National Academy of Sciences, Washington, D.C., (1977), pp. 106-118

92. C. L. Hosler and H. E. Landsberg, "*The Effect of Localized Man-Made Heat and Moisture Sources in Mesoscale Weather Modification*," ibid., pp. 96-105

93. D. D. Davis and G. Klauber, "*Atmospheric Gas Phase Oxidation Mechanism for the Molecule SO_2*," Proc. Sym. on Chemical Kinetics Data for the Upper and Lower Atmosphere (Interscience, New York, 1975), pp. 543-556

94. J. Heicklen and M. Luria, "*Kinetics of Homogeneous Particle Nucleation and Growth*," ibid, pp. 567-580

95. A. W. Castleman, Jr., R. E. Davis, H. R. Munkelwitz, I. N. Tang, and W. P. Wood, "*Kinetics of Association Reactions Pertaining to H_2SO_4 Aerosol Formation*," ibid., pp. 629-640

96. K. Ya. Kondratyev, L. S. Ivlev, and G. A. Nikolsky, "*Investigations of the Stratospheric Aerosol*," Proc. Third Conf. on the Climatic Impact Assessment Program, U. S. Dept. of Transportation Report No. DOT-TSC-OST-74-15 (1974), pp. 143-152

97. G. V. Ferry and H. Y. Lem, "*Aerosols in the Stratosphere*," ibid, pp. 310-317

98. R. P. Turco, P. Hamill, O. B. Toon, and R. C. Whitten, "*A One-Dimensional Model for the Stratospheric Aerosol Layer*," Int. Conf. on Problems Related to the Stratosphere, Jet Propulsion Laboratory Report No. 77-12 (1977), pp. 207-209

99. V. A. Pogodaev, et al., "*Thermal Explosion of Water Drops on Exposure to High-Power Laser Radiation*," Sov. J. Quant. Electron. 7, 85 (1977)

100. R. C. Haymes, "*Introduction to Space Science*," Wiley, New York (1971)

101. D. L. Book, "*NRL Plasma Formulary*," Naval Research Laboratory Report No. 2898

102. B. K. Ching and Y. T. Chiu, "*A Phenomenlogical Model of Global Ionospheric Electron Density in the E-, Fl-, and F2-Regions*," J. Atmos. Terr. Phys. 35, 1615 (1973)

103. F. S. Johson, "*Energy Input to the Lower Thermosphere*," J. Atmos. Terr. Phys. 36, 1707 (1974)

104. R. S. Stolarski, "*Energetics of the Midlatitude Thermosphere*," J. Atmos. Terr. Phys. 38, 863 (1976)

105. E. Bauer, R. H. Kummler, and M. H. Bortner, "*The Natural Atmosphere: Energy Balance in the Upper Atmosphere*," Reaction Rate Handbook, 2nd Ed., Defense Nuclear Agency Report No. DNA 1948H (sixth revision, 1975), Ch. 4

106. D. F. DuBois, "*Laser-Induced Instabilities and Anomalous Absorption in Dense Plasmas*," in Laser Interaction and Related Plasma Phenomena, Vol. 3A, edited by H. Schwarz and H. Hora (Plenum, New York, 1974), pp. 267-289

107. J. F. Drake, P. K. Kaw, Y. C. Lee, G. Schmidt, C. S. Liu, and M. N. Rosenbluth, "*Parametric Instabilities of Electromagnetic Waves in Plasmas*," Phys. Fluids 17, 778 (1974)

108. R. White, P. Kaw, D. Pesme, M. N. Rosenbluth, G. Laval, R. Huff, and R. Varma, "*Absolute Parametric Instabilities in Inhomogeneous Plasmas*," Nucl. Fusion 14, 45 (1974)

109. D. W. Forslund, J. M. Kindel, and E. L. Lindman, "*Theory of Stimulated Scattering Processes in Laser-Irradiated Plasmas*," Phys. Fluids 18, 1002 (1975)

110. C. S. Liu and M. N. Rosenbluth, "*Parametric Decay of Electromagnetic Waves into Two Plasmons and Its Consequences*," Phys. Fluids 19, 967 (1976)

111. G. Meltz, L. H. Holway, Jr., and N. M. Tomljanovich, "*Ionospheric Heating by Powerful Radio Waves*," Radio Sci. 9, 1049 (1974)

112. J. Weinstock, "*Enhanced Airglow, Electron Acceleration, and Parametric Instabilities*," Radio Sci. 9, 1085 (1974)

113. J. C. Haslett and L. R. Megill, "*A Model of the Enhanced Airglow Excited by RF Radiation*," Radio Sci. 9, 1005 (1974)

114. A. A. Biondi, D. P. Sipler, and R. D. Hake, Jr., "*Optical (λ6300) Detection of Radio Frequency Heating of Electrons in the F Region*," J. Geophys. Res. 75, 6421 (1970)

115. K. W. Billman and J. R. Stallcop, "*Adequacy of Classical Inverse Bremsstrahlung Theory for Low Temperature Plasmas*," Appl. Phys. Lett. 28, 704 (1976)

116. L. M. Biberman, G. E. Norman, and K. N. Ul'yanov, "*The Photoionization of Complex Atoms and Ions*," Sov. Astron. 6, 77 (1962)

117. J. P. Kennealy and F. P. DelGreco, "*The Kinetics of Atmospheric Radiative Processes in the Infrared*," Reaction Rate Handbook, op. cit., Ch. 11

118. G. M. Martynkevich, "*Ion-Hydrates, Their Precursors and Water Vapor in the Mesosphere and the Lower Thermosphere*," J. Atmos. Terr. Phys. 36, 1781 (1974)

119. A. D. Danilov, "*Ionization-Recombination Cycle of the D-Region*," J. Atmos. Terr. Phys. 37, 885 (1975)

120. L. Thomas, "*NO^+ and Water Cluster Ions in the D-Region*," J. Atmos. Terr. Phys. 38, 61 (1976)

121. A. W. Ali, W. S. Knapp, and F. E. Niles, "*Application of Computer Solutions to Atmospheric Deionization Processes*," Reaction Rate Handbook, op. eit., Ch. 22

122. J. Heicklen, "*Atmospheric Chemistry*," Academic, New York (1976), pp. 143-155

123. C. Wittig, "*Stimulated Emission in HCN Near 4* μm," University of Southern California, Department of Electrical Engineering preprint (1975)

124. A. B. Peterson, C. Wittig, and S. R. Leone, "*Infrared Molecular Lasers Pumped by Electronic-Vibrational Energy Transfer from $Br(4^2P_{1/2})$: CO_2, N_2O, HCN, and C_2H_2*," Appl. Phys. Lett. 27, 305 (1975)

125. S. R. Leone, "*Fundamental Kinetic Rate Processes Occurring in Polyatomic Vibrational Lasers*," Joint Institute for Laboratory Astrophysics Report No. RADC-TR-77-294 (1977)

126. W. M. Clark, Jr., "*A Proposed 4-5* μm *Energy Transfer Laser*," IEEE J. Quant. Electron, QE-13, 735 (1977)

127. B. K. Ching, "*Space Power Systems -- What Environmental Impact?*" Astronaut. Aeronaut. 15(2), 60 (1977)

10.0 COST ANALYSIS

10.0 COST ANALYSIS

The SPS cost analysis consists of project development costs (DDT&E plus development TFU) and project average costs allocated to each satellite, equipment replacement and operations and maintenance. Details of the overall analysis and methodology utilized are contained in Volume II, Part 2.

The cost factors pertinent to satellite construction, operations and maintenance include the SCB with its ancillary equipment, the LEO base, satellite construction, materials, and the satellite operations/maintenance bases. The costs have been distributed across the program, depending on the nature of the cost and the time of occurrence. Table 10.0-1 summarizes the costs relating to the major items.

Table 10.0-1. Space Construction and Support Cost Summary (Cost in Millions of Dollars)

ITEM	DDT&E	DEV. TFU	TOTAL	INV PER SATELLITE	RCI	O&M	TOTAL OPS	TOTAL
CONST. FACILITIES (SCB)	3653.2	6575.2	10228.4	123.6	19.1	11.3	30.4	154.0
LOGISTIC SUPPORT FACILITIES - LEO	3677.9	917.2	4595.1	16.3	18.3	-	18.3	34.6
O&M SUPPORT FACILITIES - SATELLITE	-	1110.2	1110.2	1008.4	14.0	-	14.0	1022.4
			15933.7					1211.0

Construction facility costs, in addition to the basic SCB structure, include beam machines, various dispensing devices (e.g., solar blankets), gantries, cranes, and crew support bases. The LEO base costs reflect the modules which comprise the base and which provide the accommodations required for cargo routing, EOTV maintenance, etc. The O&M support facilities, installed on each satellite, provide shelter, working and storage facilities to house the maintenance crew and to support satellite maintenance.

It is noted that the DDT&E and TFU costs of the SCB and LEO base are rather large; however, these items will be in use for 30 years. No DDT&E costs have been allocated to the O&M support facilities in that the equipment and facilities involved will have been developed for the SCB and for satellite construction. The costs of these items in the right side of the table are low by comparison; however, the values under "INV per satellite" must be multiplied by a factor of 60 to reflect the total build. This would result in a value which far exceeds the initial program costs.

APPENDIX— SPECIFIC SATELLITE PLASMA CHARGING CONSIDERATIONS

APPENDIX

SPECIFIC SATELLITE PLASMA CHARGING CONSIDERATIONS

For a solar powered spacecraft at GEO the plasma environment can cause undesirable effects such as spacecraft charging and power losses from high voltage solar arrays. For estimating the effects of the P.C. it can be assumed that a plasma with density me=mp=2 particle/cm^3 and electron energy of $RT_e \cong 5$ kev. These are not the worst possible conditions but are typical of a severe substorm. The effects of plasma charging are summarized in Table A-1.

Table A-1. Possible Effects of Plasma Charging

1. ARC GENERATION DUE TO EXCEEDING THE BREAKDOWN VOLTAGES
2. DIRECT ELECTRICAL DAMAGE TO COMPONENTS FROM THE TRANSIENT
3. EMI DISRUPTION OF LOGIC AND SWITCHING CIRCUITS
4. CHANGE OF REFLECTIVE OR THERMAL CONTROL SURFACES DUE TO OUTGASSING AND PITTING
5. SHOCK HAZARD FOR EVA AND DOCKING ACTIVITIES

To calculate the parasitic plasma power losses the plasma current at GEO is required. The parasitic current will come from plasma thermal current and photoelectron currents to the solar cell array.

The photoelectron current density is obtained by integrating the product of the photoelectron yield function for synthetic sapphire and the solar spectrum. This yields a photocurrent density of $J_{ph}=3\times10^{-9}$ amp/cm^2. The thermal ion and electron currents are given by

$$J = \frac{ne}{4}\sqrt{\frac{8kT}{\pi m}}$$

which gives approximately $Je=3\times10^{-10}$ amp/cm^2 and $Ji=1\times10^{-11}$ amp/cm^2. Therefore at GEO the photoelectron current is found to dominate the thermal ion and electron currents. The power loss is given approximately by;

$$P_p \cong J_{ph} \cdot A \cdot \overline{V}$$

where A is the solar cell area and $\overline{V}$ is the average voltage. This figure has been calculated to be about .7% of output power.

The voltage developed on the solar cells have the potential to break down the kapton insulation, and make the solar arrays vulnerable. Figure A-1 shows the voltage drops resulting from photoelectron and plasma thermal currents.

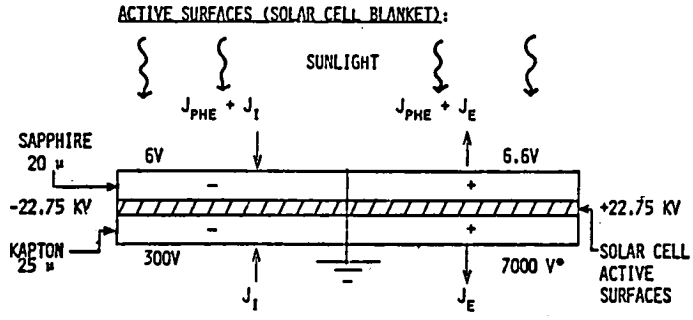

Figure A-1. Plasma Effects on Voltage

The largest voltage would be across the kapton blanket on a positive array. This may exceed the breakdown voltage for kapton 2 10^6 V/cm.

The voltages on the darkside passive (unbiased) surfaces of the satellite can be estimated using Chopra's equation

$$\phi\equiv = \frac{kTe}{2e} \ln\left(\frac{MiTe}{MeTi}\right)$$

For sunlet surfaces, the potential is several times the mean photoelectron energy. Thus we expect +10 to +100 volts for the sunlet surfaces and -10,000 to -20,000 volts for the darkside surfaces (Figure A-2). If this exceeds the insulation breakdown voltage then arcing is to be expected.

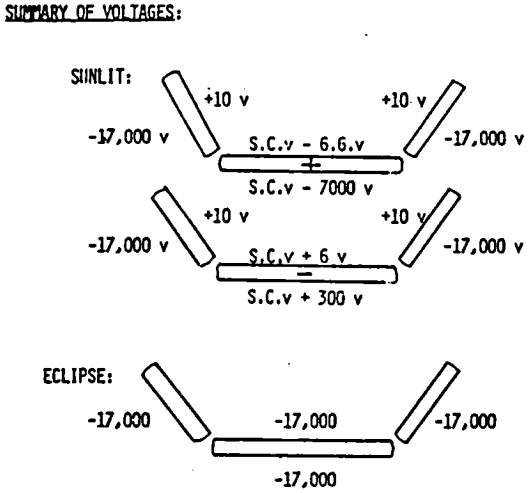

Figure A-2. Summary of Voltages

It should be noted that this is an approximate theoretical treatment and that tests should be run in a substorm test facility or on orbit to obtain accurate assessments of plasma losses and charging problems.

For a satellite in a 400 NM orbit we have somewhat different current values;

$J_I = 7\ 10^{-9}$ amp/cm^2

$J_e = 3\ 10^{-7}$ amp/cm^2

$J_{ph} = 3\ 10^{-9}$ amp/cm^2

in addition there is a RAM current associated with the vehicles movement in the plasma. This is estimated to be about

$J_{RAM} = 2\times10^{-7}$ amp/cm^2.

For a large array ($>1\times10^6$m^2) the plasma losses have been estimated at from 3% to 6%.[1]

If the spacecraft is ion thruster powered; then there is a parasitic load associated with thruster charge exchange ions. Following an approach taken by H.R. Kaufman+ for a mercury thruster we integrate the ion production along the beam path,

$$\dot{N}_{CE} = \frac{2\ G_{CE}\ J_{BEAM}(1-n_u)}{e^2\overline{V}_o R_b \pi} \quad \frac{\text{argon ions}}{\text{sec. col.}}$$

where

G_{CE} = charge exchange cross sec.

N_u = beam utilization

$\overline{V}_o = \sqrt{\frac{8kTo}{\pi m_o}}$ = mean neutral thermal velocity

Then assuming a collection efficiency of 25% to form a parasitic current. The parasitic load from thruster charge exchange ions is then

$P_{PAR} \cong J_p \cdot \overline{V} \cdot A$;

which has been estimated at around 50% of array output.

Another possible source of plasma loss is thruster neutralizer electrons, but if the portion of the array closest to the thruster is negative it can be assumed that the positive arrays are shielded from thruster neutralizer electrons.

[1]Kenneaud NASA CR-121280 + NASA CR-135099

These losses may be lessened by the addition of a conductive shield on both ends of the spacecraft to prevent thruster ion/electron feedback to the solar cells. In addition the solar cell arrays should be mounted with the grounded end toward the outside.

1. Report No.	2. Government Accession No.	3. Recipient's Catalog No.
NASA CR-3322		

4. Title and Subtitle	5. Report Date
SATELLITE POWER SYSTEMS (SPS) CONCEPT DEFINITION STUDY VOLUME V - SPECIAL EMPHASIS STUDIES	September 1980
	6. Performing Organization Code

7. Author(s)	8. Performing Organization Report No.
G. M. Hanley	SSD 79-0010-5
	10. Work Unit No.

9. Performing Organization Name and Address	11. Contract or Grant No.
Rockwell International 12214 Lakewood Boulevard Downey, CA 90241	NAS8-32475
	13. Type of Report and Period Covered
12. Sponsoring Agency Name and Address	Contractor Report
National Aeronautics and Space Administration Washington, D.C. 20546	14. Sponsoring Agency Code

15. Supplementary Notes

Marshall Technical Monitor: C. H. Guttman
Volume V of Final Report

16. Abstract

This volume contains a number of studies that received special emphasis during the contract period. Three of these were related to construction operation and included: (1) rectenna construction, (2) satellite construction, and (3) support system construction. A study was conducted to determine resource requirements and to assess manufacturing capabilities. Launch vehicle propellant requirements were assessed and power required to generate the propellants was determined. The space environment was defined to determine a baseline for future studies. The control characteristics of a single satellite and rectenna system were defined under subcontract by IBM. Finally, environmental impacts of laser transmission systems were assessd by Dr. R. Beverly, also under a subcontract.

17. Key Words (Suggested by Author(s))	18. Distribution Statement
Satellite Construction Rectenna Construction Support System Construction SPS Operations Space Environment SPS Manufacturing SPS Control Laser Power	Unclassified - Unlimited Subject Category 44

19. Security Classif. (of this report)	20. Security Classif. (of this page)	21. No. of Pages	22. Price
Unclassified	Unclassified	276	A13

For sale by the National Technical Information Service, Springfield, Virginia 22161

NASA-Langley, 1980

End of Document